NASA TM X-122

TECHNICAL MEMORANDUM

X-122 DECLASSIFIED-AUTHORITY-MEMO US: 2313. TAINE TO SHAUKLAS DATED JUNE 15, 1967

THE EFFECT OF TRAILING-EDGE CONTROL DEFLECTION ON THE LOADING OVER A 60° DELTA-WING—BODY COMBINATION AT TRANSONIC SPEEDS

By Leland B. Salters, Jr., and Charles E. Mercer

Langley Research Center
Langley Field, Va.

NATIONAL AERONAUTICS AND SPACE ADMINISTRATION
WASHINGTON
October 1959

NATIONAL AERONAUTICS AND SPACE ADMINISTRATION

TECHNICAL MEMORANDUM x-122

THE EFFECT OF TRAILING-EDGE CONTROL DEFLECTION ON THE LOADING OVER A 60° DELTA-WING—BODY COMBINATION AT TRANSONIC SPEEDS*

By Leland B. Salters, Jr., and Charles E. Mercer

SUMMARY

An investigation has been conducted in the Langley 16-foot transonic tunnel to determine the effect of constant-chord trailing-edge control deflection on the aerodynamic loading characteristics of a 3-percent-thick, 60° delta-wing—body combination. Chord length of the control was 15 percent of the wing mean aerodynamic chord. Pressure data were obtained on the wing with aileron deflected and with both aileron and elevator deflected simultaneously. The aileron and combined control deflections varied from 15° to -15° in 7.5° increments with angles of attack up to 26°. Test Mach numbers covered the range from 0.80 to 1.05 and the Reynolds number was approximately 10 × 10⁶ based on a mean aerodynamic chord length of 30.23 inches.

In general, the aileron maintained positive control over the whole range of the investigation. Greater control effectiveness was obtained for negative control deflection than for positive deflection. A positive deflection of 15° maintained local supersonic type flow over the upper control surface to Mach numbers as low as 0.94 and subsonic-type flow on the undersurface up to 1.05.

At an angle of attack of 4° and a Mach number of 0.94 aileron deflection variation from 15° to -15° moved the chordwise center of pressure forward from the 61- to the 23-percent station of the mean aerodynamic chord and at an angle of attack of 20°, from the 54- to the 45-percent station. Under similar conditions the spanwise center of pressure moved inboard from the 60- to the 42-percent semispan station and from the 49- to the 46-percent semispan station.

---

*Title, Unclassified.

INTRODUCTION

Because of inadequate theory for calculating the effects of deflected controls on wing aerodynamic loading in the transonic range, at present (see ref. 1), it is necessary to resort to experimental data for airplane control design for the transonic regime. The need for experimental data on typical airplane configurations in the transonic regime is, therefore, greater than for subsonic and supersonic ranges where present theory is adequate. Experimental investigations of various control configurations on wing-body combinations with thin wings of unswept, swept, and triangular plan forms have been conducted in the Langley 16-foot transonic tunnel as indicated in references 1 to 3.

That part of the investigation which deals with wings of triangular plan form consisted of tests to determine the aerodynamic characteristics of a 60° delta-wing—body combination with a 3-percent-thick wing. The longitudinal aerodynamic characteristics have been reported in reference 4, the wing loading characteristics with undeflected controls in reference 5, and the wing loading characteristics with deflected constant-chord controls are presented in this paper. The chord length of the control was 15 percent of the wing mean aerodynamic chord. A Mach number range of 0.80 to 1.05 was covered in this investigation over an angle-of-attack range from 0° to 26°. Deflections of aileron and combined controls (aileron with elevator) varied from 15° to -15° in approximately 7.5° increments. The Reynolds number was approximately 10×10^6 based on a mean aerodynamic chord length of 30.23 inches.

SYMBOLS

A	aspect ratio
b	wing span
c	local chord
c'	wing mean aerodynamic chord, $\frac{2}{S}\int_0^{b/2} c^2 dy$
$\bar{c}$	average wing chord, S/b
$c_{m_{0.35c}}$	wing-section pitching-moment coefficient about 0.35c, $\int_0^{1.0} \left(C_{p,l} - C_{p,u}\right)\left(0.35 - \frac{x}{c}\right) d\frac{x}{c}$

c_m wing-section pitching-moment coefficient about 0.35c', $c_{m_{0.35c}} - c_n\left(0.35 - \frac{x'}{c}\right)$

C_b wing bending-moment coefficient about body center line, $\int_{0.19}^{1.0} c_n \frac{c}{\bar{c}} \frac{y}{b/2} \, d\frac{y}{b/2}$

C_m wing pitching-moment coefficient about 0.35$\bar{c}$', $\int_{0.19}^{1.0} c_m \frac{c^2}{\bar{c}c'} \, d\frac{y}{b/2}$

c_n wing-section normal-force coefficient, $\int_0^{1.0} \left(C_{p,l} - C_{p,u}\right) d\frac{x}{c}$

C_N wing normal-force coefficient, $\int_{0.19}^{1.0} c_n \frac{c}{\bar{c}} \, d\frac{y}{b/2}$

l body length

M Mach number

P free-stream static pressure

C_p pressure coefficient, $\frac{p_{local} - p}{q}$

q free-stream dynamic pressure

r body radius

R radius of wing tip

S wing area (includes area covered by body)

x distance from wing leading edge or body nose (positive rearward)

x' distance from wing leading edge to a line perpendicular to plane of symmetry and passing through 0.35c'

$\frac{x_{cp}}{c}$	section chordwise center-of-pressure position
$\frac{x_{cp}}{c'}$	wing chordwise center-of-pressure position, $0.35 - \frac{C_m}{C_N}$
Y	spanwise distance measured from body center line
$\frac{y_{cp}}{b/2}$	wing spanwise center-of-pressure position
a	angle of attack of body center line
λ	taper ratio
δ	angle of control deflection, in plane normal to hinge line (positive when trailing edge deflected down)

Subscripts:

a	aileron
c	combined control (aileron with elevator)
2	wing lower surface
u	wing upper surface
cp	center of pressure

APPARATUS AND METHODS

Wind Tunnel and Support System

This investigation was conducted in the Langley 16-foot transonic tunnel which is a single-return atmospheric wind tunnel with an octagonal slotted test section. It has a speed range from a Mach number of 0.20 to about 1.10 and the Mach number is varied over this range simply by variation of tunnel drive power. The model was sting supported from a single swept cantilever strut that was arranged so that the model was always located near the tunnel center line for all angles of attack.

Model

Figure 1 shows the model with left aileron deflected 15° mounted in the Langley 16-foot transonic tunnel test section. Figure 2 is a sketch showing model details and a list of wing pressure orifices. These pressure orifices were located on the top and bottom surfaces of the left-wing panel and control surfaces only. The steel wing has 60° leading-edge sweepback, 0° trailing-edge sweep, and NACA 65A003 airfoil sections parallel to free stream. The wing was mounted in the midwing position on the fuselage and was designed to have no geometric twist, incidence, or dihedral. The wing tips were slightly rounded; thus, differences in the actual and theoretical values of aspect ratio, area, and the wing mean aerodynamic chord were created. These differences are shown in figure 2. Actual values were used in data reduction.

The control shown in figure 2 consisted of wing trailing-edge ailerons and elevators. The aileron was deflected individually and the aileron and elevator were deflected simultaneously as a full-span trailing-edge combined control. The parting line between aileron and elevator was located at $0.67b/2$.

Tests

Pressure data were obtained for Mach numbers of 0.80, 0.90, 0.94, 1.00, and 1.05 at angles of attack from 0° to 26°. Nominal control deflections of 0°, ±7.5°, and ±15° were obtained for each Mach number. At Mach numbers of 1.00 and above, the angle-of-attack range was limited by tunnel drive power. For this investigation the Reynolds number based on the wing mean aerodynamic chord varied from 9.5×10^6 to 11.5×10^6 over the Mach number range.

The relationship between the control deflections of the right- and left-wing panels is shown in the following table:

Left wing panel (Instrumented)		Right wing panel (Not instrumented)	
Aileron	Elevator	Elevator	Aileron
Aileron alone			
0°	0°	0°	0°
7.5	0	0	0
15.0	0	0	0
-7.5	0	0	0
-15.0	0	0	0
Combined controls			
0	0	0	0
7.5	7.5	-7.5	-7.5
15.0	15.0	-15.0	-15.0
-7.5	-7.5	-7.5	-7.5
-15.0	-15.0	-15.0	-15.0

Instrumentation

Pressures over the wing and trailing-edge controls of the left-wing panel were measured at six spanwise stations with the pressure orifices located as listed in figure 2. These orifices were connected directly to manometer boards. At the innermost station the orifices were installed on the fuselage shell about 1/16 inch from the wing surface at the wing-fuselage juncture. These orifices are listed but the pressures obtained were not used in the analysis of the combined control data for this investigation since they are closely associated with the pressures over the entire wing chord only for a $\delta = 0^\circ$ deflection of combined controls.

Model angles of attack were measured by means of a calibrated pendulum strain-gage angle-of-attack indicator mounted in the model nose. The resulting angles of attack are independent of sting and balance deflections due to load.

Reduction of Data

Pressures were recorded by photographing 100-tube mercury manometer boards. A film reader converted the individual pressure tube deflections recorded on the film into punch card readings. The data were then processed on electronic computing machines to obtain individual pressure

coefficients. Wing-section normal-force and pitching-moment coefficients were machine processed by the use of a rectangular step Integration. The data cards were also fed into an automatic plotting device for the preparation of chordwise pressure-distribution plots which will be discussed later in this paper.

Accuracy

Measurements and coefficients are accurate to within the following limits:

C_p	±0.01
C_N	±0.01
C_m	±0.001
C_b	±0.05
M	±0.005
α	±0.1

The local wing section angles of attack have not been corrected for twisting characteristics due to aerodynamic loads. However, the twisting characteristics at several chordwise and spanwise stations were determined from static loadings. The method used is described in reference 6. The maximum twist at the 0.90b/2 station was about -0.5° for conditions of maximum load.

The additional control deflections due to load was determined by a calibration using static loadings applied only to the controls. Deflections due to wing twist were not considered, inasmuch as they were believed to be small. The maximum deflection for maximum loading was found to be approximately -1.40°. For this paper the nominal deflection angles were used for all basic data but the corrected deflection values were used in the wing chordwise and spanwise center-of-pressure location analysis figures.

RESULTS

The results of the investigation are presented as follows:

	Figures
Wing chordwise pressure distributions with controls deflected	3 to 10
Variation of wing chordwise pressure distributions with control deflection	11 to 14

DISCUSSION

Basic Chordwise Pressure Distributions

In figures 3 to 10 are presented the basic control deflection data, consisting of pressure coefficient distributions for the upper and lower wing surfaces for six spanwise stations. In interpreting these data it should be noted that the ratios of the control-surface chord lengths to the wing-chord lengths vary along the semispan. For instance at $0.19b/2$ the control surface comprises about 12 percent of the wing chord while at $0.90b/2$ it comprises about 65 percent of the wing chord. The sudden breaks in the curves, denoting where the control surface begins, may be seen to vary in percentage of the chord at each spanwise station. A complete discussion on the pressure distribution and flow characteristics of the basic wing (with controls undeflected) is given in reference 5. Reference 3 indicates that carryover loads from the elevator deflection on the right wing may be expected. Although the magnitude of the carryover is not evaluated in this paper, the fact of carryover should be considered in studying these figures.

Effect of Control Deflection On Wing Chordwise Pressure Distribution

In figures 11 to 14 are presented pressure coefficient distribution comparisons between the basic wing, with controls undeflected (from ref. 5), and the wing with various aileron and combined control deflections. The differences between the dashed and solid lines of figures 11 to 14 represent the effect of control surface deflection upon wing chordwise pressure distributions and may be termed additional pressures.

The effect of a positive aileron deflection of 15° upon the wing pressure pattern is shown in figure 11. The additional pressure produced on the lower surface of the wing and aileron was positive in sign and usually approximated a triangle in shape with the apex at the aileron

[redacted]

leading edge and with rapid tapering down from the apex in both upstream and downstream directions. (See fig. 11(a).) The limit of the influence of aileron deflection upon the wing undersurface was about one aileron chord length forward of the aileron. This positive pressure pattern was not greatly affected by angle of attack or Mach number from $M = 0.80$ to 1.05.

The additional-pressure pattern on the upper surface of the wing produced by a positive aileron deflection of 15° was more complicated in shape, the pattern being greatly affected by Mach number and angle of attack. At a Mach number of 0.80 the pressure pattern had definite subsonic characteristics whereas at $M = 0.94$ and 1.05 it had supersonic characteristics. At $M = 0.80$ the additional pressure, although negative in sign, showed peak pressures at the aileron leading edge (as on the undersurface) and influenced the wing pressure field also about one aileron chord length forward of the aileron leading edge. At $M = 0.94$ and higher, however, the influence did not extend upstream but was confined mainly to the aileron itself. (See fig. 11(b), for $\alpha = 0.3^\circ$.) The pattern on the aileron also tended to the rectangular shape which is typical of supersonic flow. (See ref. 7.) In general, the influence of control deflection on the additional pressure patterns decreased with increase in angle of attack. This decrease in influence is associated with stall on the aileron and the part of the wing covered by the aileron. At an angle of attack of 8° stall was usually evident at one of the two aileron stations ($y = 0.74b/2$ or $0.90b/2$) and at an angle of attack of 12° at both stations.

The fact that the undersurface seemed unaffected by Mach number and the upper surface was definitely affected may be explained by circulation due to lift. On the upper surface the circulation added to the general flow and produced local supersonic flow at free-stream Mach numbers as low as 0.94, whereas on the undersurface of the wing the circulation opposed the general flow and produced local subsonic type flow even to Mach numbers as high as 1.05.

The remarks concerning the positive aileron deflection of 15° apply in general to the combined control deflection of figure 13 except that the spanwise influence of the combined controls extend undiminished inboard to the body. The deflection of the elevator in addition to the aileron on the left-wing panel appears to strengthen the additional pressure field of the aileron and to extend its influence slightly farther forward upon the wing pressure pattern. It should be noted here that the combined control on the opposite (right) wing panel was deflected -15°, whereas for the aileron the opposite aileron was not deflected. Therefore some influence from carryover associated with this -15° deflection on the right-wing panel may be expected in the pressure data of the combined controls on the left-wing panel in the manner indicated in reference 3. Figures 13 and 14 indicate that the influence of combined control deflection on the wing pressure distribution is mainly limited to the vicinity of the controls.

The effect of negative aileron deflection of 15° on the wing pressure pattern is shown in figure 12. The forward and lateral extent of influence of the aileron on the pressure field of the wing is about the same as that for positive 15° aileron deflection. Perhaps the most pronounced characteristics of these pressure patterns were the peak negative pressures on the undersurface of the wing at the aileron leading edge. At a Mach number of 0.80 these had the sharp peaks characteristic of subsonic flow, but at a Mach number of 0.94 the peaks had broadened out noticeably and at a Mach number of 1.05 the peak pressure had extended back almost undiminished to the trailing edge which resembled the expansion phenomena of supersonic flow. (See ref. 7.) At a Mach number of 0.94 and above, these peak negative pressures as a rule do not carry over onto the wing either in a chordwise or spanwise direction, but are confined mainly to the aileron itself. As was the case for positive aileron deflection, angle-of-attack variation had little effect on the wing undersurface pressure pattern but a pronounced effect on that of the upper surface. In general, the onset of the stall on the upper surface occurred at lower angles of attack than for positive deflection. The influence of aileron deflection on the upper-surface pressure pattern at angles of attack above the stall angle was small.

A visual indication of the effects of negative 15° aileron deflection on the flow pattern on the upper surface of the wing is provided from boundary-layer studies by means of ink-flow and tuft photographs of figure 15. It may be noted that both ailerons are deflected at -15°. Comparable ink-flow photographs for undeflected controls are shown in reference 5.

A comparison of figure 15 with the photographs of reference 5 indicates that negative aileron deflection makes the pressures more positive in the region of the aileron. The ink-flow pattern indicates that the spanwise flow near the aileron noted in reference 5 has been eliminated by negative control deflection. This is believed to be associated with the more positive pressure field connected with negative control deflection. Pressure distributions and ink flow both show the vortex existing near the leading edge, and tufts indicate the spanwise extent of the vortex. Although aileron deflection did affect spanwise flow, it did not influence the position or appearance of the vortex.

The negative 15° deflection of the elevator in addition to the aileron as shown in figure 14 reinforces the additional pressures produced by the aileron and extends the pressure pattern undiminished inboard to the body. The deflection of the combined control on the opposite wing panel was -15°. The carryover from the opposite control would be expected to reinforce the additional pressure field in this case. This should be considered when these data are compared with those of figure 13, where the carryover would be expected to oppose and diminish the additional pressure field.

Effect of Control Deflection on Wing Spanwise Loading Characteristics

In figures 16 to 23 the spanwise loadings for undeflected controls are compared directly with those for deflected controls. Figure 17(a) indicates that the main effect of the aileron deflection was on the loading of that part of the span covered by the aileron although there was some carryover to the remainder of the wing. A comparison of figure 17(a) with figure 17(c) shows the effect of Mach number on the lateral carryover, namely, that the magnitude of the carryover pressures decreased with increase in Mach number through the transonic range. It may be observed that for positive aileron deflection (fig. 17 for instance) an increase in the angle of attack produced a marked decrease in the additional loading caused by deflection of the aileron, whereas for negative aileron deflection (fig. 19 for instance) an increase in the angle of attack had much smaller effect on the additional pressure patterns. This difference between positive and negative deflection could not be caused by carryover from the opposite wing because in both cases the opposite aileron was not deflected. It would therefore appear that wing normal force was more greatly influenced by negative aileron deflection than by positive aileron deflection.

When figures 21 are compared with figures 23 it is apparent that negative combined control deflection was more effective than positive deflection in influencing wing normal force. However, in both cases the combined control on the opposite wing panel was deflected -15° which would tend to enhance this effect since it might be expected that carryover from the opposite panel would decrease the additional normal-force pattern for 15° deflection and increase it for -15° deflection.

Effect of Control Deflection on Center of Pressure Characteristics

Section chordwise center of pressure.- Variation of the section chordwise center-of-pressure location with control deflection at the typical transonic Mach number of 0.94 is shown in figures 24 and 25. Figure 24 indicates the localized nature of the influence of the aileron alone upon the section centers of pressure along the semispan. Both figures clearly emphasize the decrease in center-of-pressure movement with increase in angle of attack. This, of course, does not necessarily mean that the controls are less effective in producing changes in pitching moment at the higher angles of attack (see ref. 4) but only less in proportion to the normal force.

Wing chordwise center of pressure.- In figures 26 and 27 is presented the effect of control deflections on the wing chordwise center-of-pressure location. For both aileron and combined control, increasing the angle of attack produced forward movement of the center of pressure for positive control deflection and rearward movement for negative deflection. Increase in Mach number in the range of the investigation moved the center of pressure slightly rearward, in general. This effect was more pronounced for combined controls than for the aileron alone. The magnitude of the center-of-pressure movement decreased with increase in angle of attack. For instance, at an angle of attack of 4° and a Mach number of 0.94, aileron-deflection variation from 15° to -15° moved the chordwise center of pressure from 61 to 23 percent of the mean aerodynamic chord but at an angle of attack of 20° from 54 to 49 percent of the mean aerodynamic chord. L 5 0 6

Deflecting the controls positively from the neutral or zero position moved the center of pressure rearward in every case and deflecting them negatively caused the center of pressure to move forward, the extent of movement being much greater for combined controls than for the aileron alone. For combined controls negative deflection often moved the center of pressure off the leading edge at the low angles of attack.

Wing lateral center of pressure.- The relation between spanwise center-of-pressure location and control deflection is shown in figures 28 and 29. With controls undeflected the center of pressure varied between 45 and 55 percent of the semispan being mainly affected by variation in angle of attack and only slightly by Mach number.

The location of the spanwise center of pressure in general was more greatly affected by aileron (fig. 28) than by combined control deflection (fig. 29), the trend in both cases being that an increase in deflection in the positive direction caused the center to move outboard. The maximum center-of-pressure movement for the aileron alone occurred between positive 15° and negative 15° deflection at a Mach number of 0.80 which caused a 25-percent shift from 0.60 to 0.35 percent of the semispan.

For all positive deflection angles of the aileron and for low negative deflection angles, an increase in the angle of attack moved the spanwise center of pressure inboard, but at the negative deflection angles, from about 6° and upward, moved the center of pressure outboard. The magnitude of the center-of-pressure movement decreased with an increase in angle of attack. For instance at an angle of attack of 4° and a Mach number of 0.94 aileron-deflection variation from 15° to -15° moved the spanwise center of pressure from 60 to 42 percent of the semispan but at an angle of attack of 20°, from 49 to 46 percent of the semispan. Increase in Mach number through the range of the investigation decreased the magnitude of the center-of-pressure travel. These remarks also apply for the case of the combined controls except that the change

from inboard to outboard movement of the center of pressure occurs, in general, at higher negative deflection angles.

The sudden movements of the center of pressure from positive to negative infinity in figure 29 for an angle of attack of 4° was caused by the wing normal force passing through zero under the influence of the negative deflection of the combined controls.

Effect of Control Deflection on Wing Normal-Force and Bending-Moment Characteristics

Wing normal force.- It is assumed for the purposes of this discussion that aileron effectiveness is determined by its ability to produce changes in normal force, positive deflection increasing and negative deflection decreasing normal force. Figure 30 indicates that the aileron is effective over the whole range of the investigation except at a Mach number of 0.94, an angle of attack of 12°, and a positive deflection of 15°, as shown in figure 30(a). As for the cause of the ineffectiveness of the aileron at this point, figure 17(b) ($\alpha = 12.3°$) indicates that the root of the trouble lies at station 0.74b/2 on the aileron, in that aileron deflection did not produce the usual increase in normal force at this station. An examination of pressure distributions in figure 11(b) for $\alpha = 12.3°$ and station 0.74b/2 indicates that aileron deflection produced the usual increase in normal force on the lower surface but a decrease on the upper surface. The decrease in normal force on the upper surface opposed the increase on the lower surface and caused the aileron to lose most of its effectiveness at this point. No explanation for this phenomena will be attempted in this paper; however, it may be significant that previous investigations of similar model configurations have indicated mixed flows at a Mach number of 0.94, and flight tests also indicate that this is a troublesome flight region.

The aileron is slightly more consistent as well as effective for negative deflection than for positive deflection as indicated by a comparison of figures 30(a) and 30(b). Also a comparison of figures 32(a) and 32(b) shows that for combined controls negative deflection is considerably more effective than positive deflection. As indicated previously, however, some of this may be caused by carryover from the opposite wing panel.

Wing bending moment.- The effect of control deflection on wing bending moment may be seen in figures 34 and 35. The influence of control deflection on bending moment shows no consistent or significant variation with Mach number; however, a slight decrease may be noted with an increase in angle of attack. Bending moment, as normal force, appears to be influenced by negative control deflection to a greater degree than by positive deflection.

CONCLUSIONS

The results of an investigation of wing loading produced by control deflection on a 60° delta wing-body combination at transonic speeds indicate the following conclusions:

1. The aileron maintained positive control over the whole range of the investigation except near an angle of attack of 12°, a Mach number of 0.94, and a control deflection of 15°.

2. In all cases negative control deflection was more effective than positive control deflection. This effect is more pronounced for combined controls than for aileron alone.

3. A positive control deflection of 15° maintained local supersonic-type flow over the upper control surface to Mach numbers as low as 0.94 and subsonic-type flow on the undersurface up to 1.05.

4. At an angle of attack of 4° and a Mach number of 0.94, aileron-deflection variation from 15° to -15° moved the chordwise center of pressure from 61 percent to 23 percent of the mean aerodynamic chord and at an angle of attack of 20°, from 54 percent to 49 percent of the mean aerodynamic chord.

5. At an angle of attack of 4° and a Mach number of 0.94, aileron-deflection variation from 15° to -15° moved the spanwise center of pressure from 60 percent to 42 percent of the semispan and at an angle of attack of 20°, from 49 percent to 46 percent of the semispan.

Langley Research Center,
National Aeronautics and Space Administration,
Langley Field, Va., July 17, 1959.

REFERENCES

1. West, F. E., Jr., and Czarnecki, K. R.: Loads Due to Controls at Transonic and Low Supersonic Speeds. NACA RM L57D26a, 1957.

2. Runckel, Jack F., and Gray, W. H.: An Investigation of Loads on Ailerons at Transonic Speeds. NACA RM L55E13, 1955.

3. Heath, Atwood R., Jr., and Igoe, Ann W.: A Wind-Tunnel Investigation of the Wing Loads Due to Deflected Inboard Ailerons on a 45° Swept-back Wing at Transonic Speeds. NACA RM L58E12, 1958.

4. Critzos, Chris C., and Foss, Willard E., Jr.: Effect of Full-Span Trailing-Edge Elevons on the Transonic Longitudinal Aerodynamic Characteristics of a Wing-Body Combination Having a 3-Percent-Thick Triangular Wing With 60° Leading-Edge Sweep. NACA RM L57G03, 1957.

5. Swihart, John M., and Foss, Willard E., Jr.: Transonic Loads Characteristics of a 3-Percent-Thick 60° Delta-Wing—Body Combination. NACA RM L57D12, 1957.

6. Runckel, Jack F., and Lee, Edwin E., Jr.: Investigation at Transonic Speeds of the Loading Over a 45° Sweptback Wing Having an Aspect Ratio of 3, a Taper Ratio of 0.2, and NACA 65A004 Airfoil Sections. NACA RM L56F12, 1956.

7. Lord, Douglas R., and Czarnecki, K. R.: Analysis of Pressure Distributions for a Series of Tip and Trailing-Edge Controls on a 60° Delta Wing at Mach Numbers of 1.61 and 2.01. NACA RM L58C07, 1958.

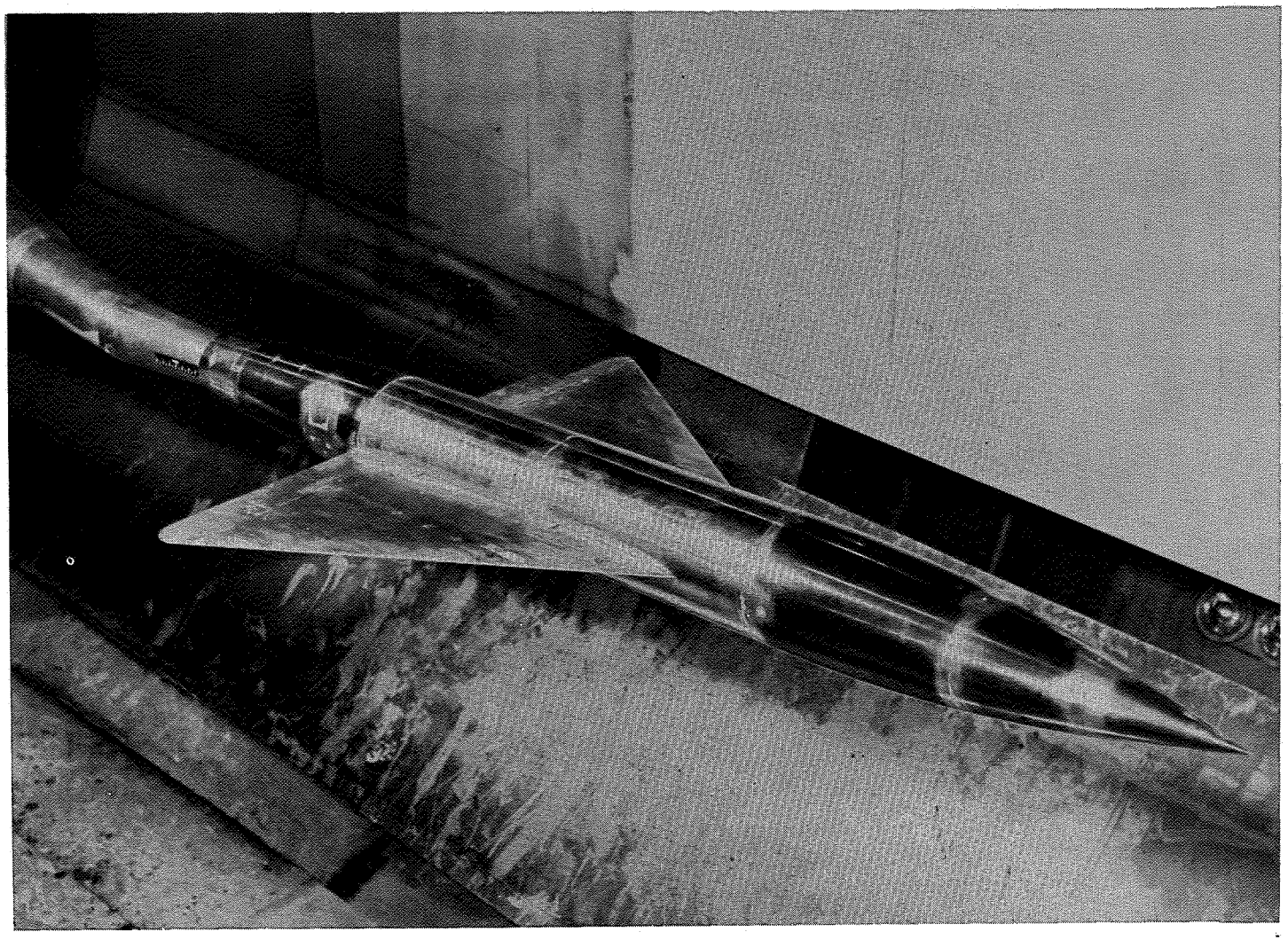

L-88122

Figure 1.- Model with left aileron deflected 15° installed in the Langley 16-foot transonic tunnel.

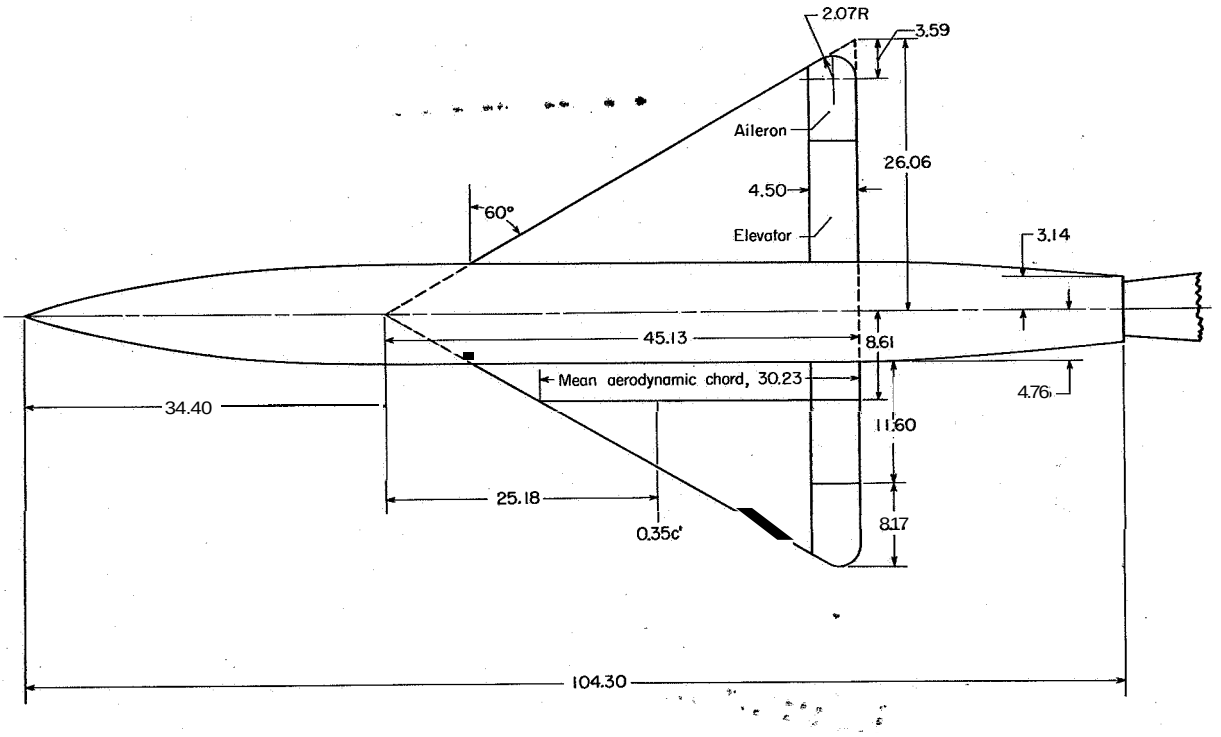

	Actual	Theoretical
A	2.06	231
b/2	24.54	26.06
S	8.13 ft^2	8.17 ft^2
λ	0	0
c'	30.23 in.	30.09 in.
Section	NACA 65A003	NACA 65A003

Body	inates
x	r
0	0
2.00	0.56
4.00	1.09
6.00	1.58
8.00	2.04
10.00	2.45
14.00	3.18
18.00	3.77
22.00	4.22
26.00	4.54
30.00	4.72
33.33	4.76
78.58	4.76
80.00	4.73
83.50	4.56
87.00	4.35
90.97	4.07
104.30	3.14

*	Wing orifice locations Station					
	x/c	x/c	x/c	x/c	x/c	x/c
	0.19 $\frac{b}{2}$	0.327 $\frac{b}{2}$	0.53 $\frac{b}{2}$	0.65 $\frac{b}{2}$	0.74 $\frac{b}{2}$	0.90 $\frac{b}{2}$
	0	0	0	0	0	0
	0.01	0.01	0.01	0.01	0.01	0.01
	.03	.03	.03	.03	.03	.05
	.05	.05	.05	.05	.05	.08
	.08	.08	.08	.08	.08	.10
	.10	.10	.10	.10	.10	.15
	.15	.15	.15	.15	.15	.19
	.20	.19	.19	.19	.19	.25
	.25	.25	.25	.25	.25	.30
	.30	.30	.30	.30	.30	.35
	.35	.35	.35	.35	.35	.40
	.40	.40	.40	.40	.40	.45
	.45	.45	.45	.45	.45	.50
	.50	.50	.50	.50	.50	.60
	.55	.55	.55	.55	.55	.70
	.60	.60	.60	.60	.60	.80
	.65	.65	.65	.65	.68	.90
	.70	.70	.70	.70	.70	
	.75	.75	.75	.77	.73	
	.80	.80	.82	.79	.75	
	.85	.85	.83	.81	.80	
	.90	.87	.85	.83	.85	
	.95	.88	.87	.87	.90	
		.89	.90	.92	.95	
		.91	.93	.96		
		.93	.97			
		.95				
		.98				

* Actually located on body

Figure 2.- Model details and list of wing and body pressure orifice locations. All model dimensions are in inches unless otherwise noted.

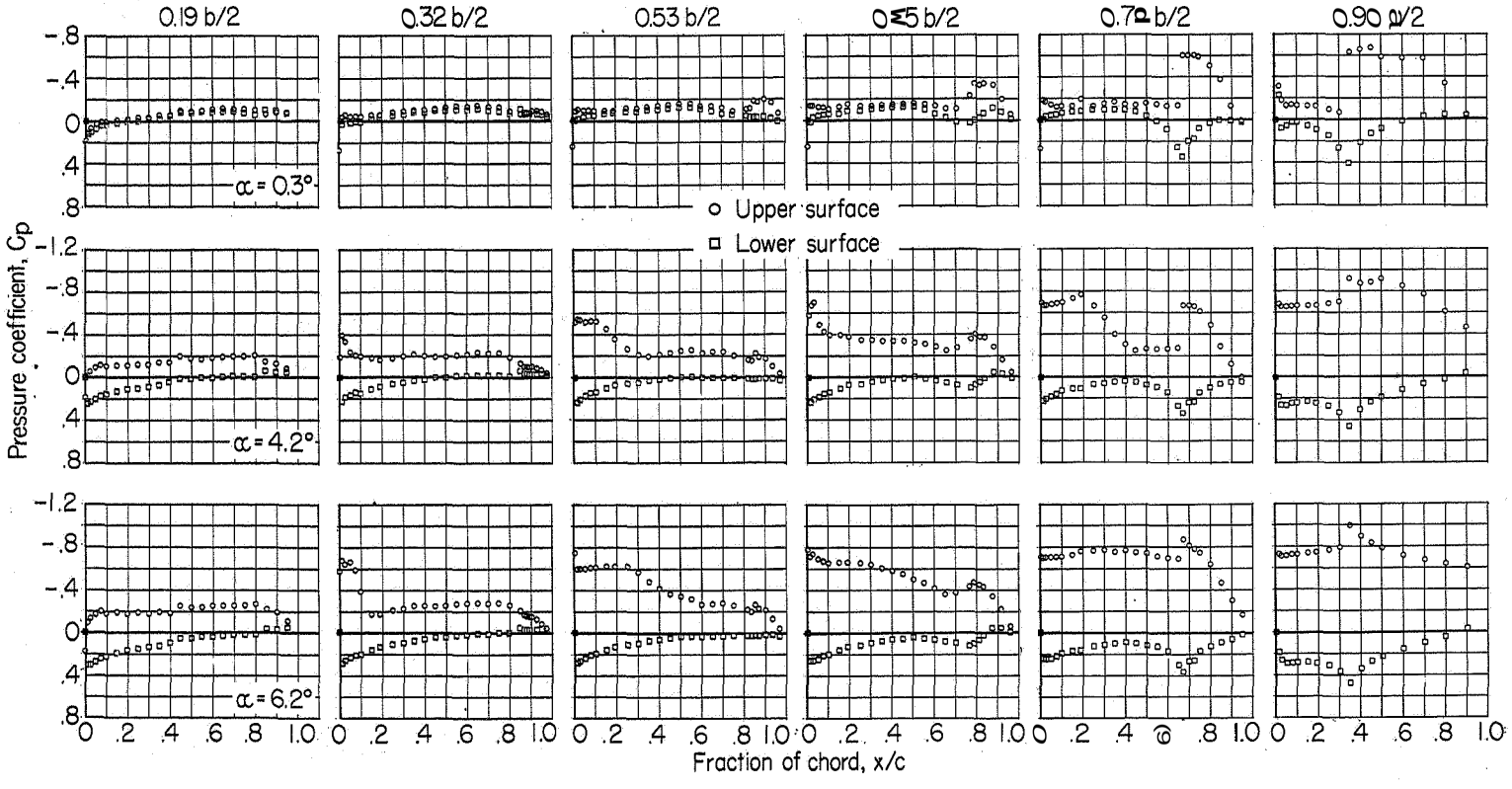

Figure 3.- Chordwise pressure distributions on a 60° delta wing with aileron deflected 7.5° M = 0.94; $C_{p,sonic}$ = -0.10.

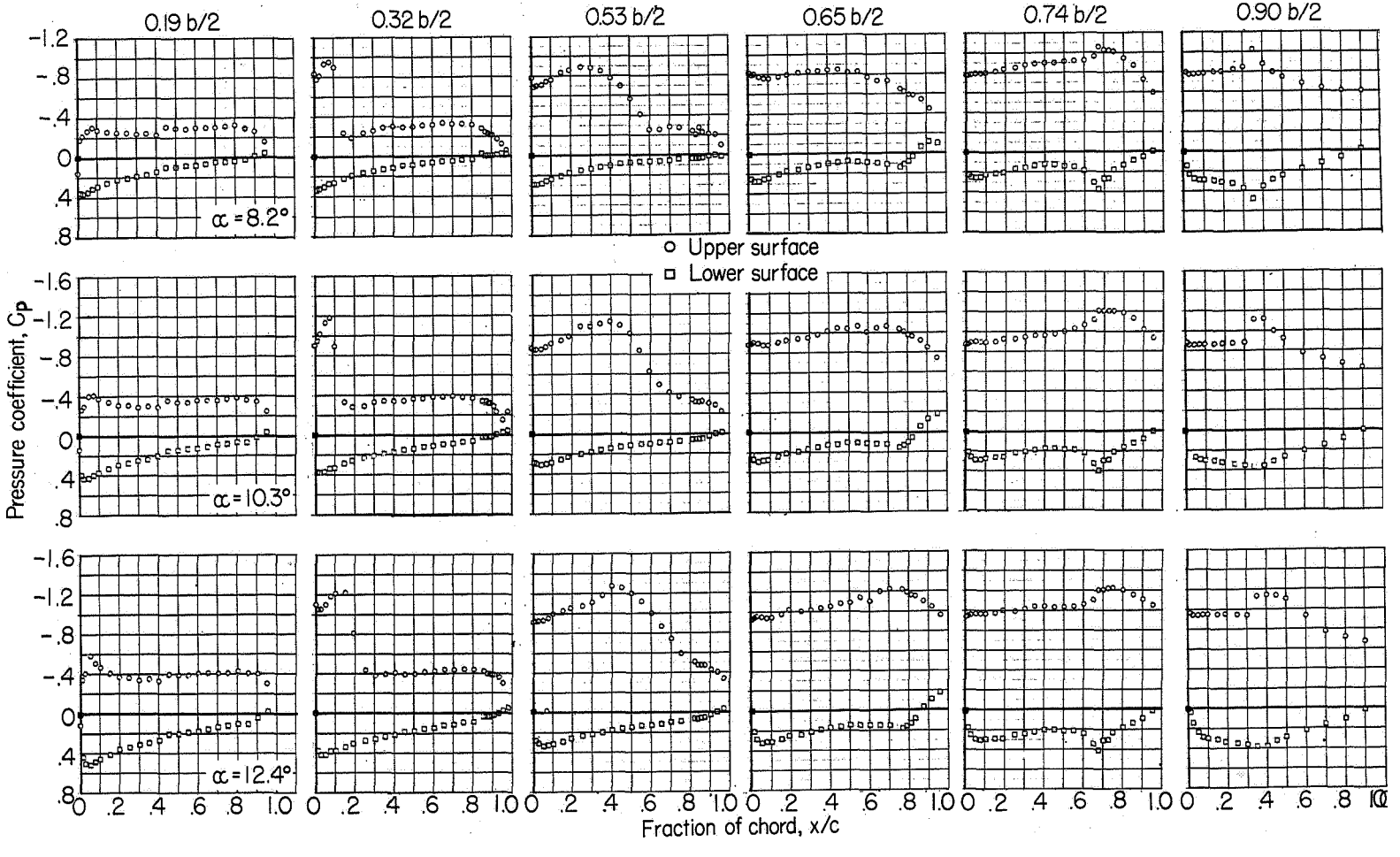

Figure 3.- Continued.

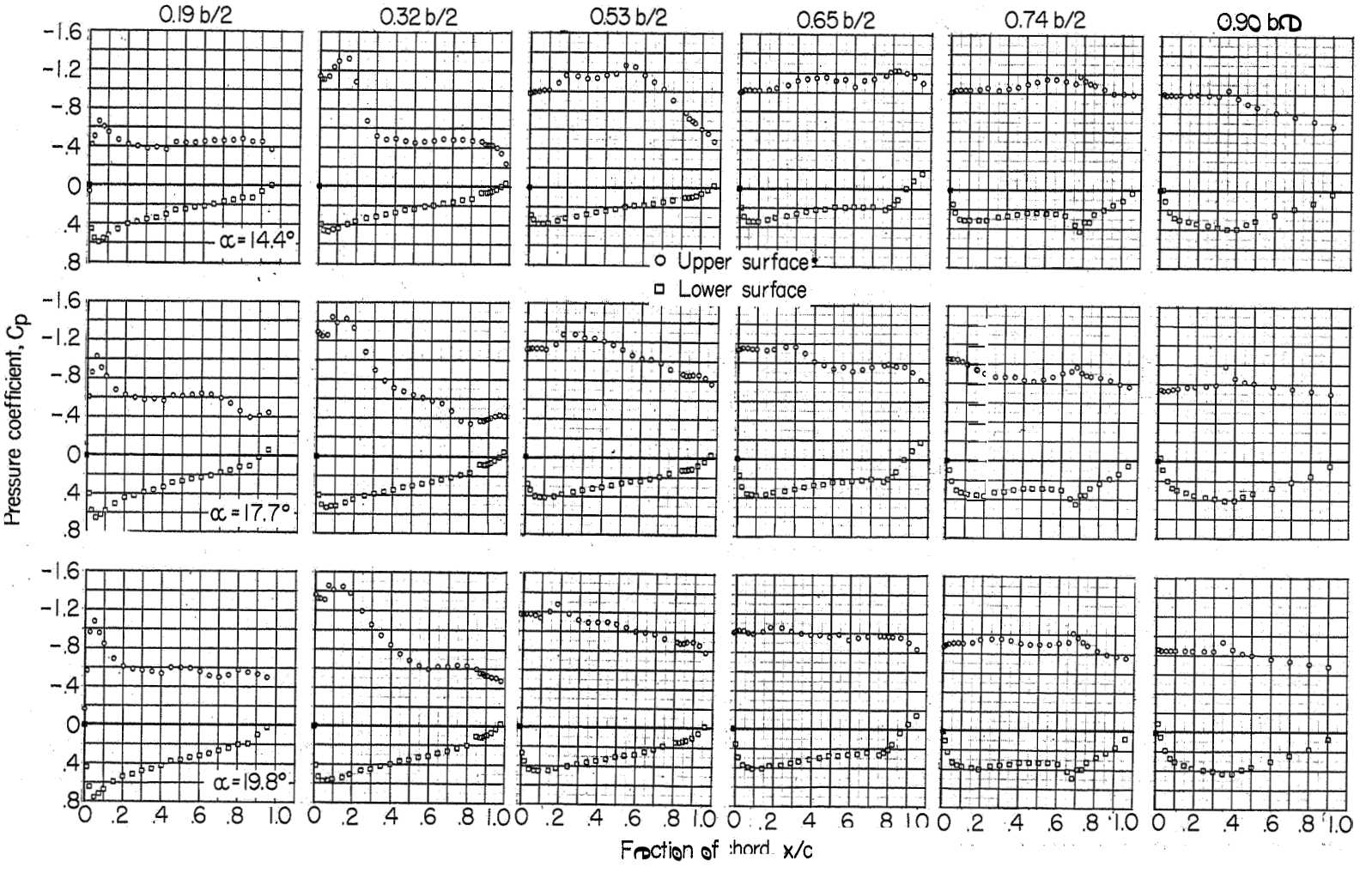

Figure 3.- Concluded.

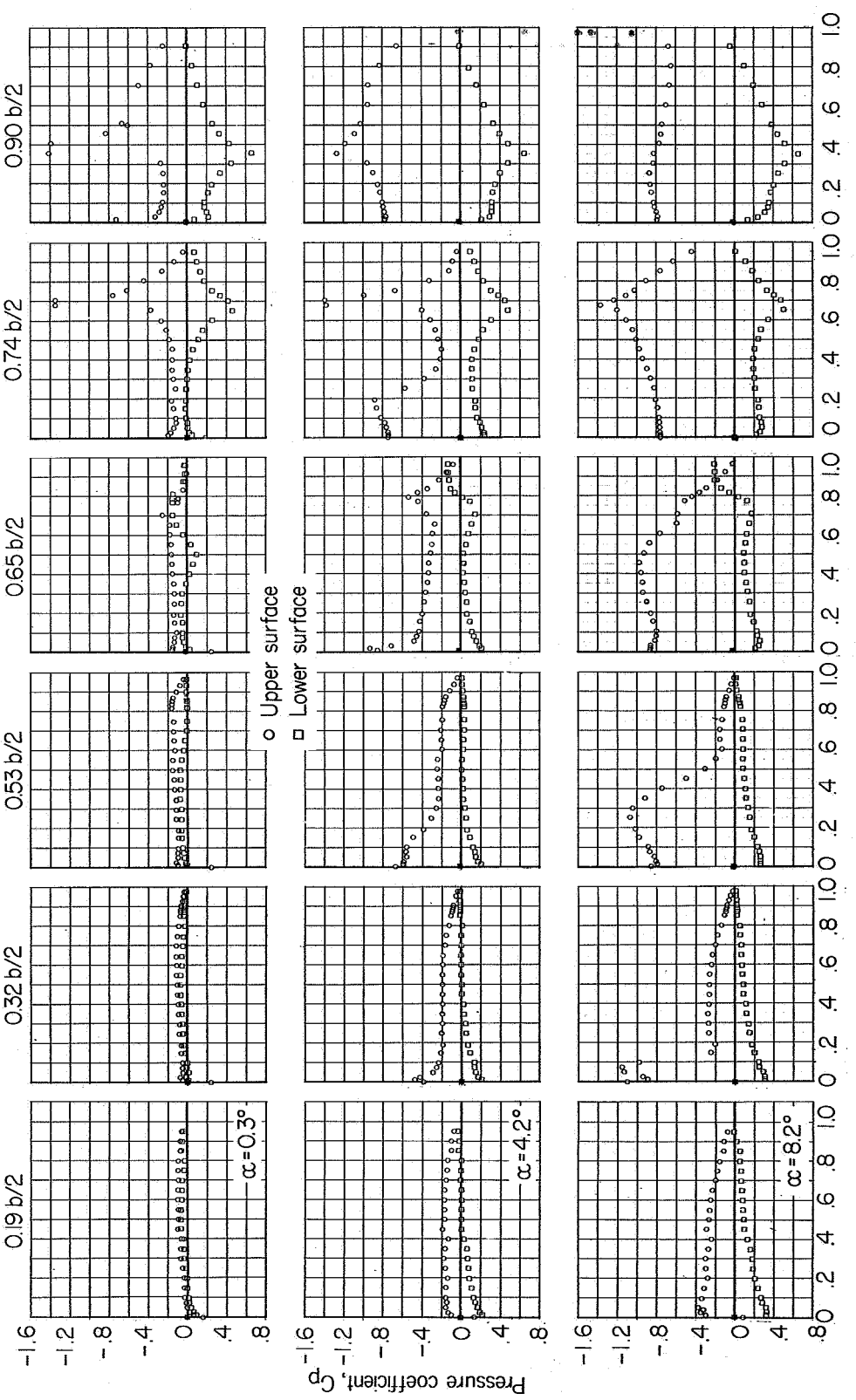

(a) M = 0.80; $C_{p,sonic}$ = -0.44.

Figure 4.- Chordwise pressure distributions on a 60° delta wing with aileron deflected 15°.

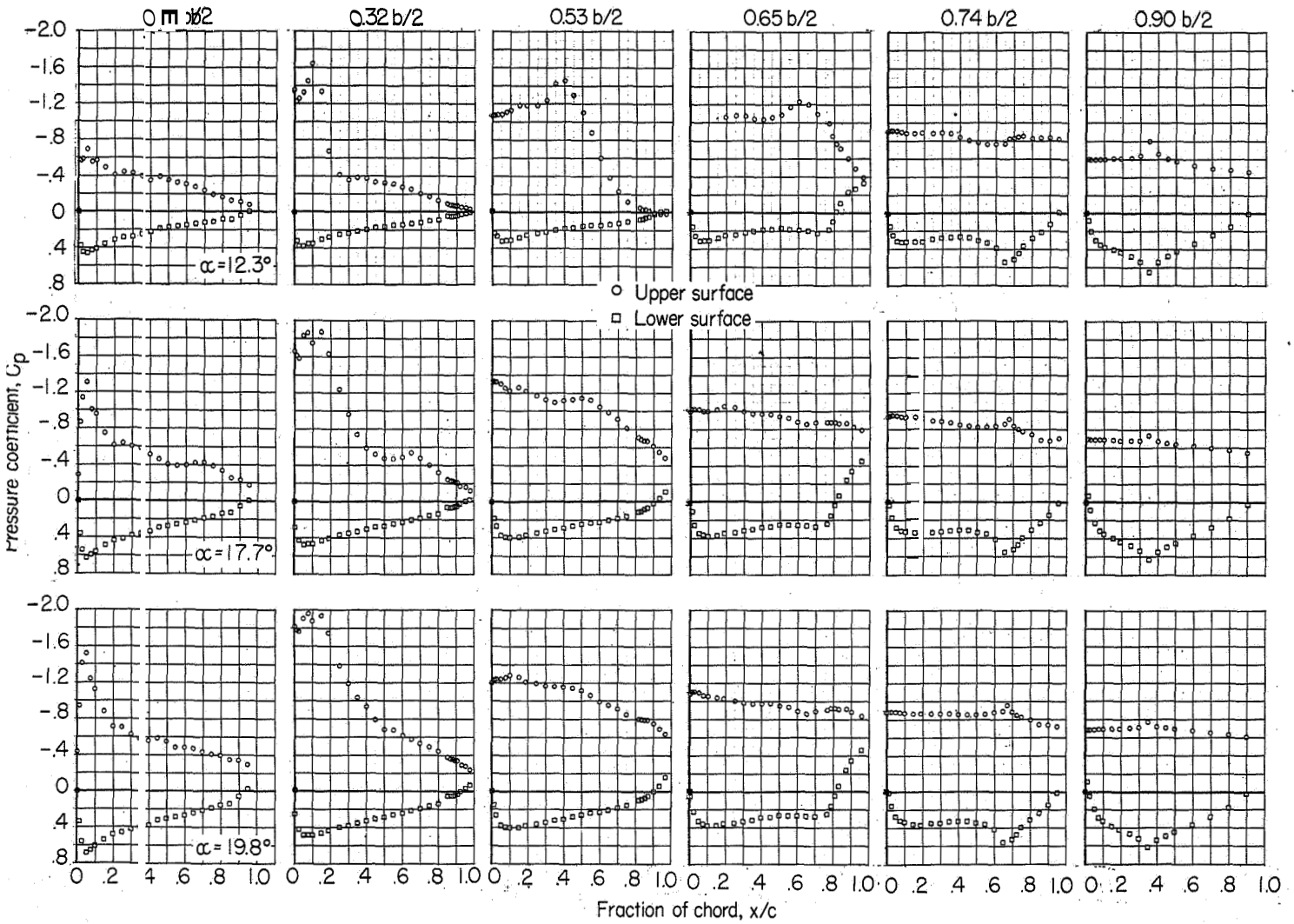

(a) Concluded.

Figure 4.- Continued.

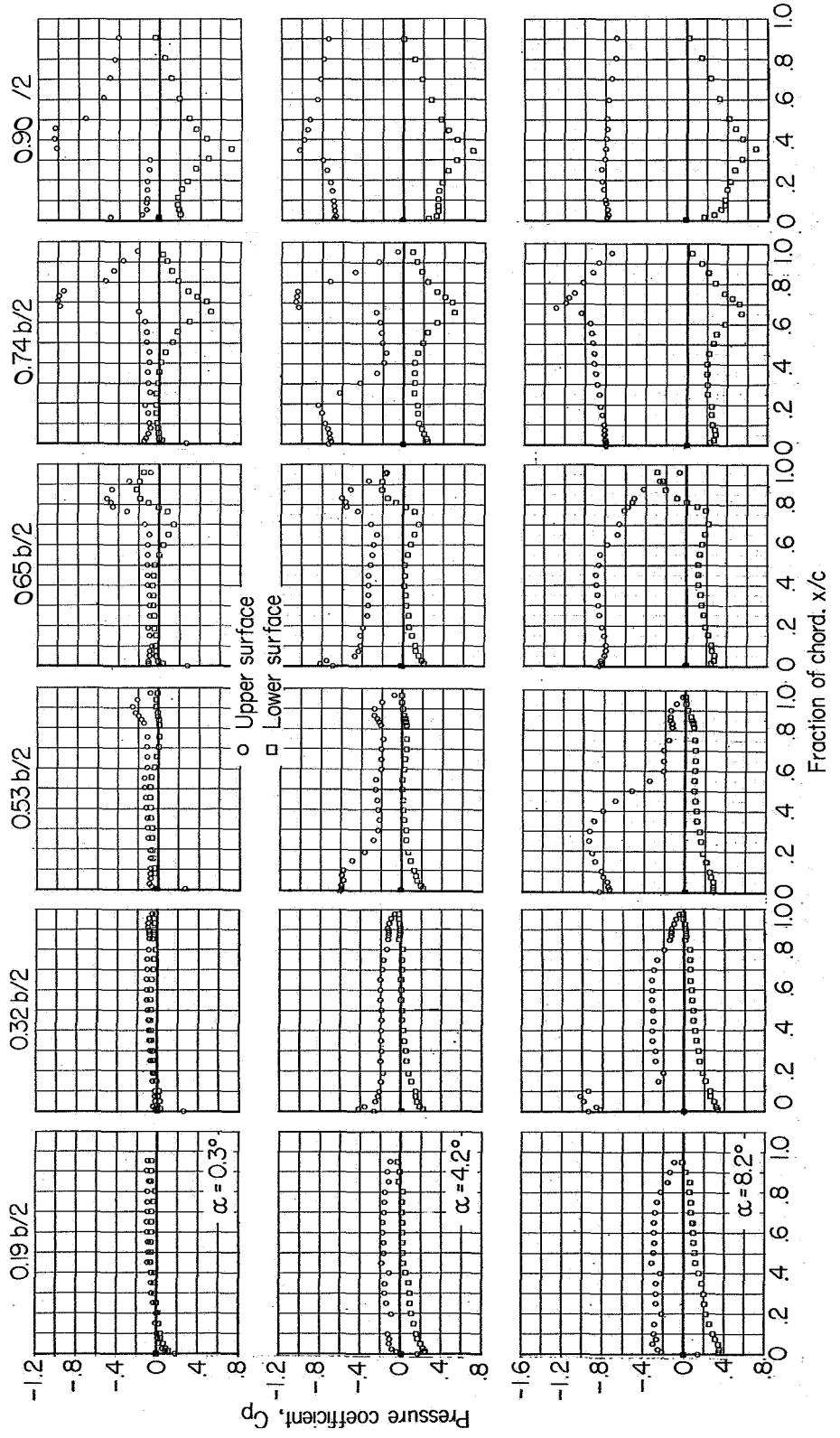

(b) M = 0.90; $C_{p,sonic}$ = 19.

Figure 4.- Continued

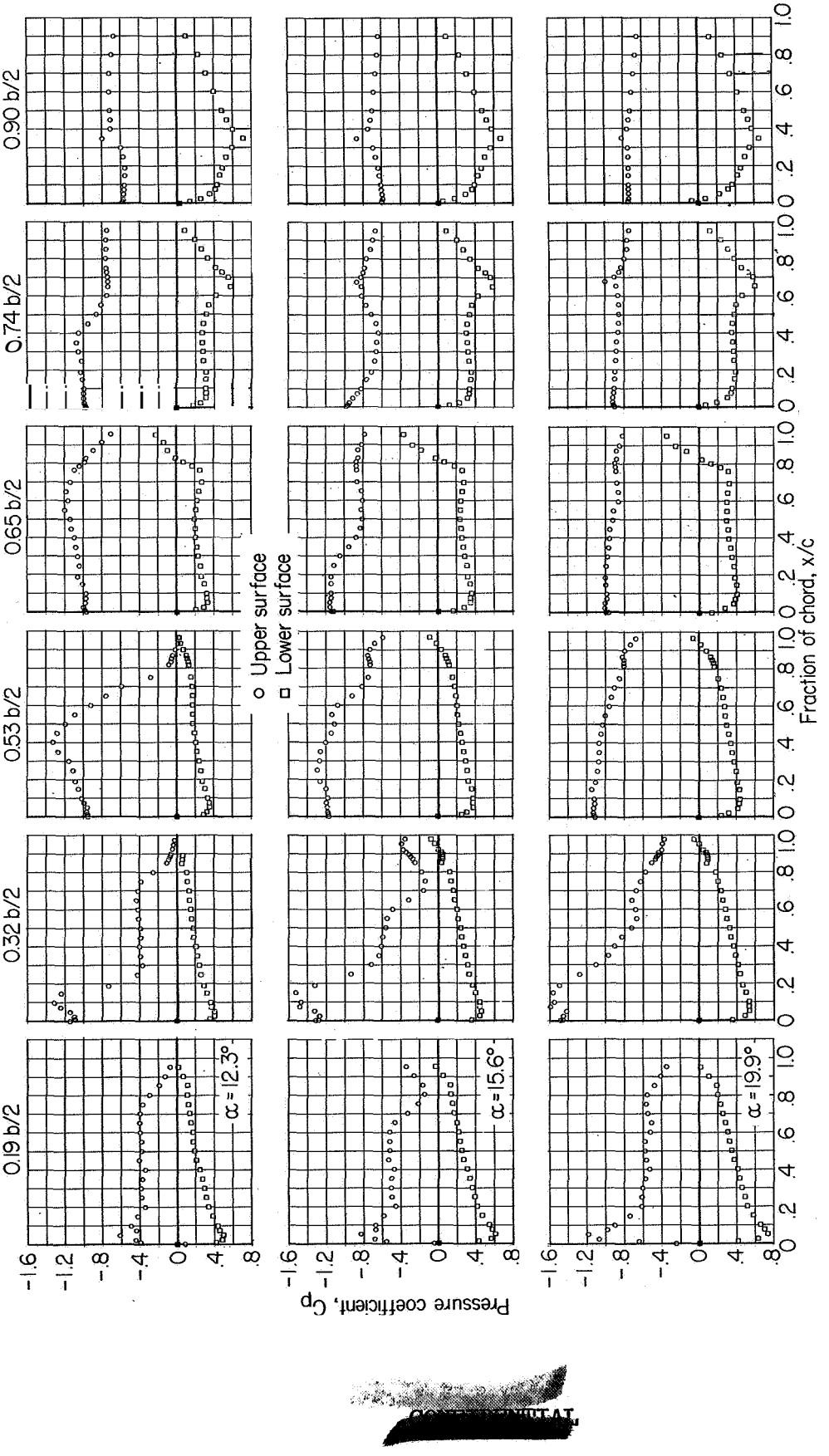

(b) Concluded.

Figure 4.- Continued.

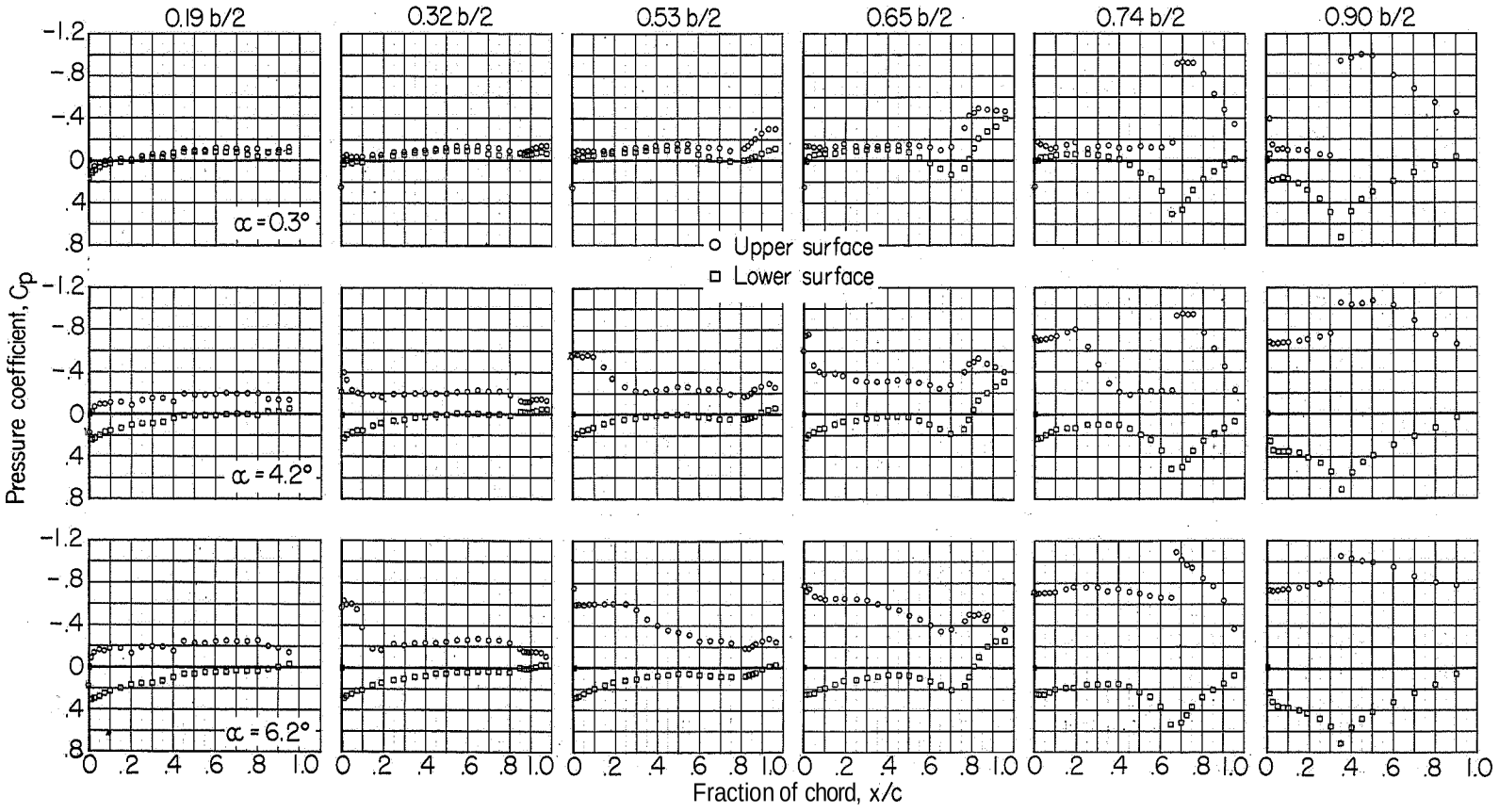

(c) $M = 0.94$; $C_{p,sonic} = -0.10$.

Figure 4.- Continued.

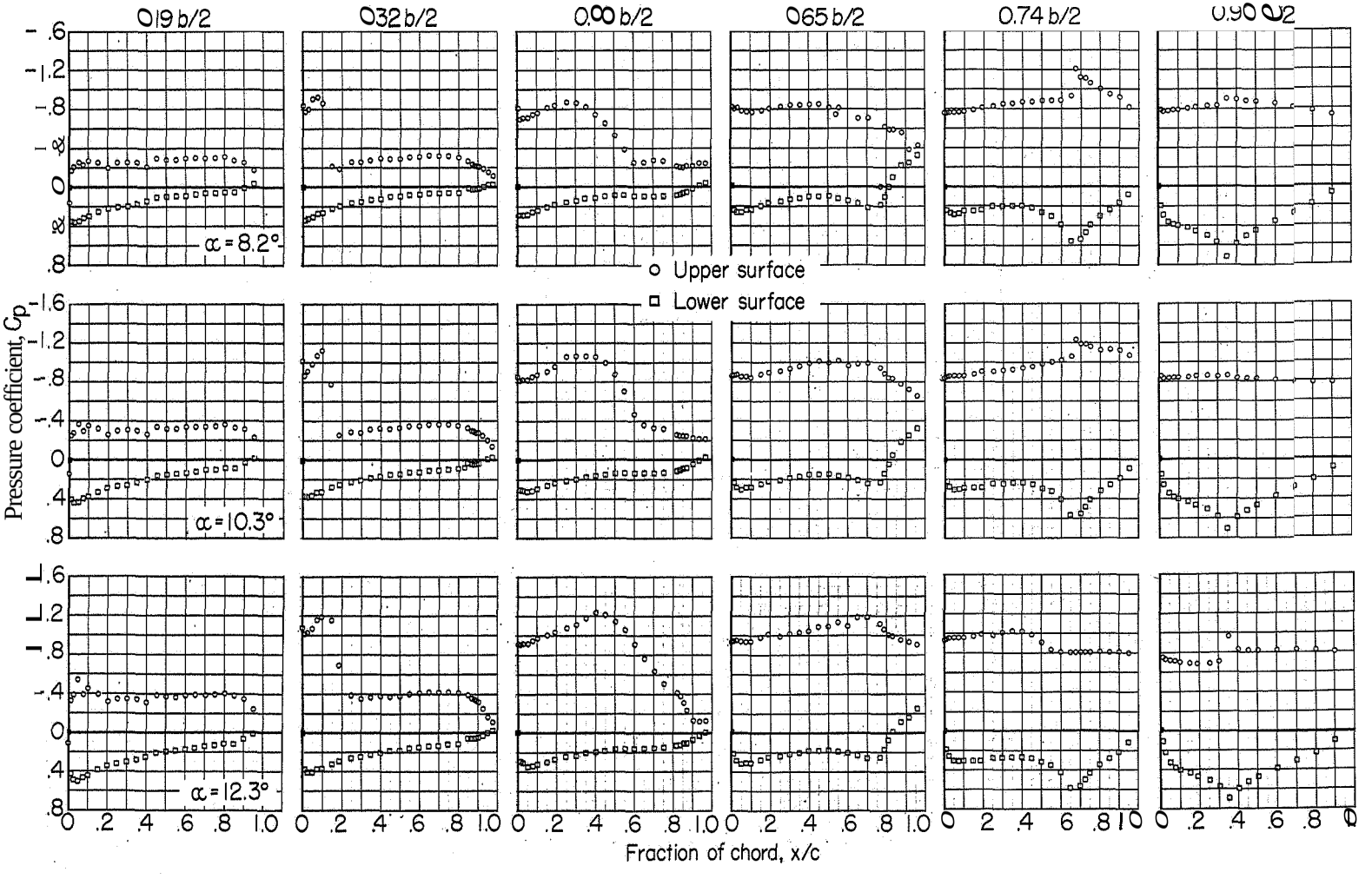

(c) Continued.

Figure 4.- Continued.

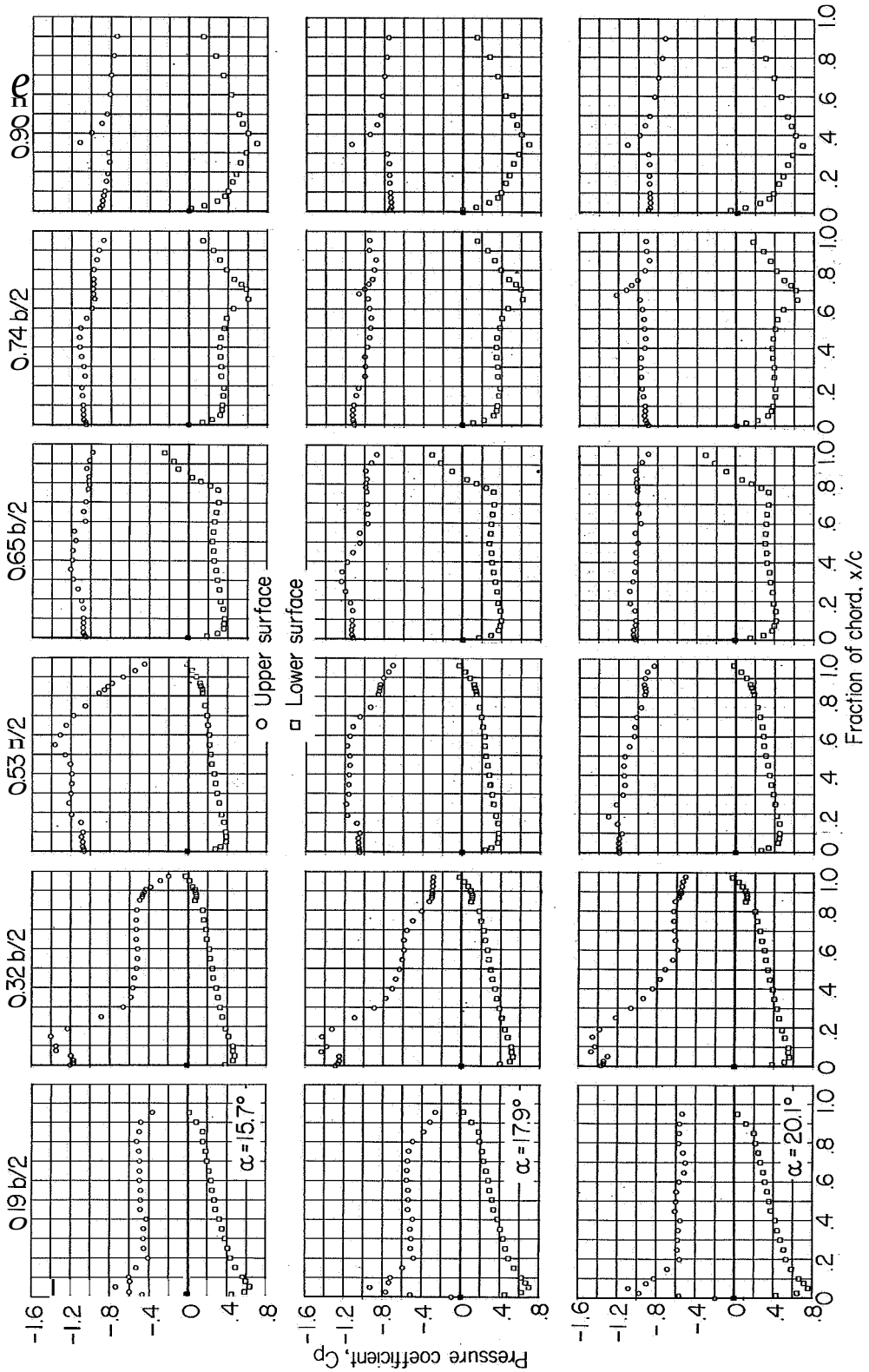

(c) Continued.

Figure 4 - Continued.

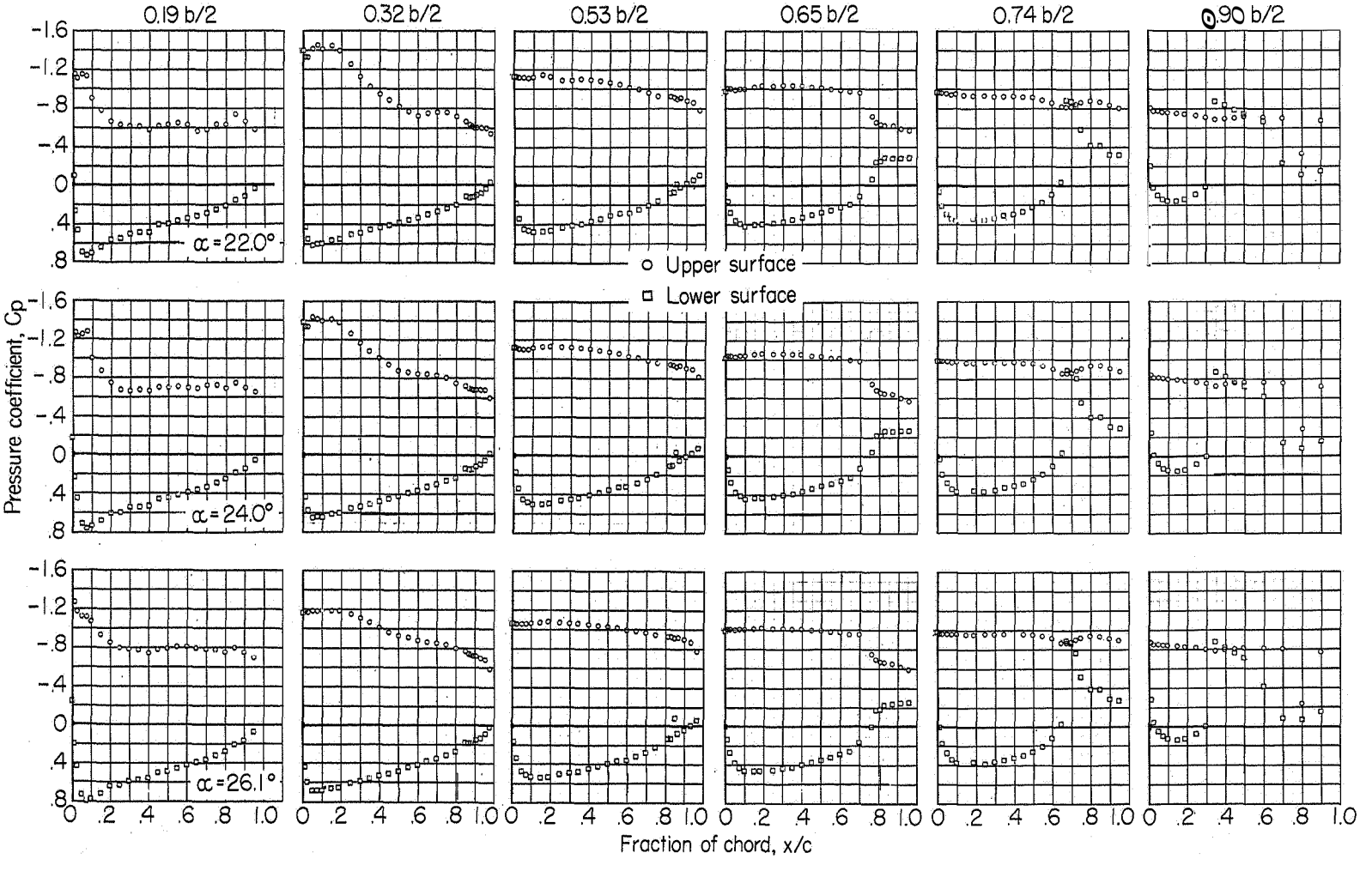

(c) Concluded.

Figure 4 - Continued.

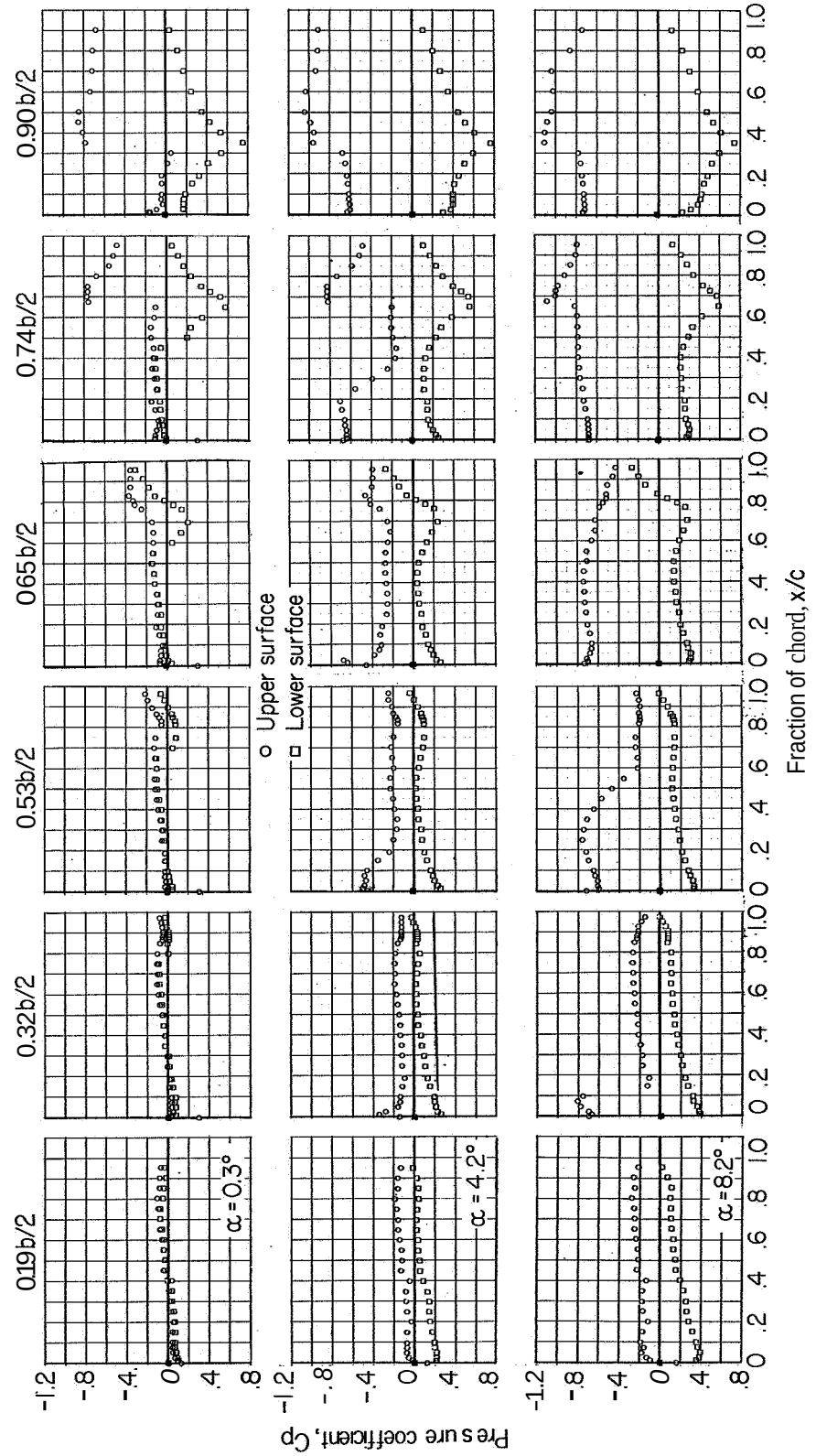

(d) M = 1.00.

Figure 4.- Continued.

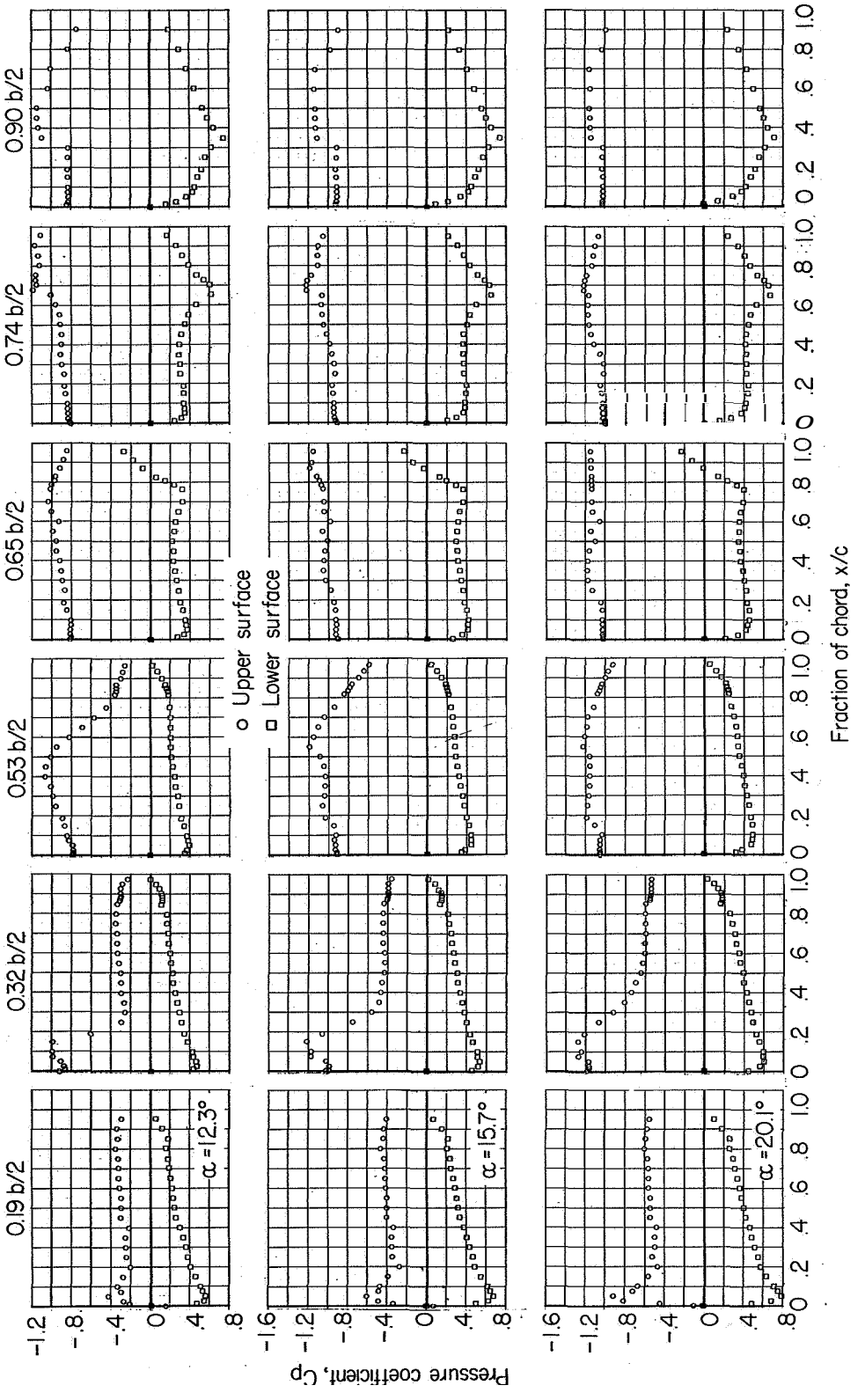

(d) Concluded.

Figure 4 - Continued.

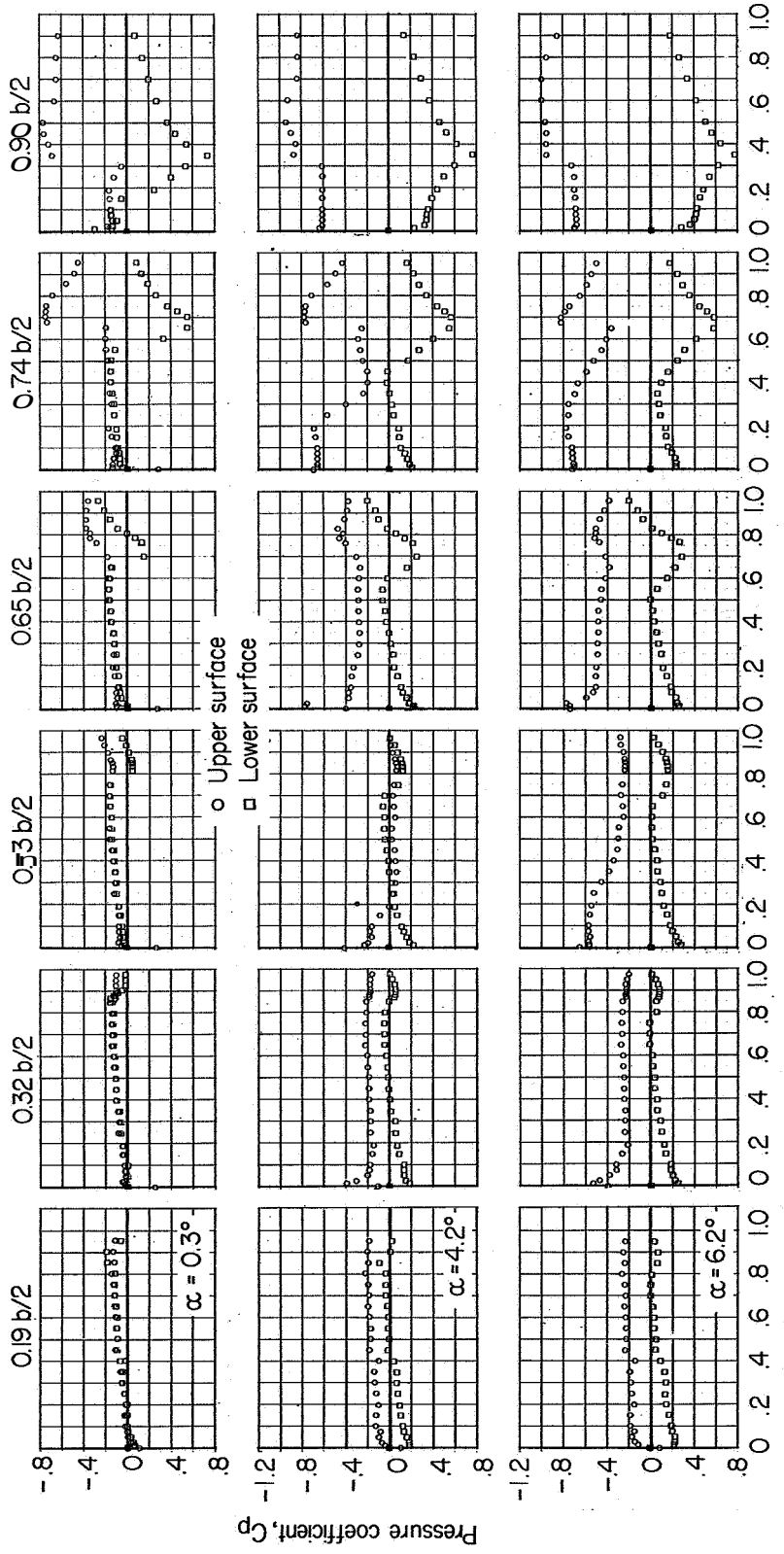

(e) M = 1.05.

Figure 4.- Continued.

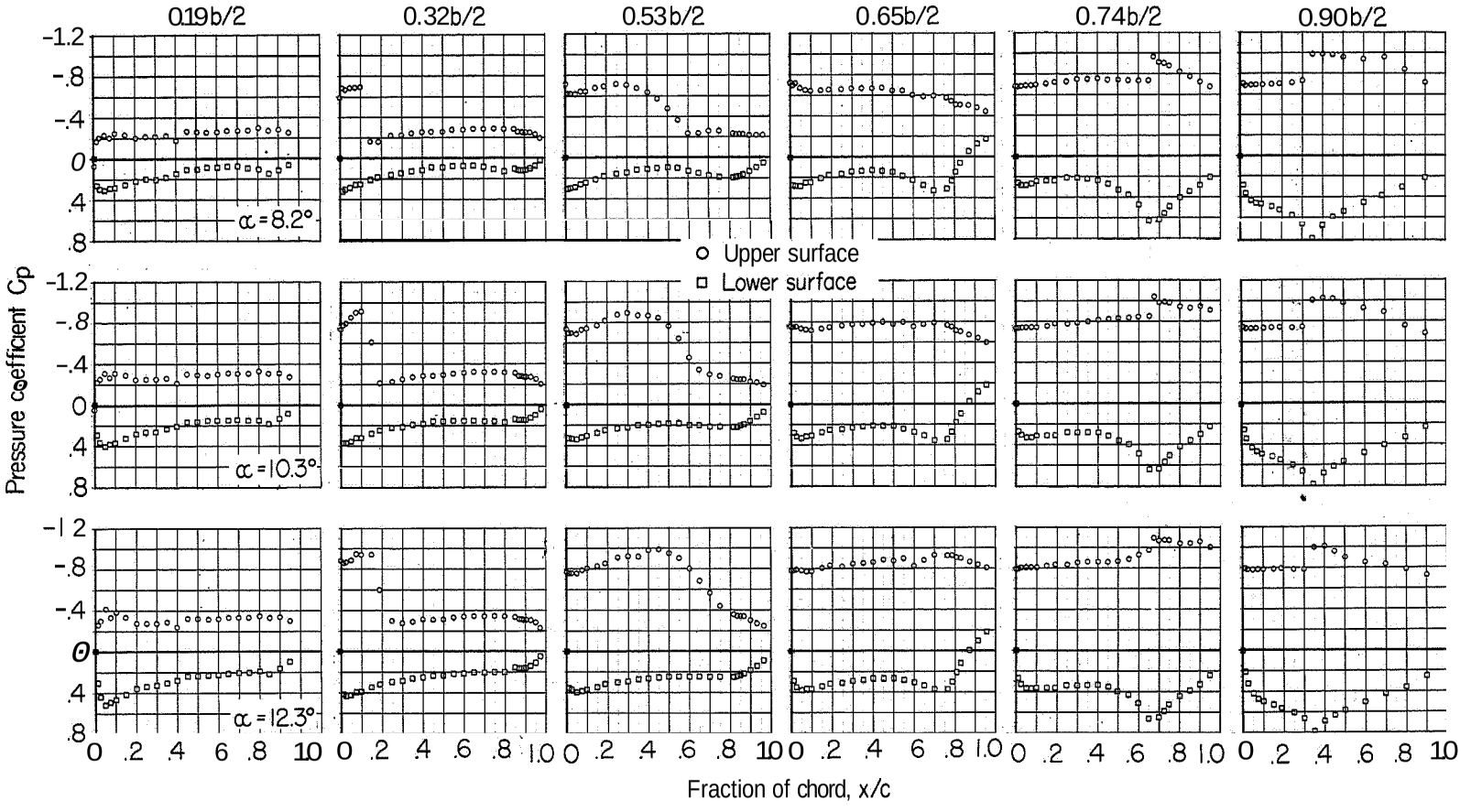

(e) Concluded.

Figure 4. - Concluded.

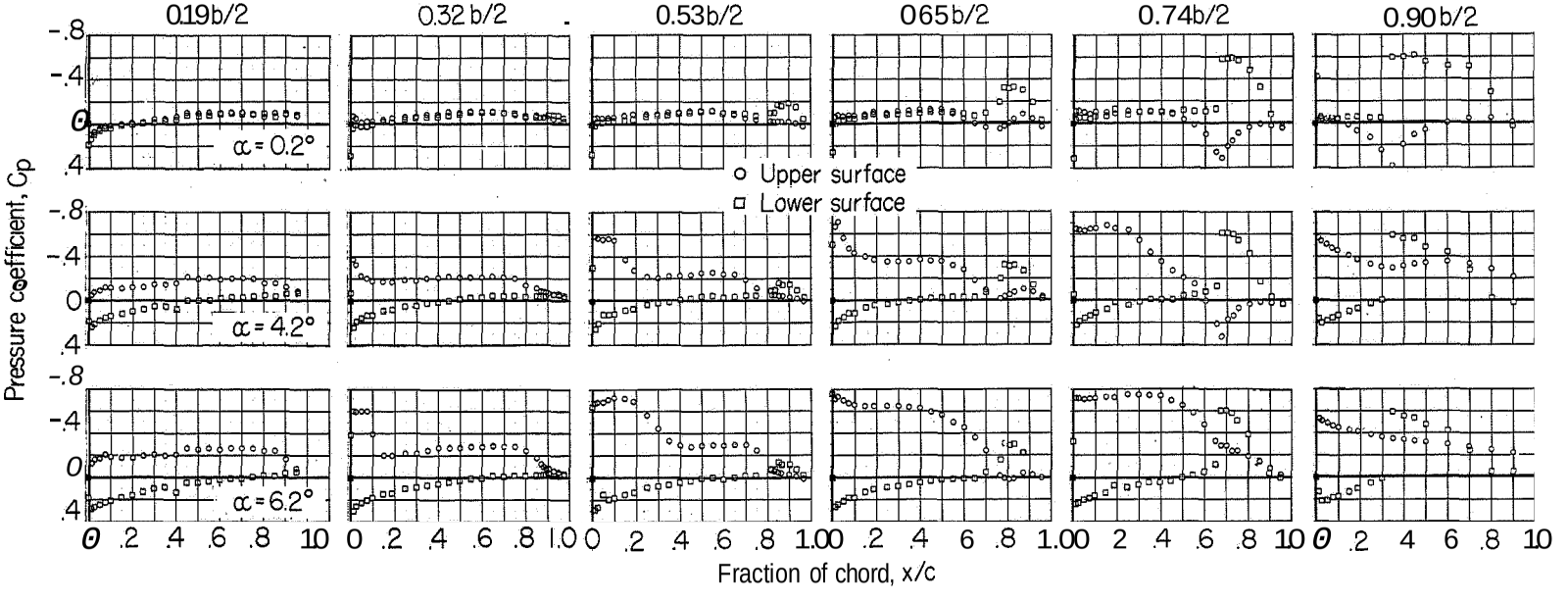

(a) M = 0.94; $C_{p,sonic}$ = -0.10.

Figure 5.- Chordwise pressure distributions on a 60° delta wing with aileron deflected -7.5°.

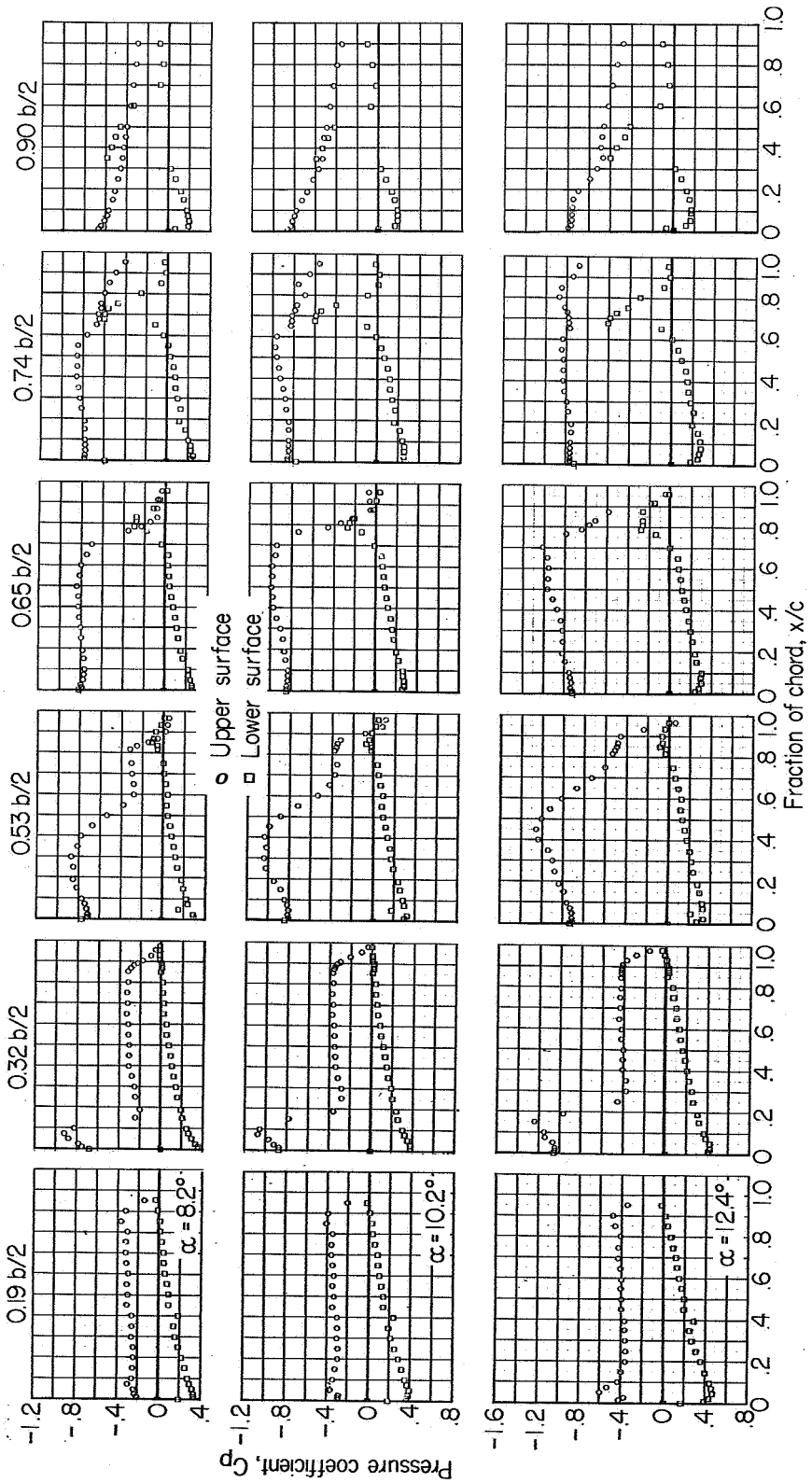

(a) Continued.

Figure 5.- Continued.

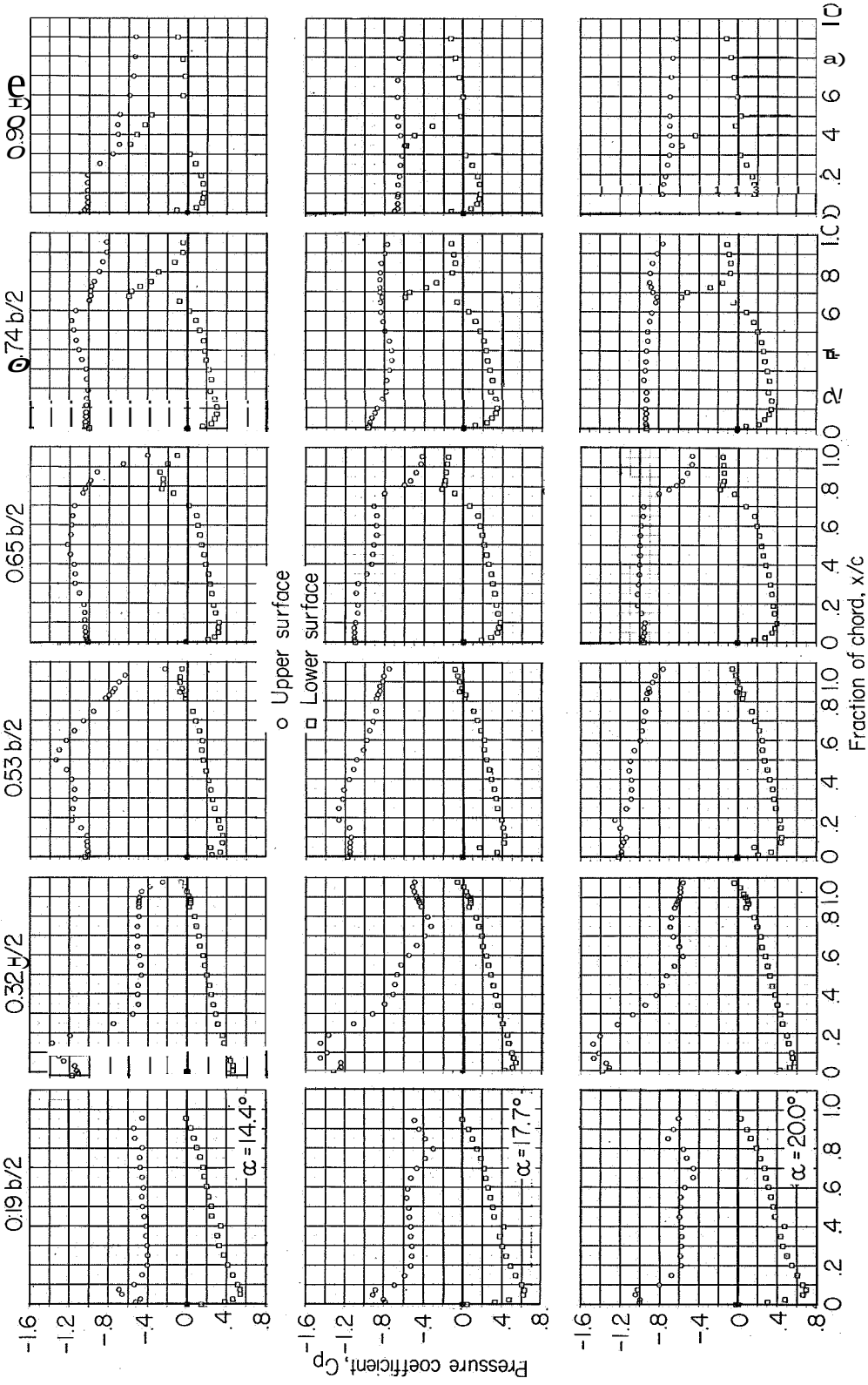

(a) Continued.

Figure 5 - Continued.

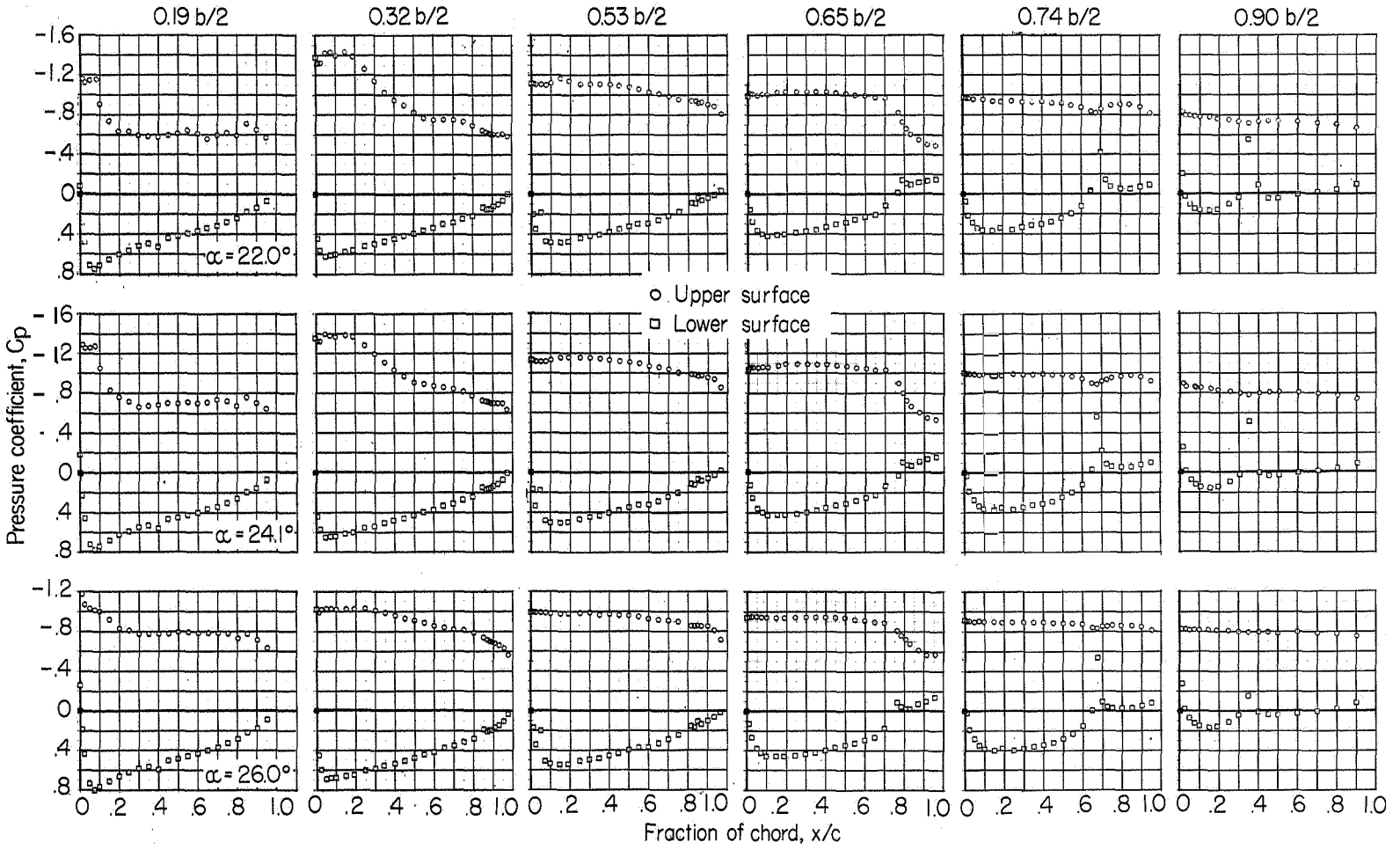

(a) Concluded.

Figure 5 - Concluded

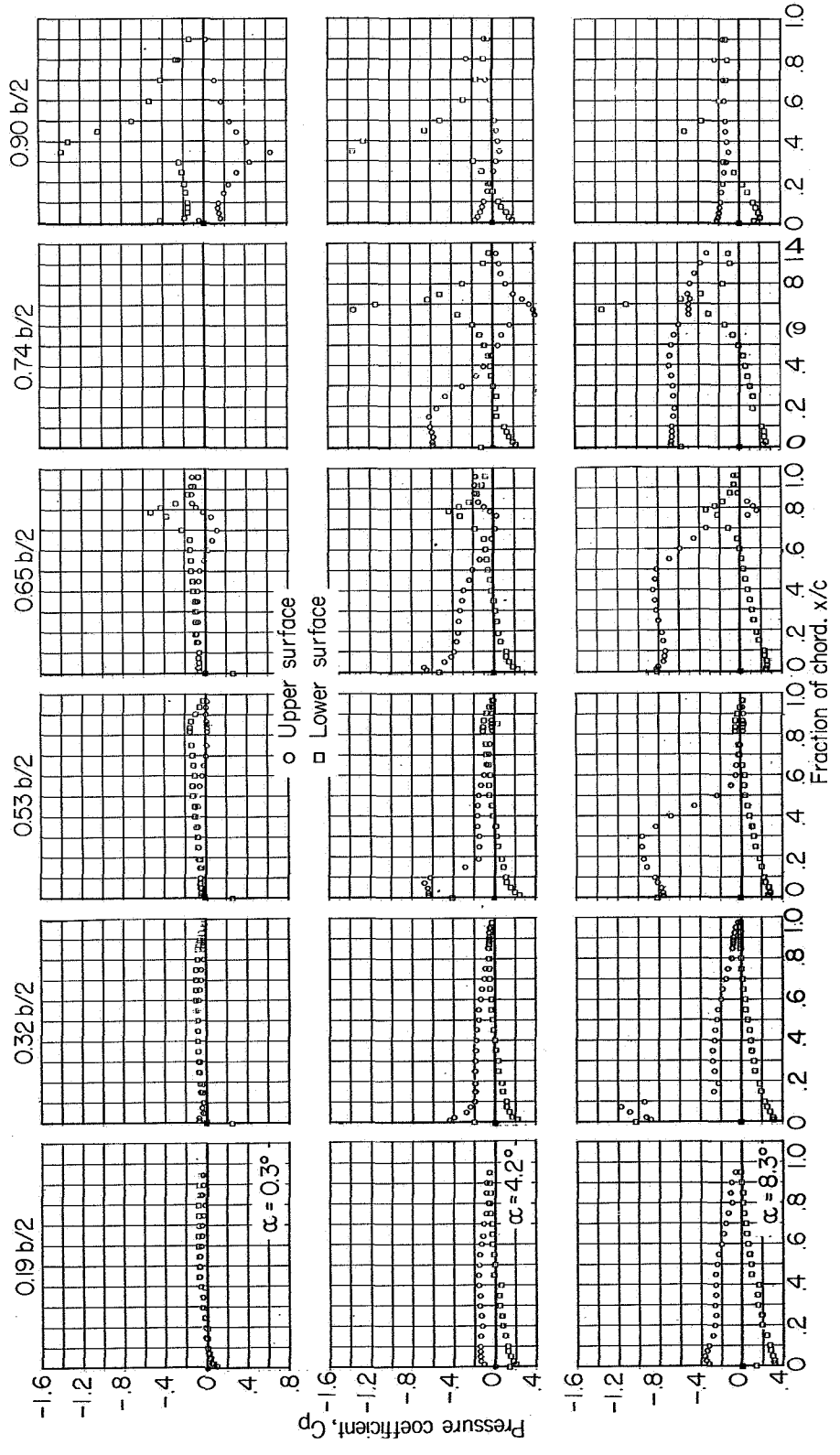

(a) M = 0.80; $C_{p,sonic}$ = -0.44.

Figure 6.- Chordwise pressure distributions on a 60° delta wing with aileron deflected -15°.

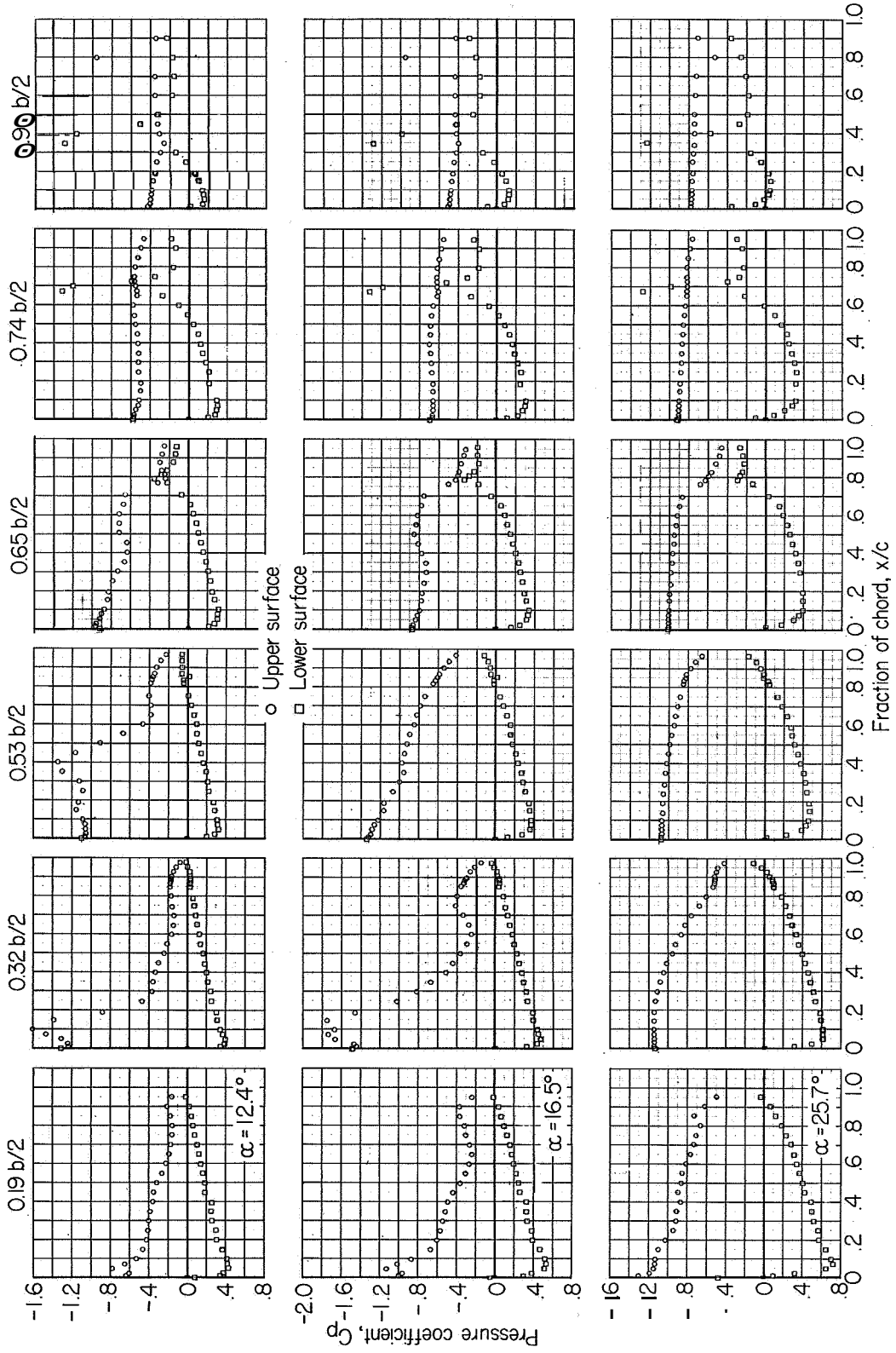

(a) Concluded.

Figure 6 - Continued.

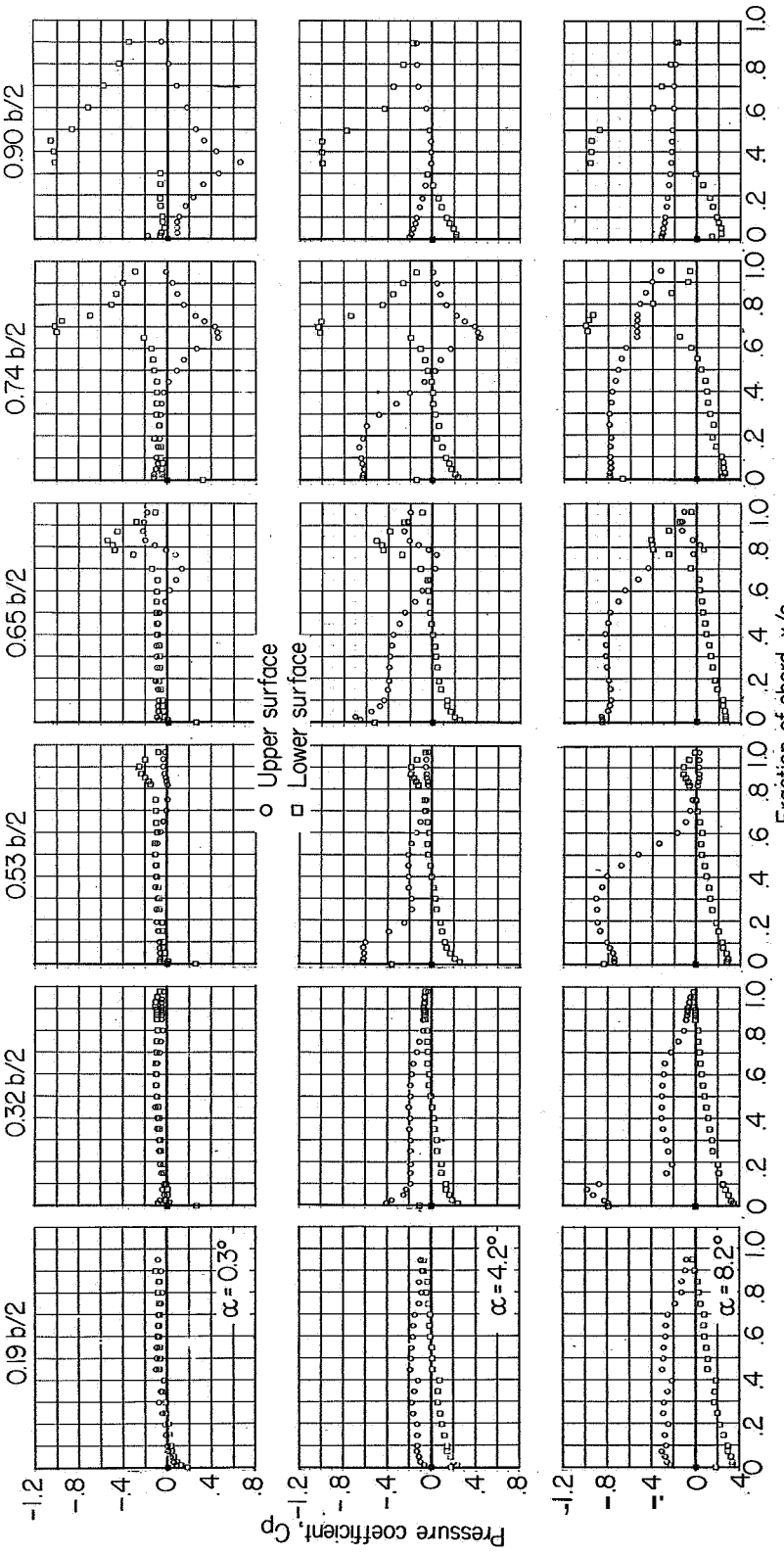

(b) M = 0.90; $C_{p,sonic}$ = -0.19.

Figure 6.- Continued.

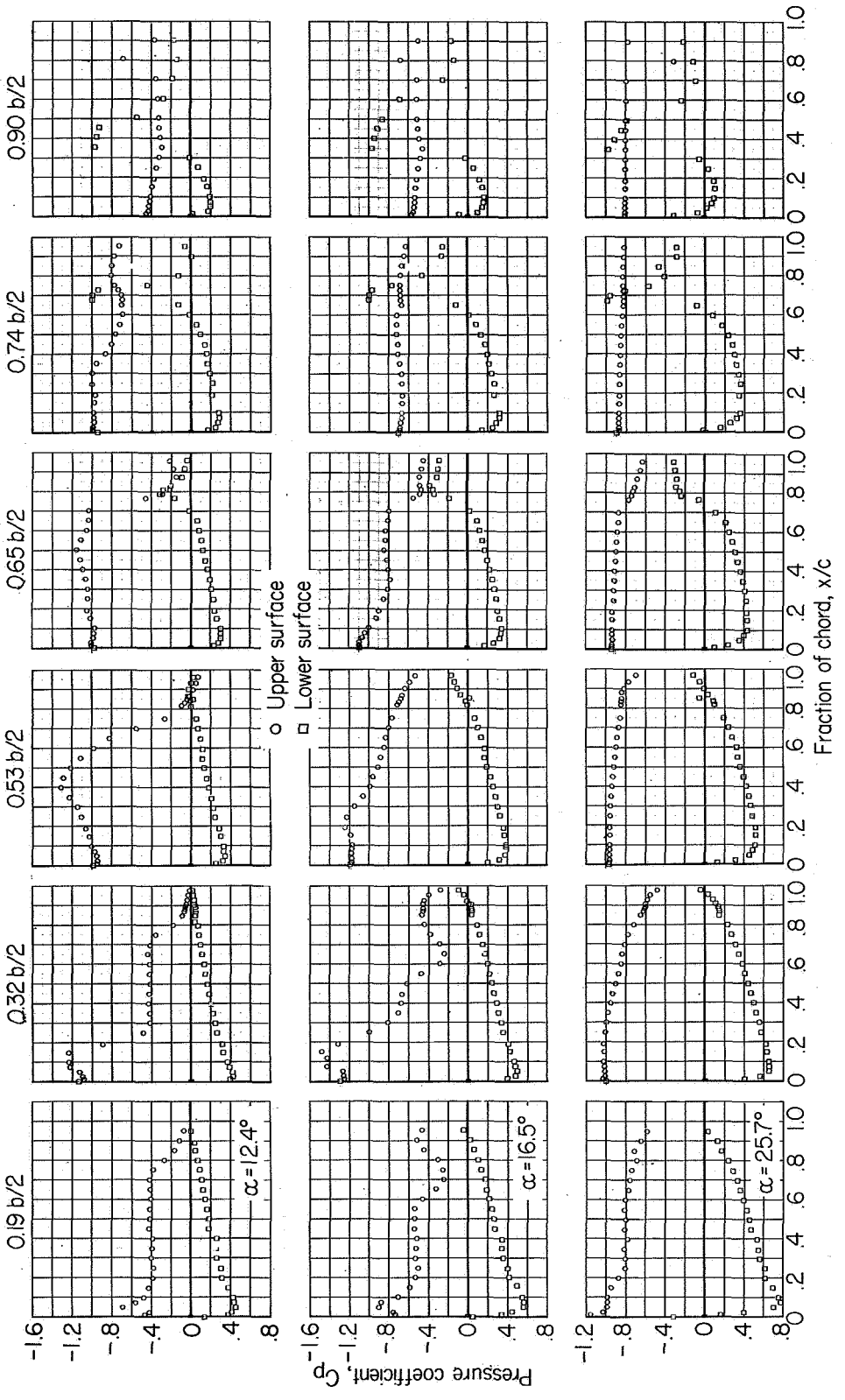

(b) Concluded.

Figure 6.- Continued.

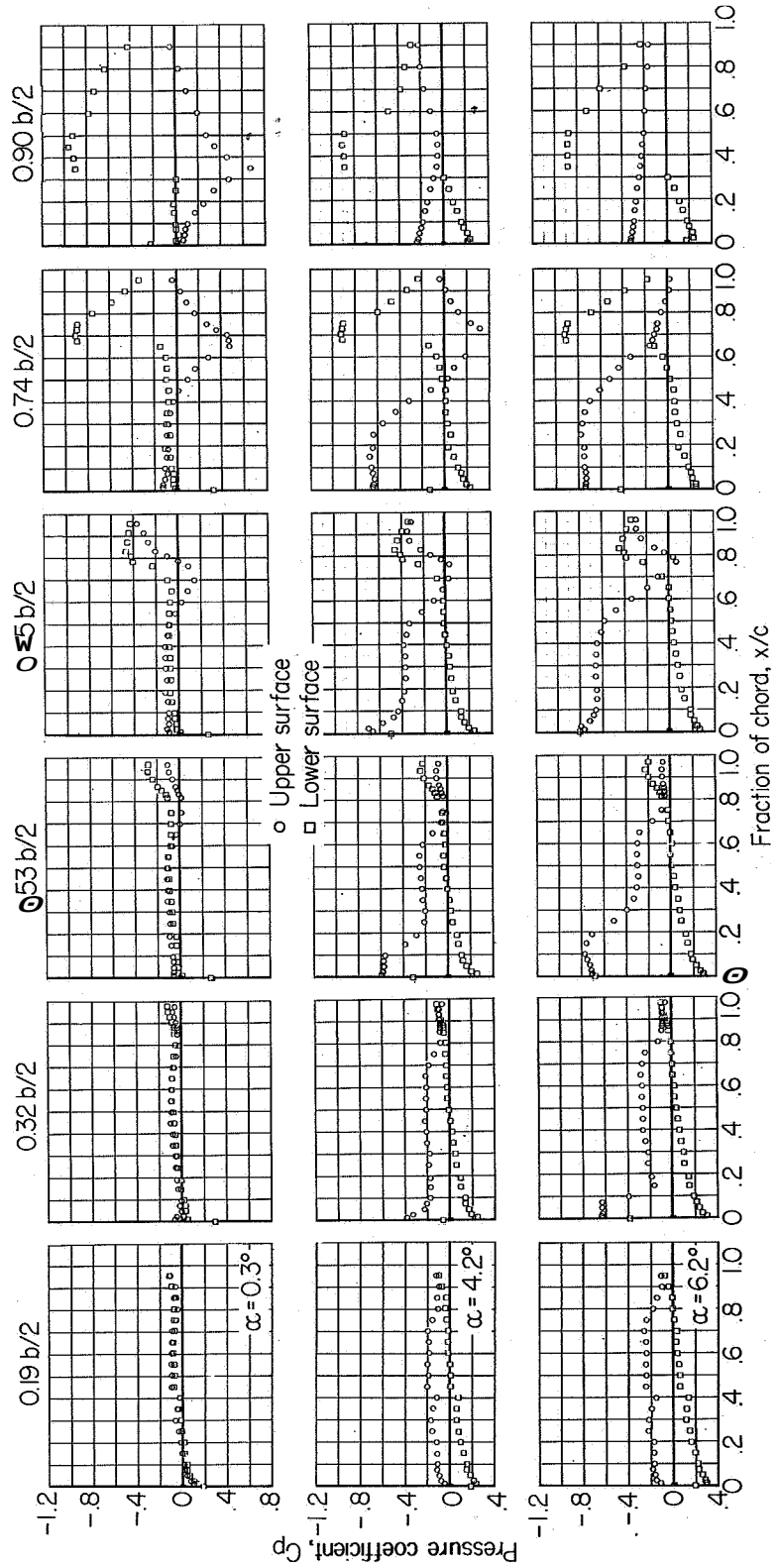

(c) M = 0.94; $C_{p,sonic}$ = -0.10.

Figure 6.- Continued.

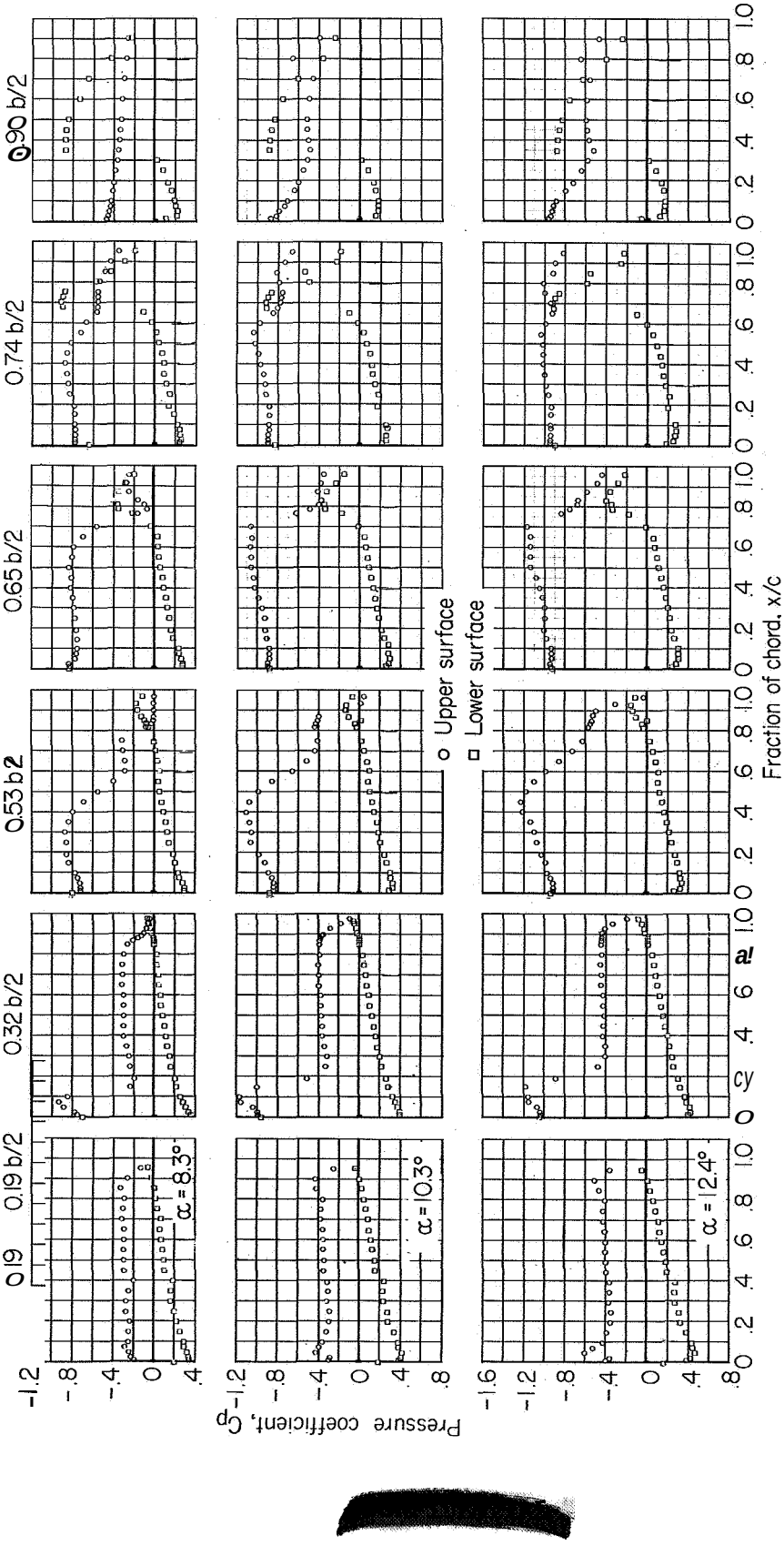

(c) Continued.

Figure 6.- Continued.

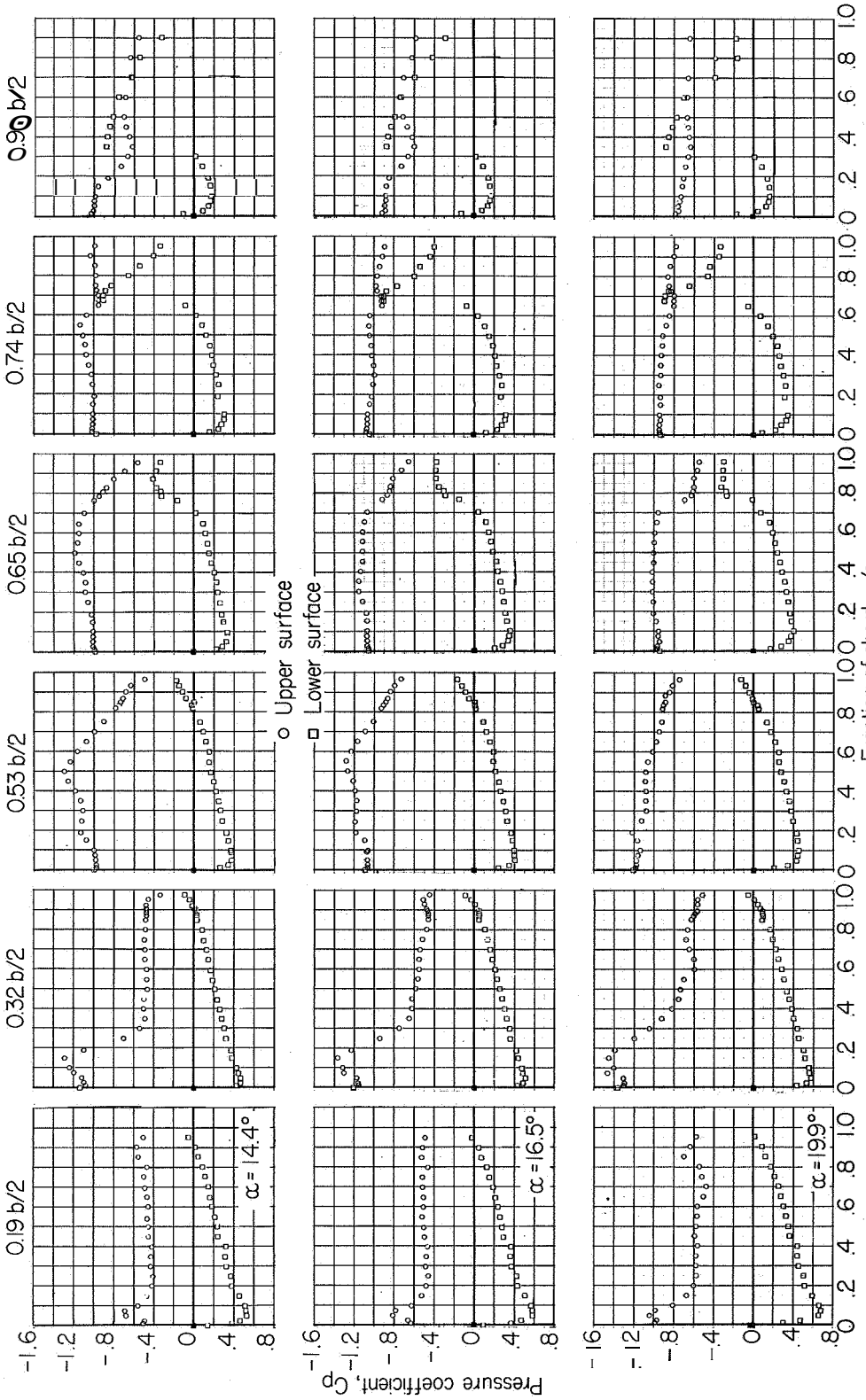

(c) Continued.

Figure 6.- Continued.

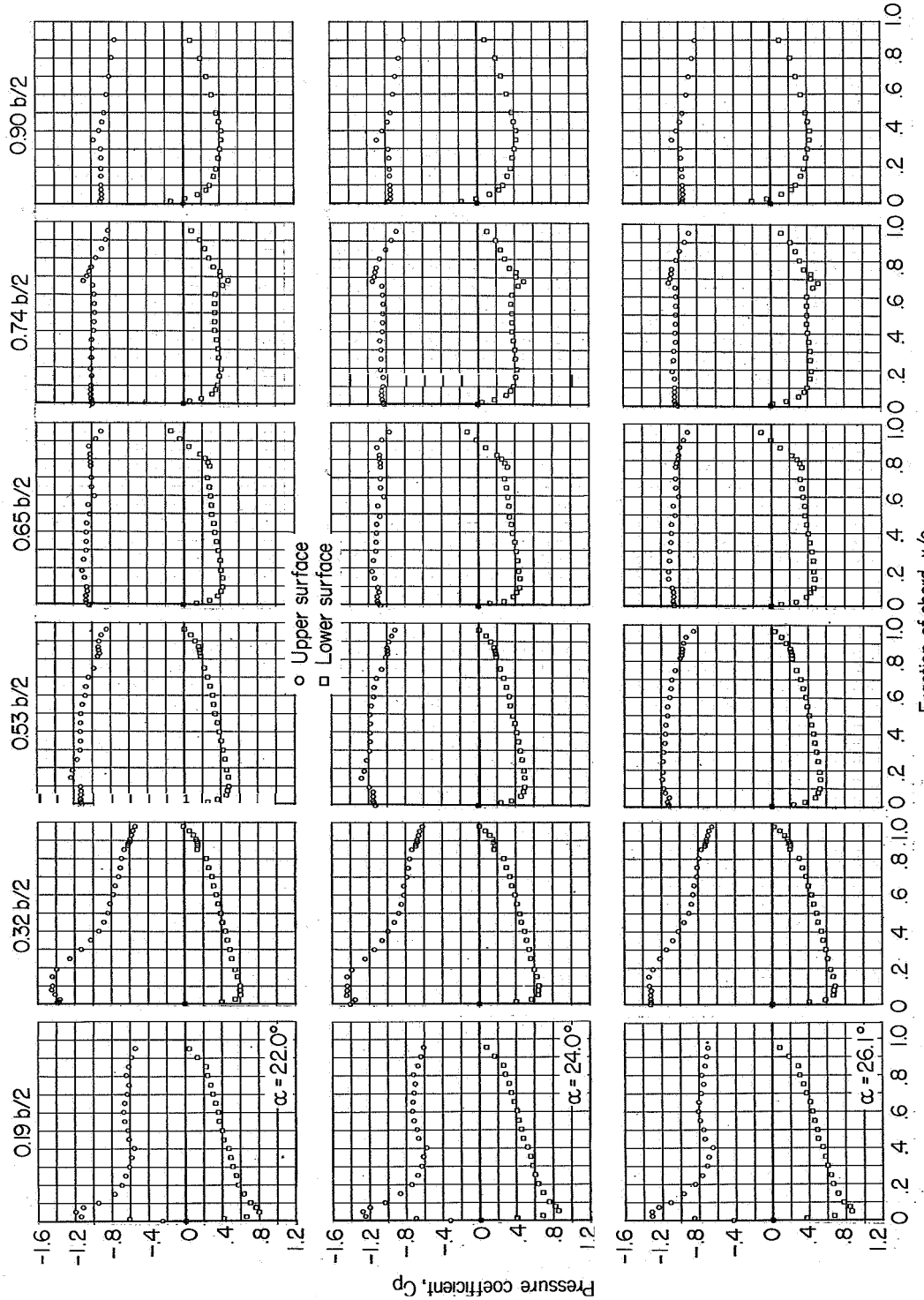

(c) Concluded.

Figure 6 - Continued.

(a) M = 1.00

Figure 6.- Continued.

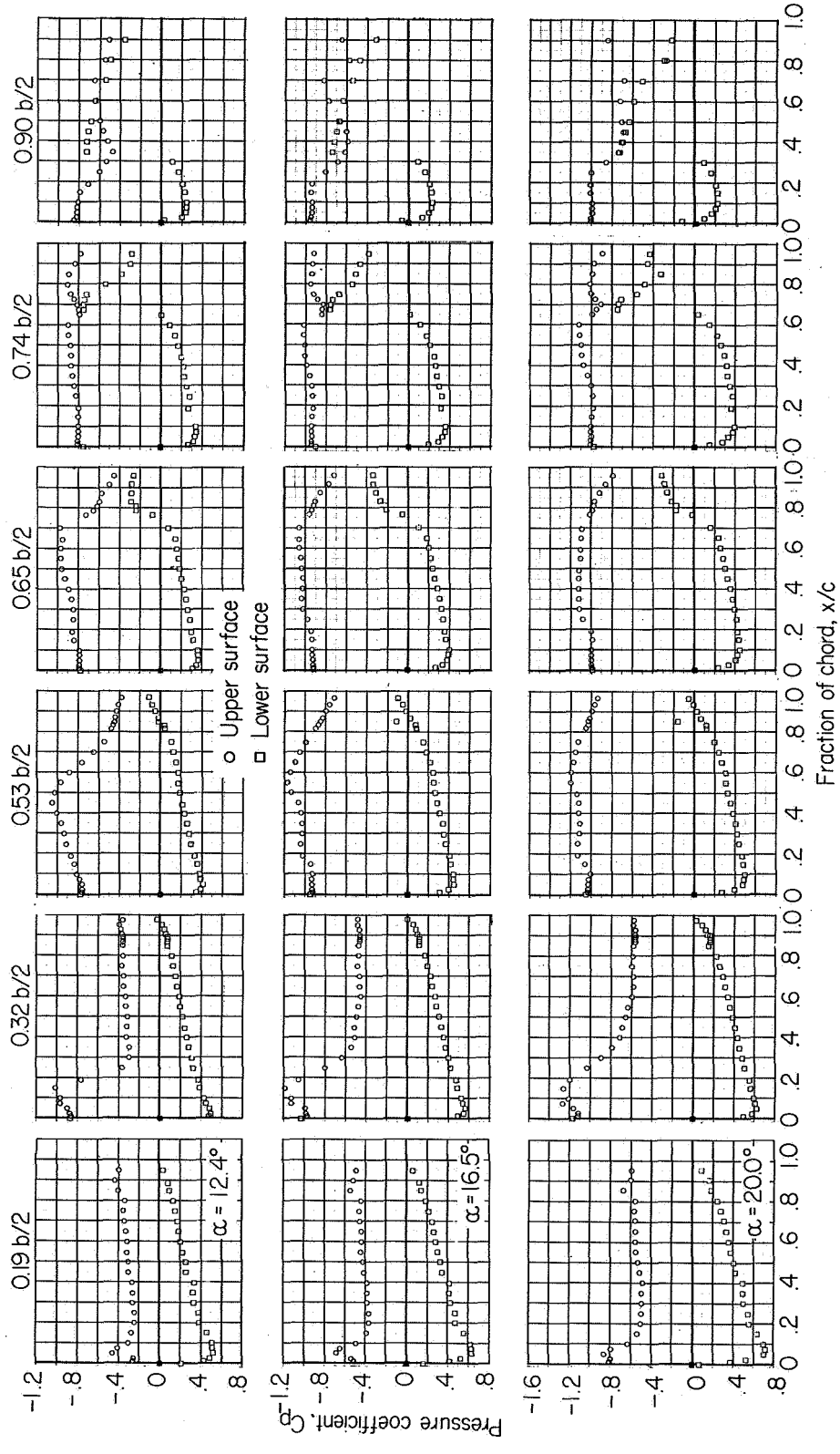

(d) Concluded.

Figure 6.- Continued.

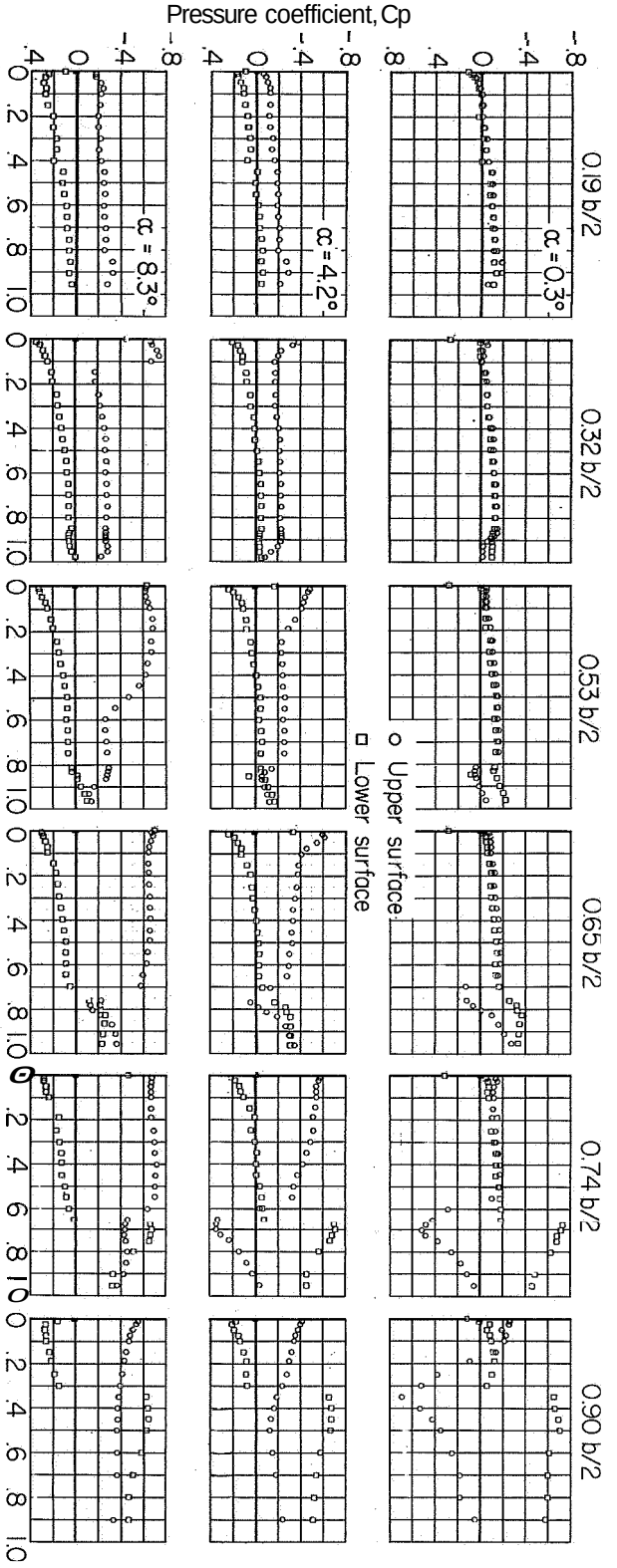

(e) M = 1.05.

Figure 6.- Continued.

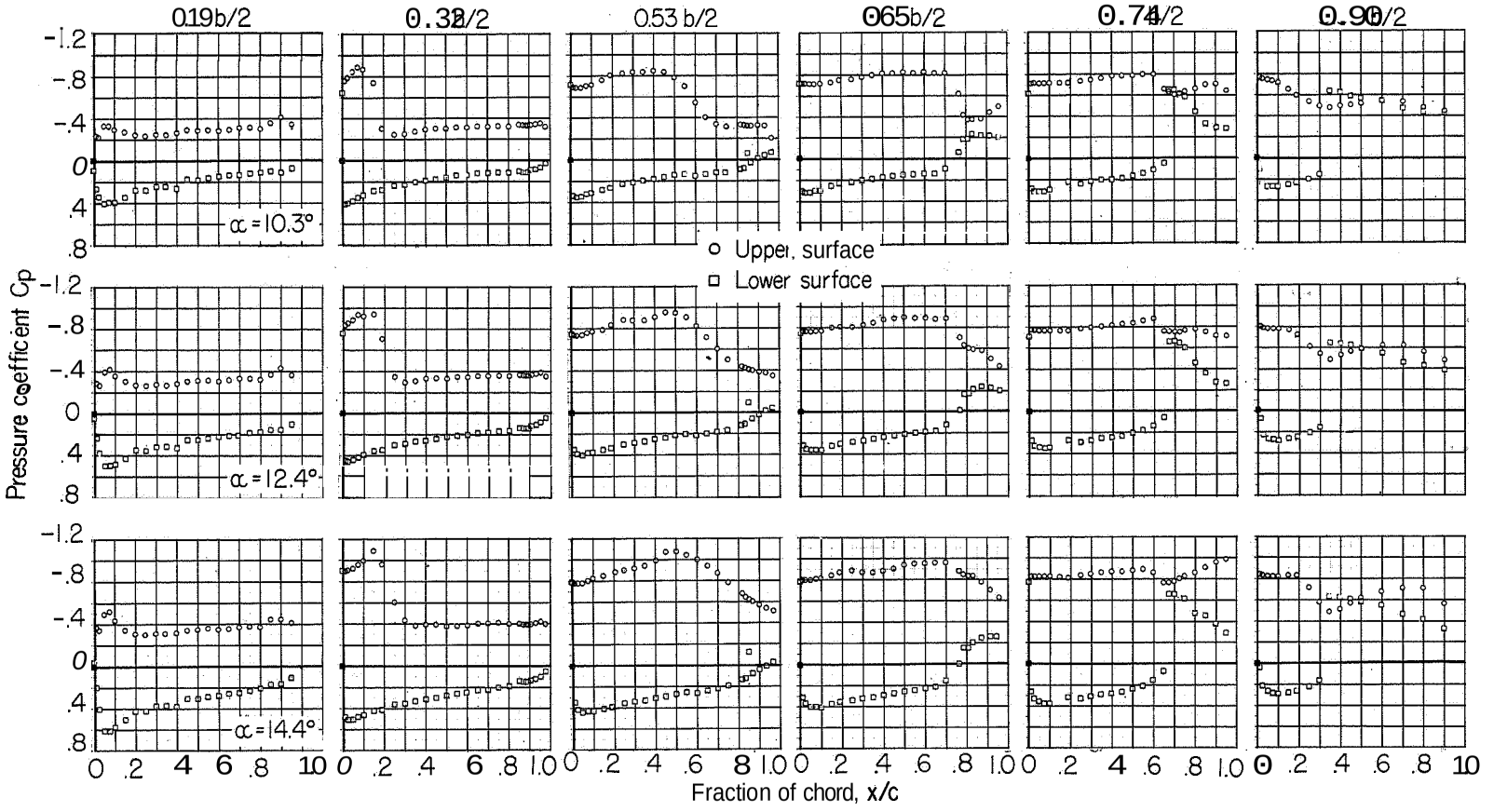

(e) Concluded.

Figure 6.- Concluded.

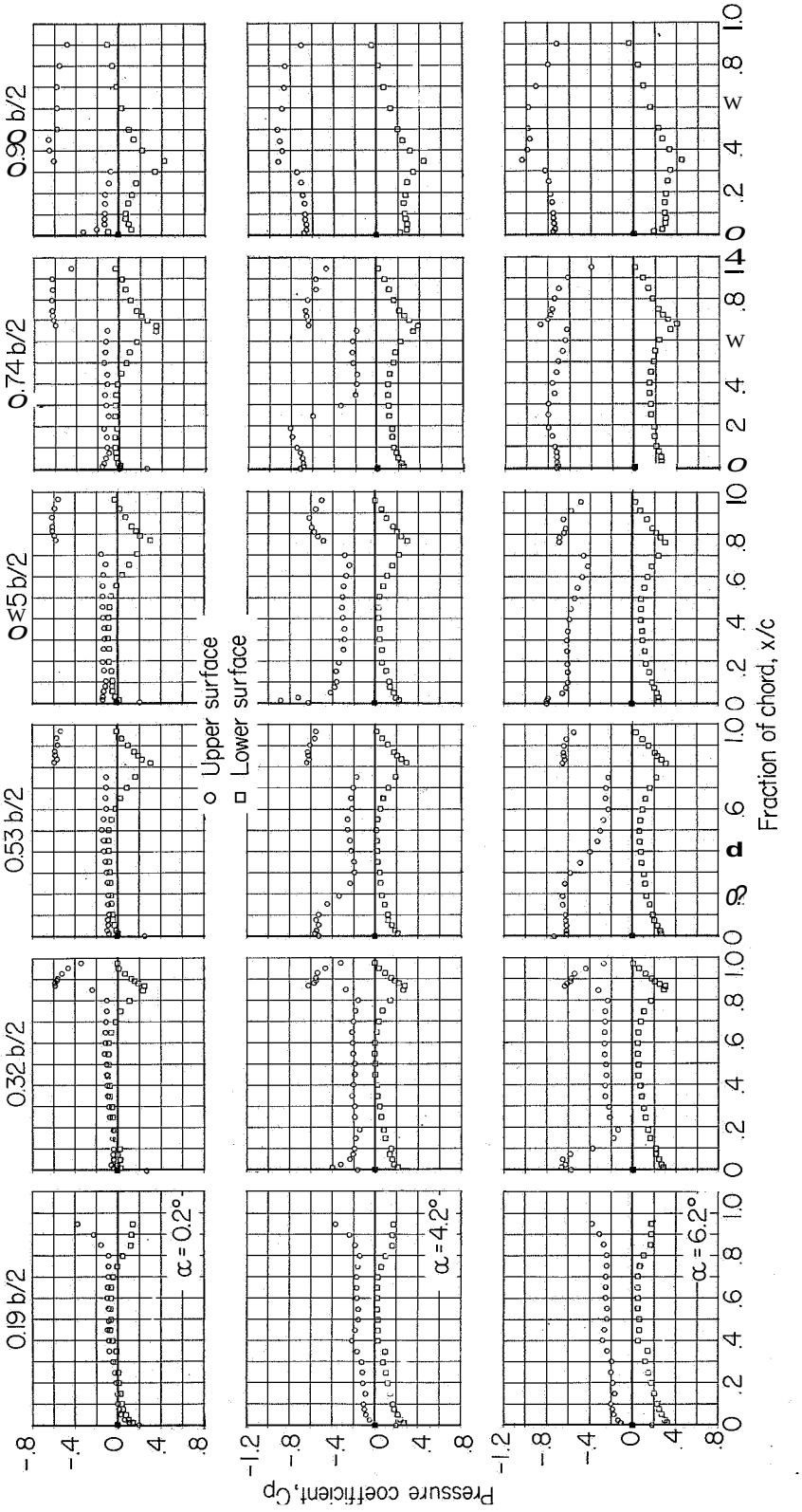

(a) M = 0.94; $C_{p,sonic}$ = -0.10

Figure 7.- Chordwise pressure distributions on a 60° delta wing with combined control deflected 7.5°.

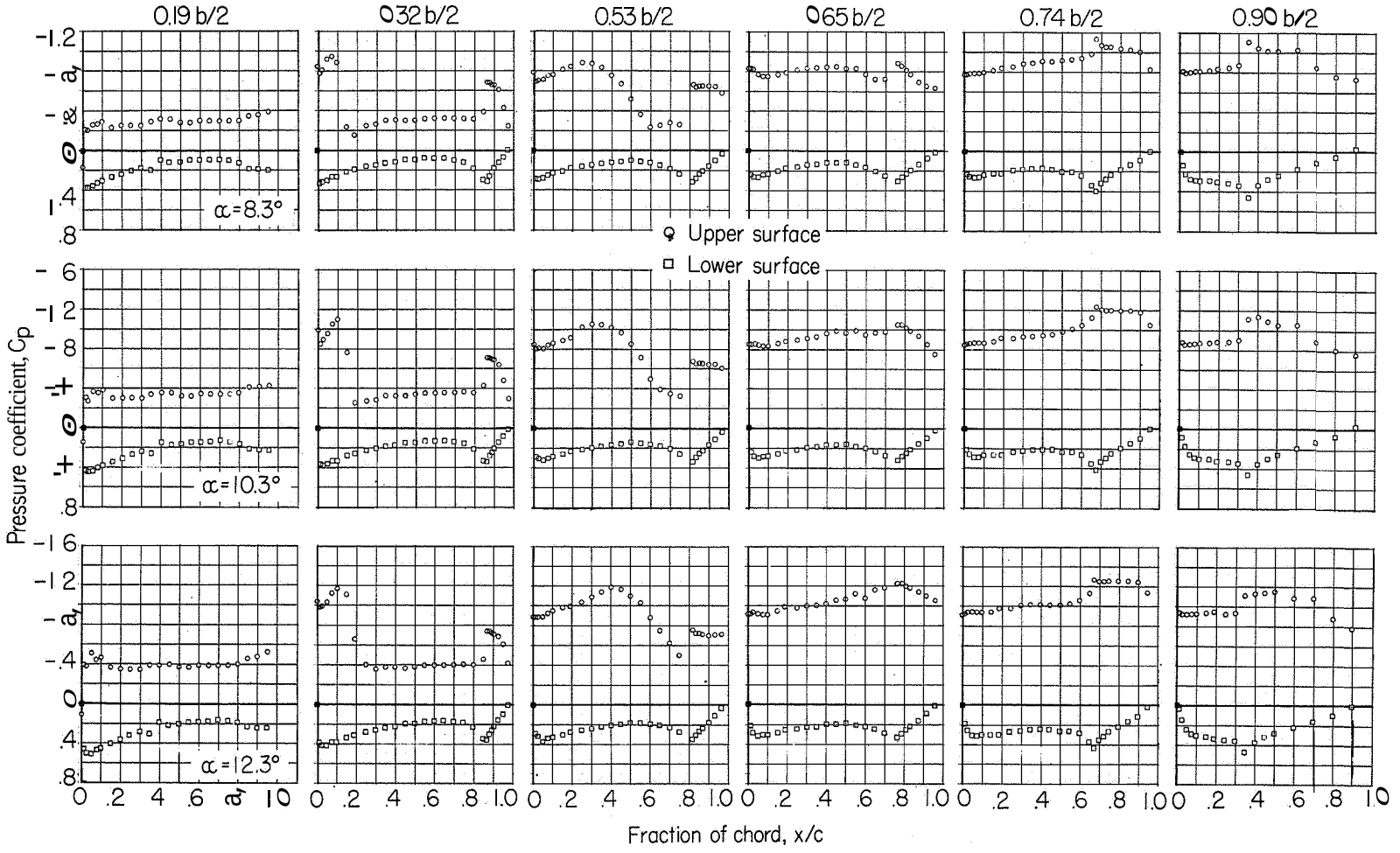

(a) Continued.

Figure 7.- Continued.

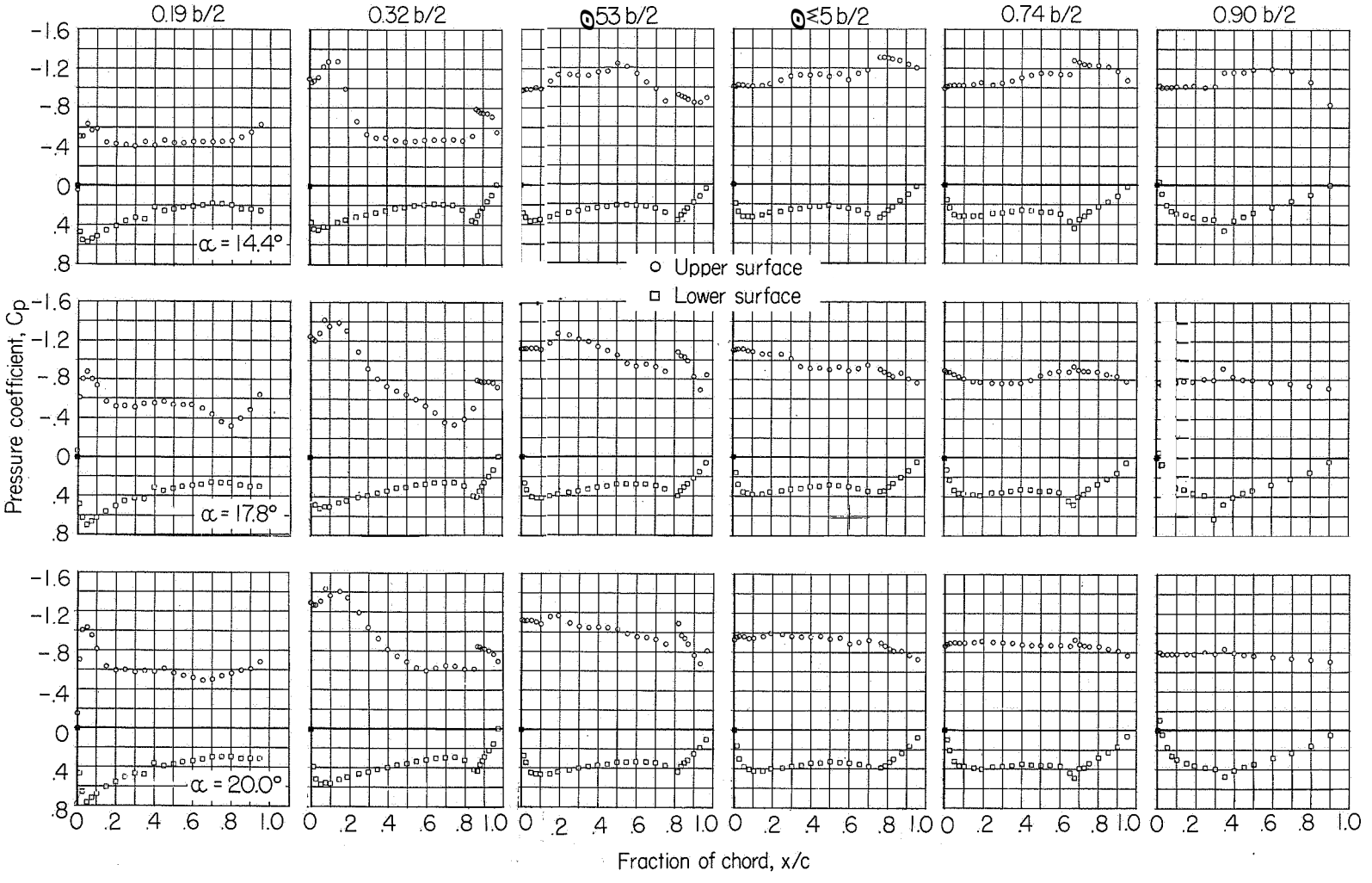

(a) Continued.

Figure 7.- Continued.

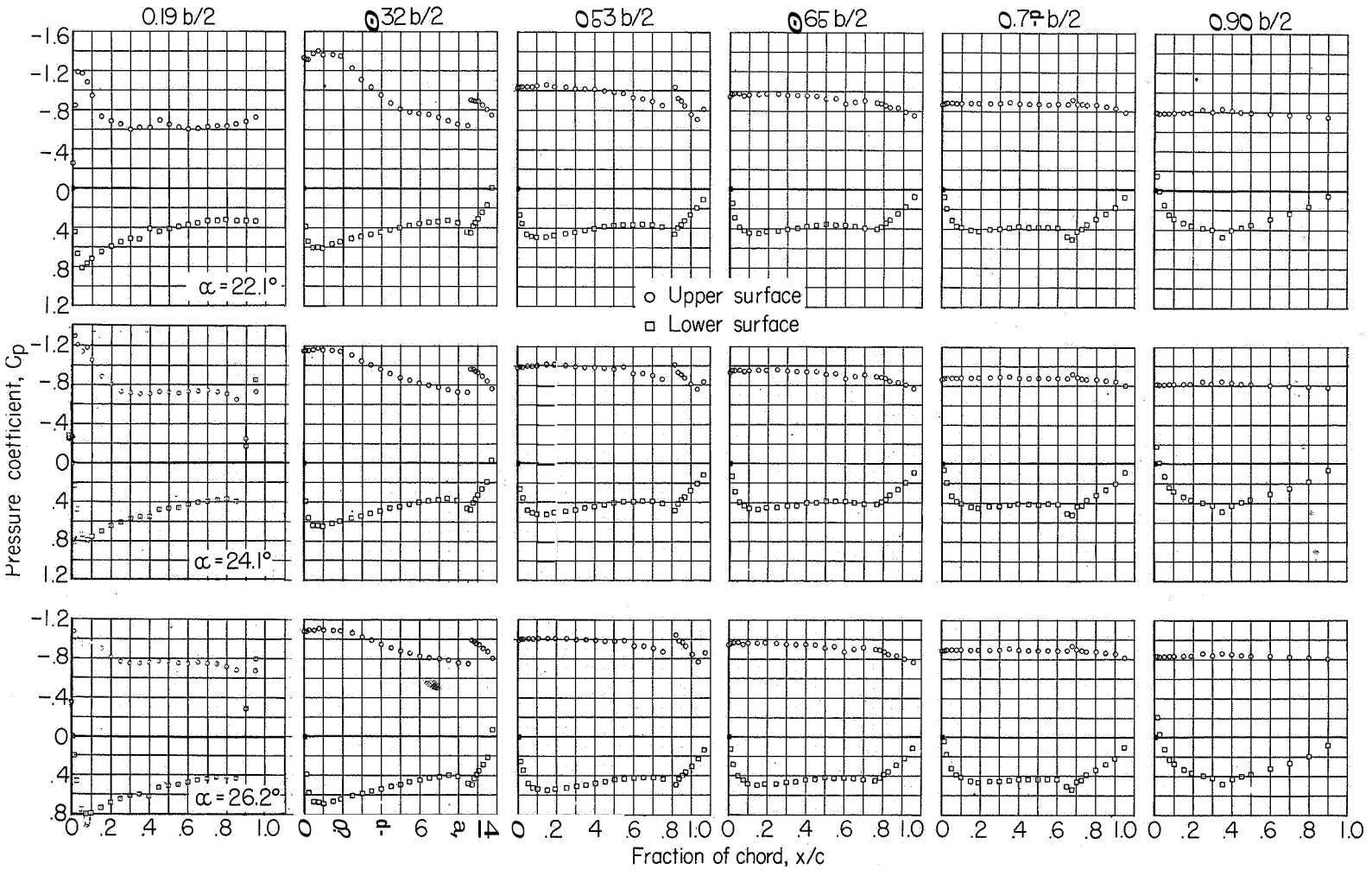

(a) Concluded.

Figure 7.- Concluded.

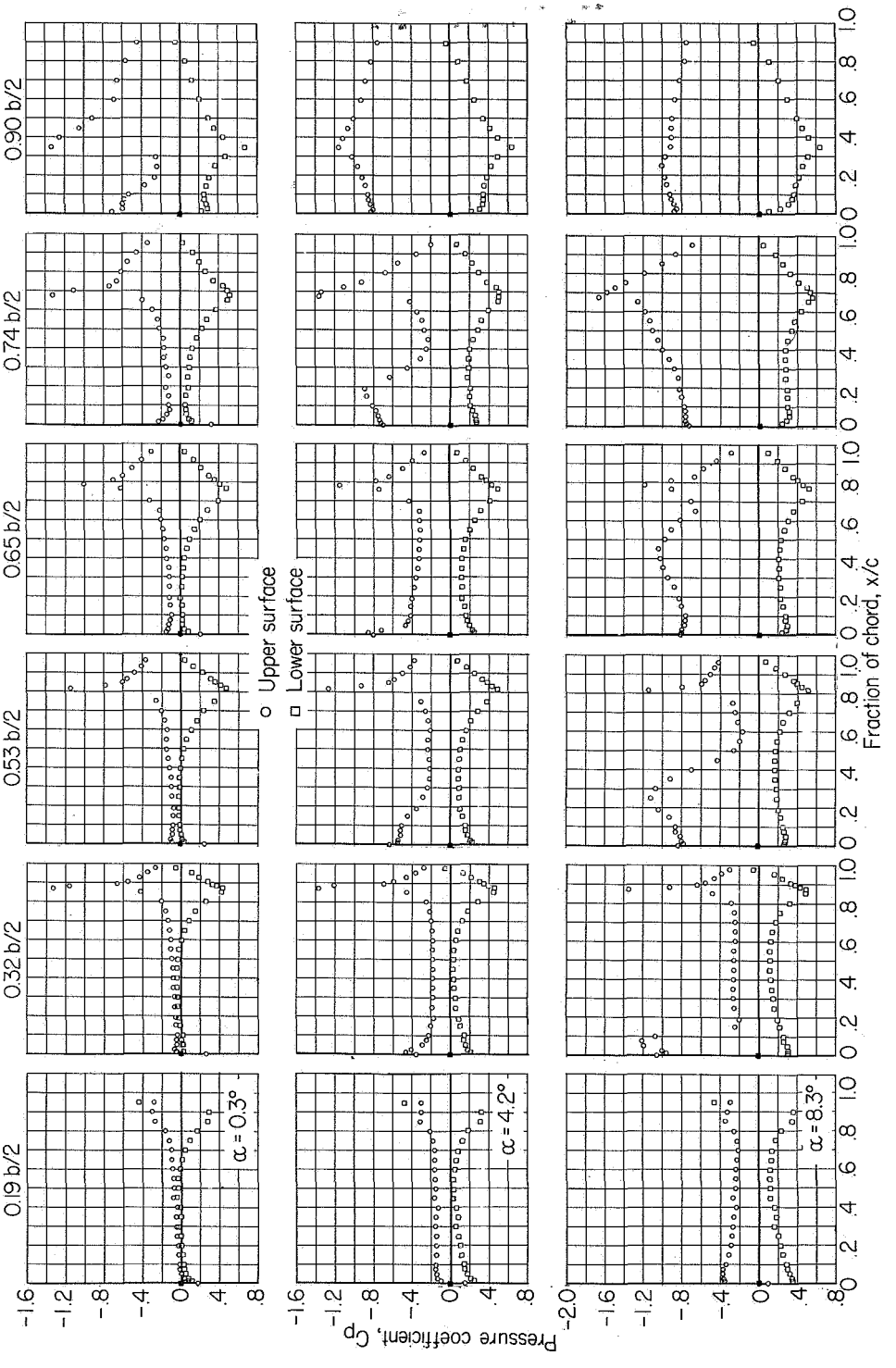

(a) M = 0.80; $C_{p,sonic}$ = -0.44.

Figure 8.- Chordwise pressure distributions on a 60° delta wing with combined controls deflected 15°.

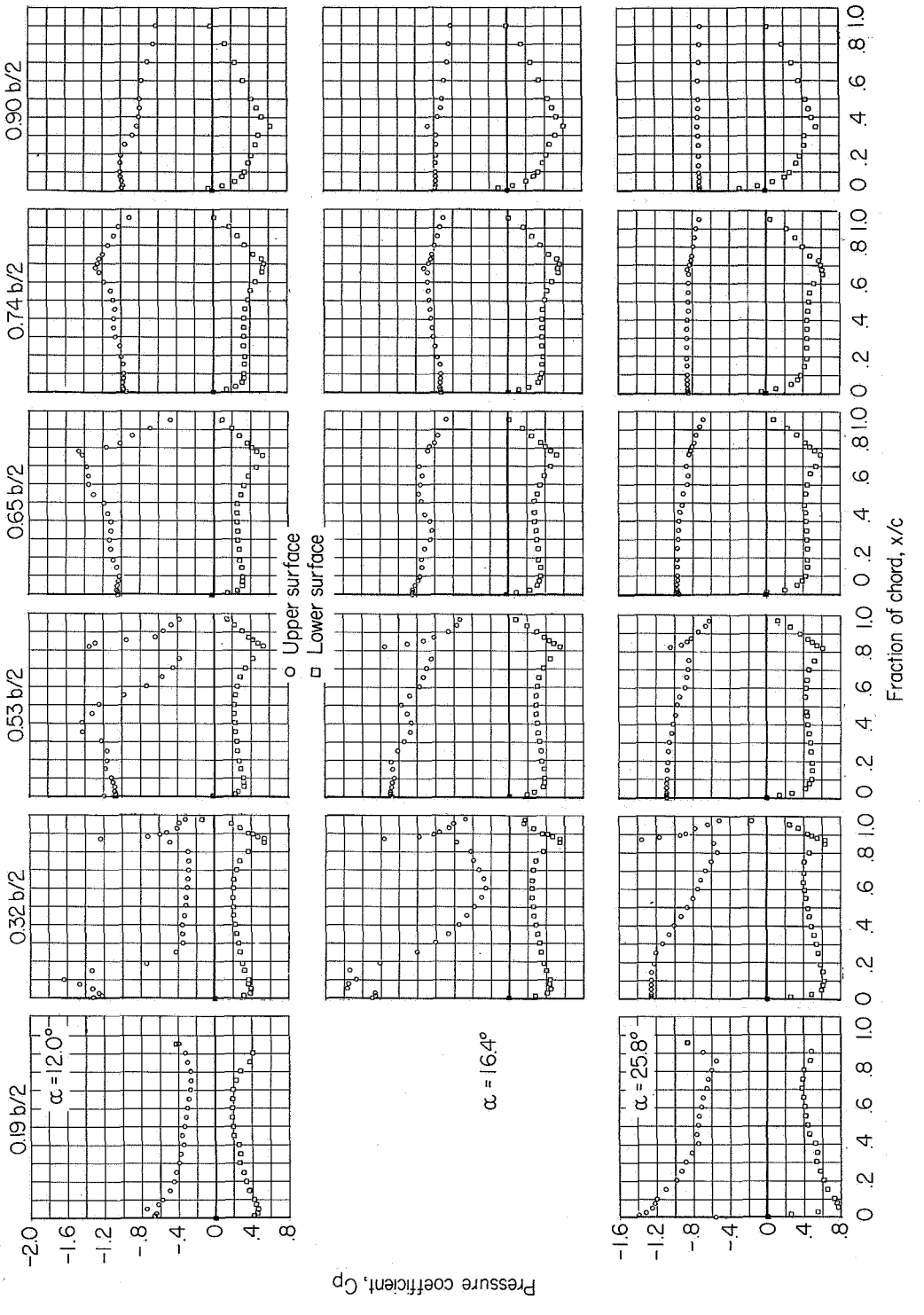

(a) Concluded.

Figure 8.- Continued.

T-505

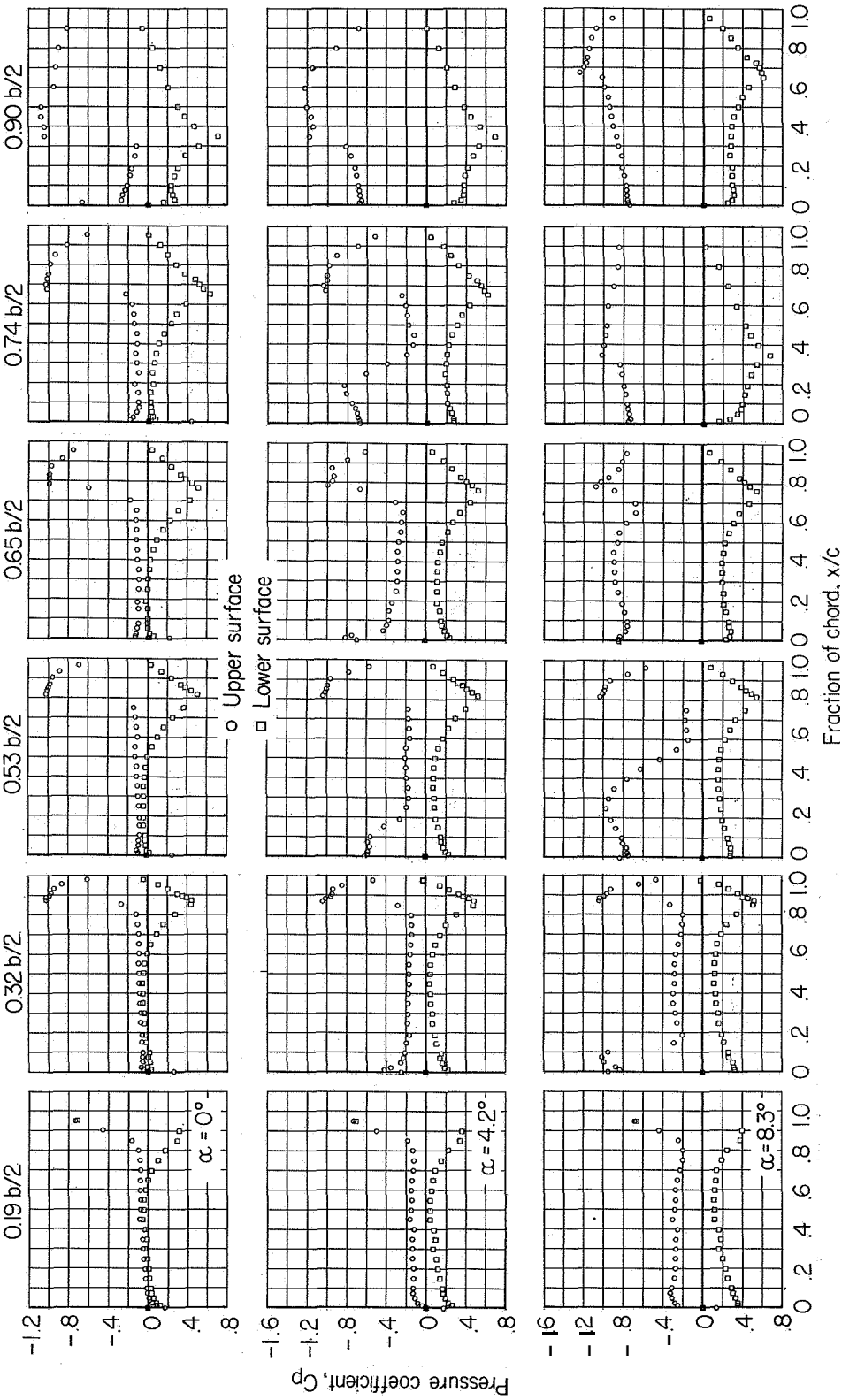

(b) M = 0.90; $C_{p,sonic}$ = -0.19.

Figure 8.- Continued.

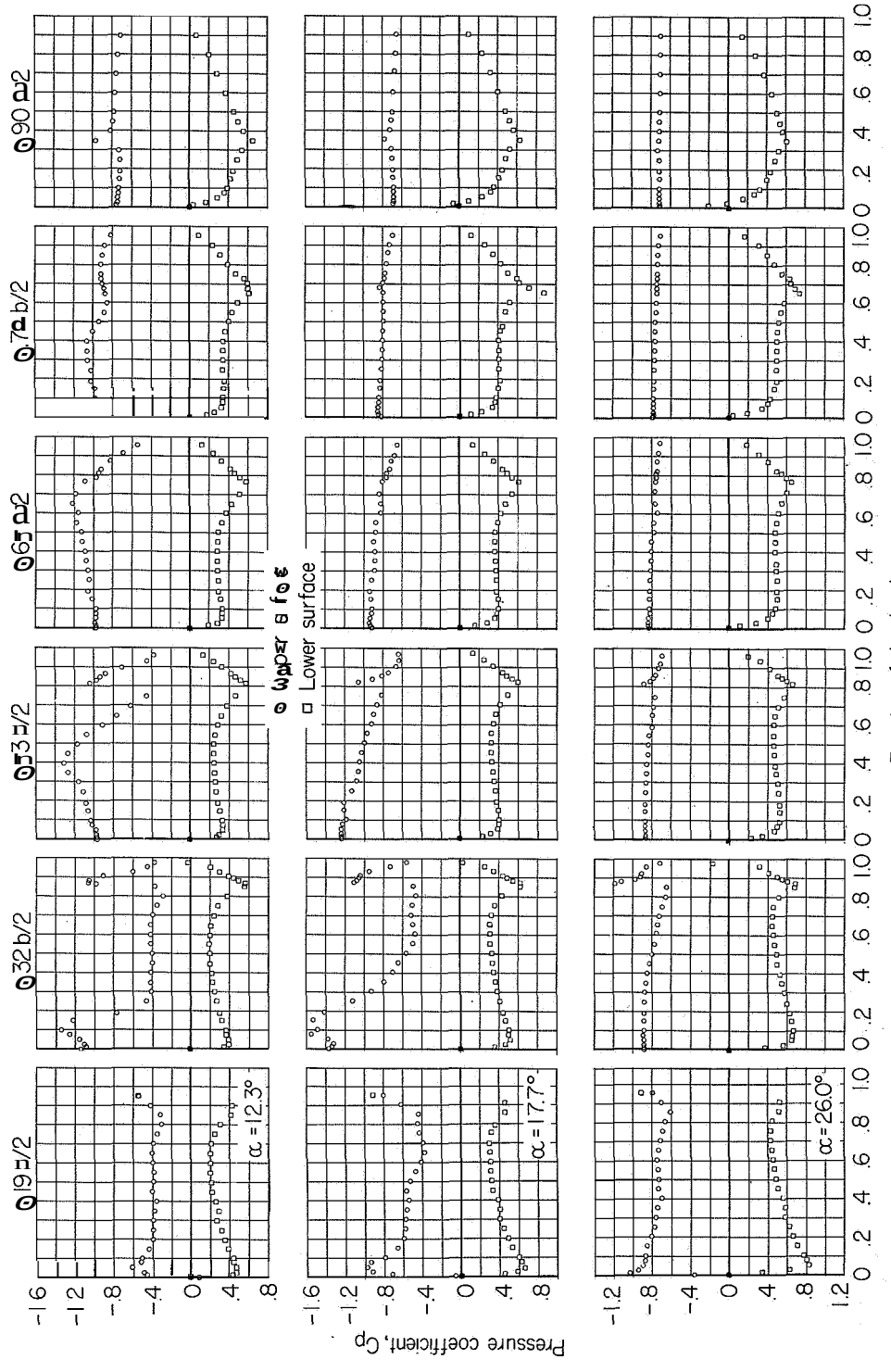

(b) Concluded.

Figure 8.- Continued.

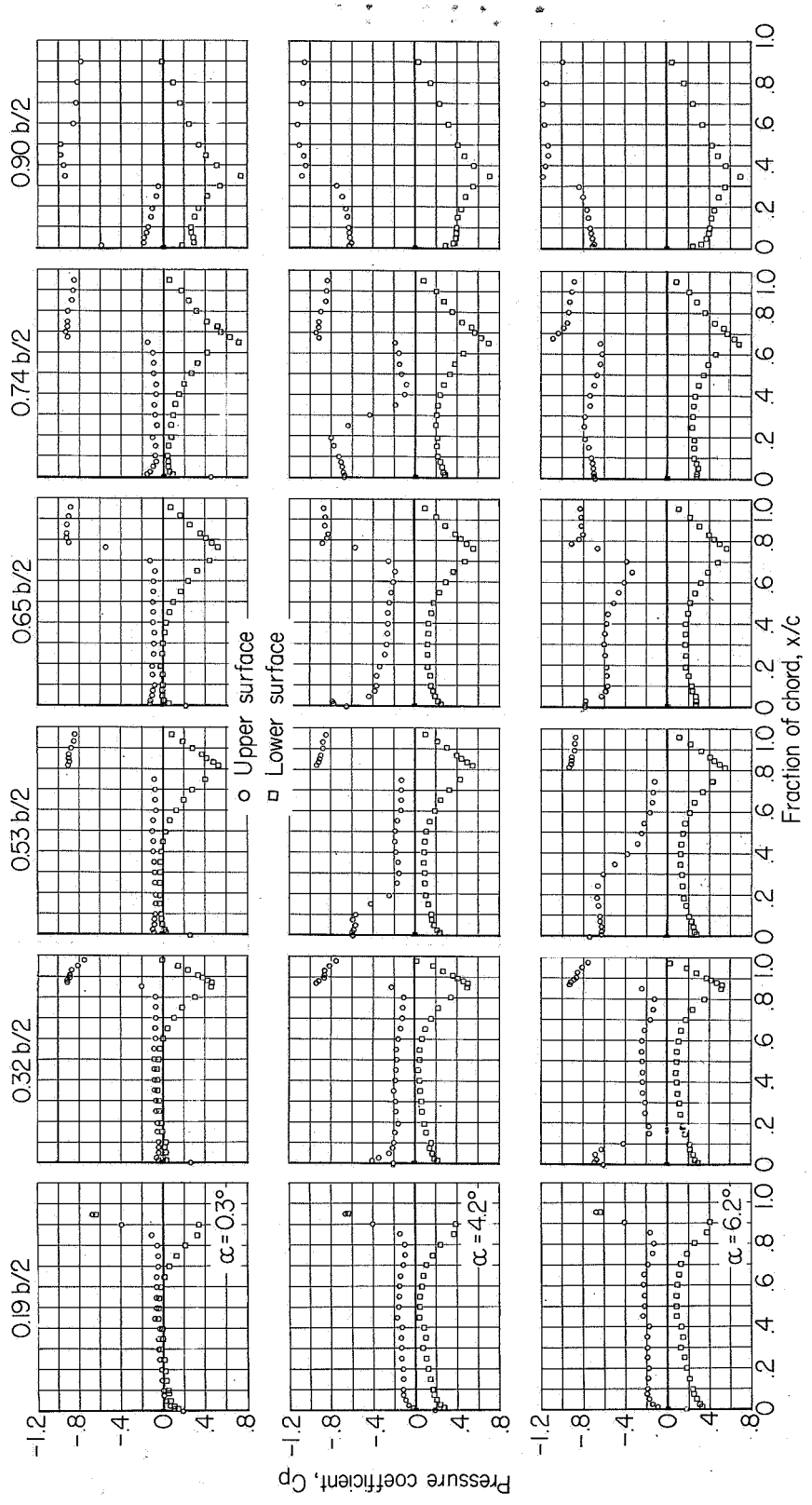

(c) M = 0.94; $C_{p,sonic}$ = -0.10.

Figure 8.- Continued.

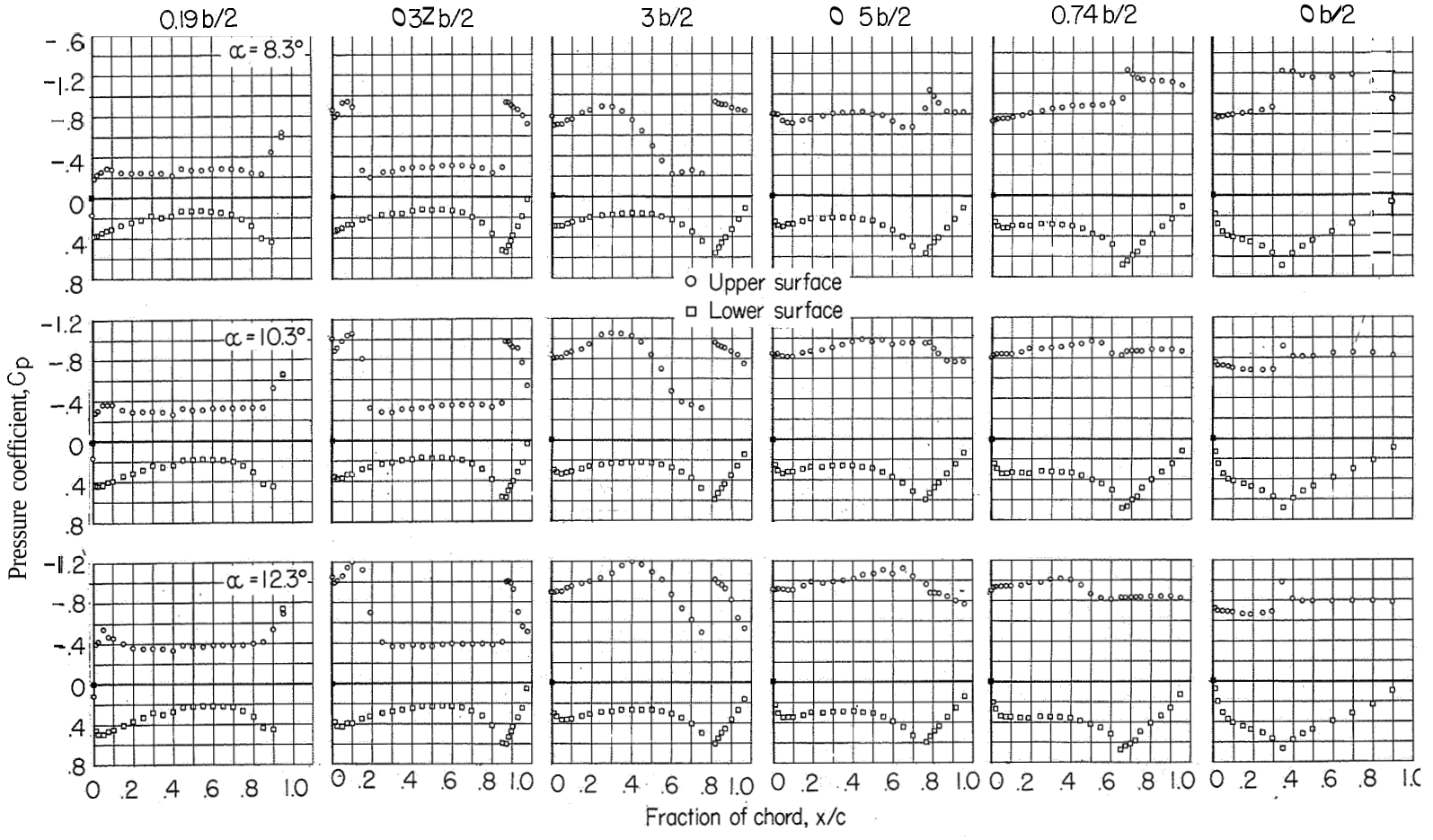

(c) Continued.

Figure 8.- Continued.

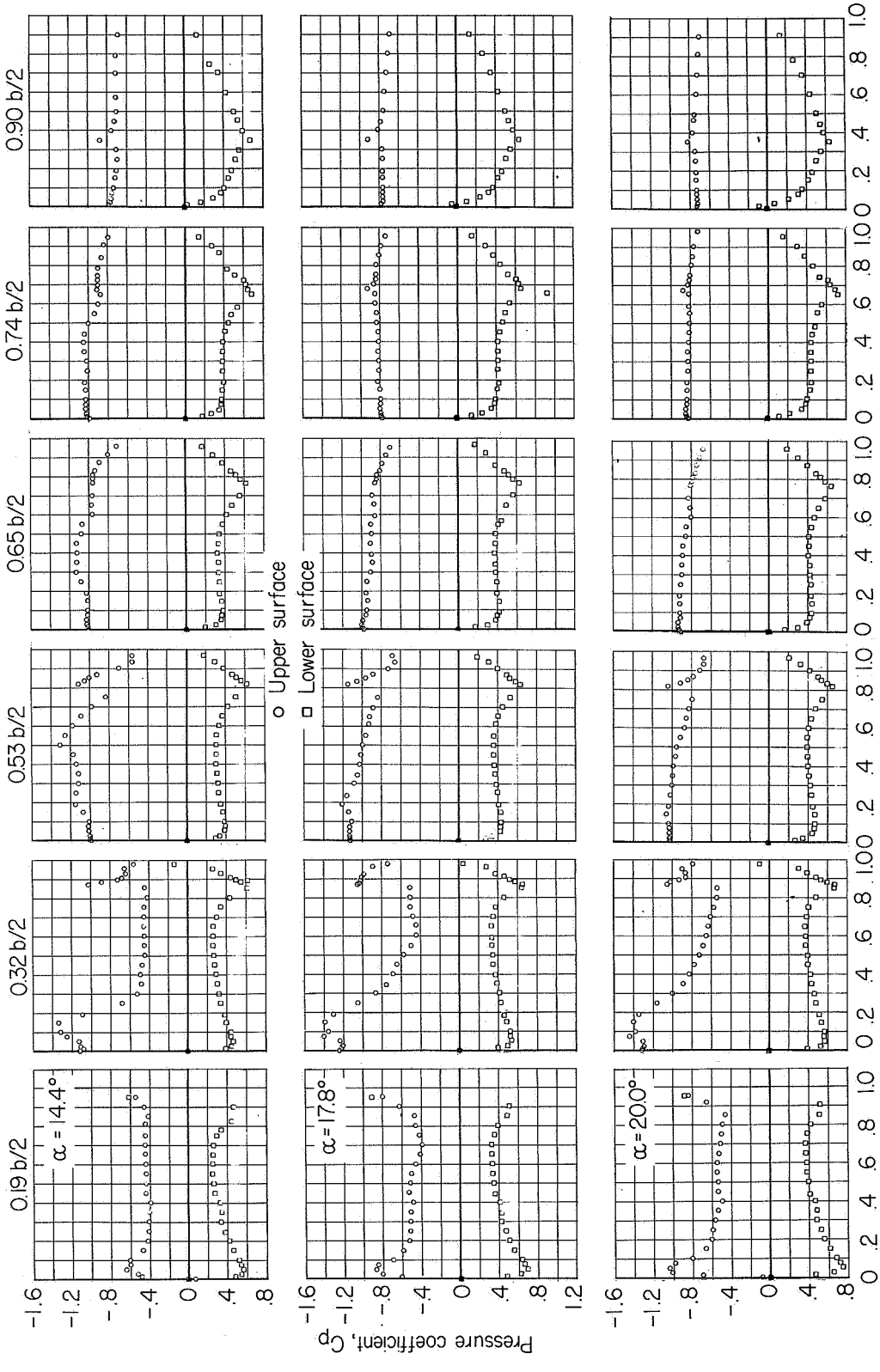

(c) Continued.

Figure 8.- Continued.

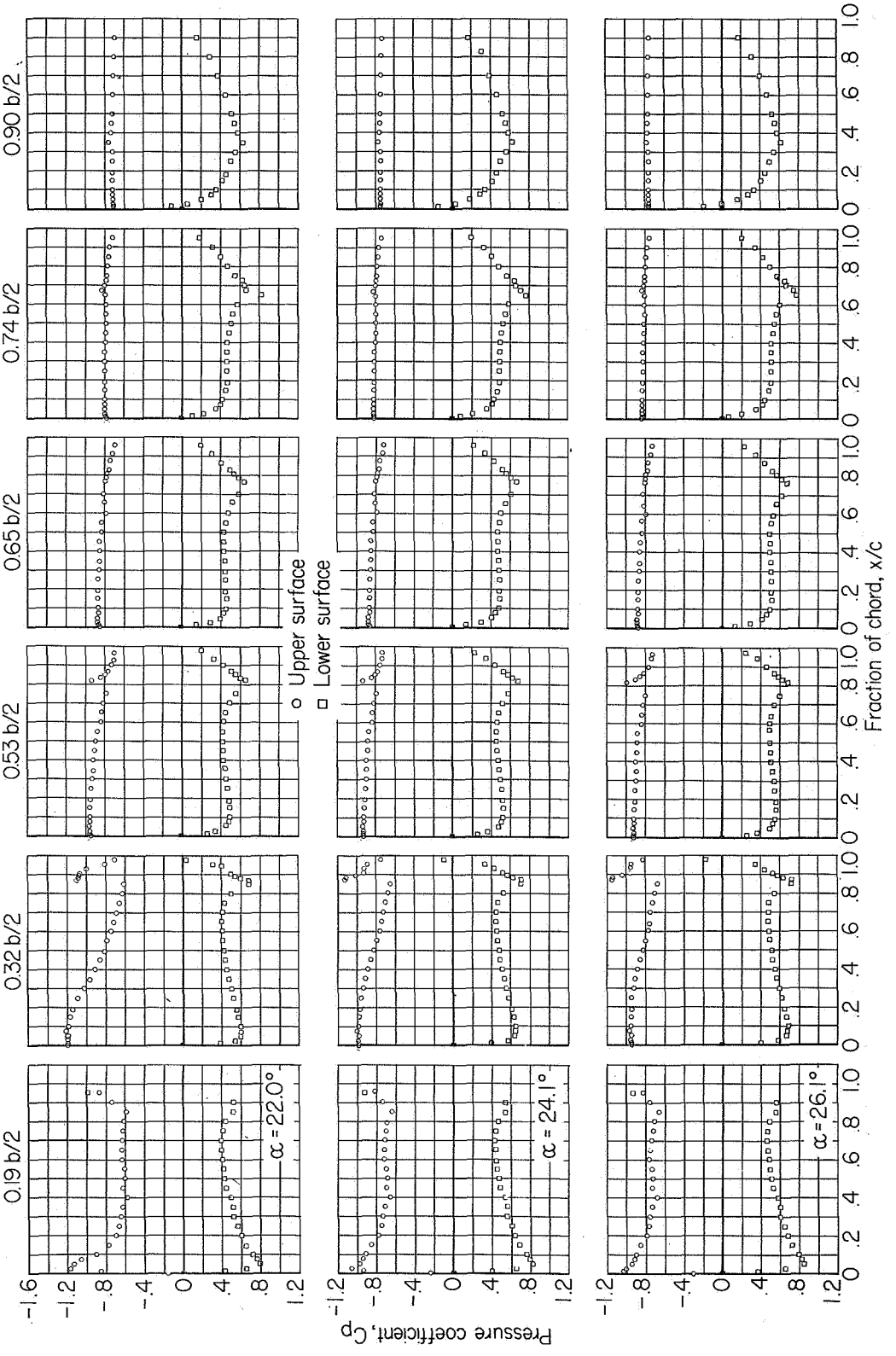

(c) Concluded.

Figure 8.- Continued.

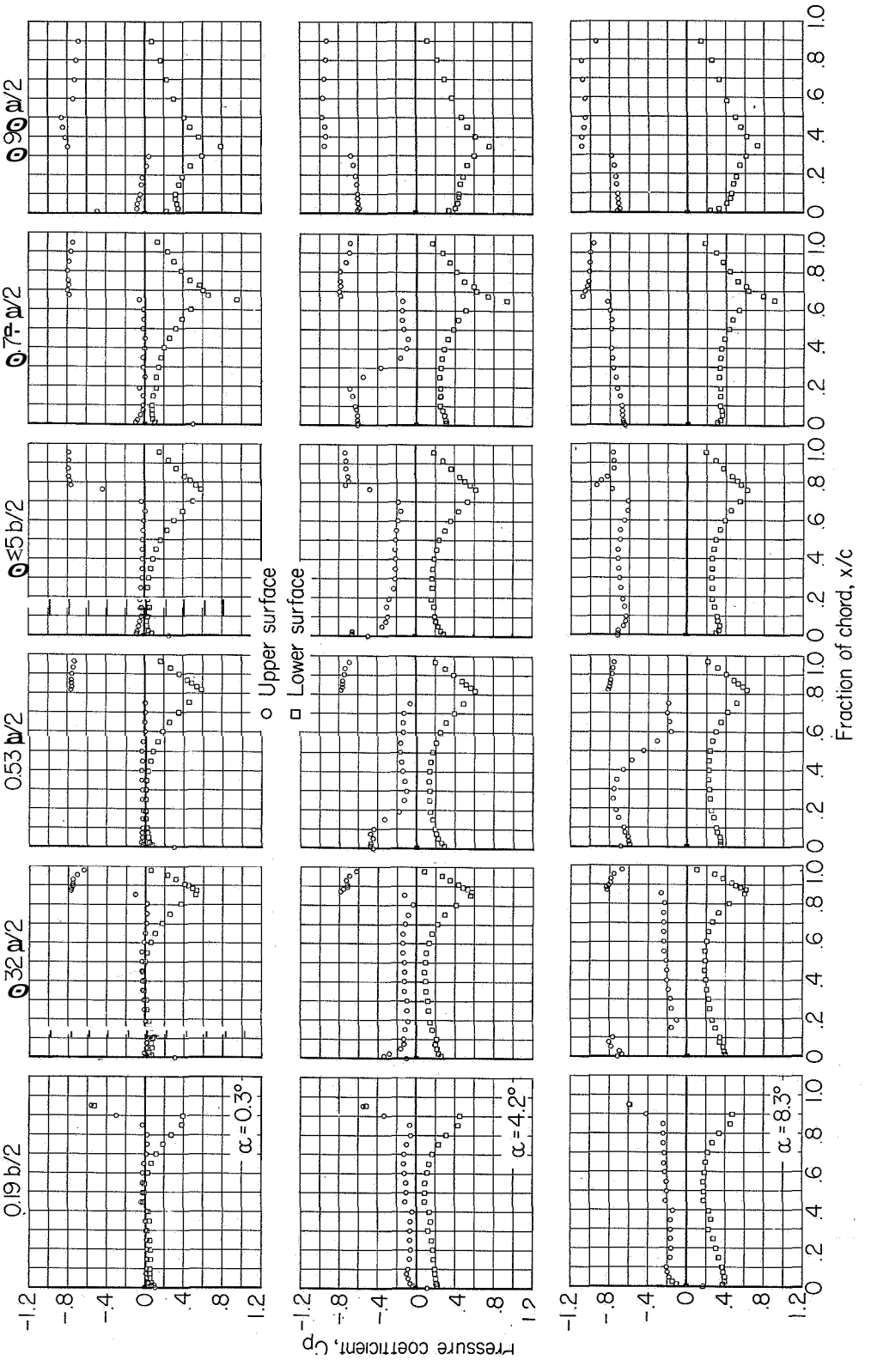

(d) M = 1.00.

Figure 8.- Continued.

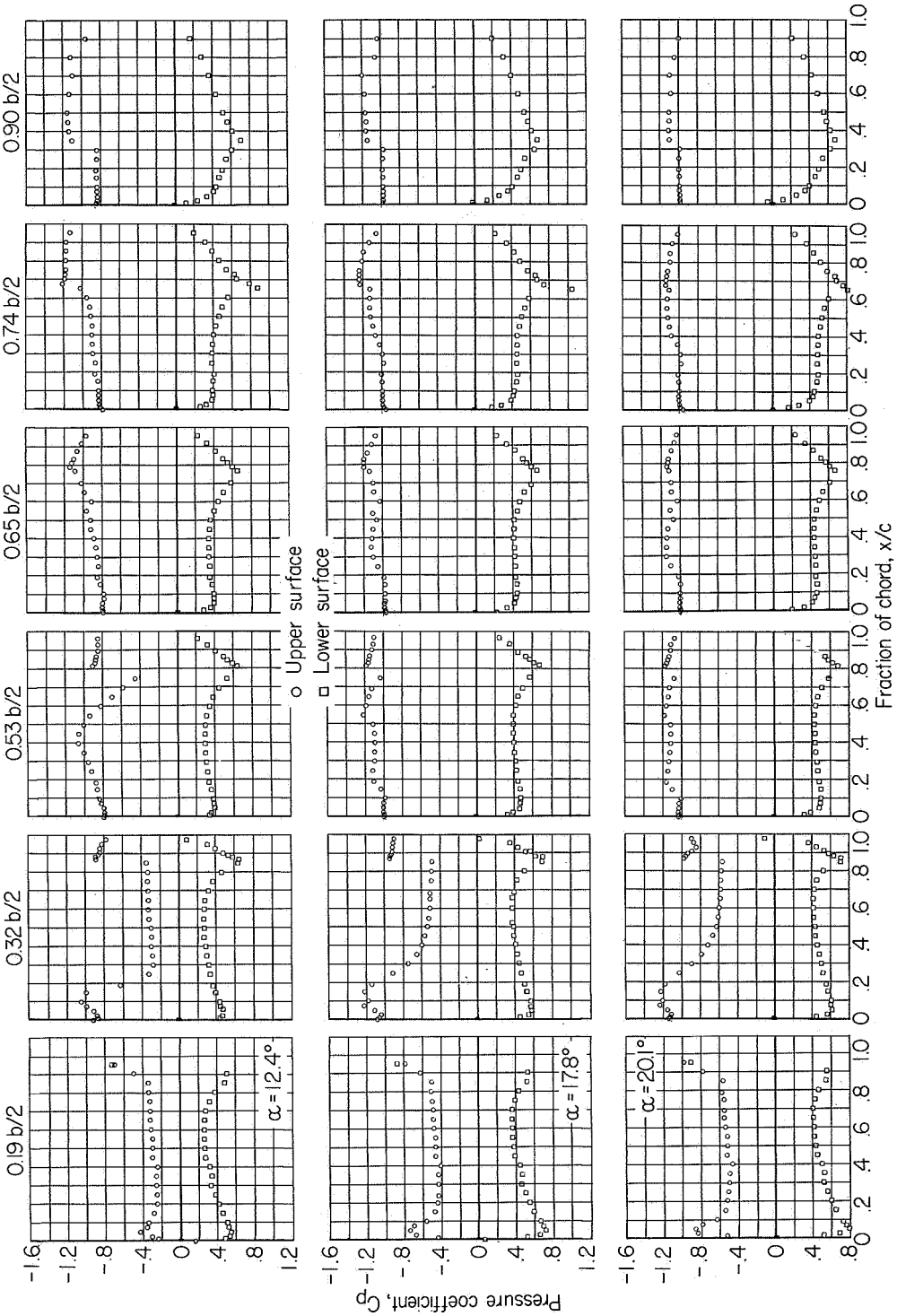

(a) Concluded.

Figure 8.- Continued.

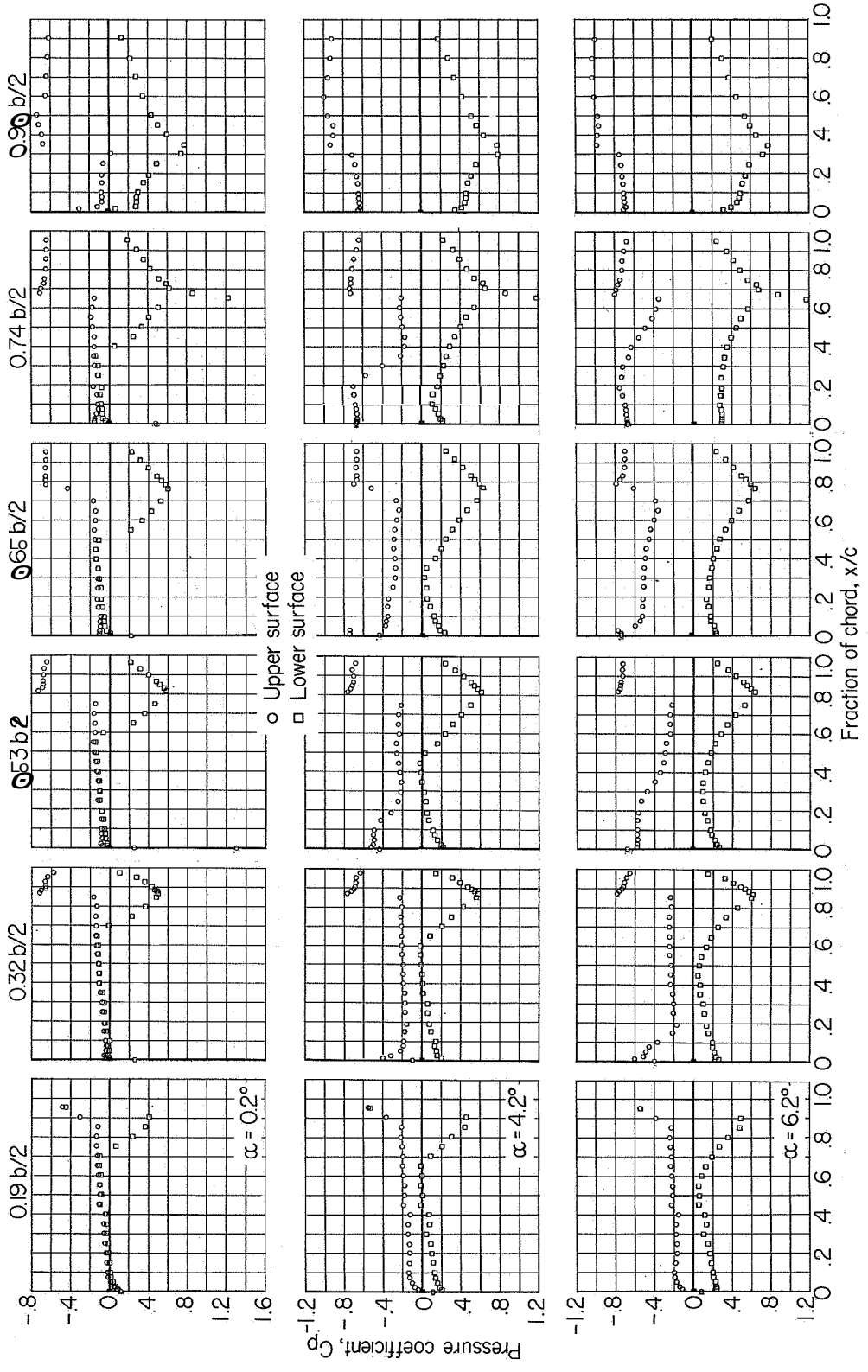

(e) M = 1.05.

Figure 8.- Continued.

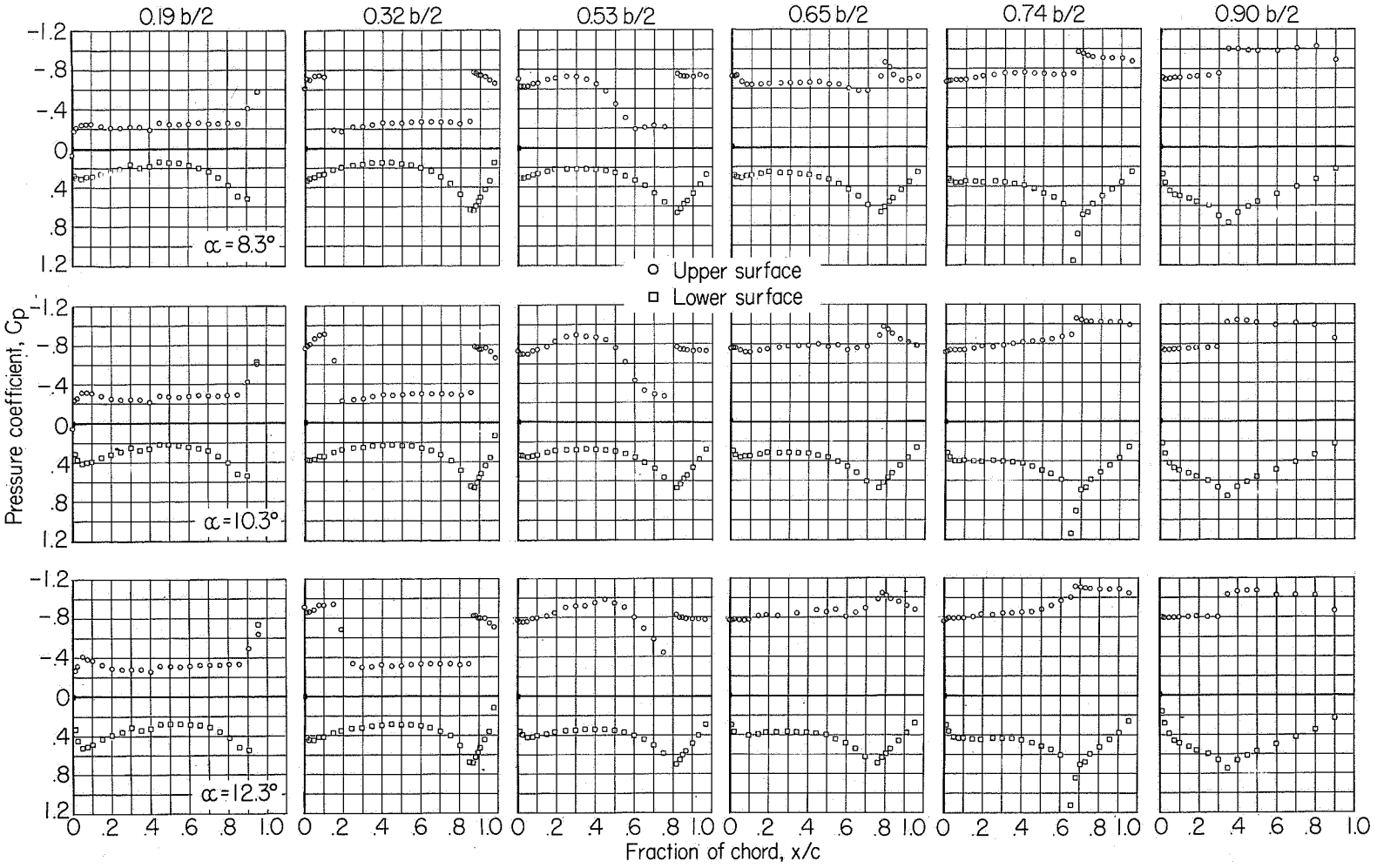

(e) Concluded.

Figure 8.- Concluded.

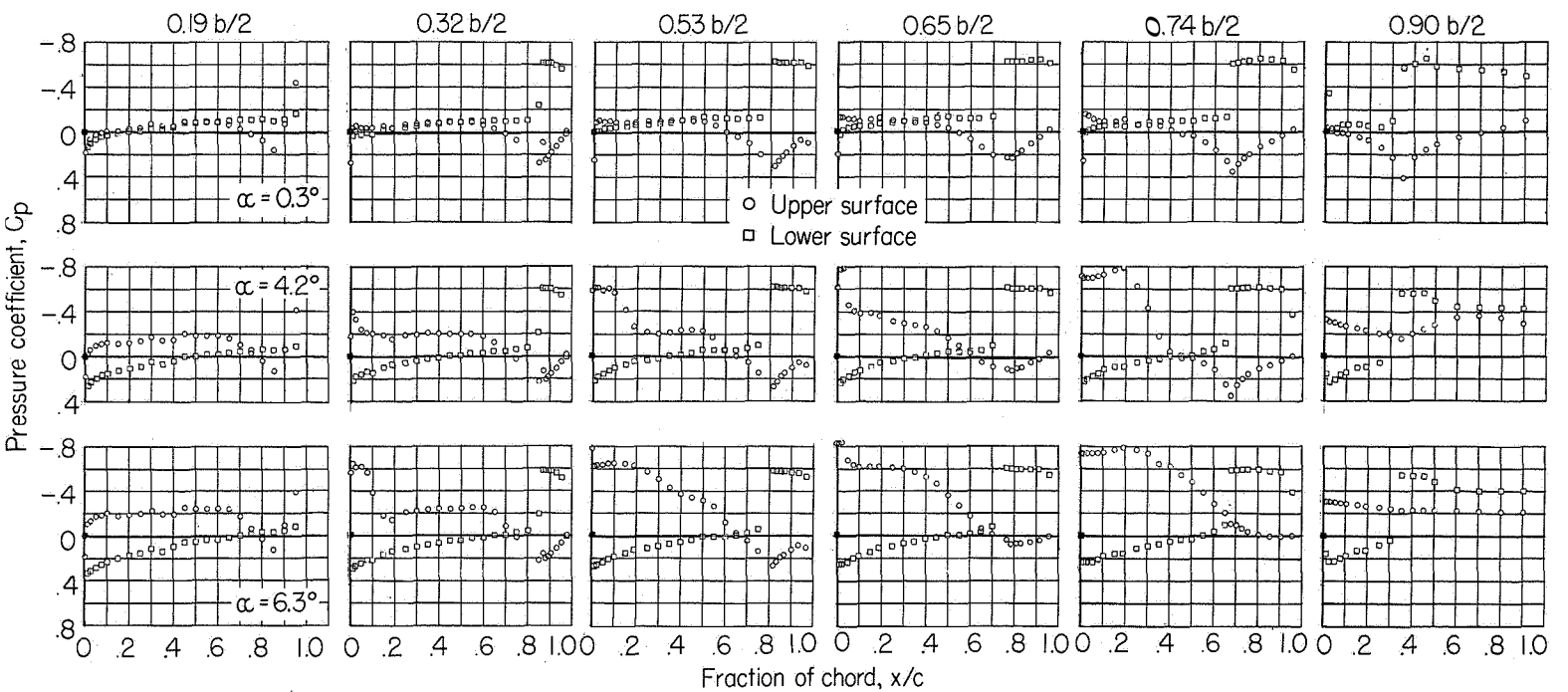

Figure 9.- Chordwise pressure distributions on a 60° delta wing with combined controls deflected -7.5°. M = 0.94; $C_{p,sonic}$ = -0.10.

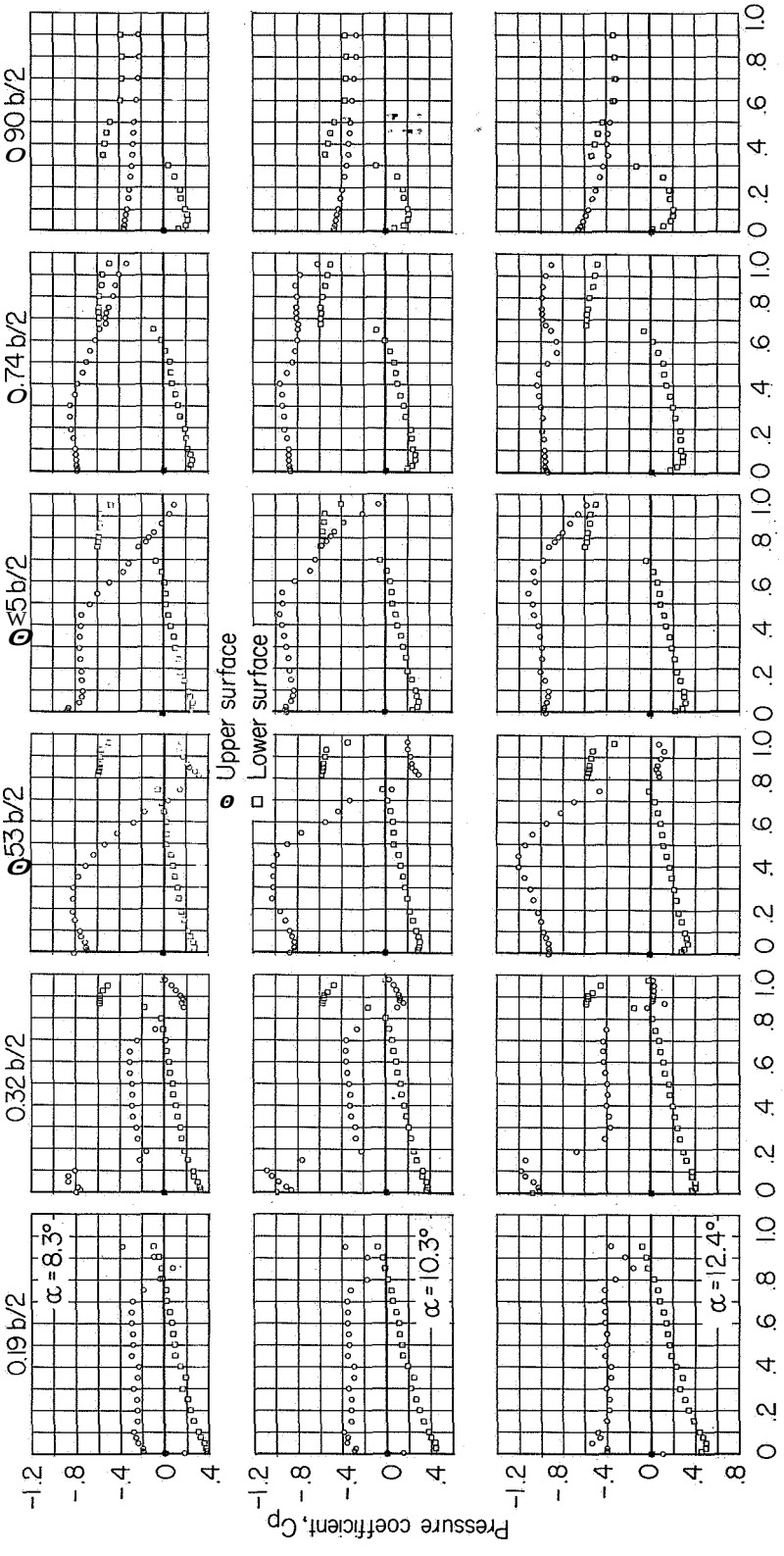

Figure 9.- Continued.

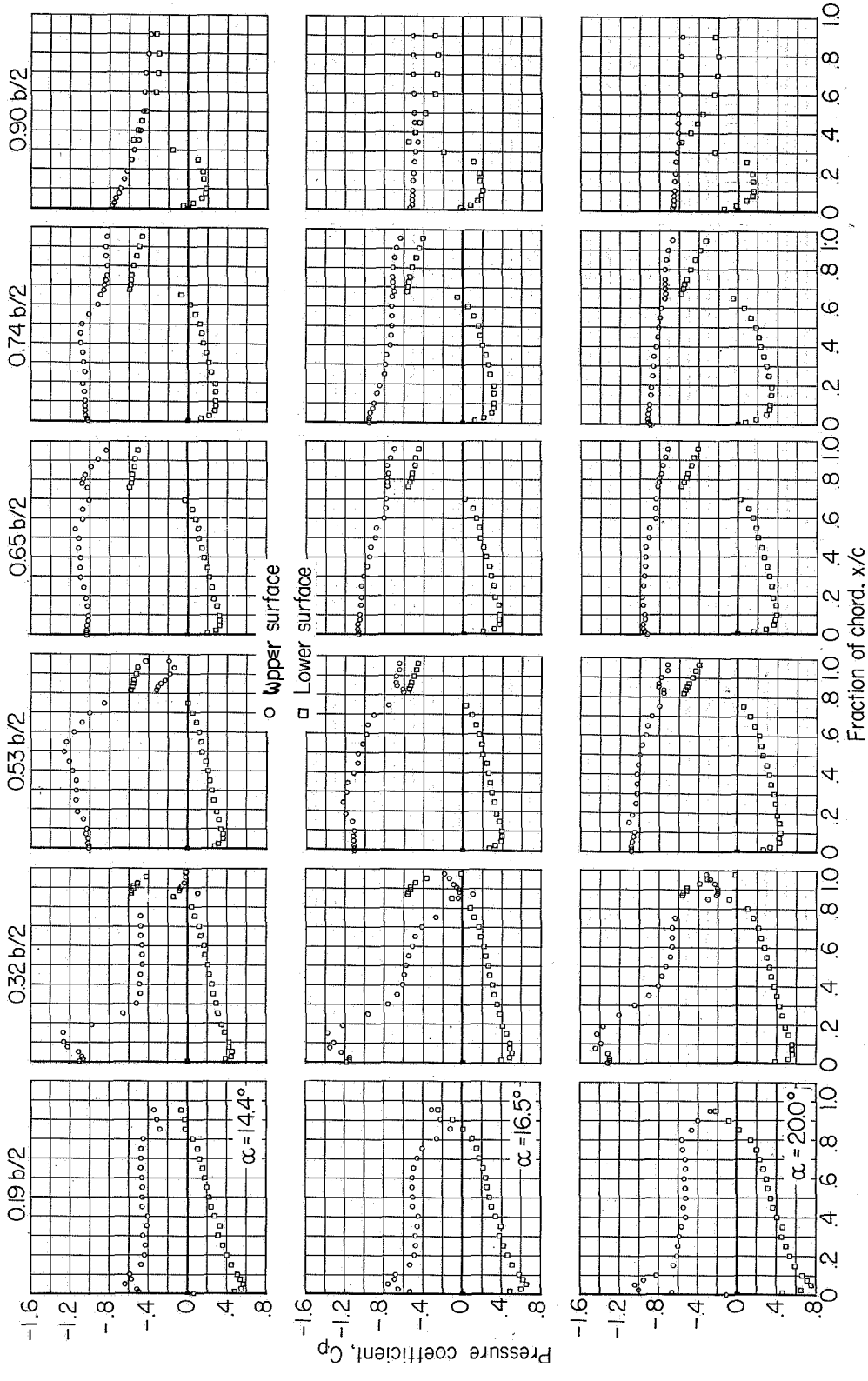

Figure 9.- Continued.

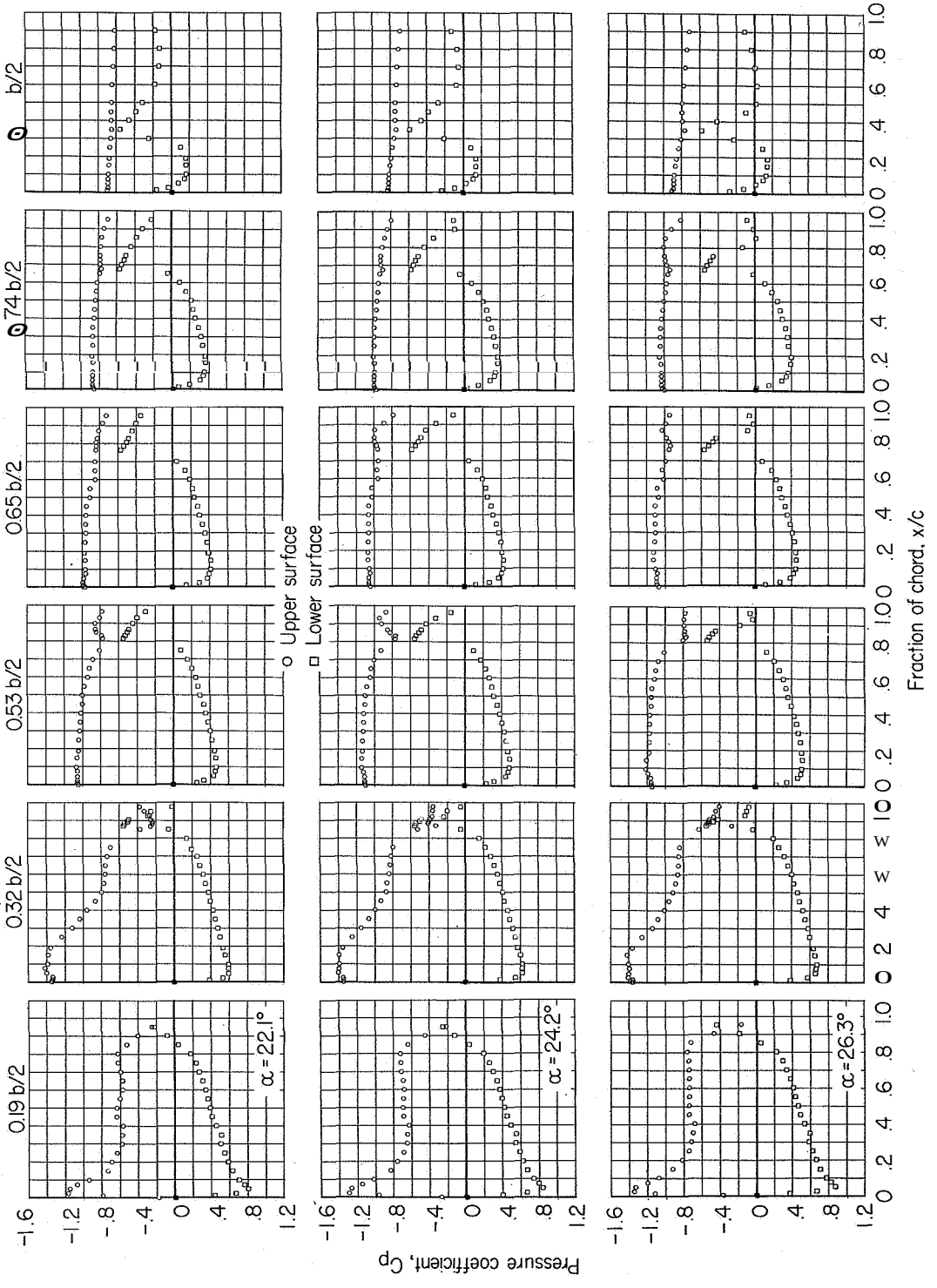

Figure 9.- Concluded.

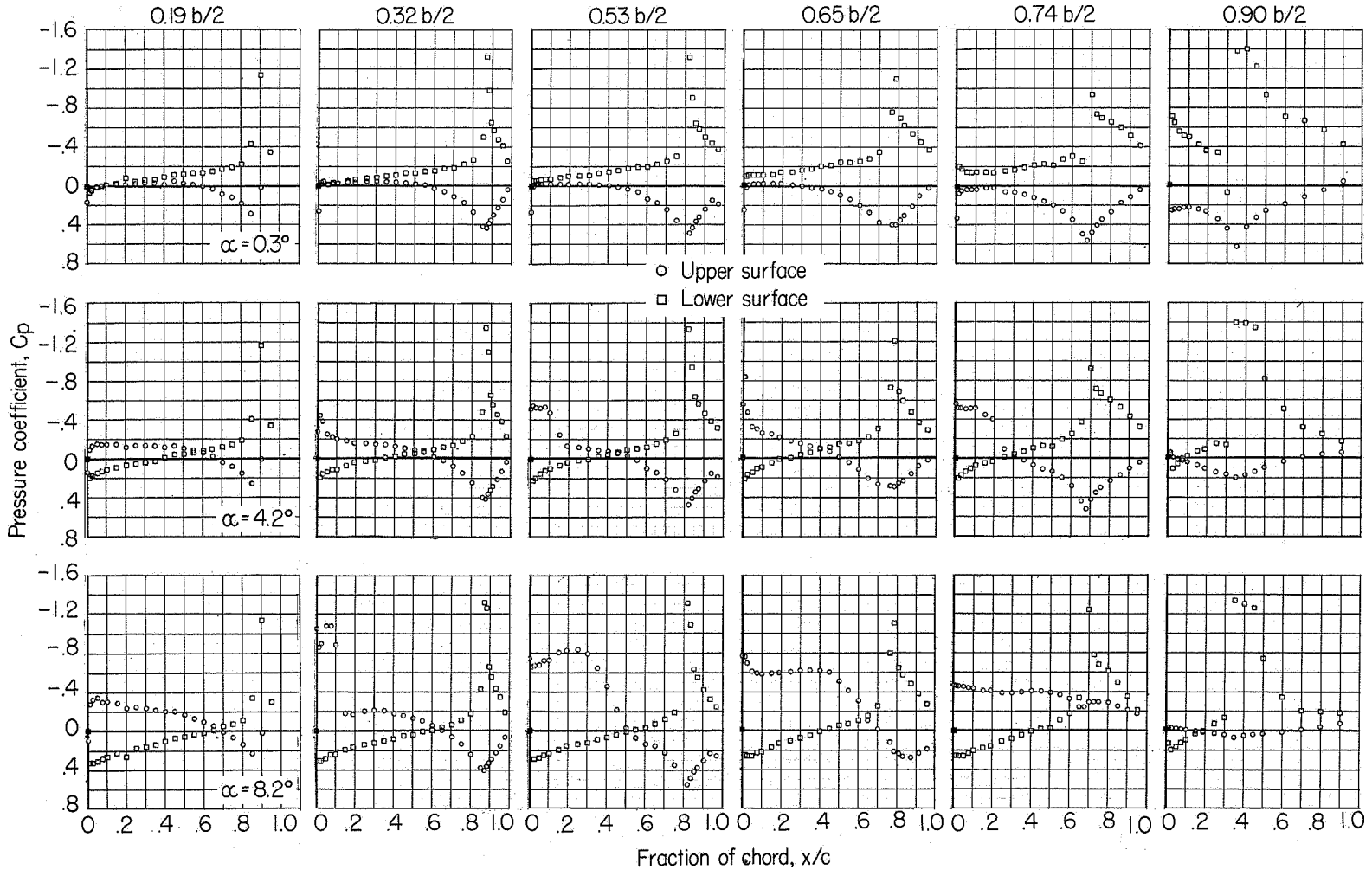

(a) M = 0.80; $C_{p,sonic}$ = -0.44

Figure 10 - Chordwise pressure distributions on a 60° delta wing with combined controls deflected -15°.

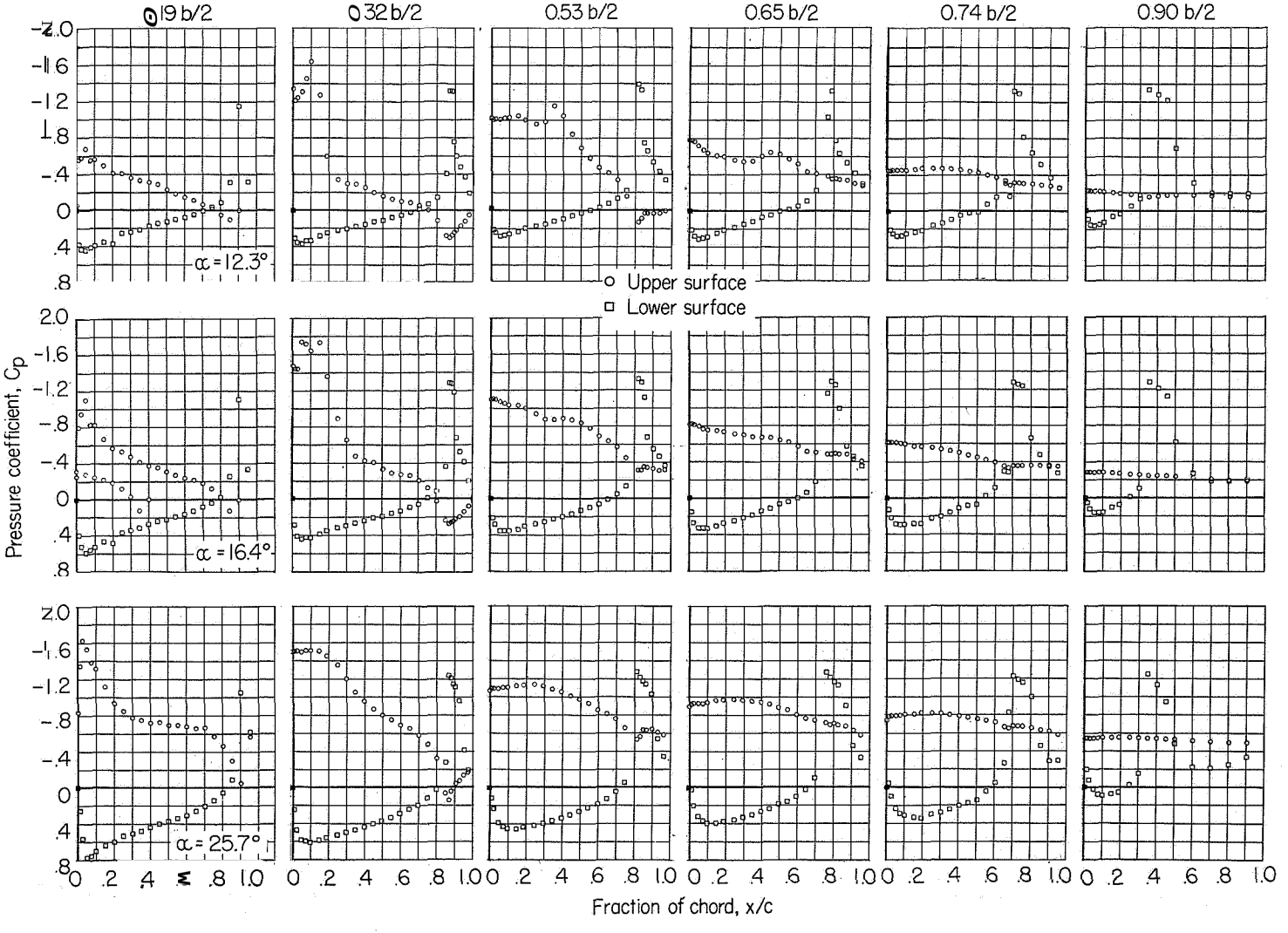

(a) Concluded.

Figure 10.- Continued.

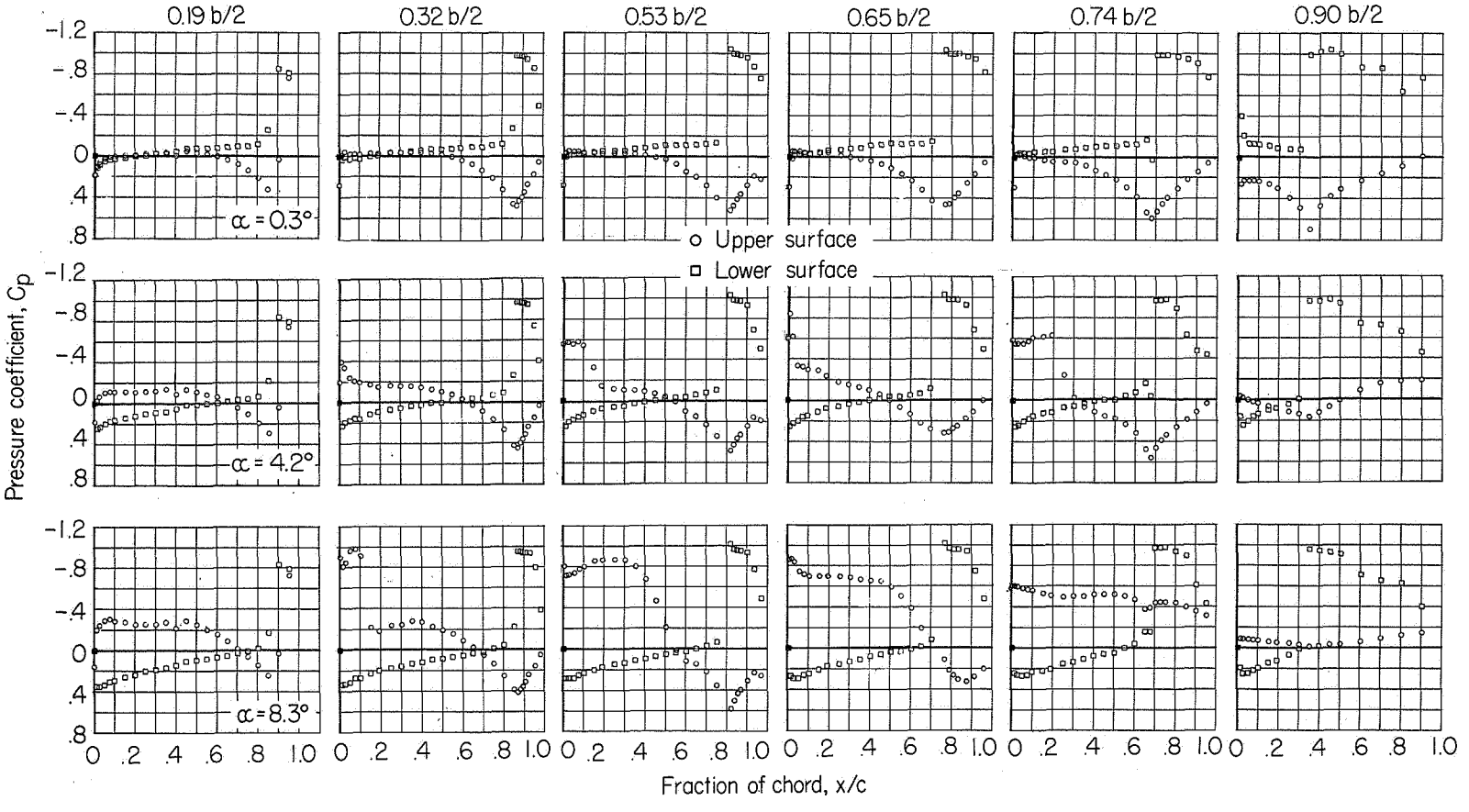

(b) M = 0.90; $C_{p,sonic}$ = -0.19.

Figure 10.- Continued.

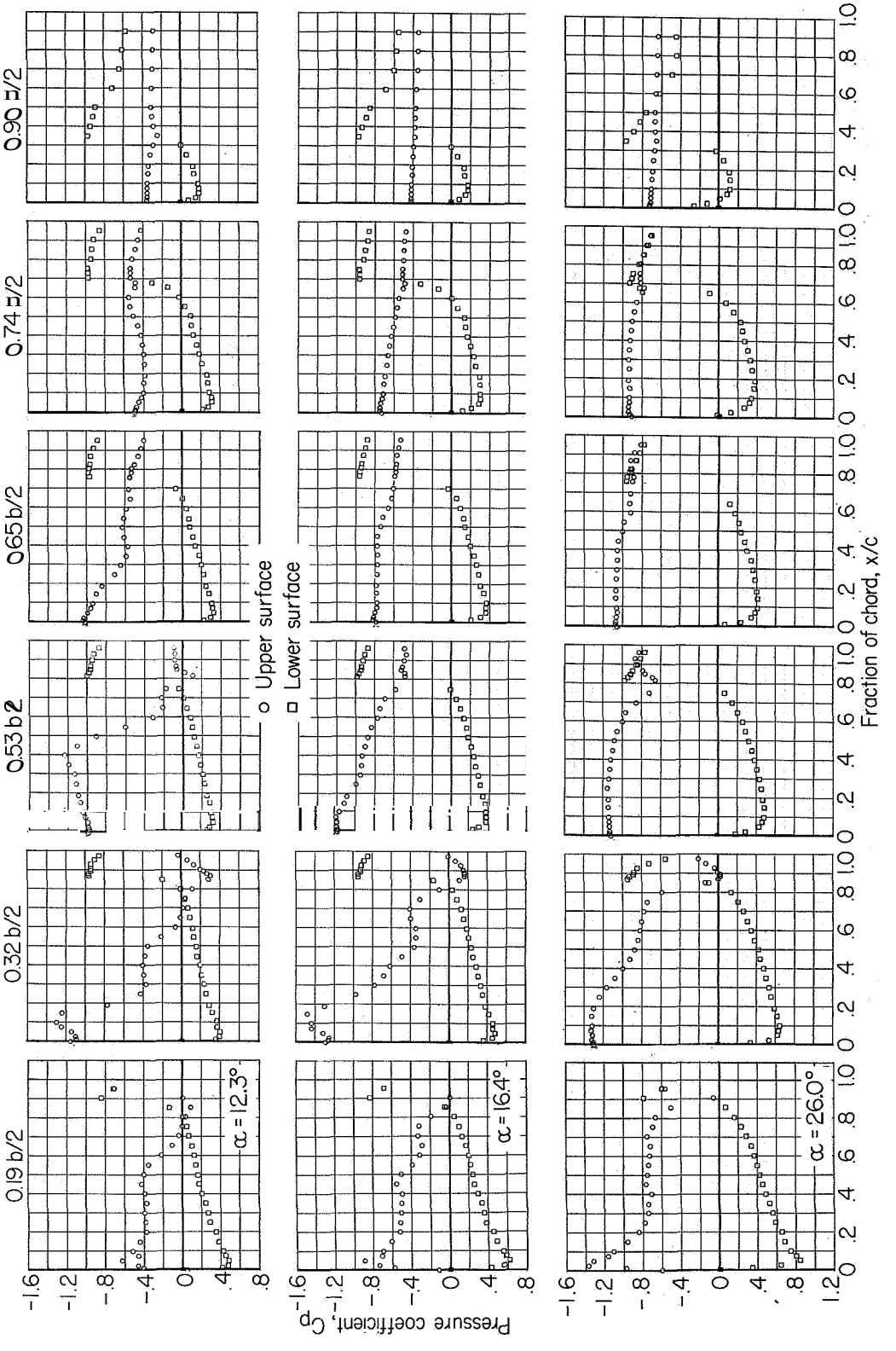

(b) Concluded.

Figure 10.- Continued.

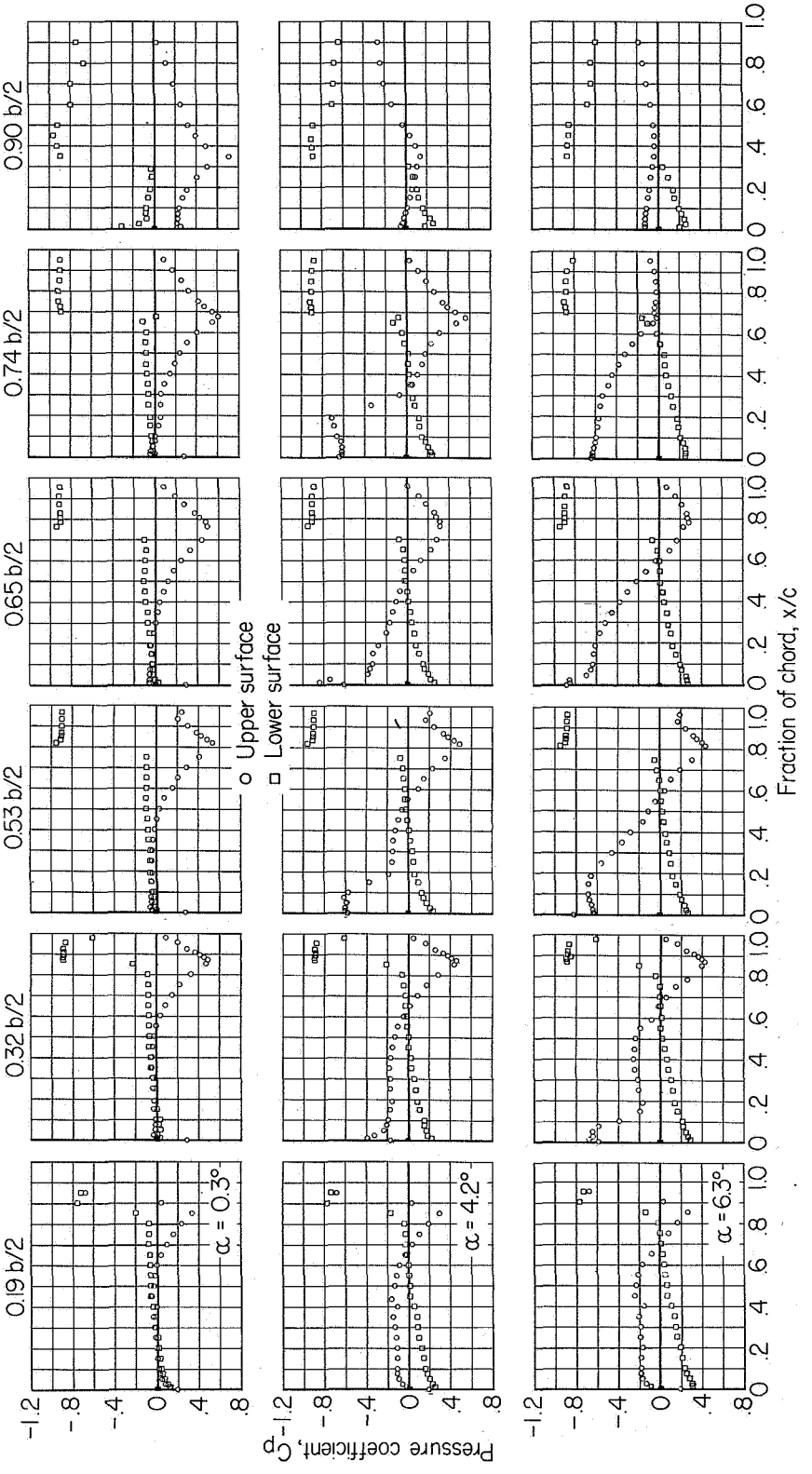

(c) M = 0.94; $C_{p,sonic}$ = -0.10.

Figure 10.- Continued.

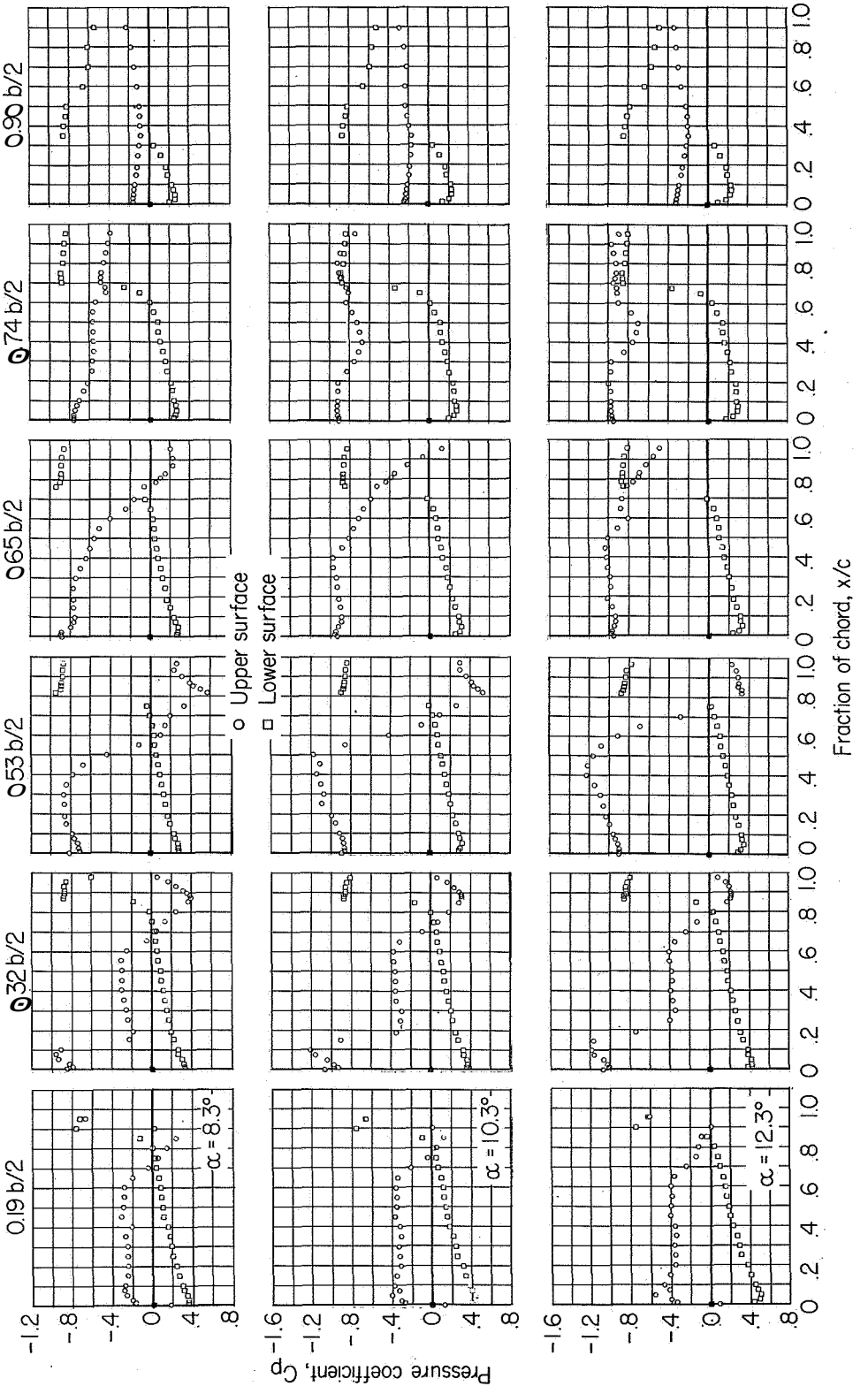

(c) Continued.

Figure 10.- Continued.

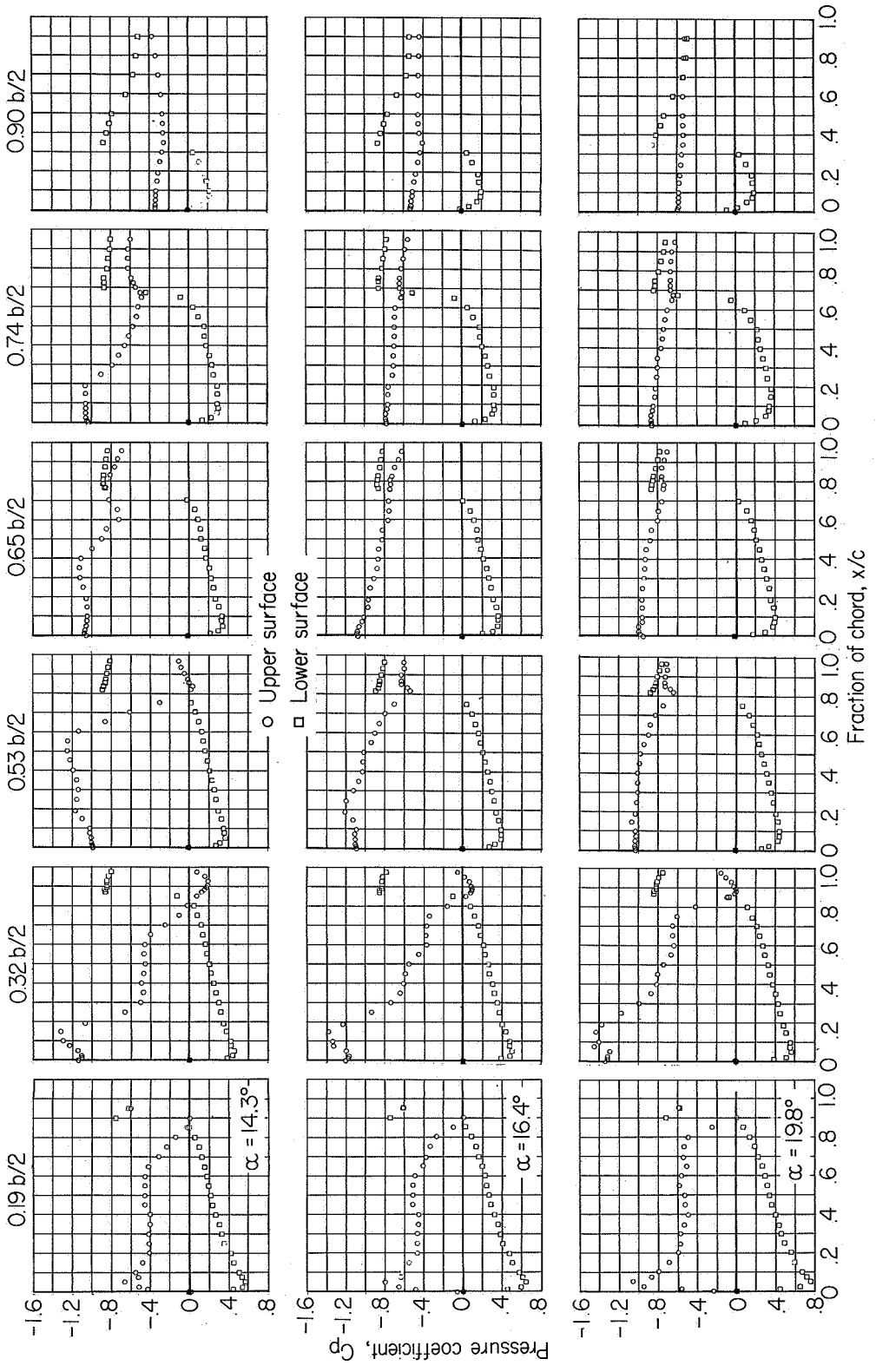

(c) Continued.

Figure 10 - Continued.

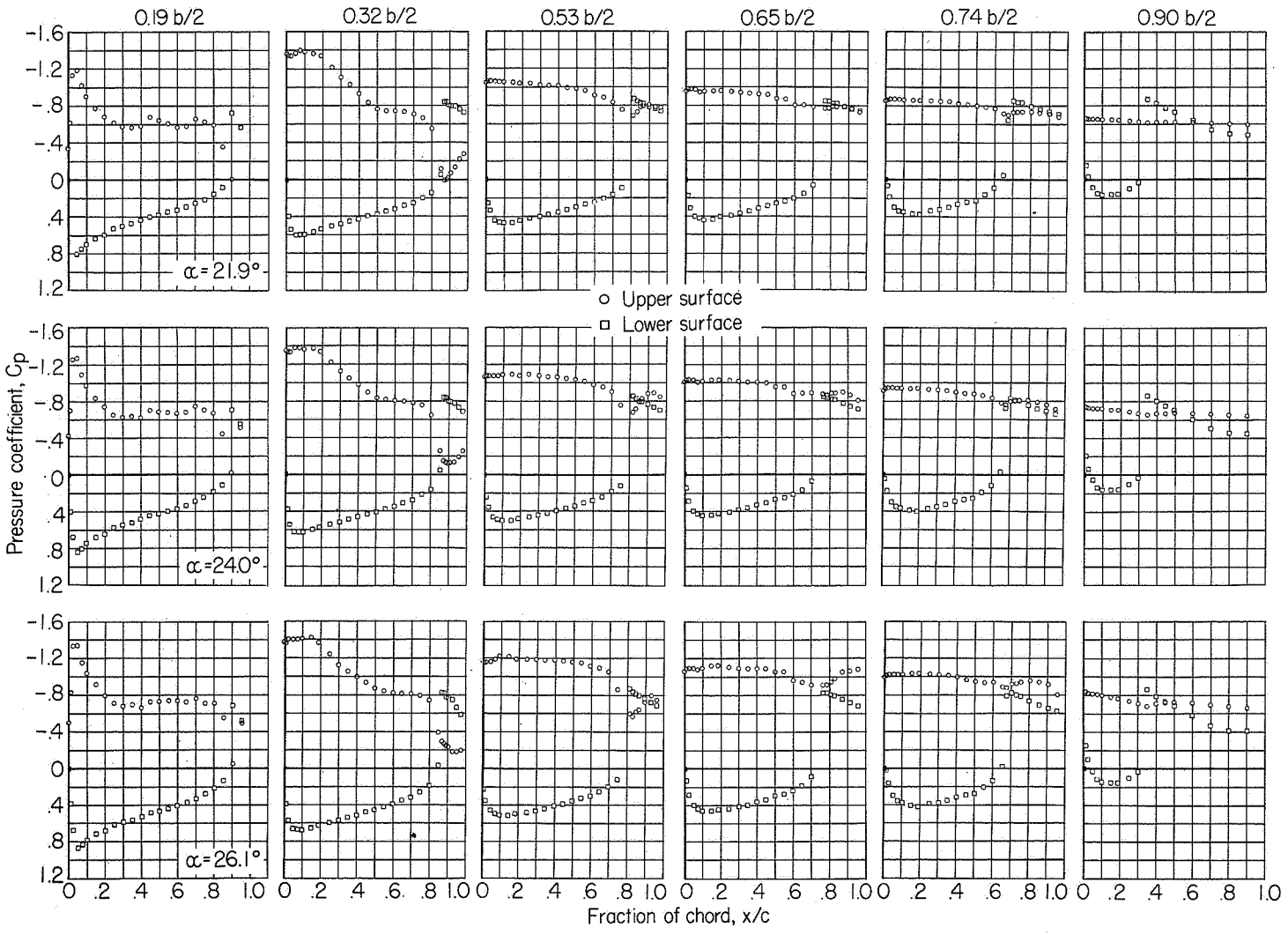

(c) Concluded.

Figure 10.- Continued.

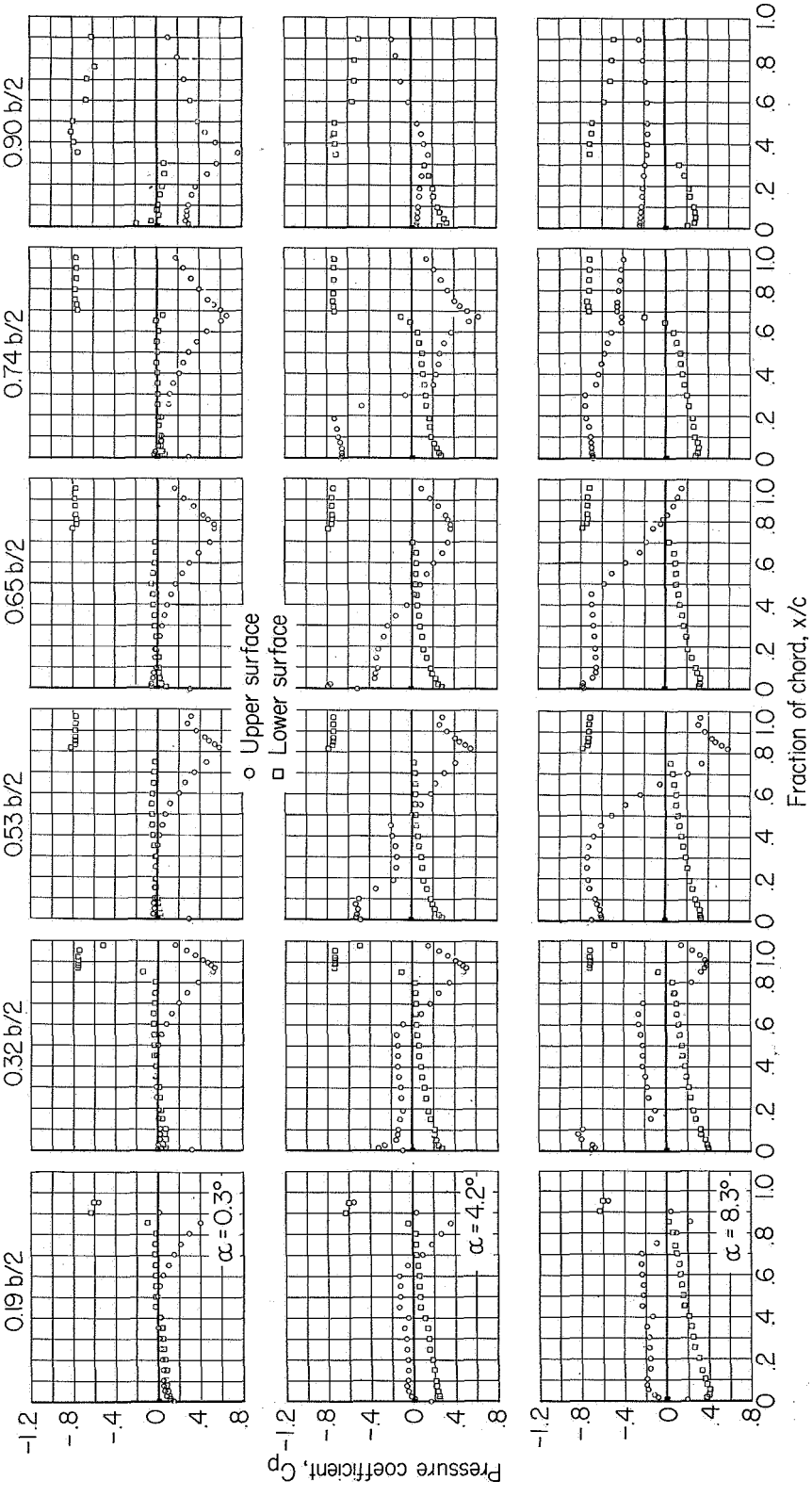

(d) M = 1.00.

Figure 10.- Continued.

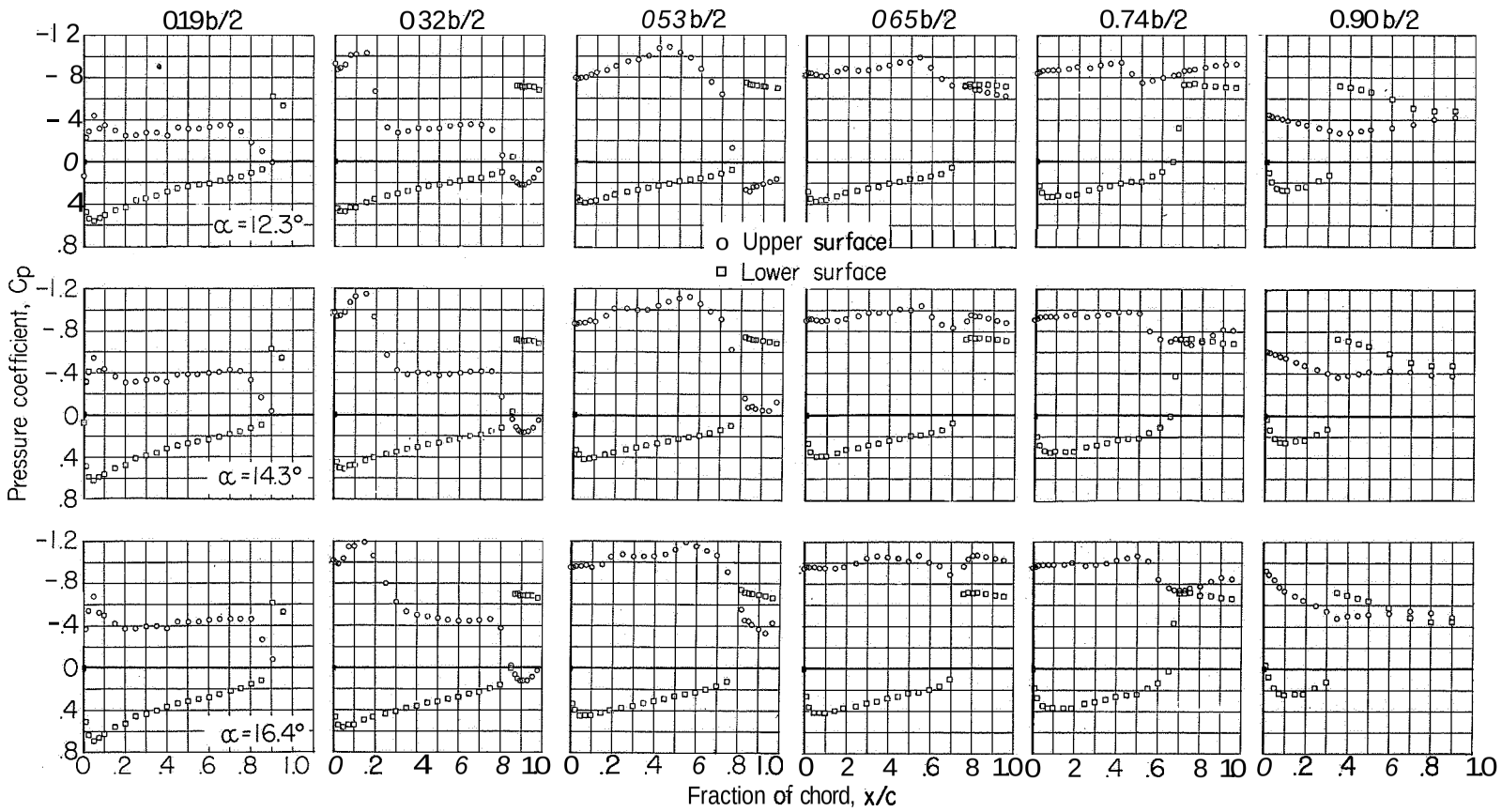

(d) Concluded.

Figure 10.- Continued.

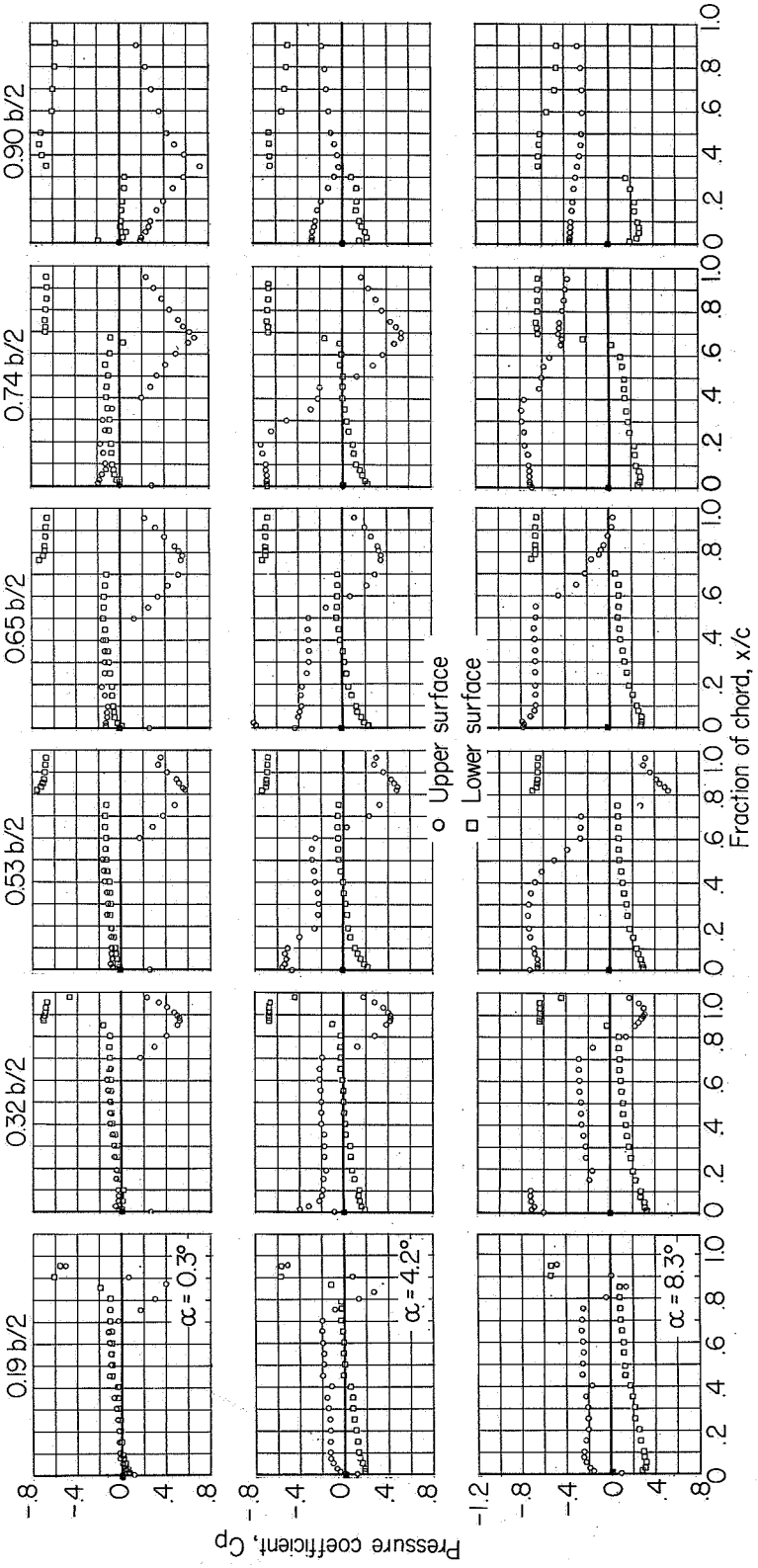

(e) M = 1.05.

Figure 10.- Continued.

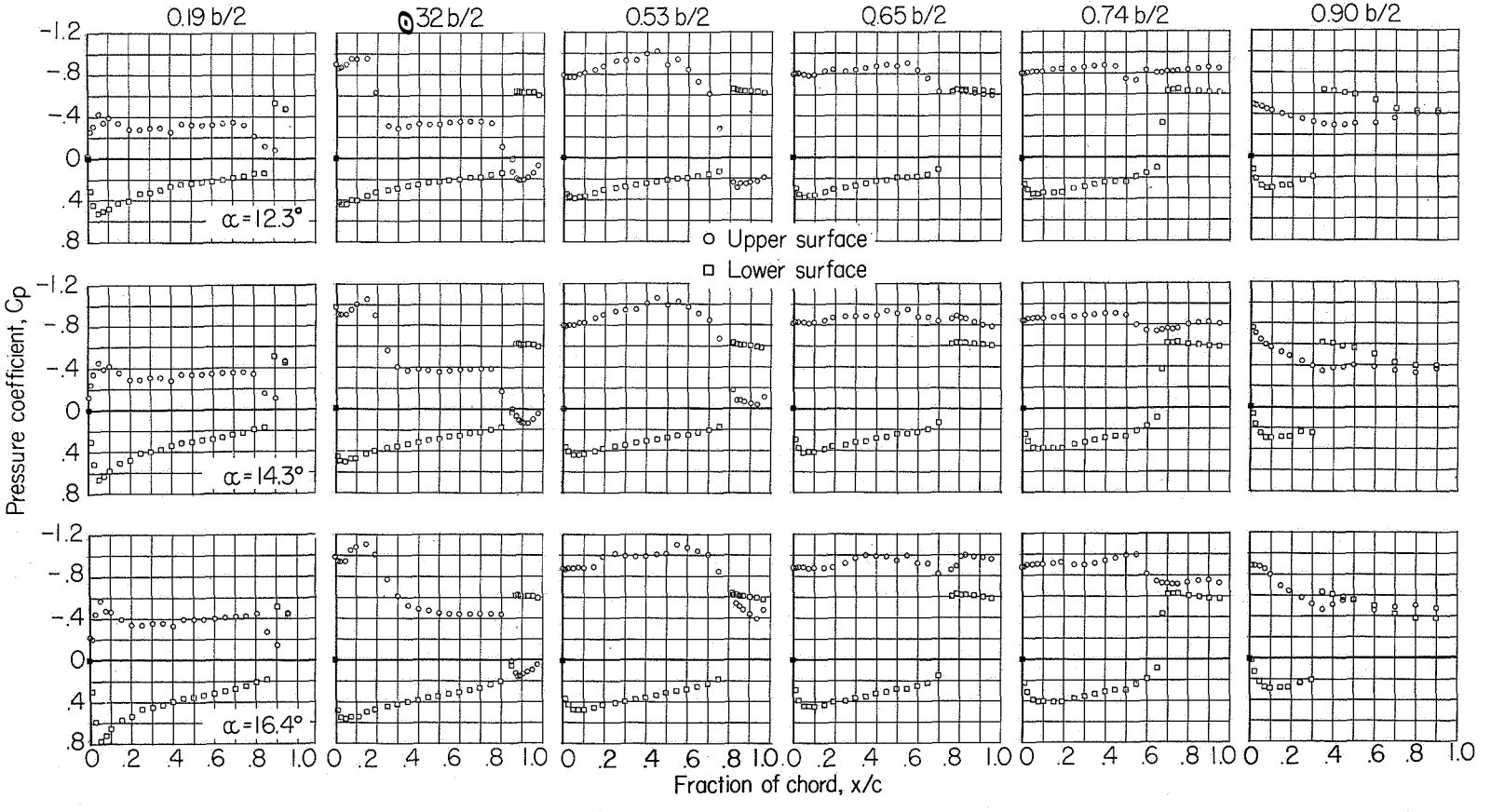

(e) Concluded.

Figure 10.- Concluded.

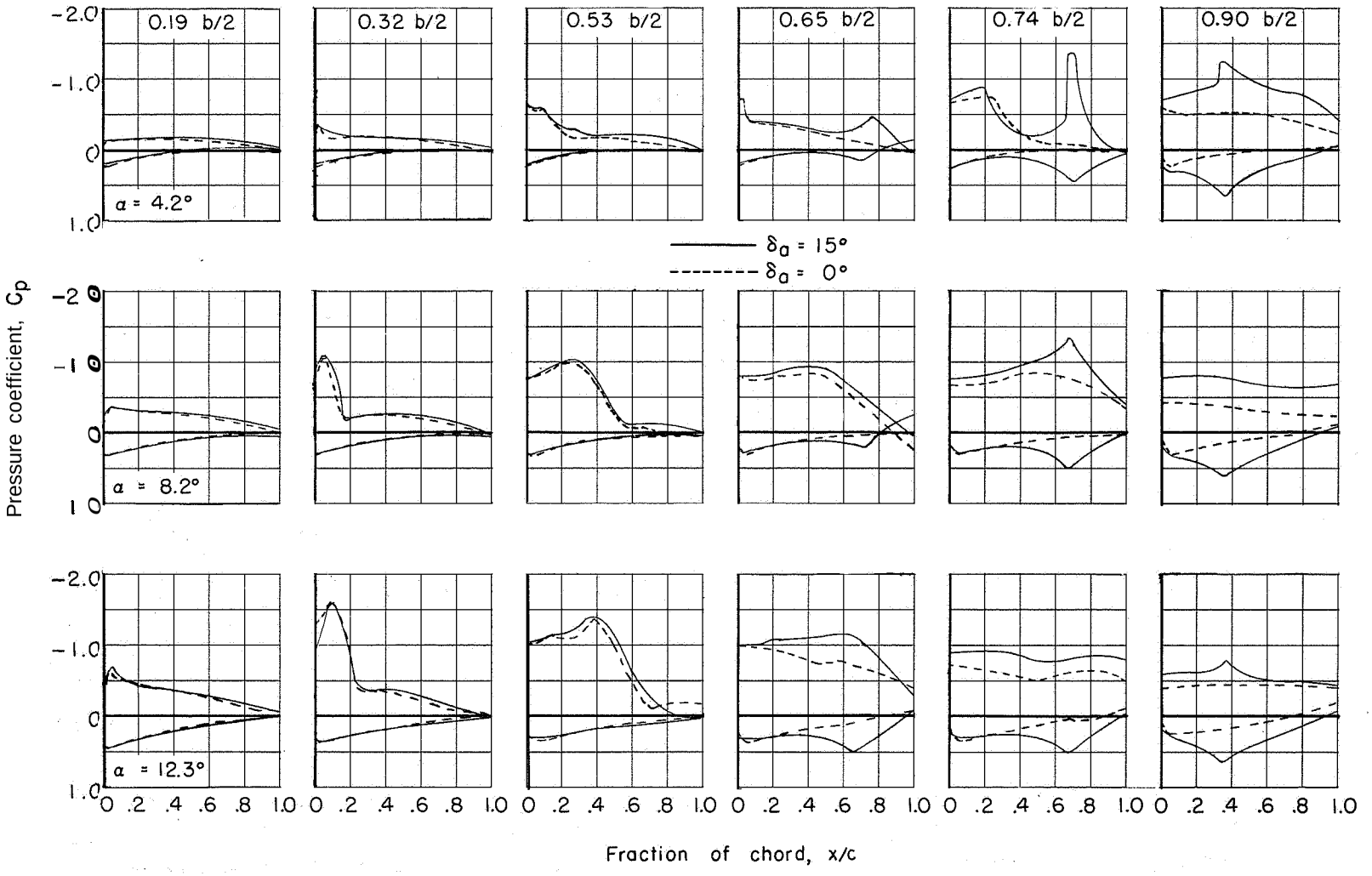

(a) M = 0.80; $C_{p,sonic}$ = -0.44.

Figure 11.- Chordwise pressure distributions with aileron deflected 15° compared with basic-wing pressure distributions.

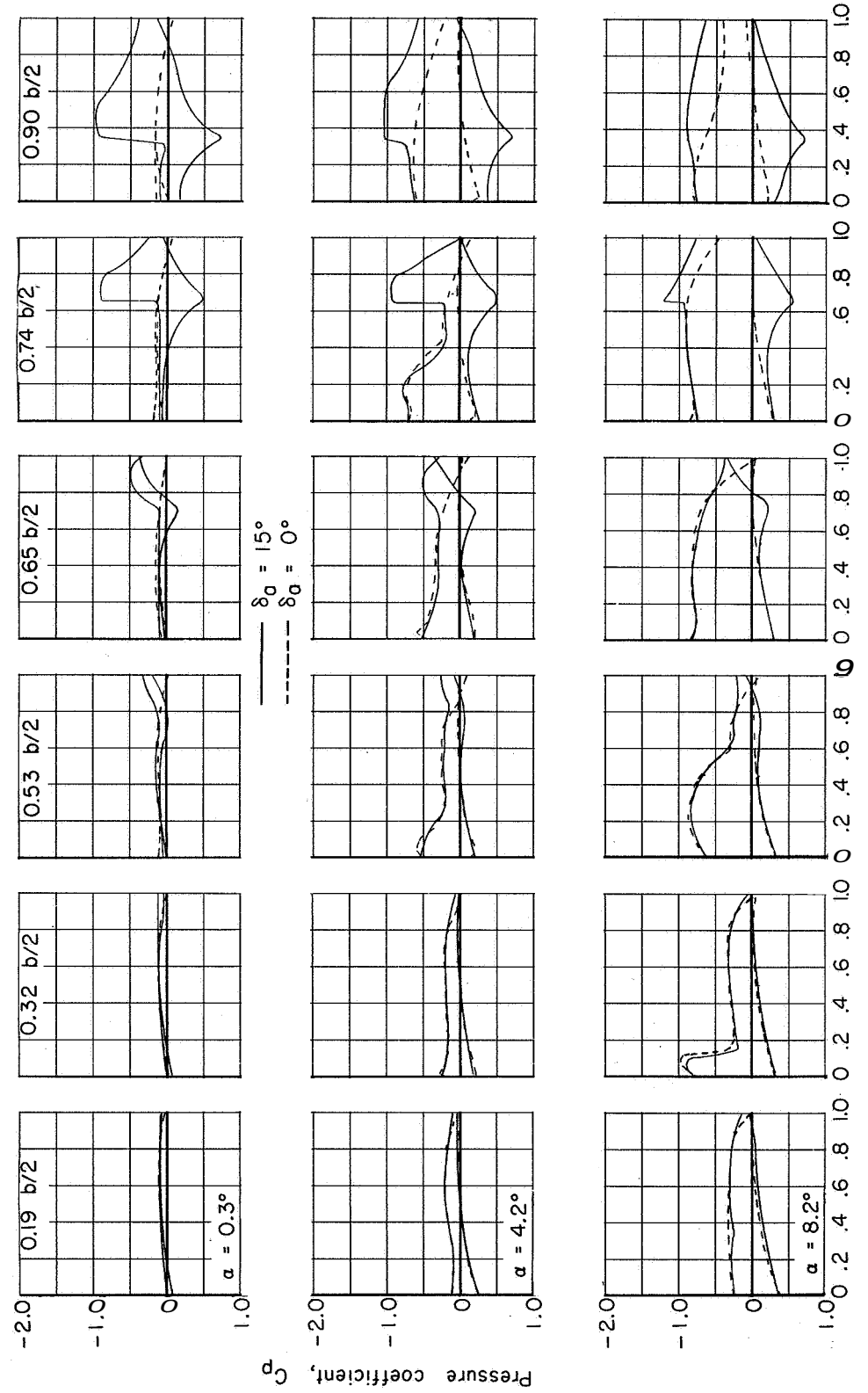

(b) M = 0.94; $C_{p,sonic}$ = -0 10

Figure 11.- Continued.

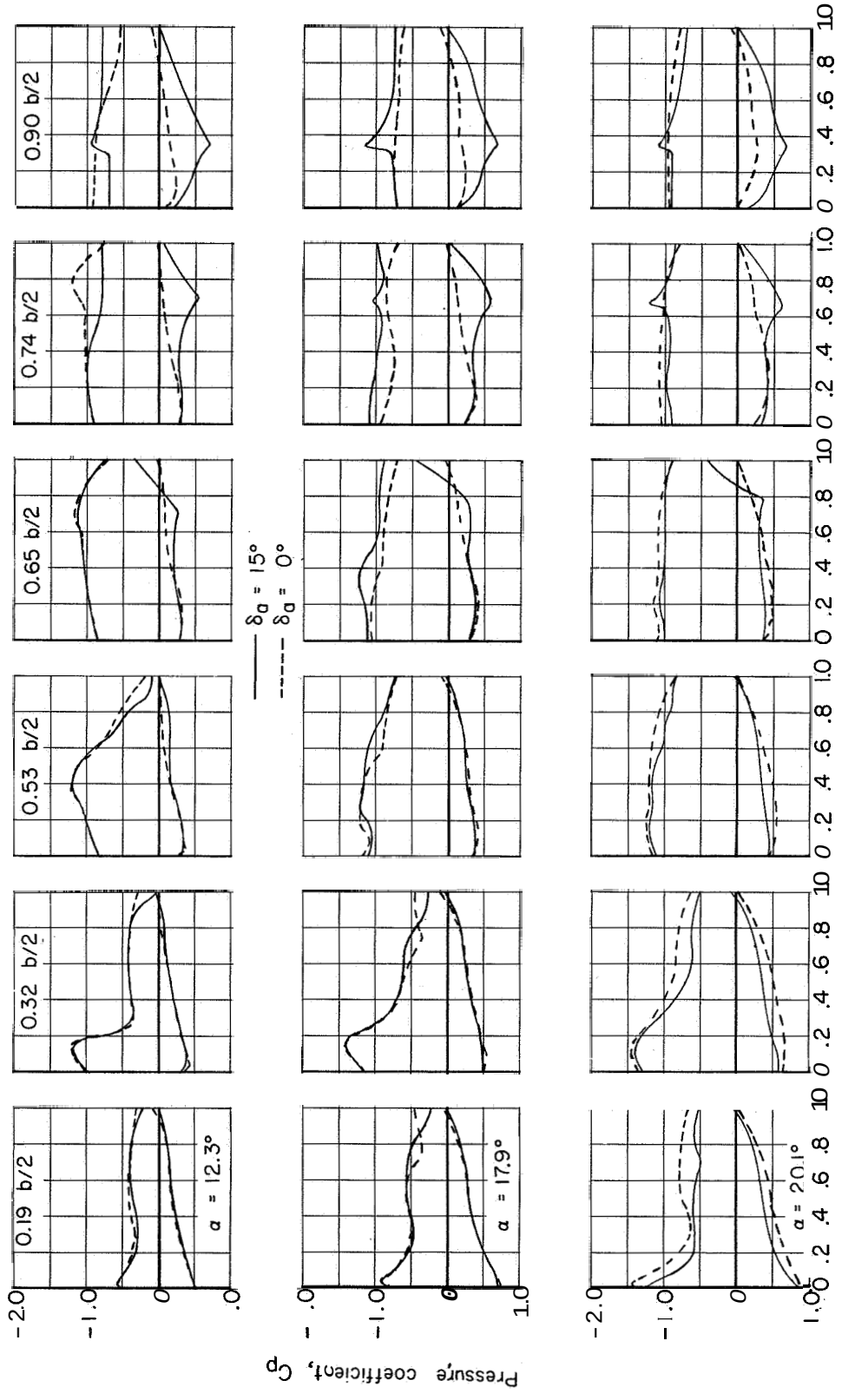

(b) Concluded.

Figure 11.- Continued.

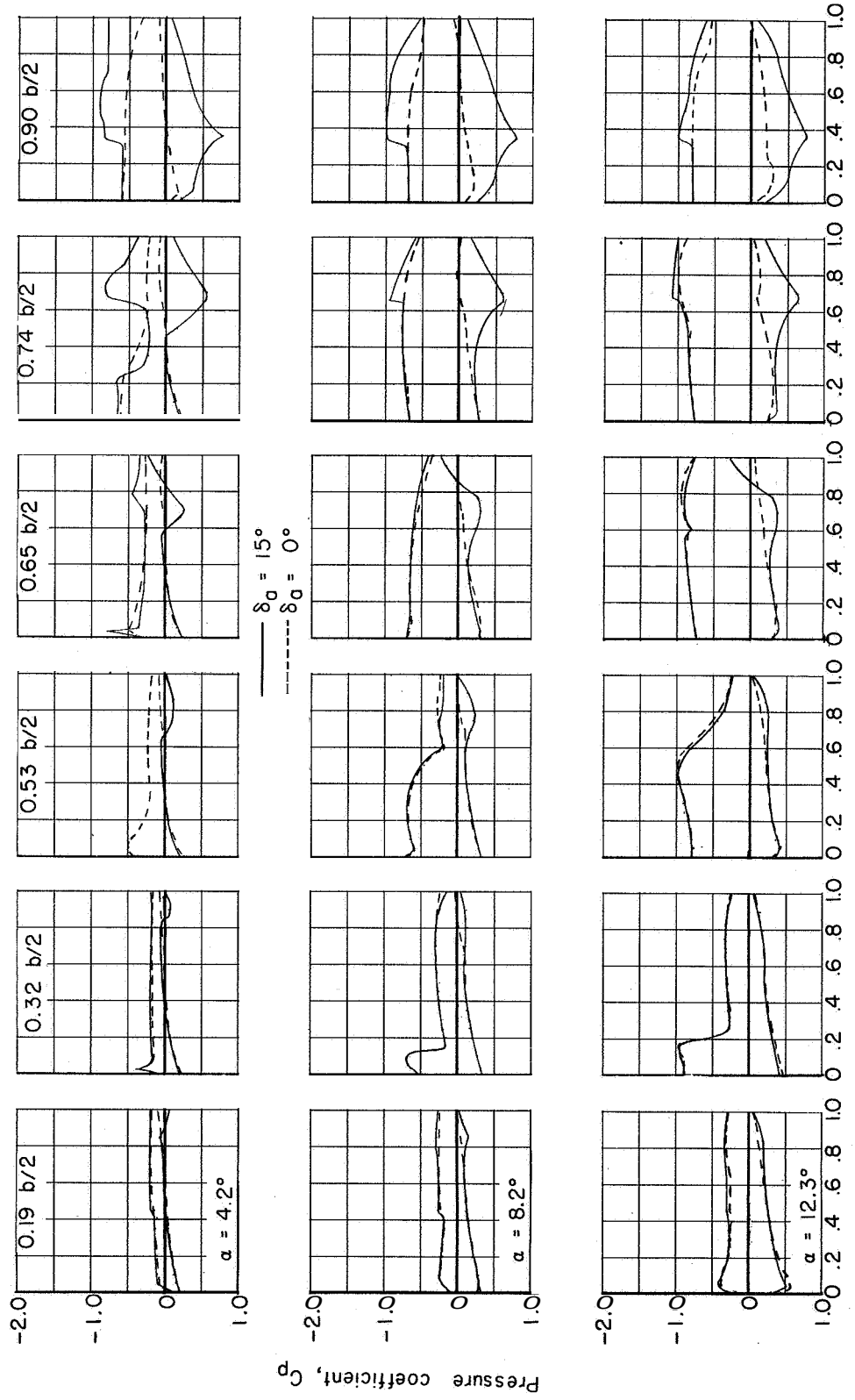

(c) M = 1.05.

Figure 11.- Concluded.

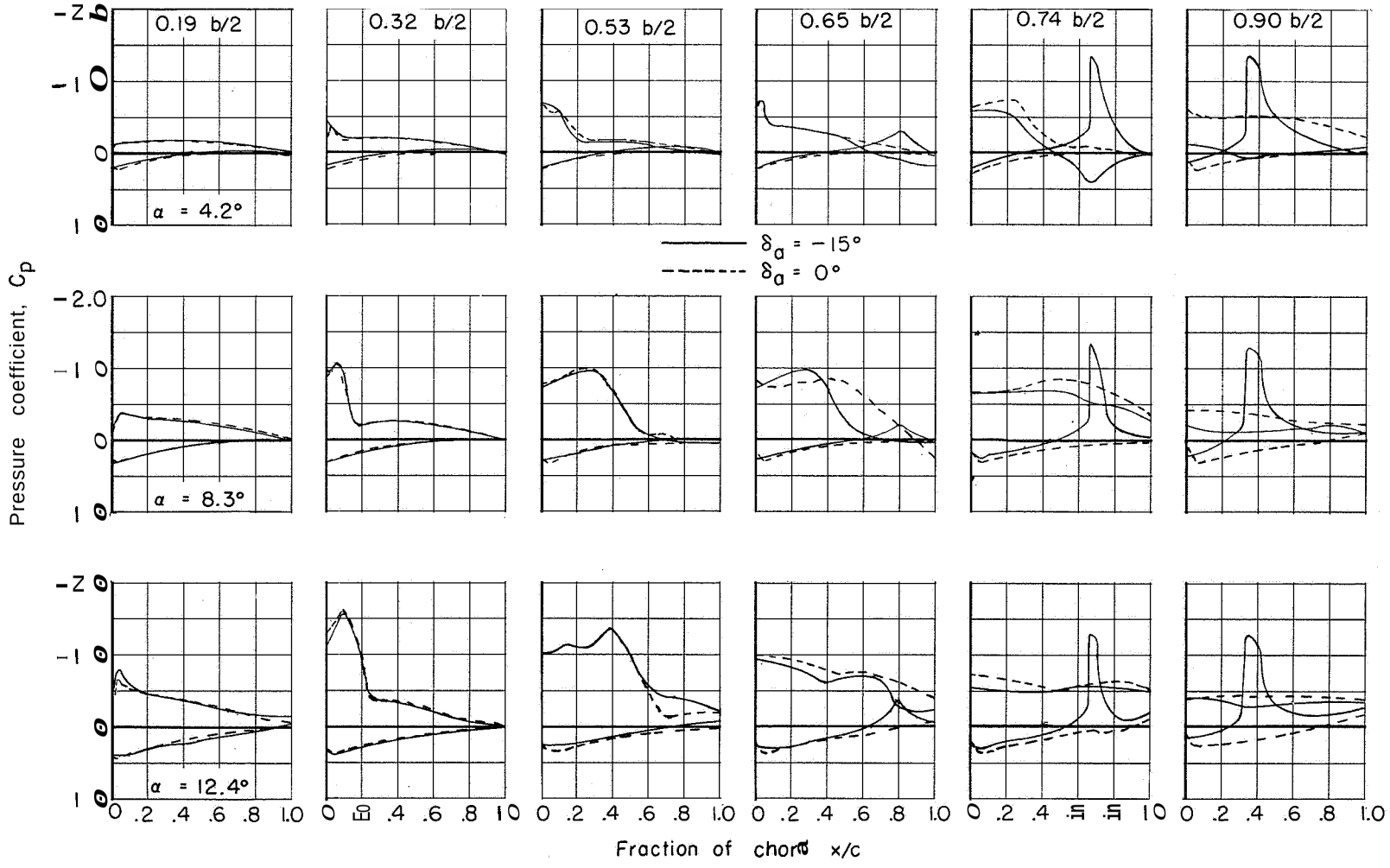

(a) M = 0.80; $C_{p,sonic}$ = -0.44.

Figure 12.- Chordwise pressure distributions with aileron deflected -15° compared with basic-wing pressure distributions.

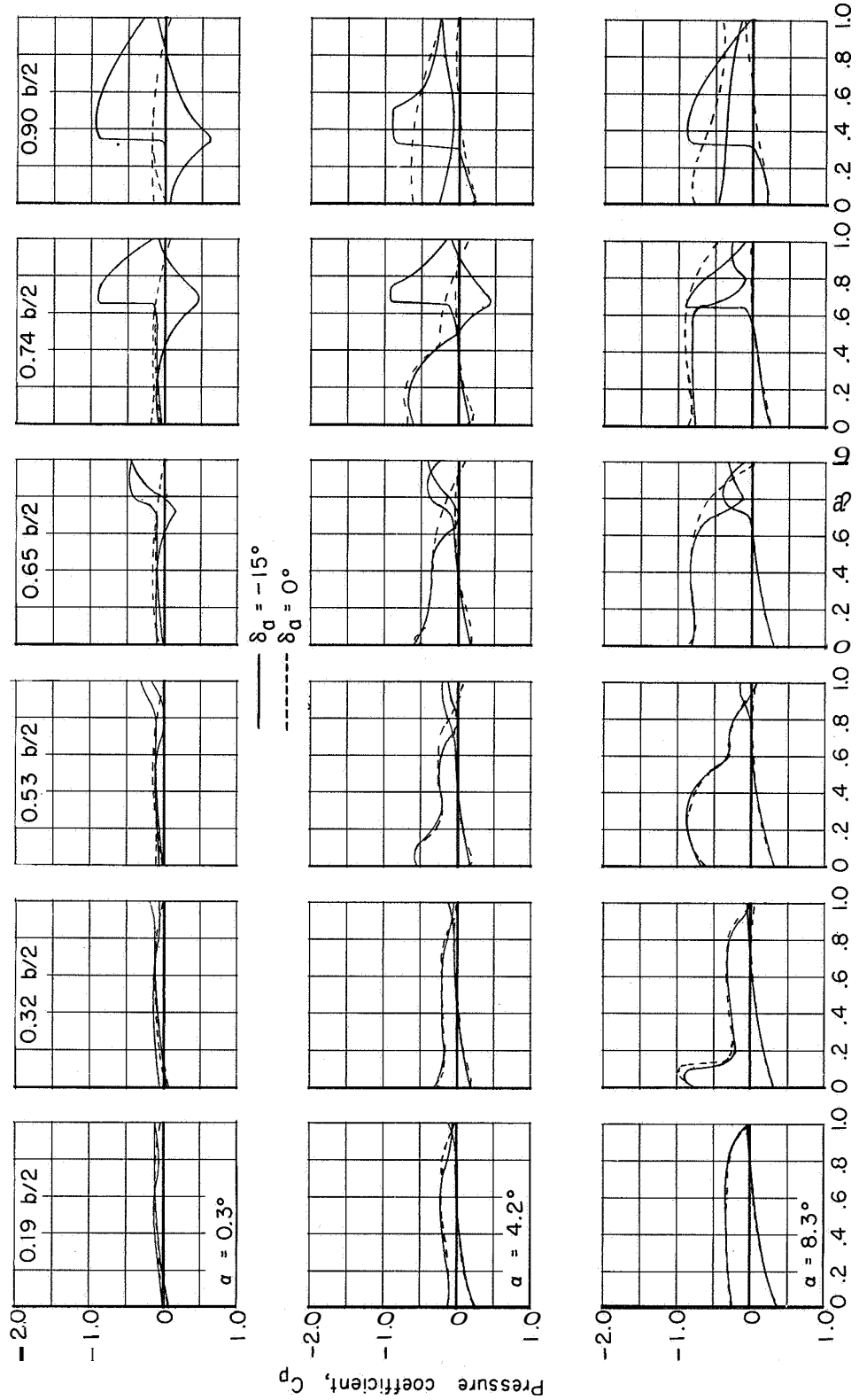

(b) M = 0.94; $C_{p,sonic}$ = -0.10.

Figure 12.- Continued.

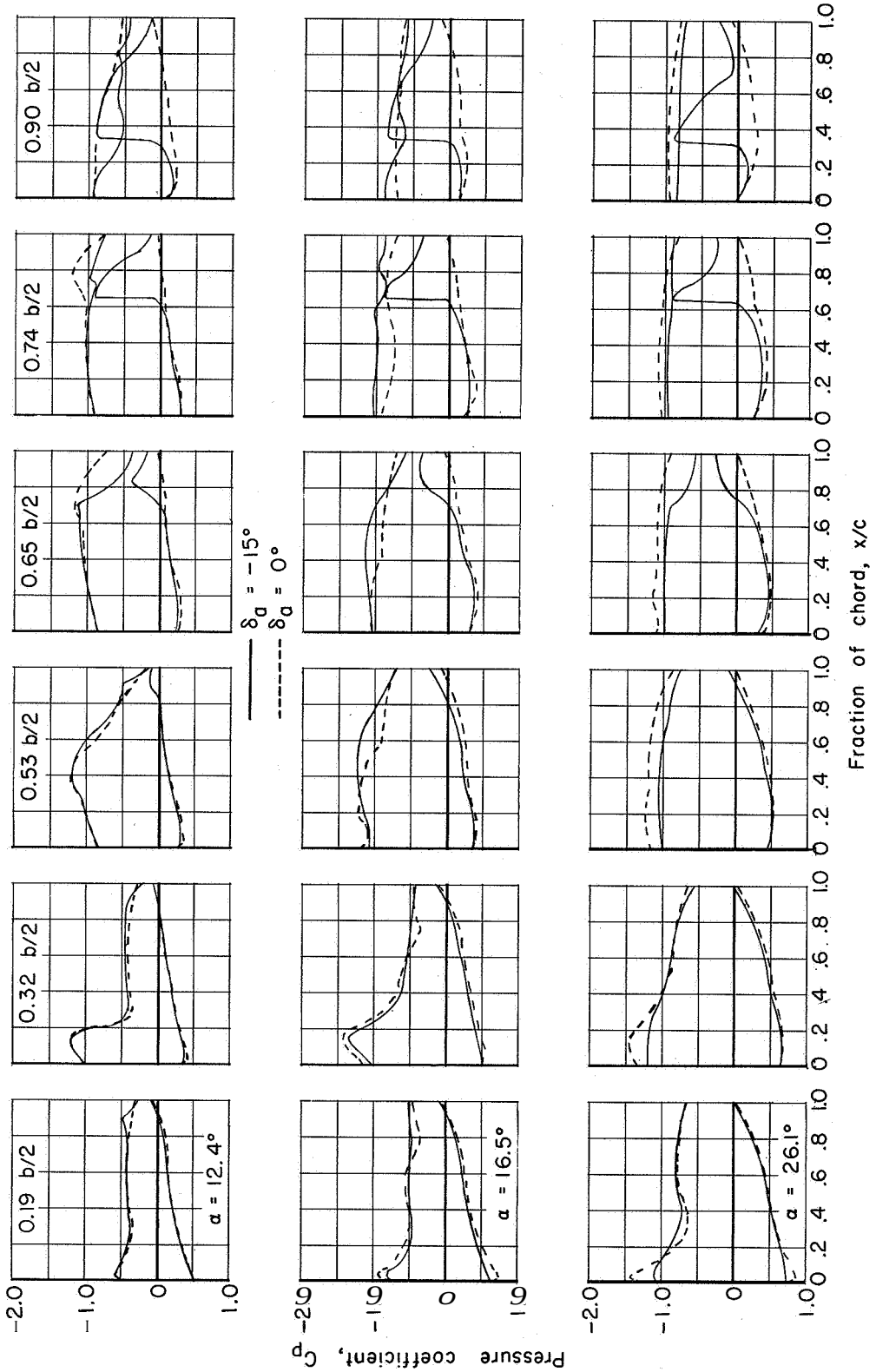

(b) Concluded.

Figure 12.- Continued.

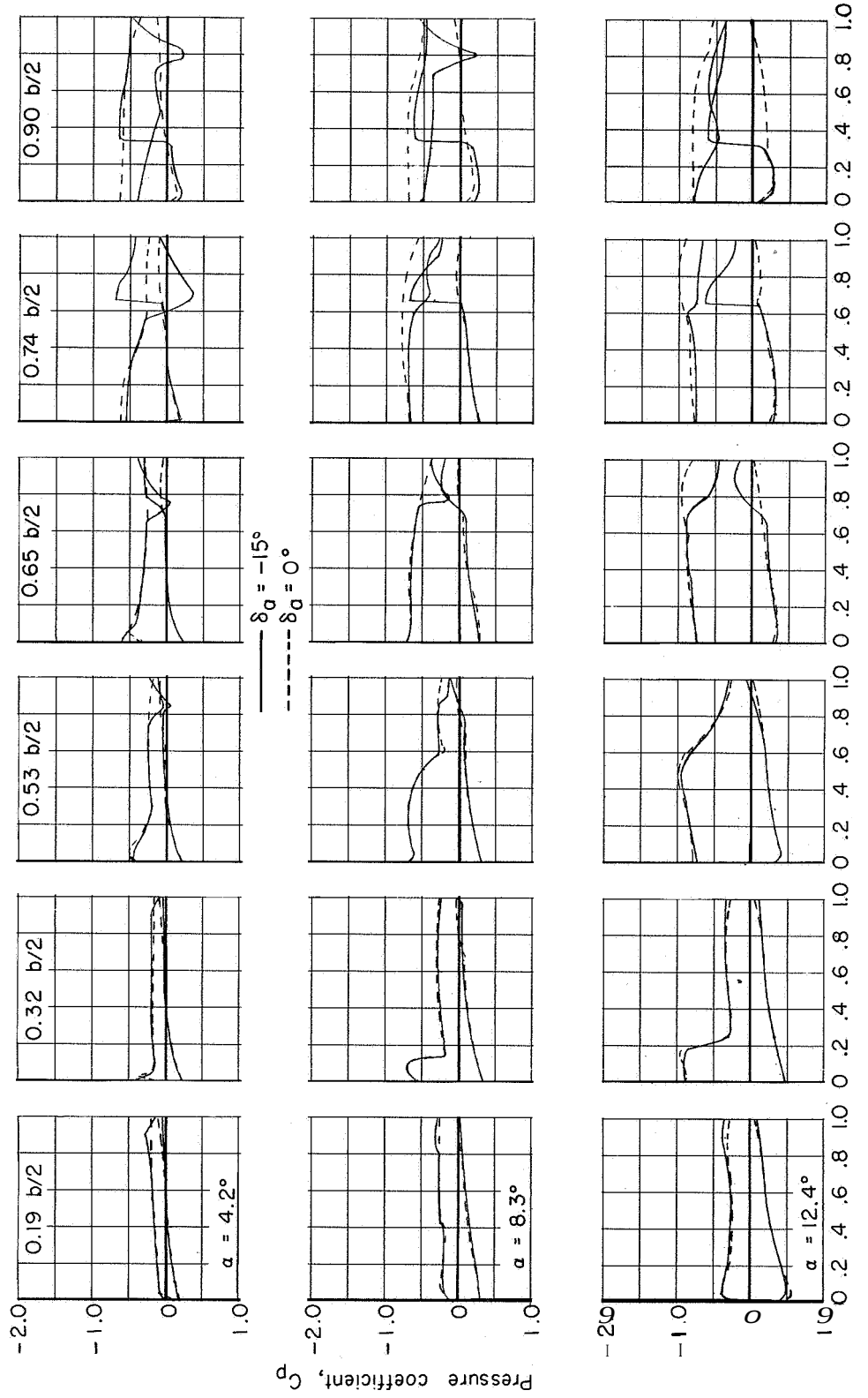

(c) M = 1.05.

Figure 12.- Concluded.

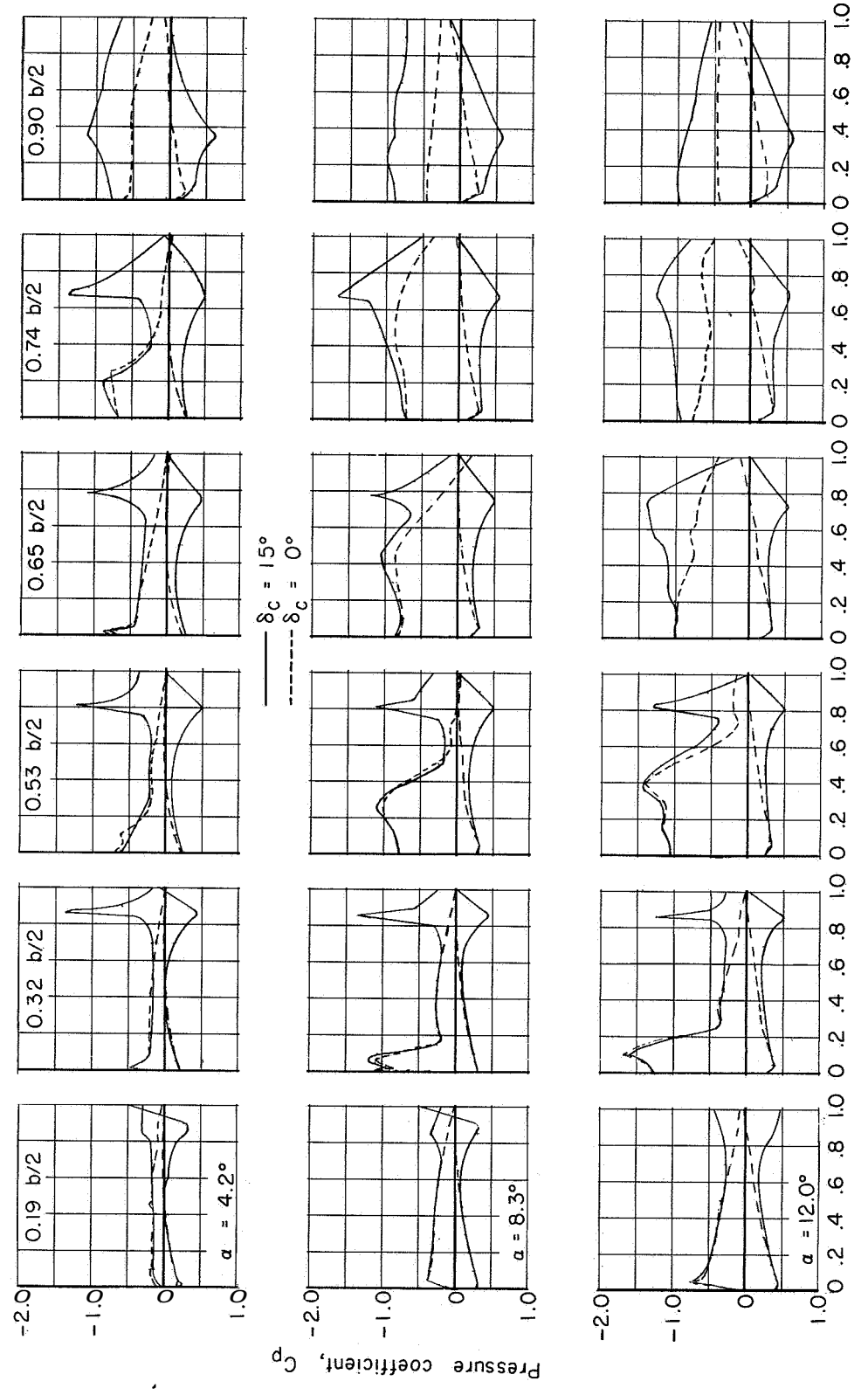

(a) M = 0.80; $C_{p,sonic}$ = -0.44.

Figure 13.- Chordwise pressure distributions with combined control deflected 15° compared with basic-wing pressure distributions.

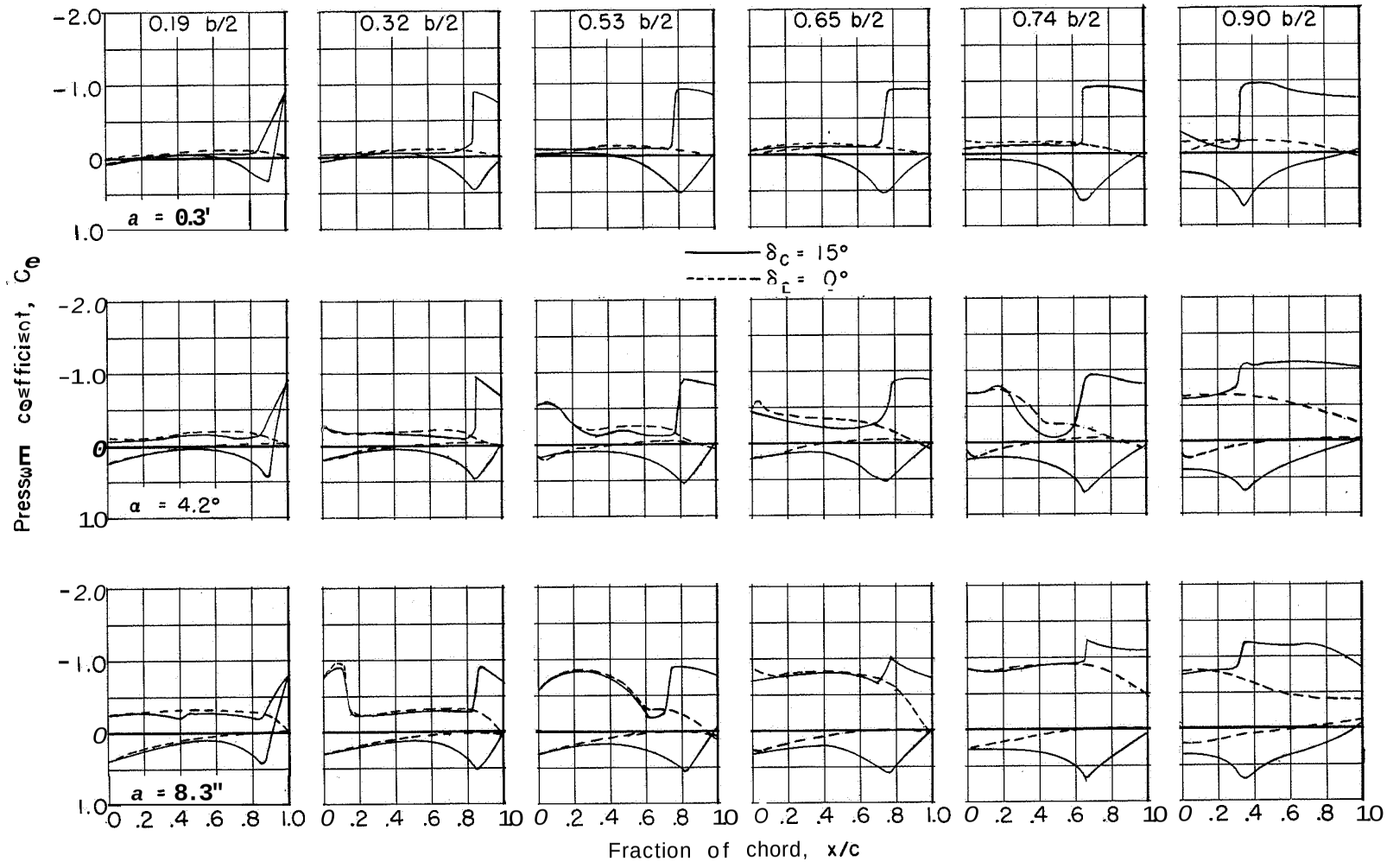

(b) M = 0.94; $C_{p,sonic}$ = -0.10.

Figure 13.- Continued.

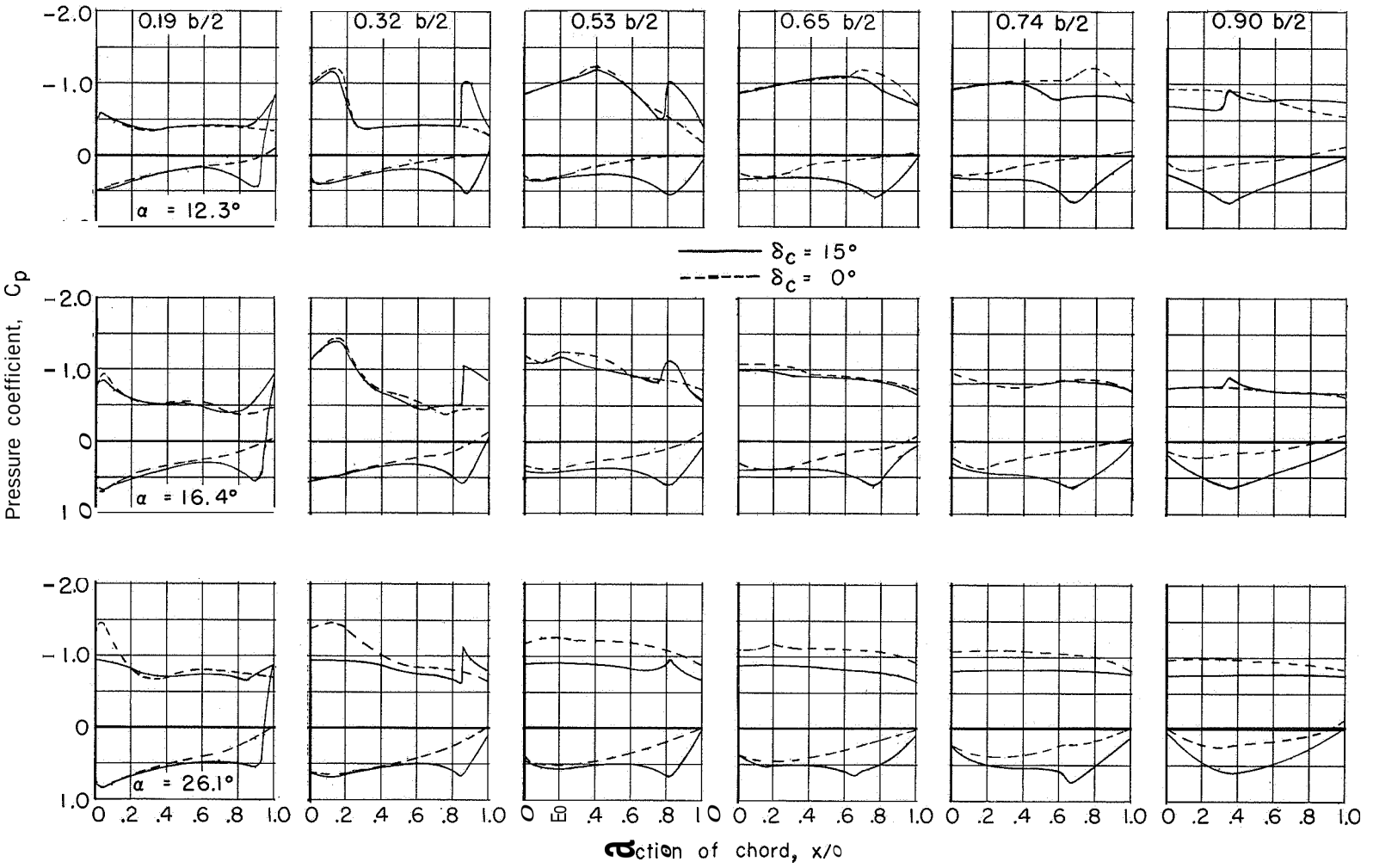

(b) Concluded.

Figure 13.- Continued.

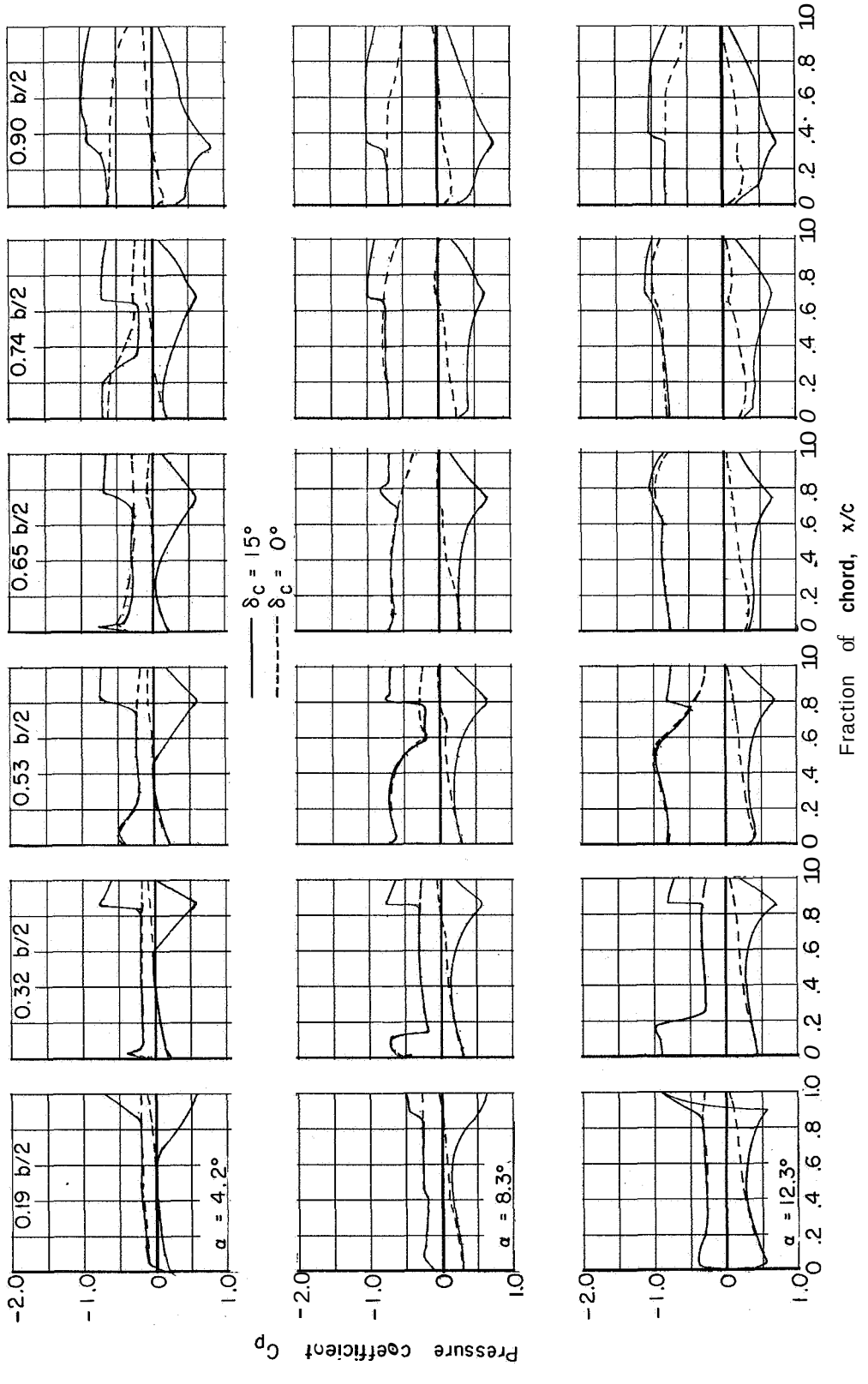

(c) M = 1.05.

Figure 13.- Concluded.

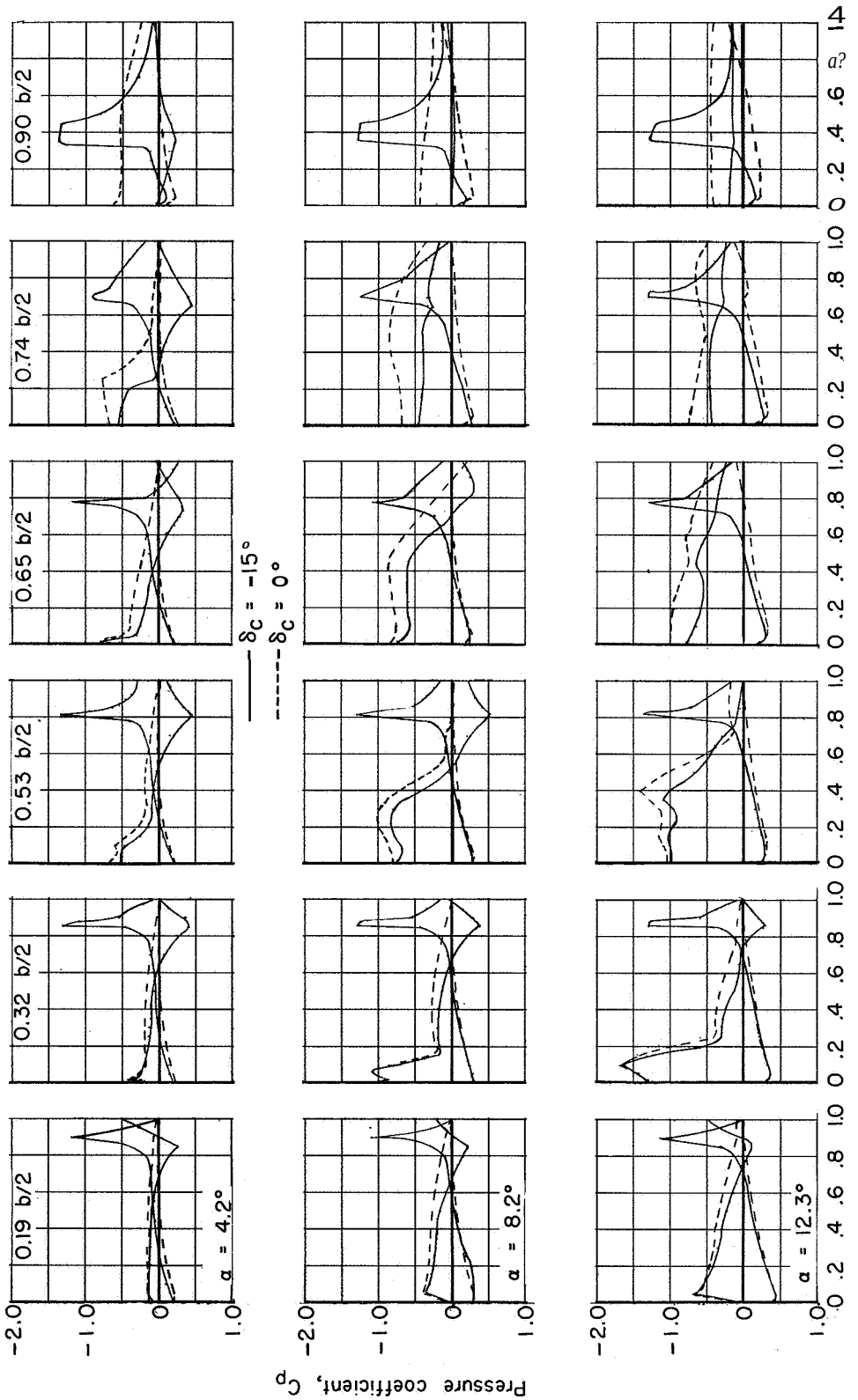

(a) M = 0.80; $C_{p,sonic}$ = -0.44.

Figure 14.- Chordwise pressure distributions with combined control deflected -15° compared with basic-wing pressure distributions.

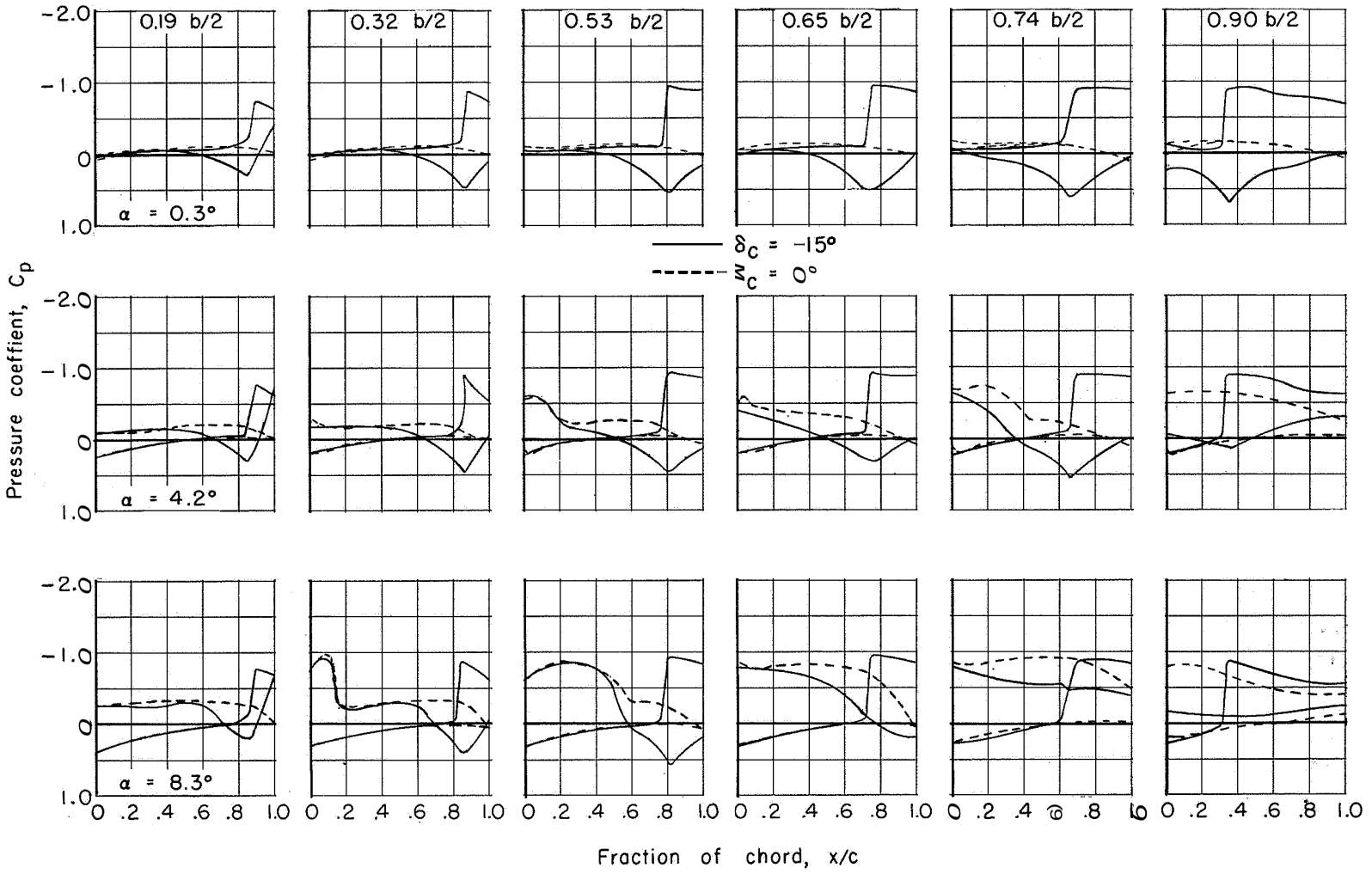

(b) M = 0.94; $C_{p,sonic}$ = -0.10.

Figure 14.- Continued.

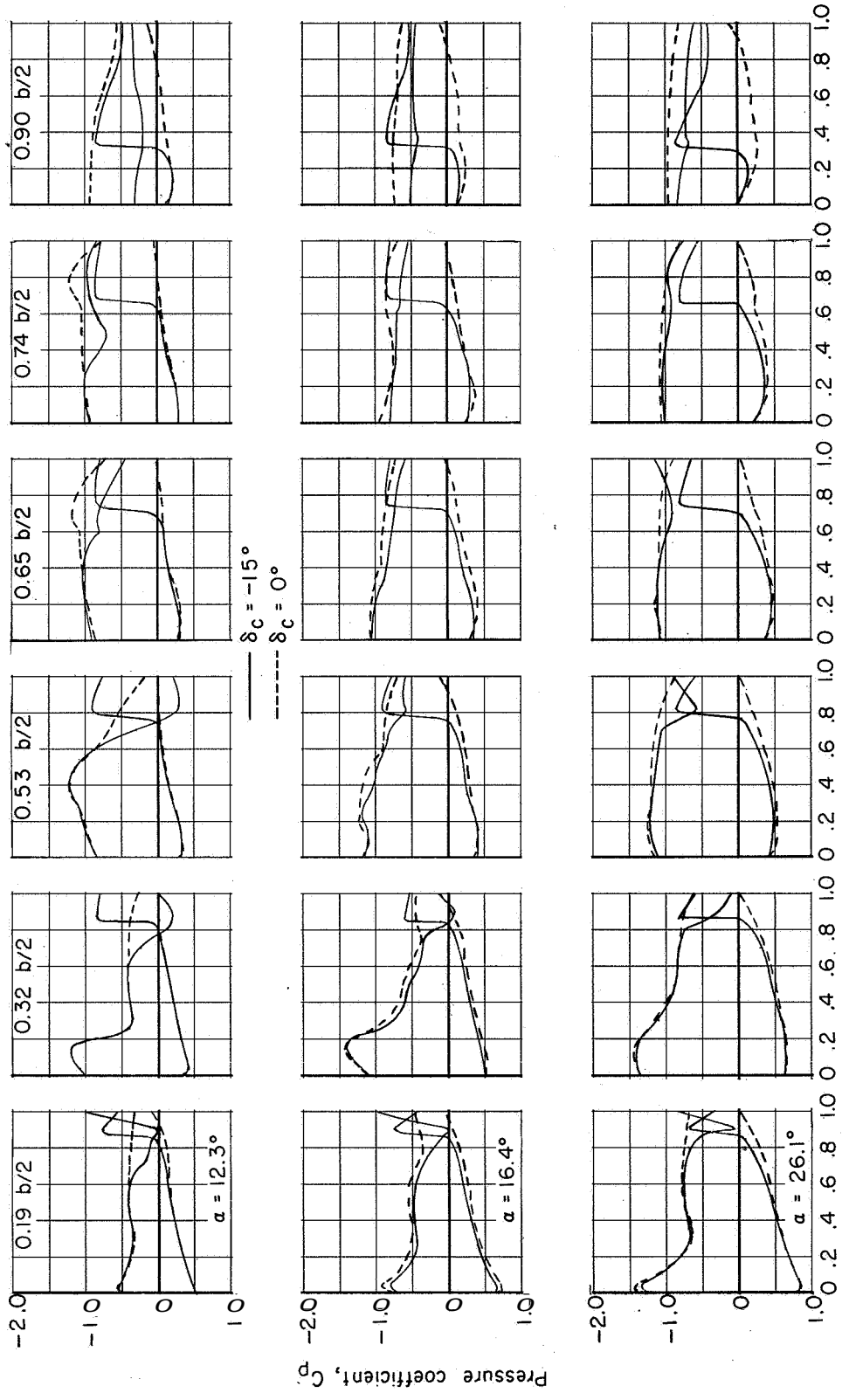

(b) Concluded.

Figure 14.- Continued.

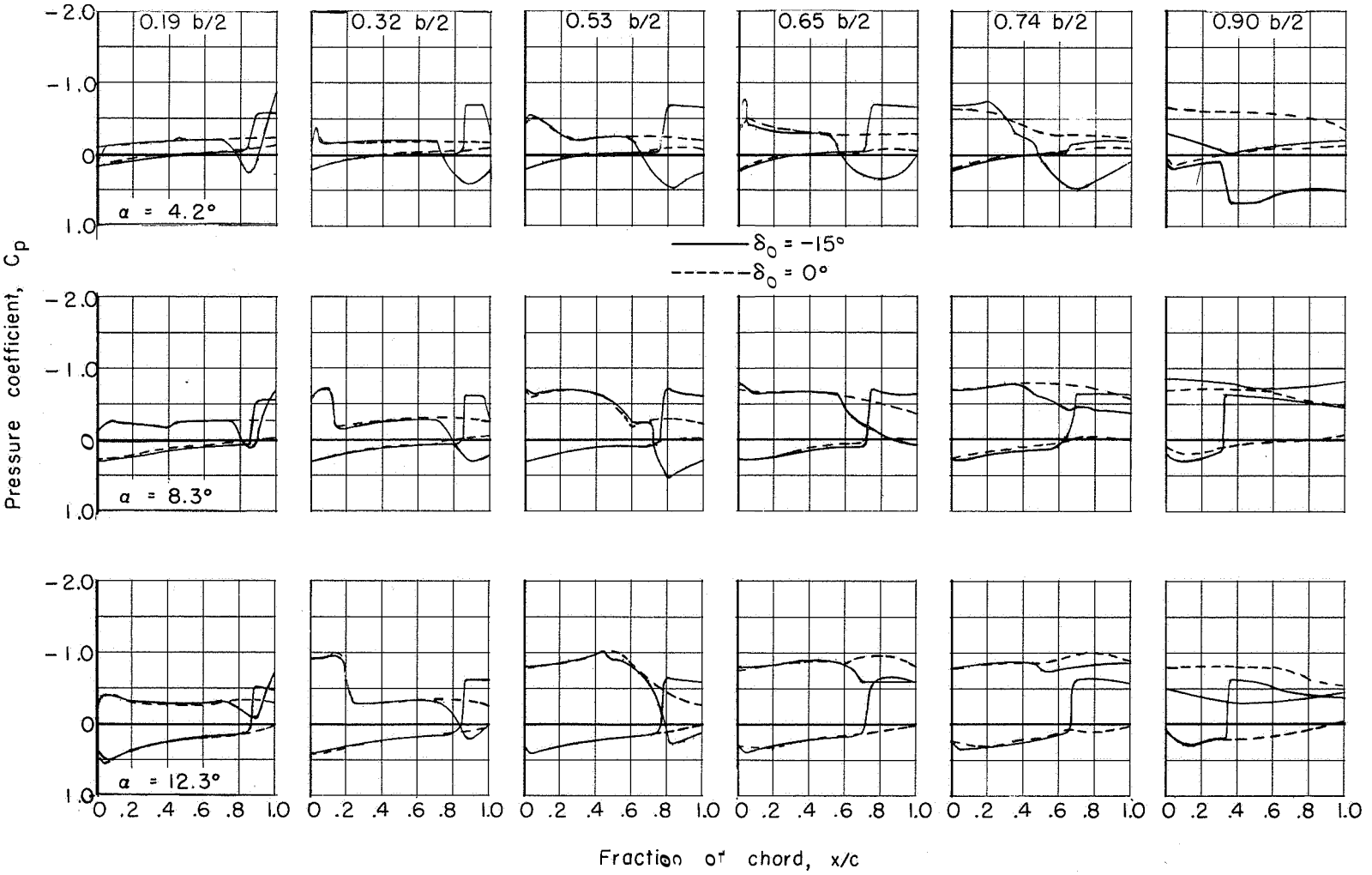

(c) M = 1.05.

Figure 14.- Concluded.

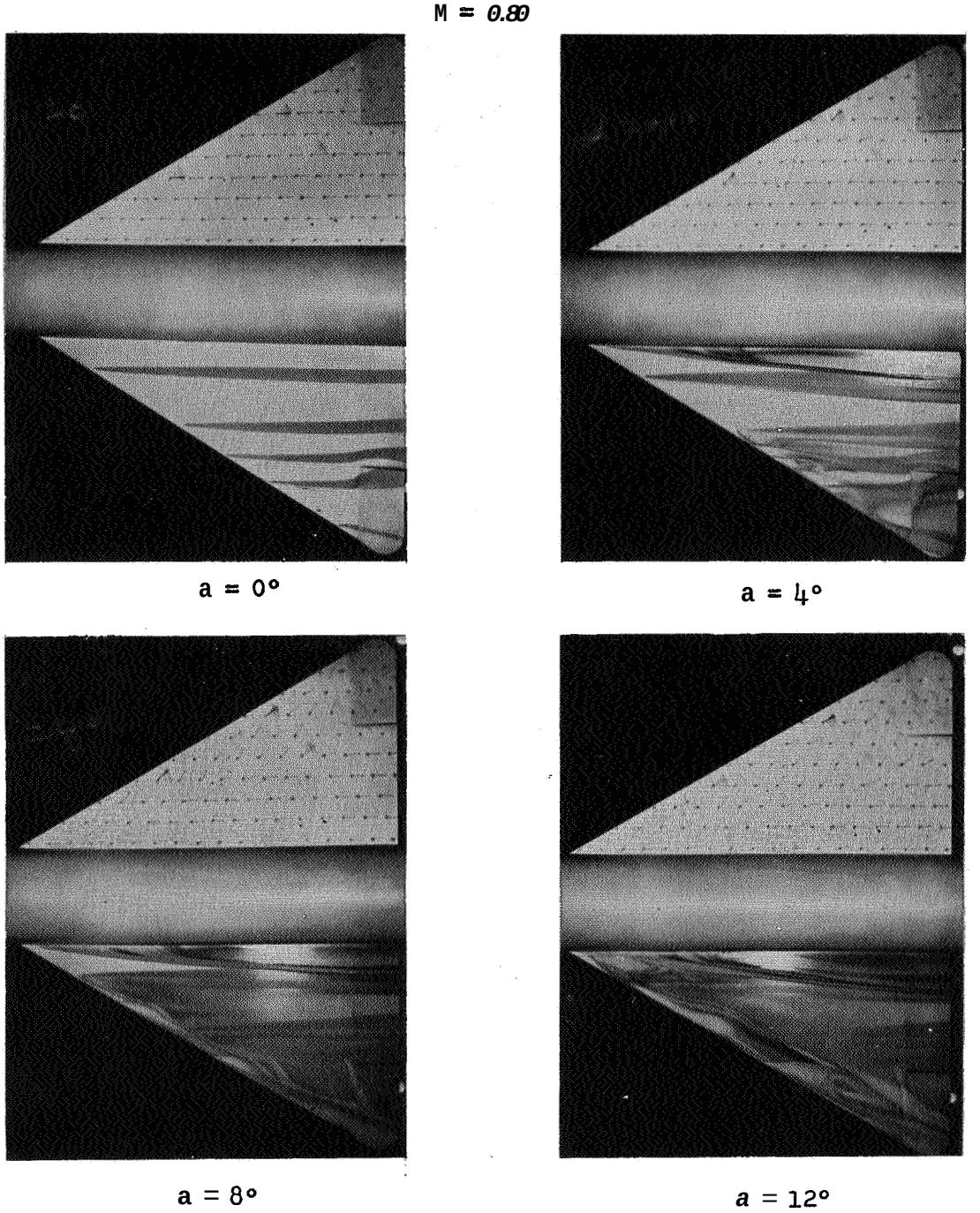

(a) M = 0.80. L-59-5000

Figure 15.- Boundary-layer flow patterns on a 60° delta wing with both ailerons deflected -15°.

M = 0.94

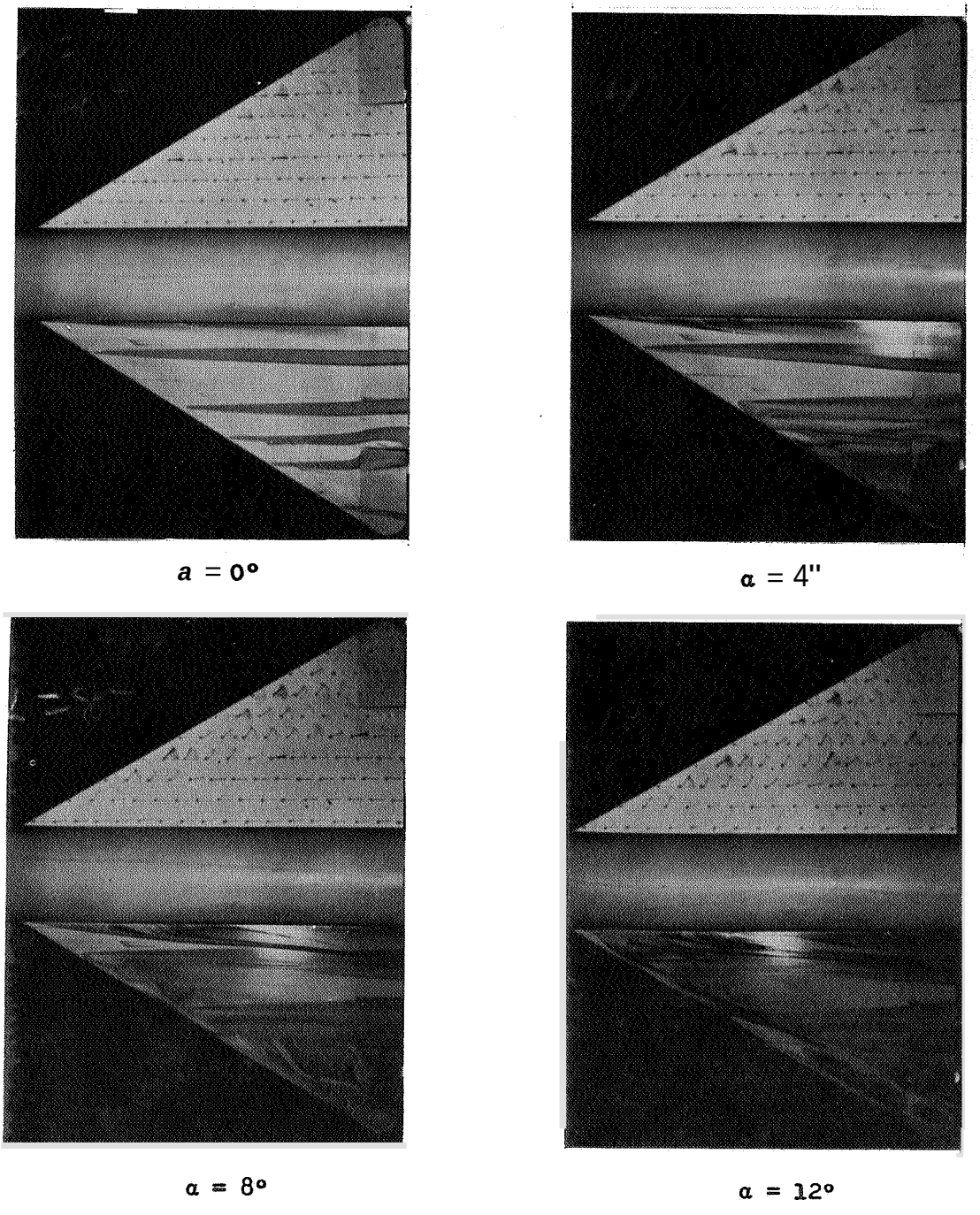

L-506

(b) M = 0.94. L-59-5001

Figure 15.- **Continued.**

M = 1.05

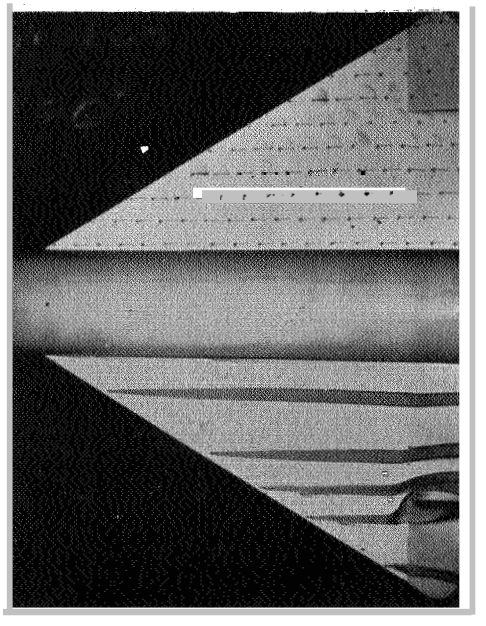

a = 0°

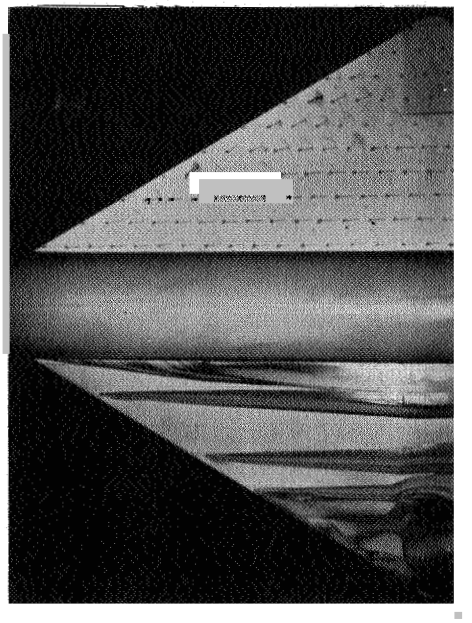

a = 4"

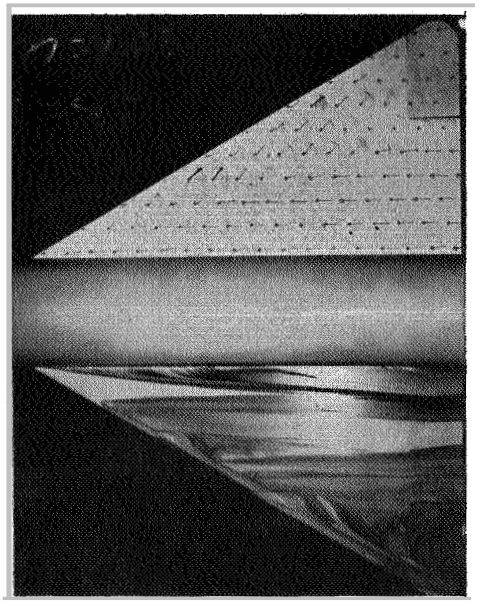

a = 8°

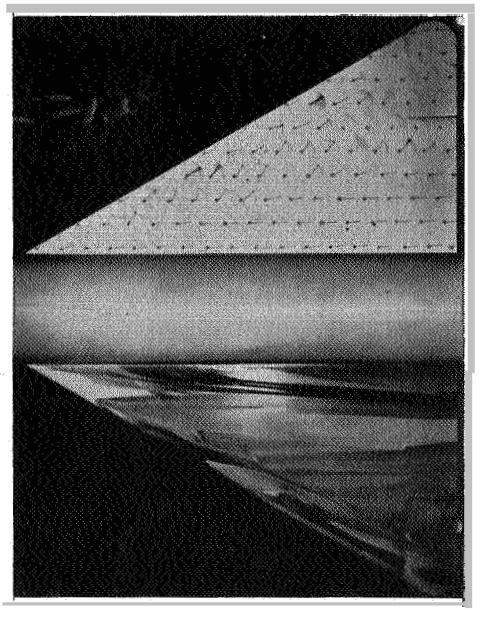

a = 12°

(c) M = 1.05. L-59-5002

Figure 15.- Concluded.

L-506

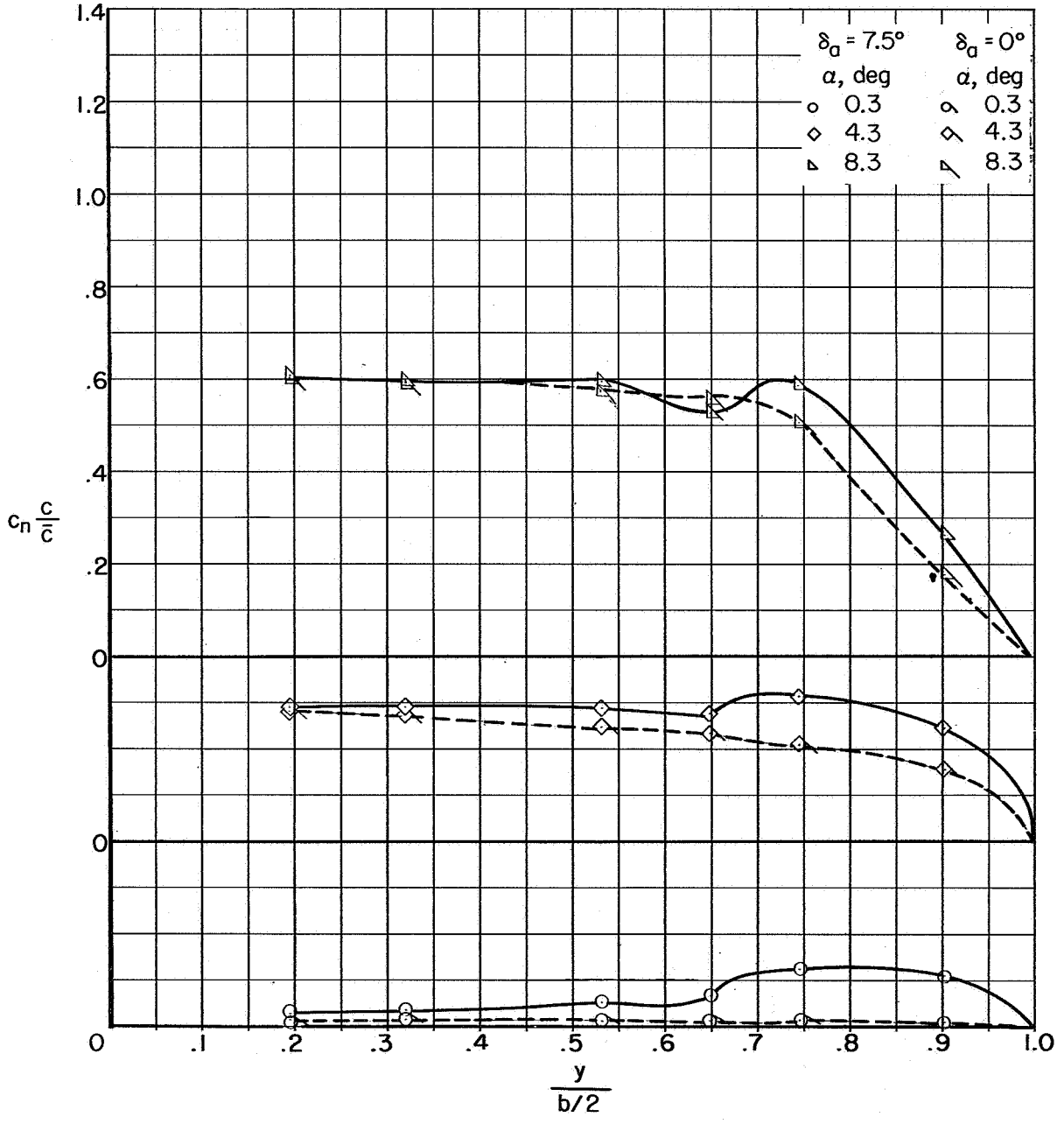

(a) M = 0.94; $\delta_a = 0^\circ$ and $\delta_a = 7.5^\circ$.

Figure 16.- Variation of section normal-load parameter with wing semispan.

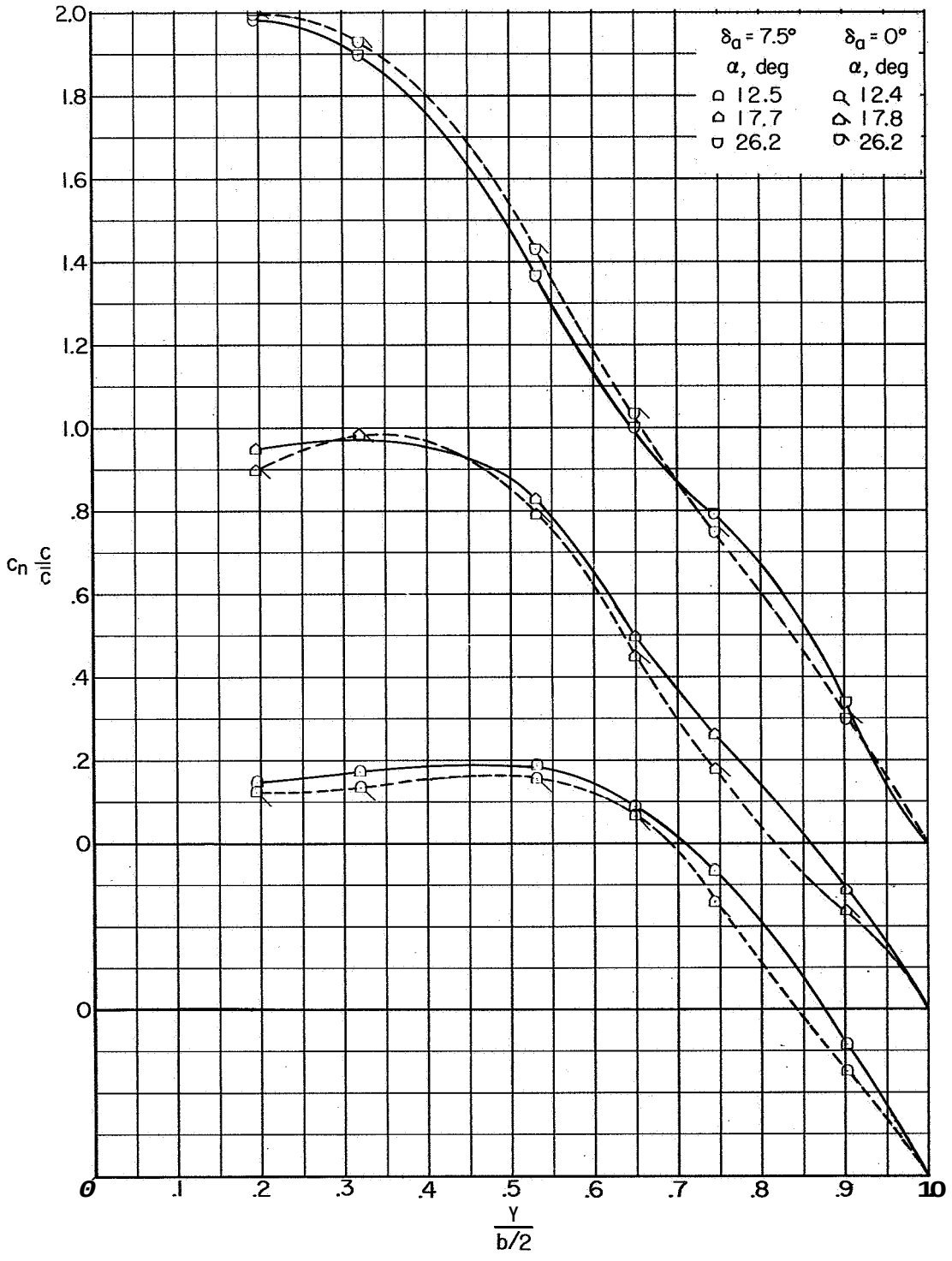

(a) Concluded.

Figure 16.- Concluded.

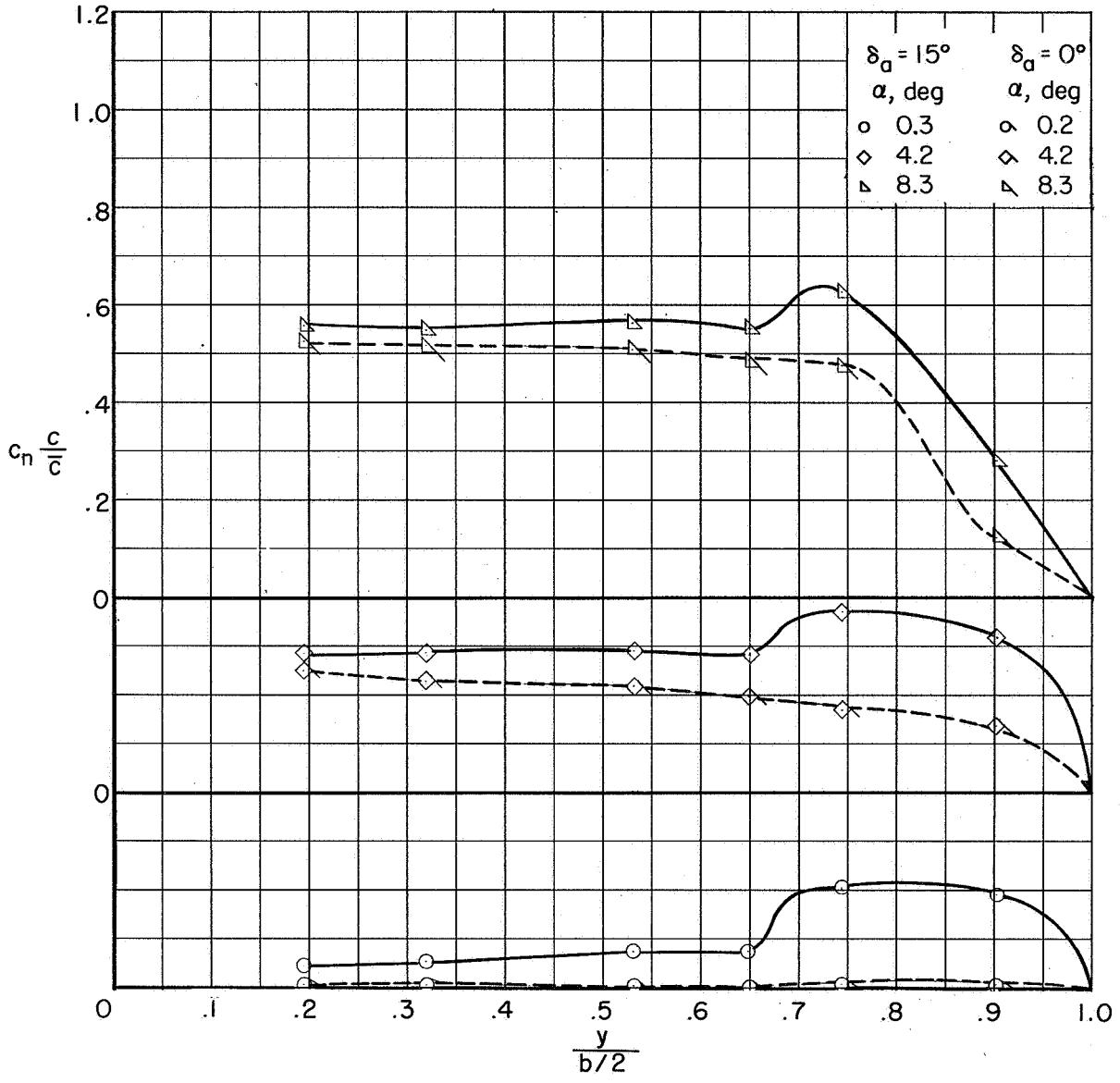

(a) M = 0.80; $\delta_a = 0^\circ$ and $\delta_a = 15^\circ$.

Figure 17.- Variation of section normal-load parameter with wing semispan.

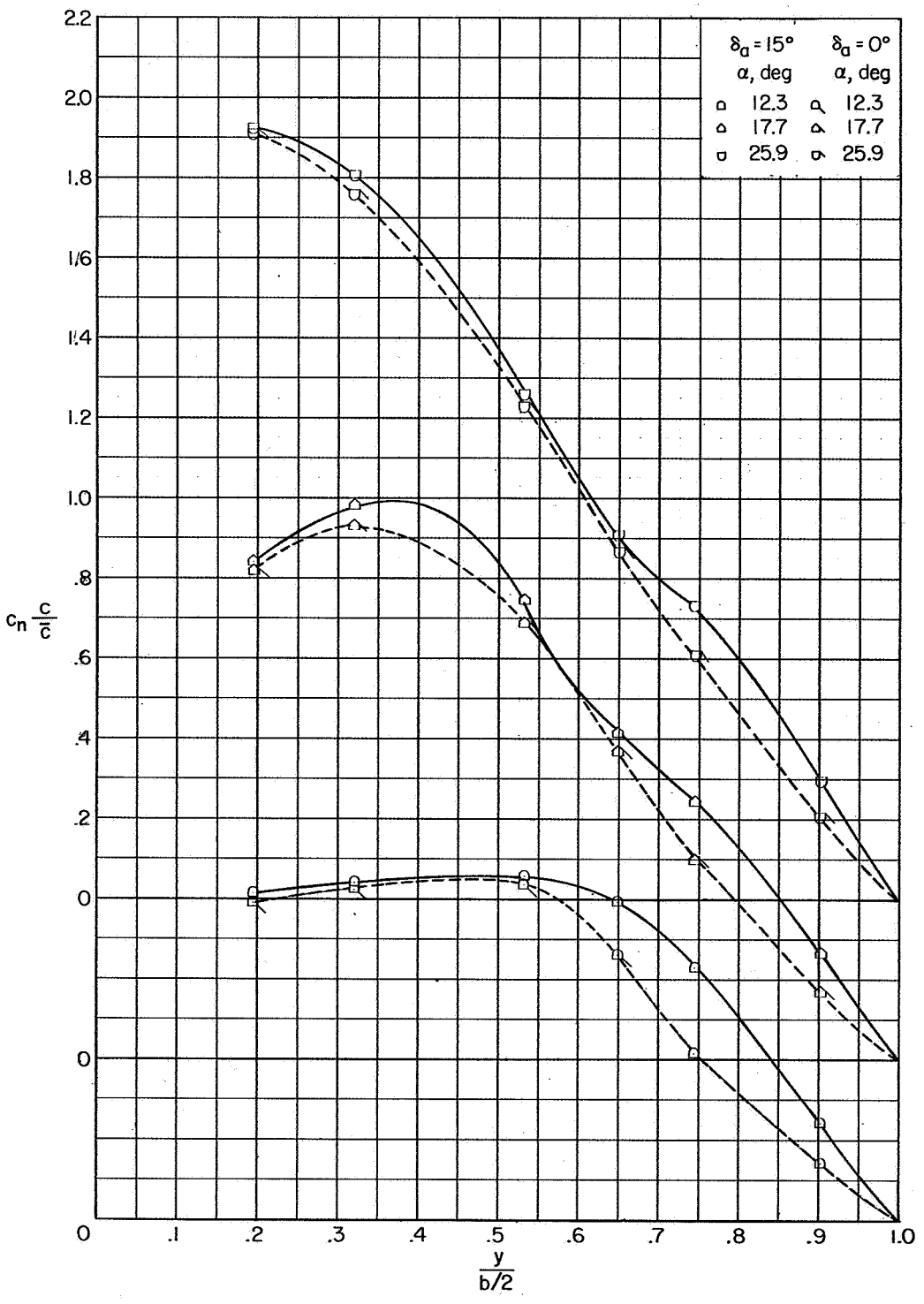

(a) Concluded.

Figure 17.- Continued.

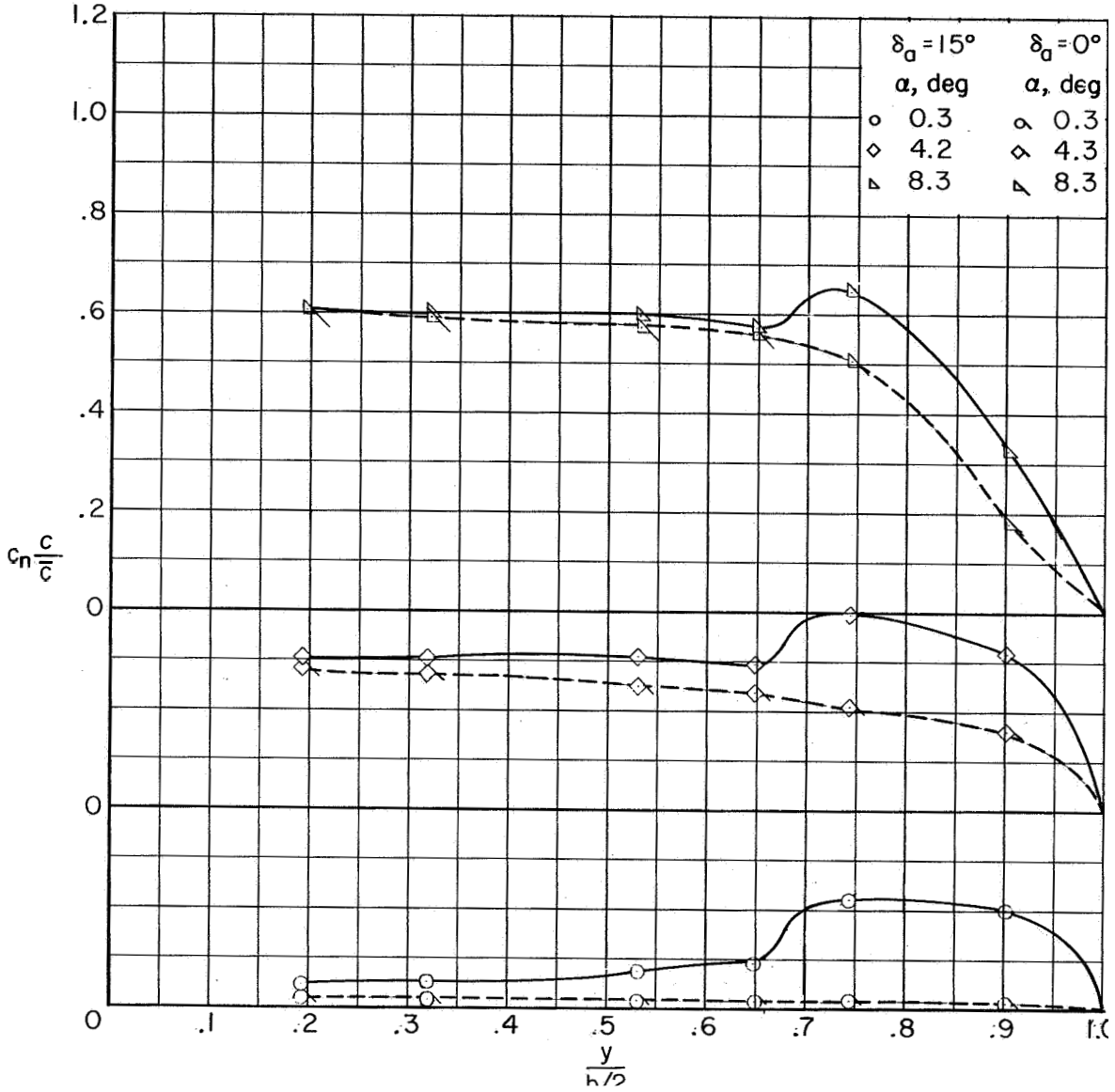

I-506

(b) M = 0.94; $\delta_a = 0°$ and $\delta_a = 15°$.

Figure 17.- Continued.

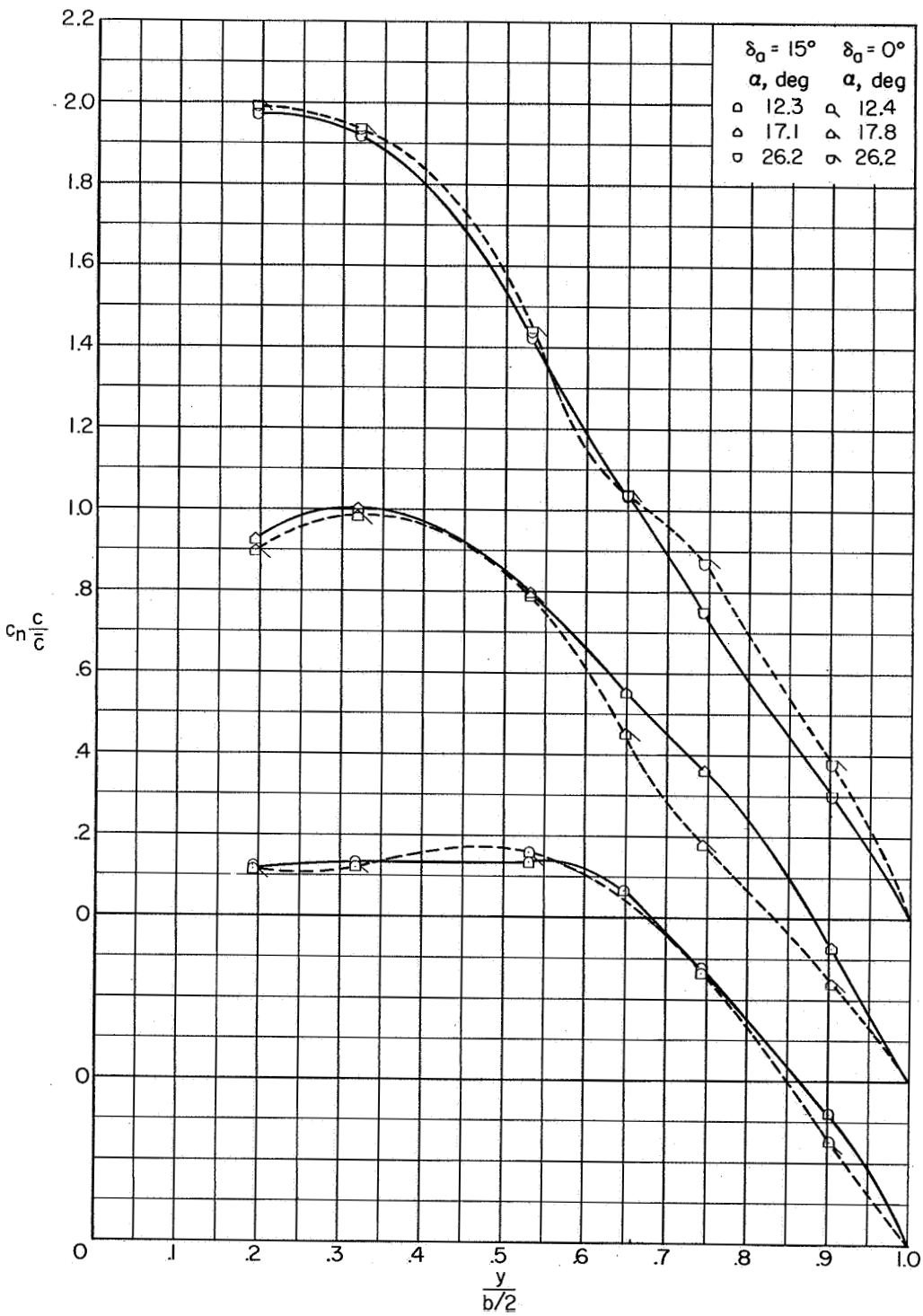

(b) Concluded.

Figure 17.- Continued.

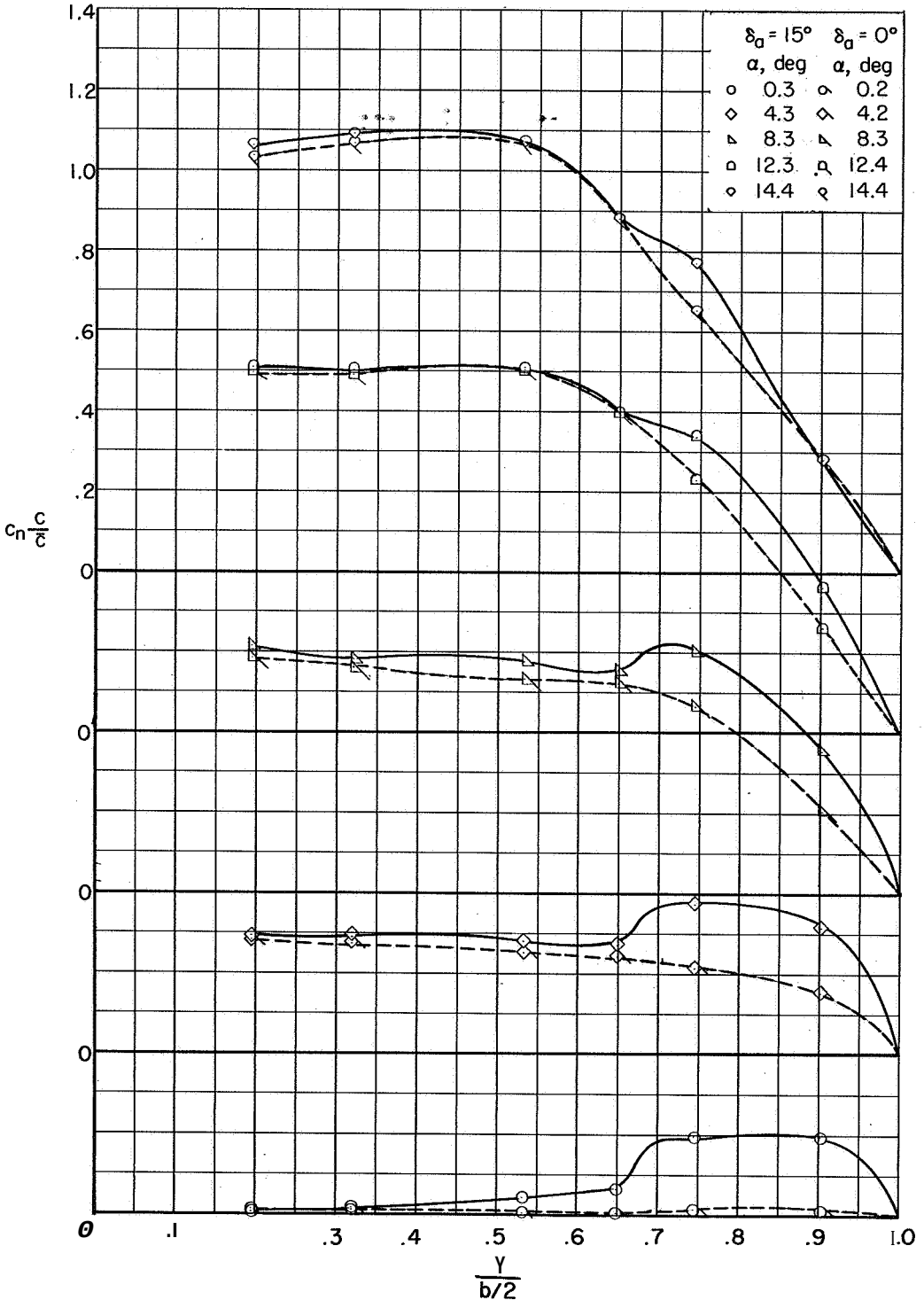

(c) M = 1.05; $\delta_a = 0^\circ$ and $\delta_a = 15^\circ$.

Figure 17.- Concluded.

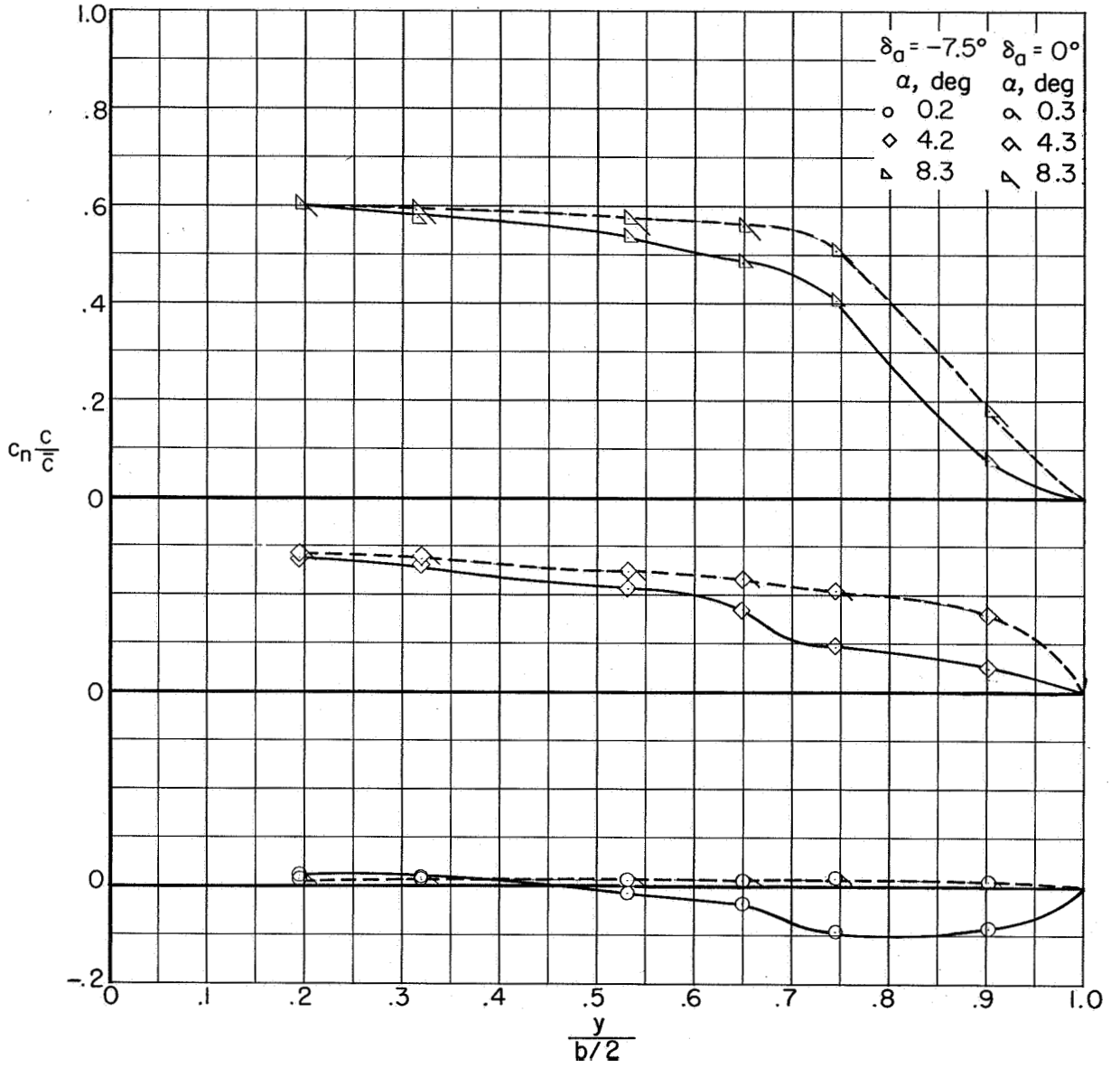

(a) M = 0.94; $\delta_a = 0^\circ$ and $\delta_a = -7.5^\circ$.

Figure 18.– Variation of section normal–load parameter with wing semispan.

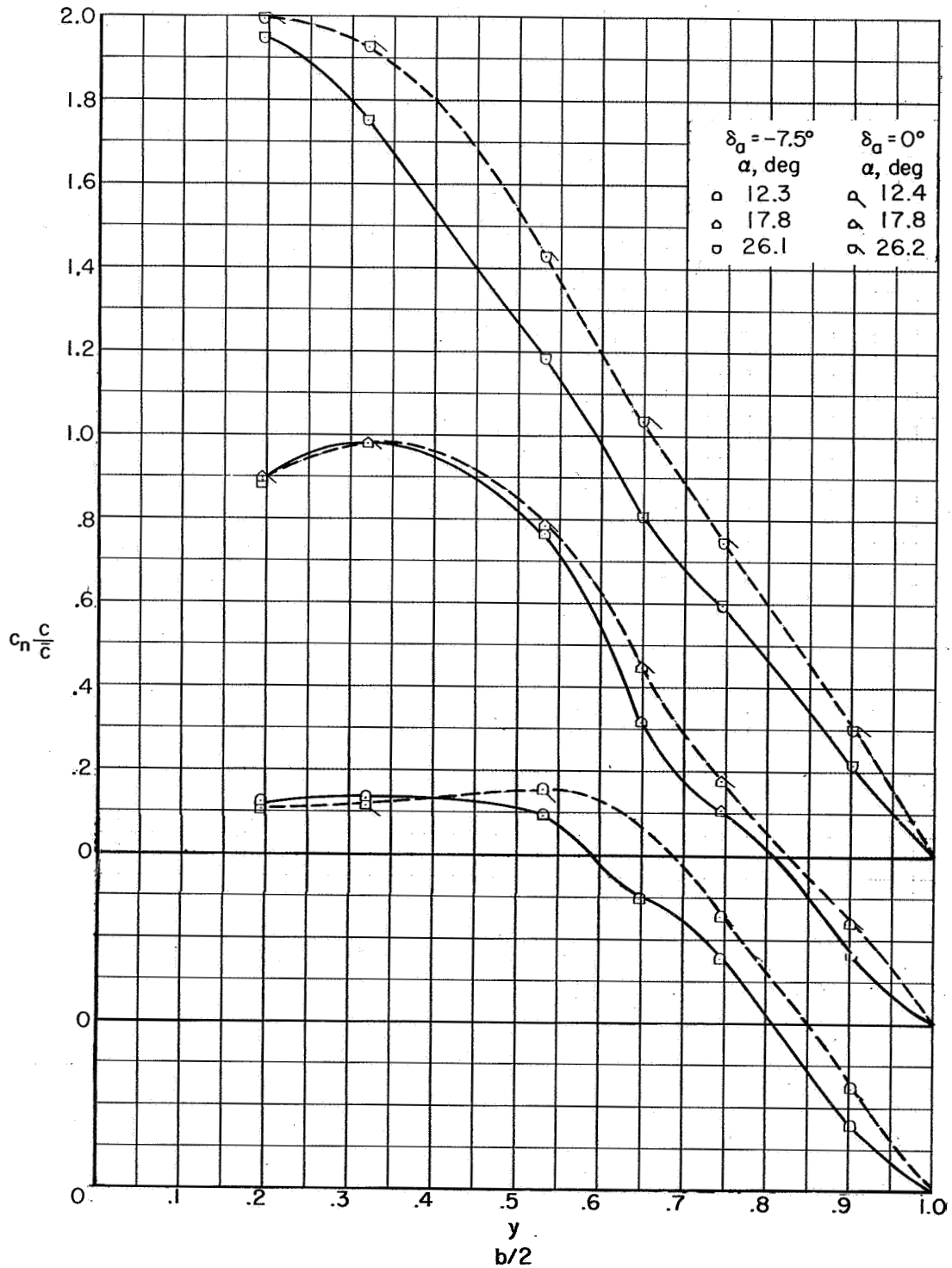

(a) Concluded.

Figure 18.- Concluded.

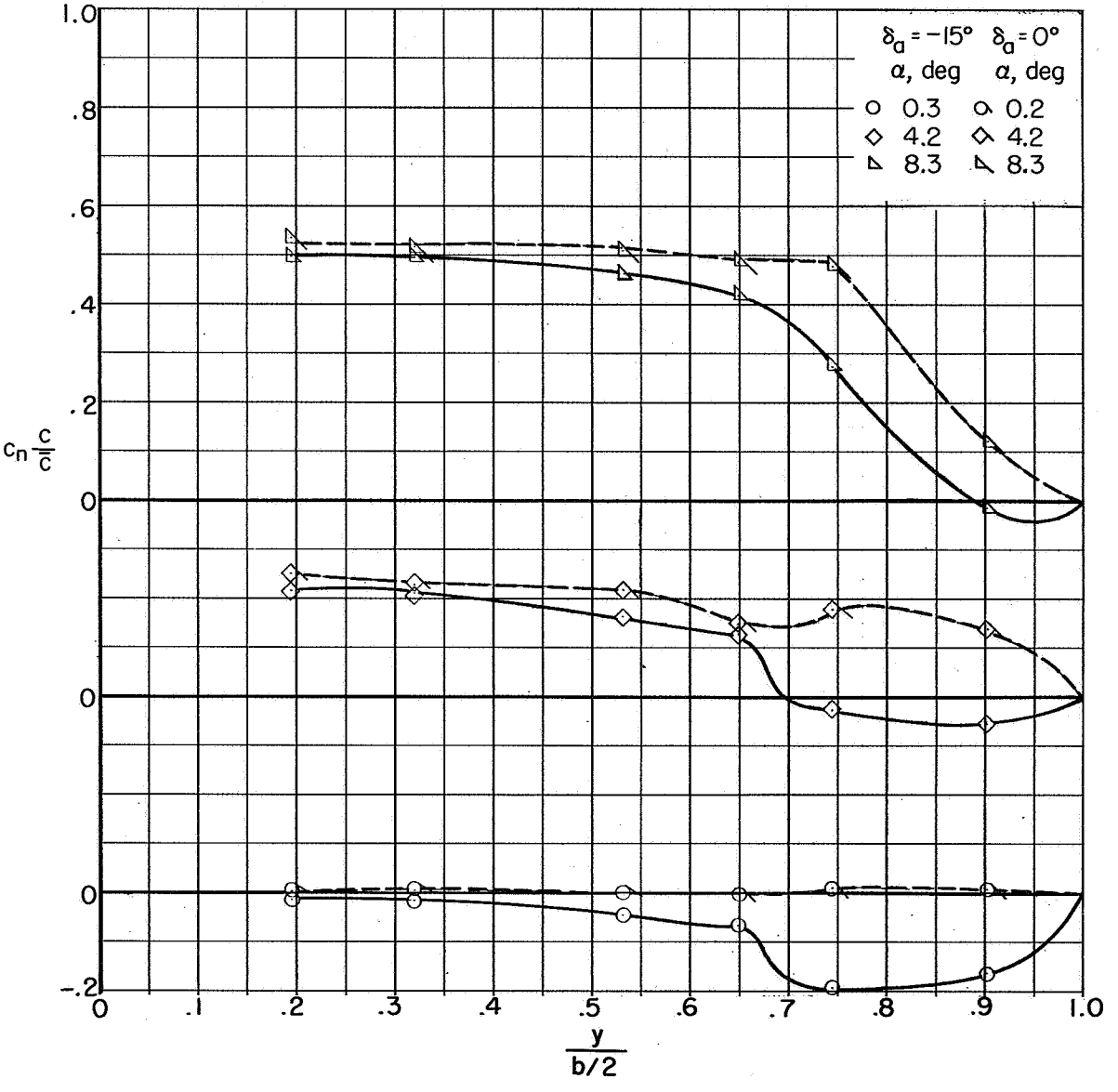

(a) M = 0.80; $\delta_a = 0^\circ$ and $\delta_a = -15^\circ$.

Figure 19.- Variation of section normal-load parameter with wing semispan.

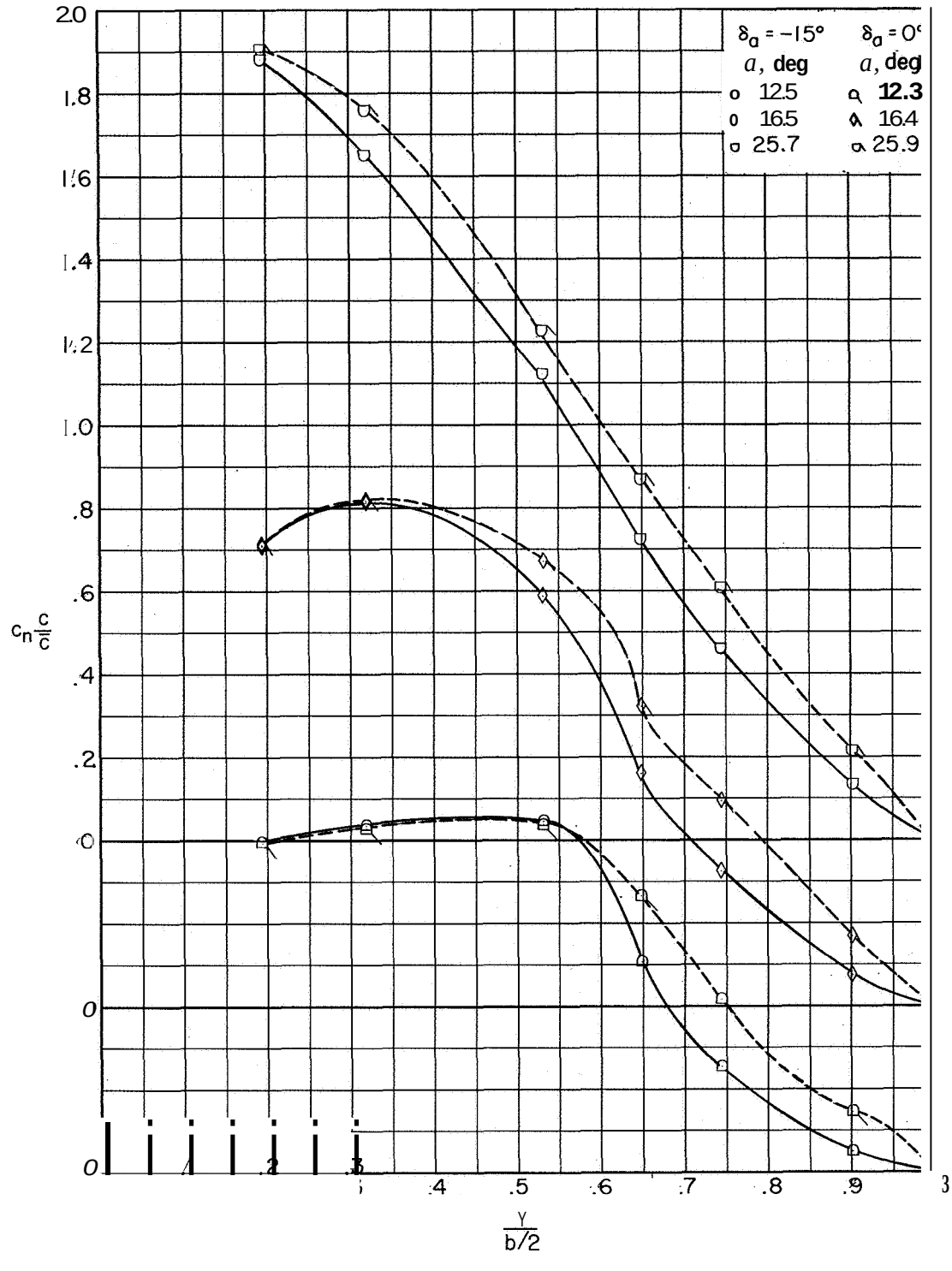

(a) Concluded.

Figure 19.- Continued.

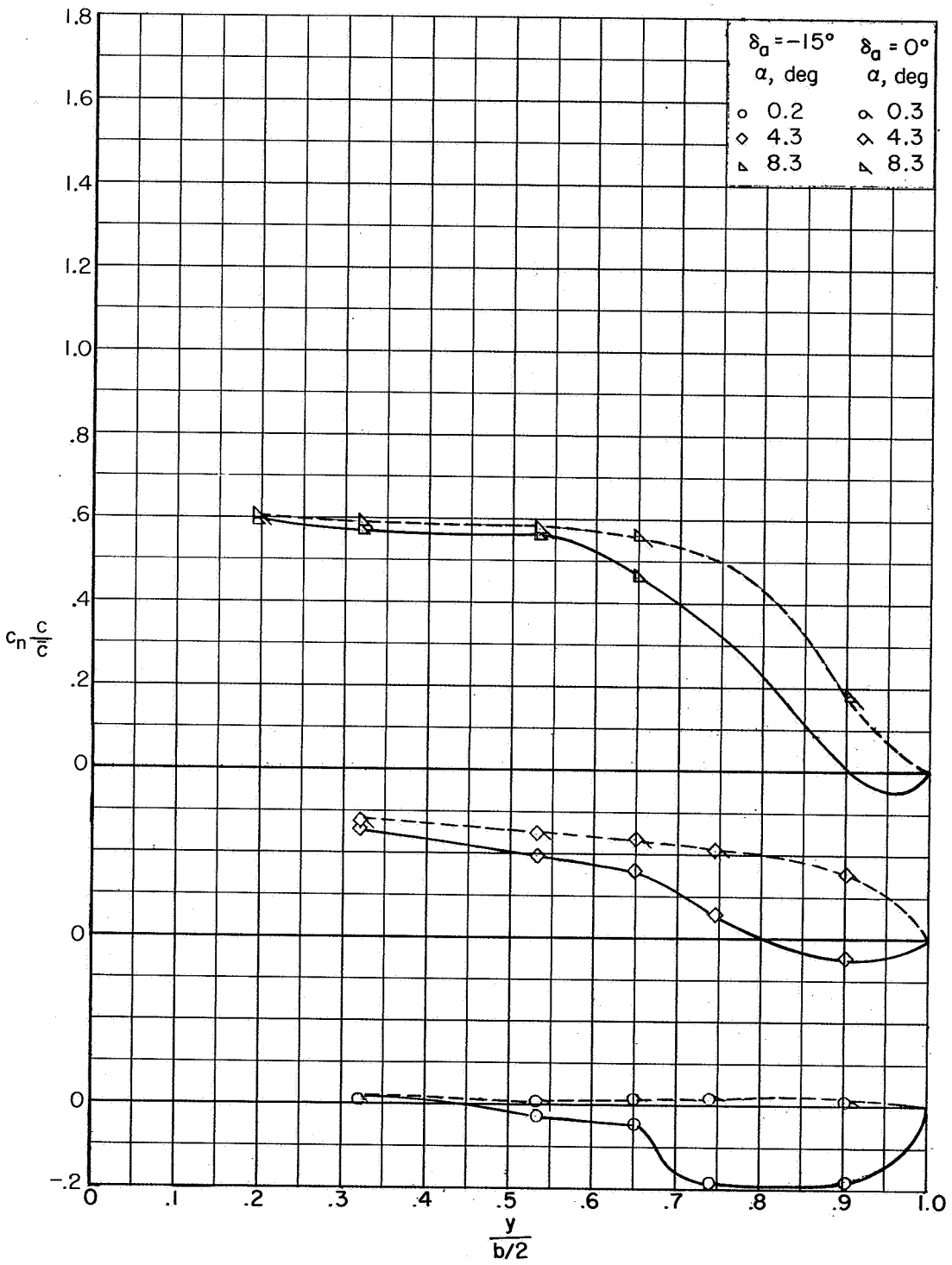

(b) M = 0.94; $\delta_a = 0^\circ$ and $\delta_a = -15^\circ$.

Figure 19.- Continued.

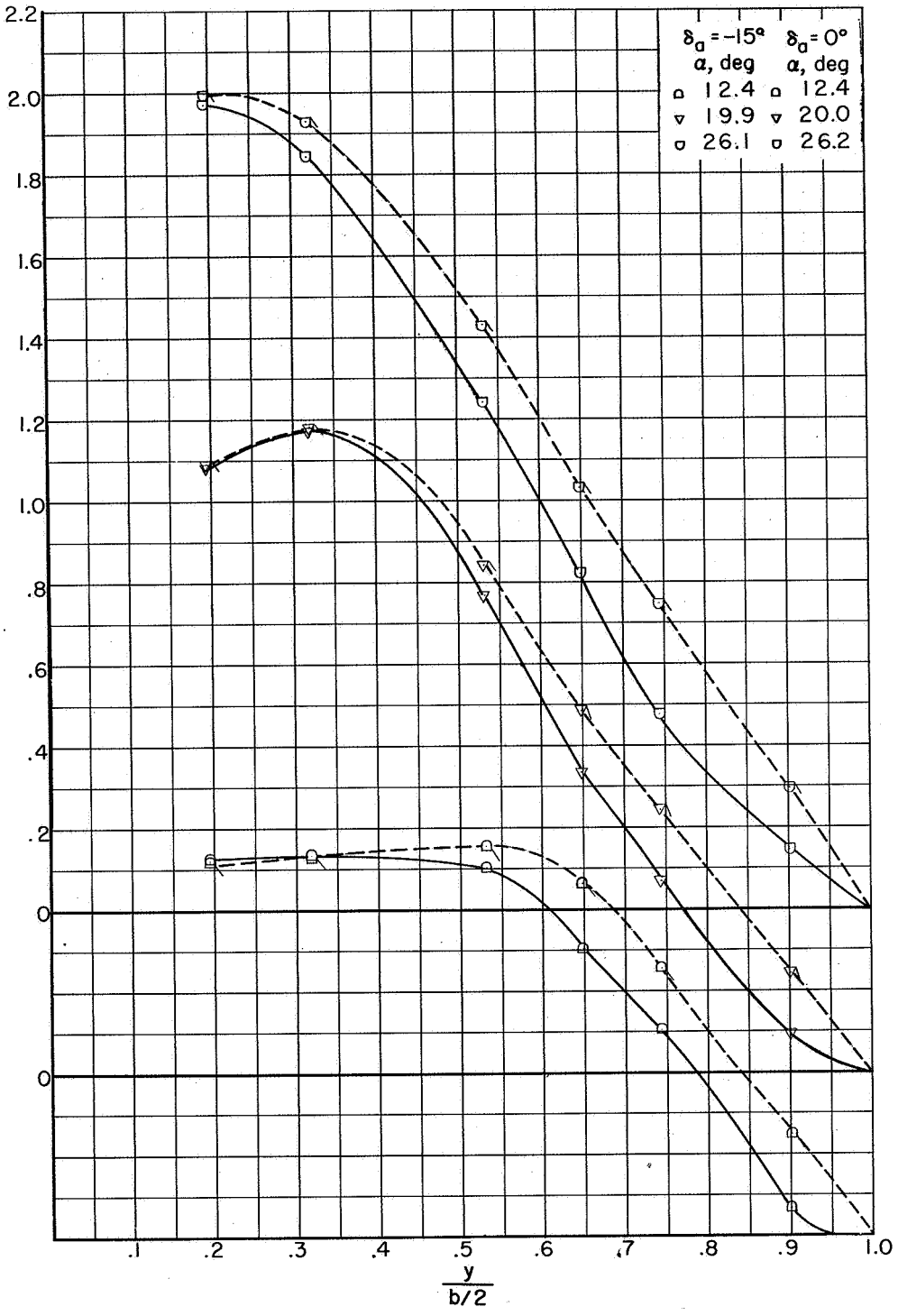

(b) Concluded.

Figure 19.- Continued.

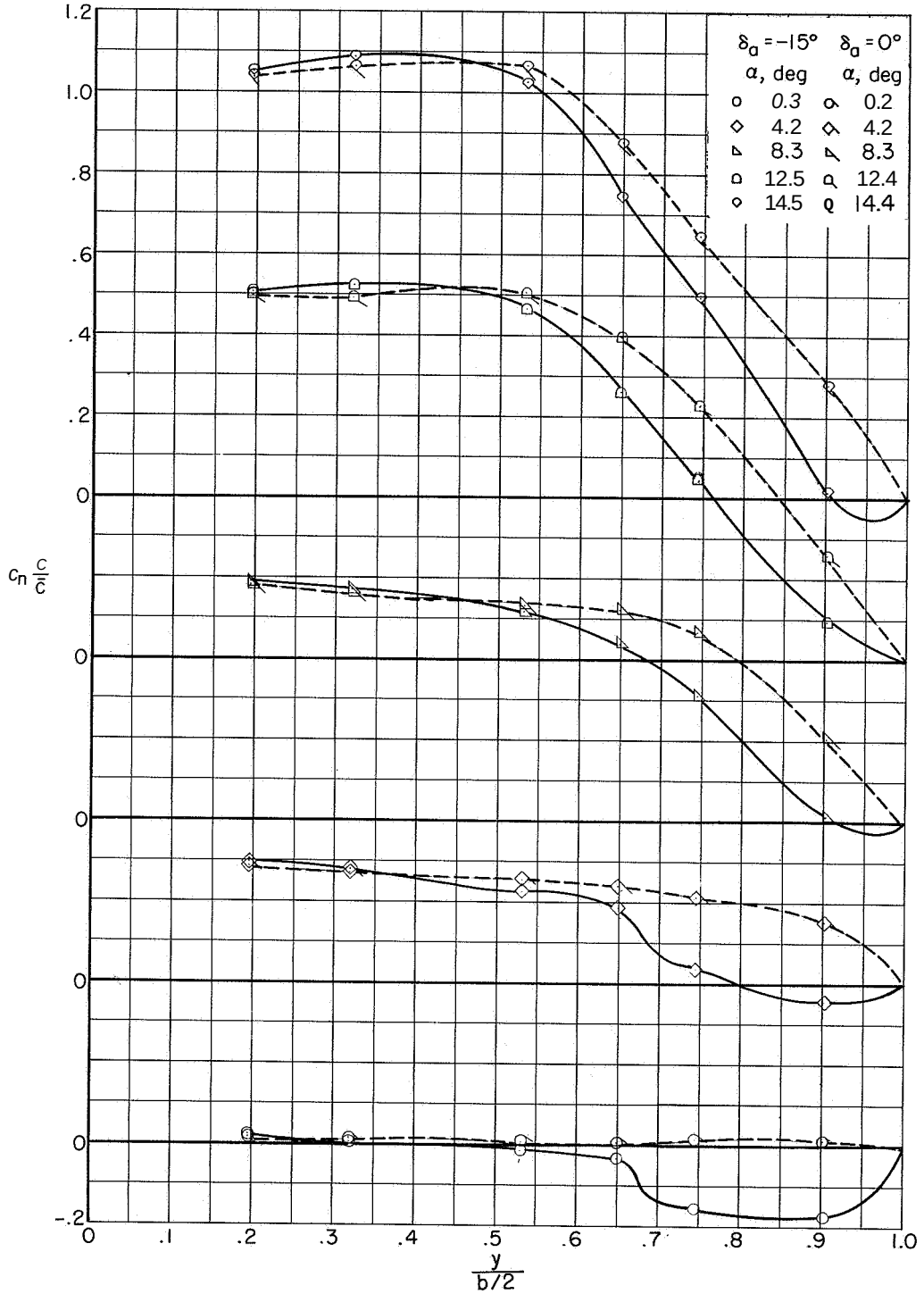

(c) M = 1.05; α = 0° and δ_a = -15°.

Figure 19.- Concluded.

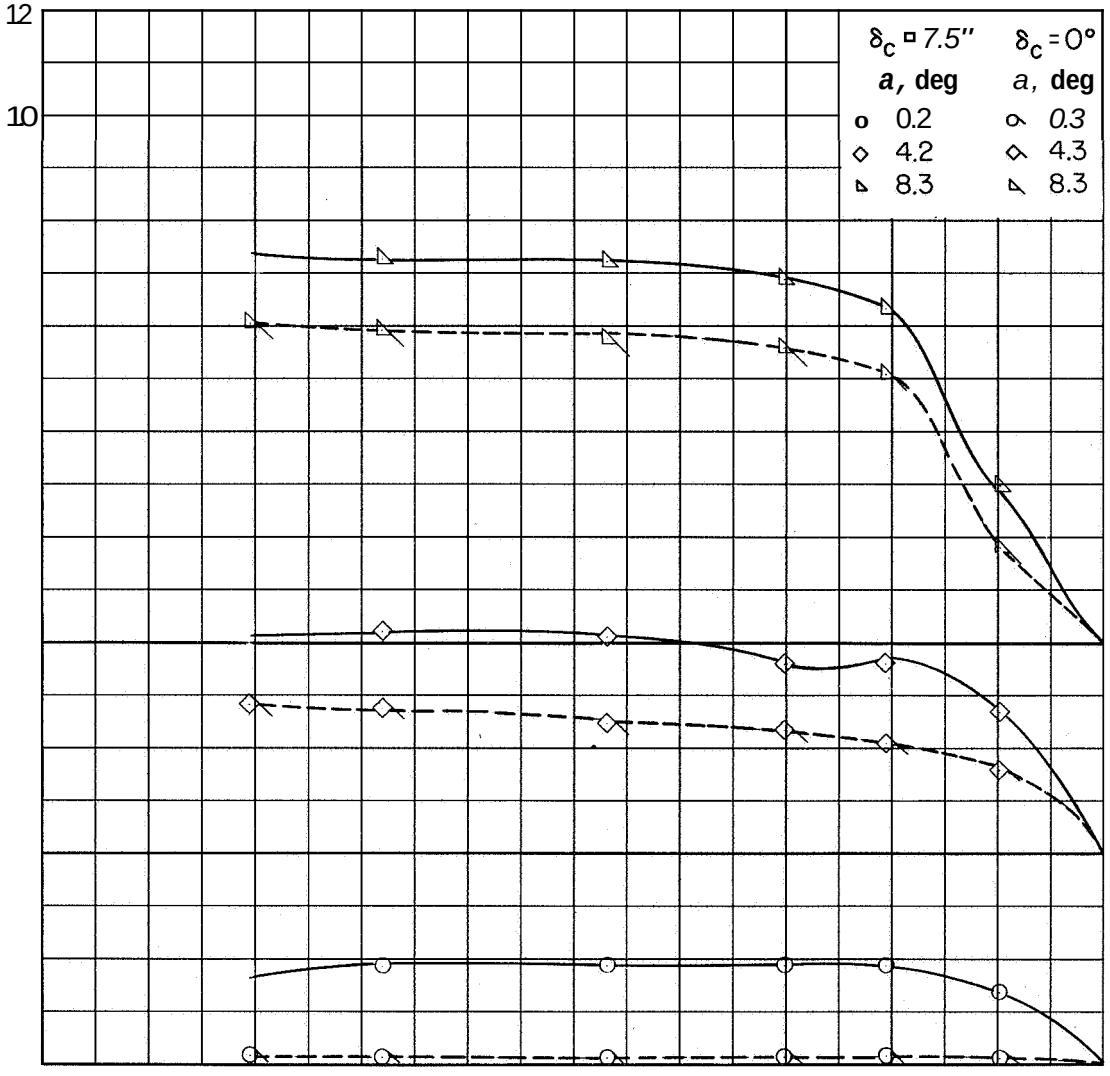
12
10
$c_n \frac{c}{\bar{c}}$
δ_c = 7.5"
δ_c = 0°
a, deg
a, deg
o 0.2
◇ 4.2
△ 8.3
o 0.3
◇ 4.3
△ 8.3

L-506

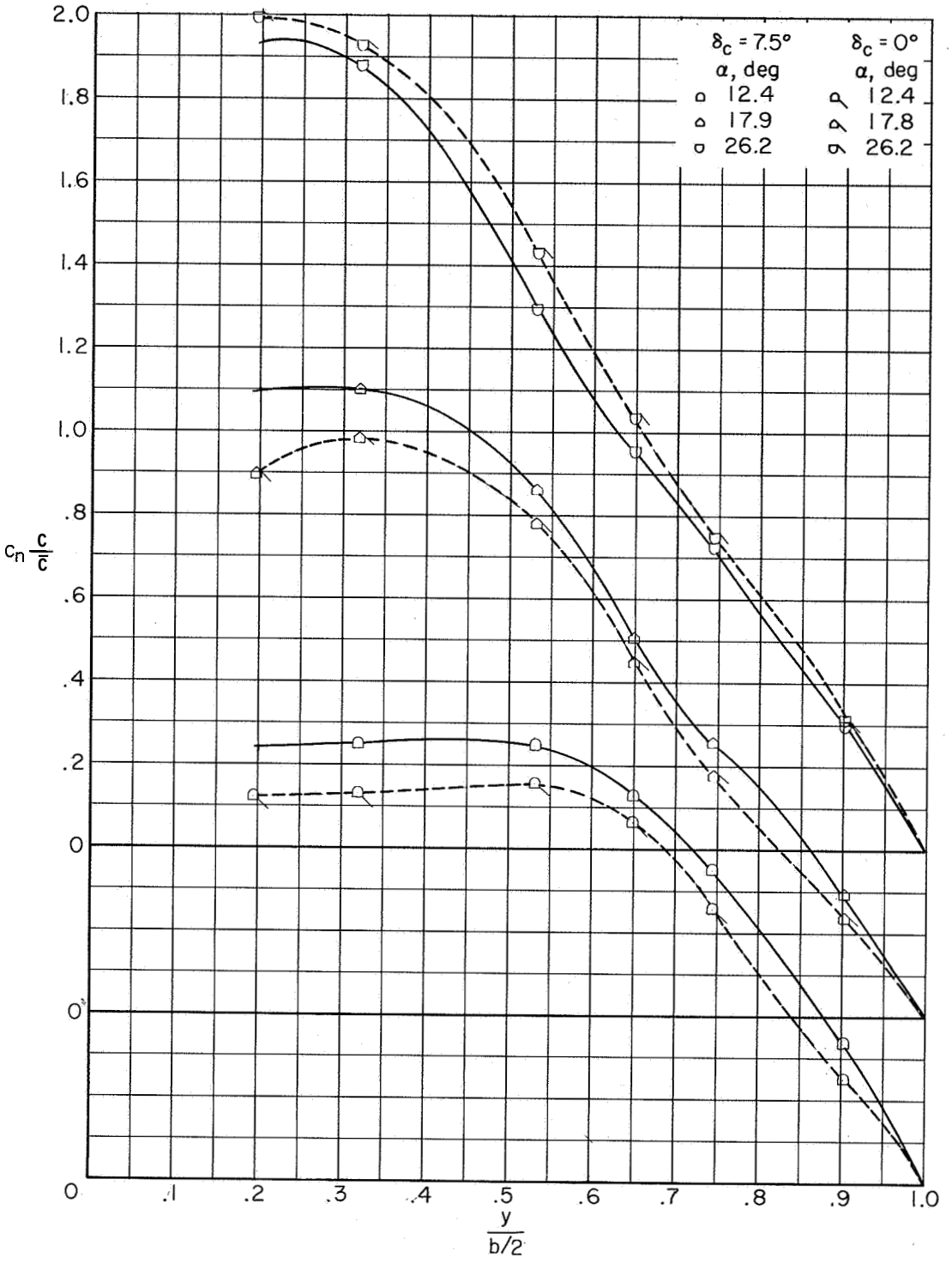

(a,) Concluded.

Figure 20.- Concluded.

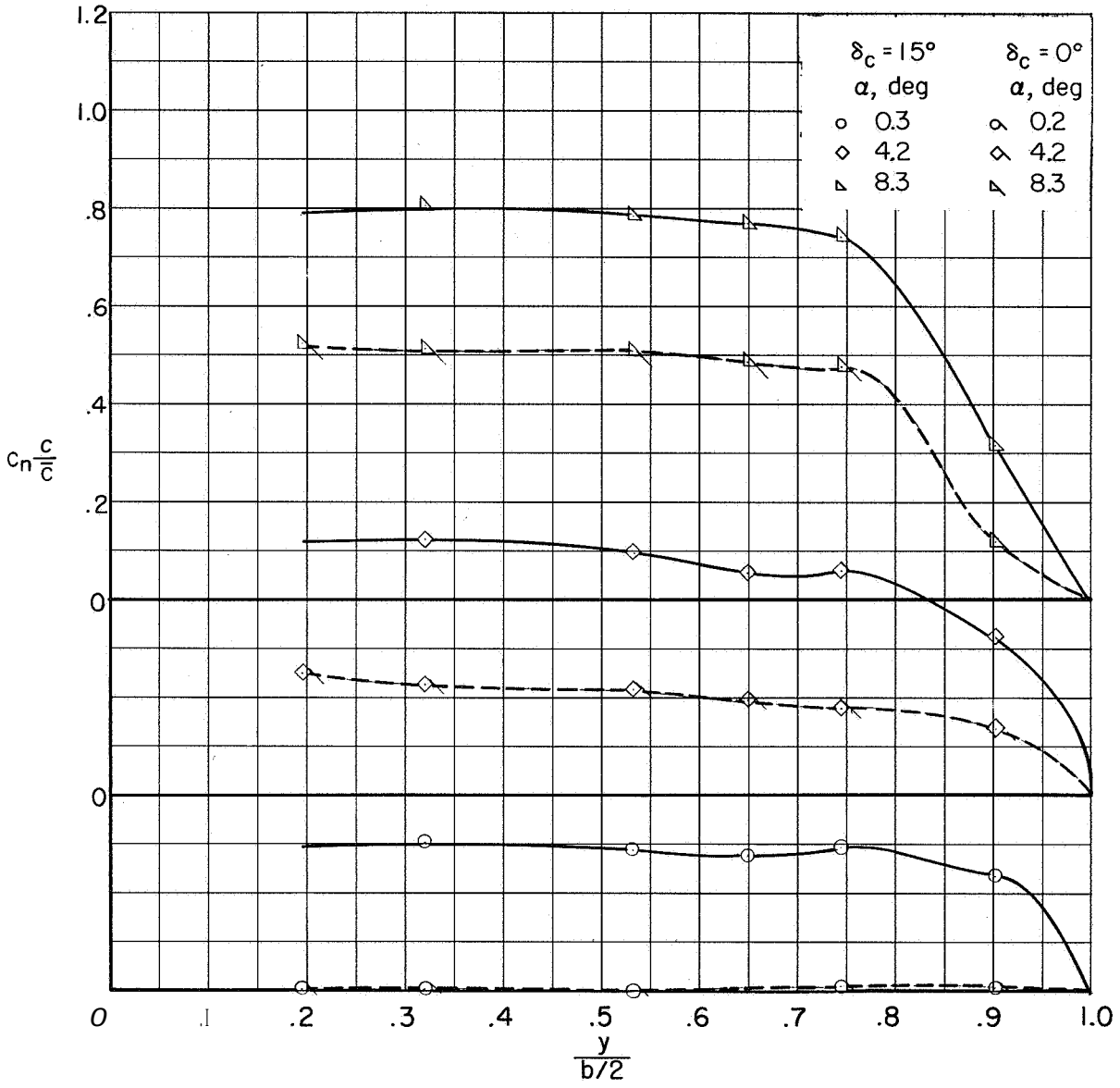

(a) $M = 0.80$; $\delta_c = 0°$ and $\delta_c = 15°$.

Figure 21.- Variation of section normal-load parameter with wing semispan.

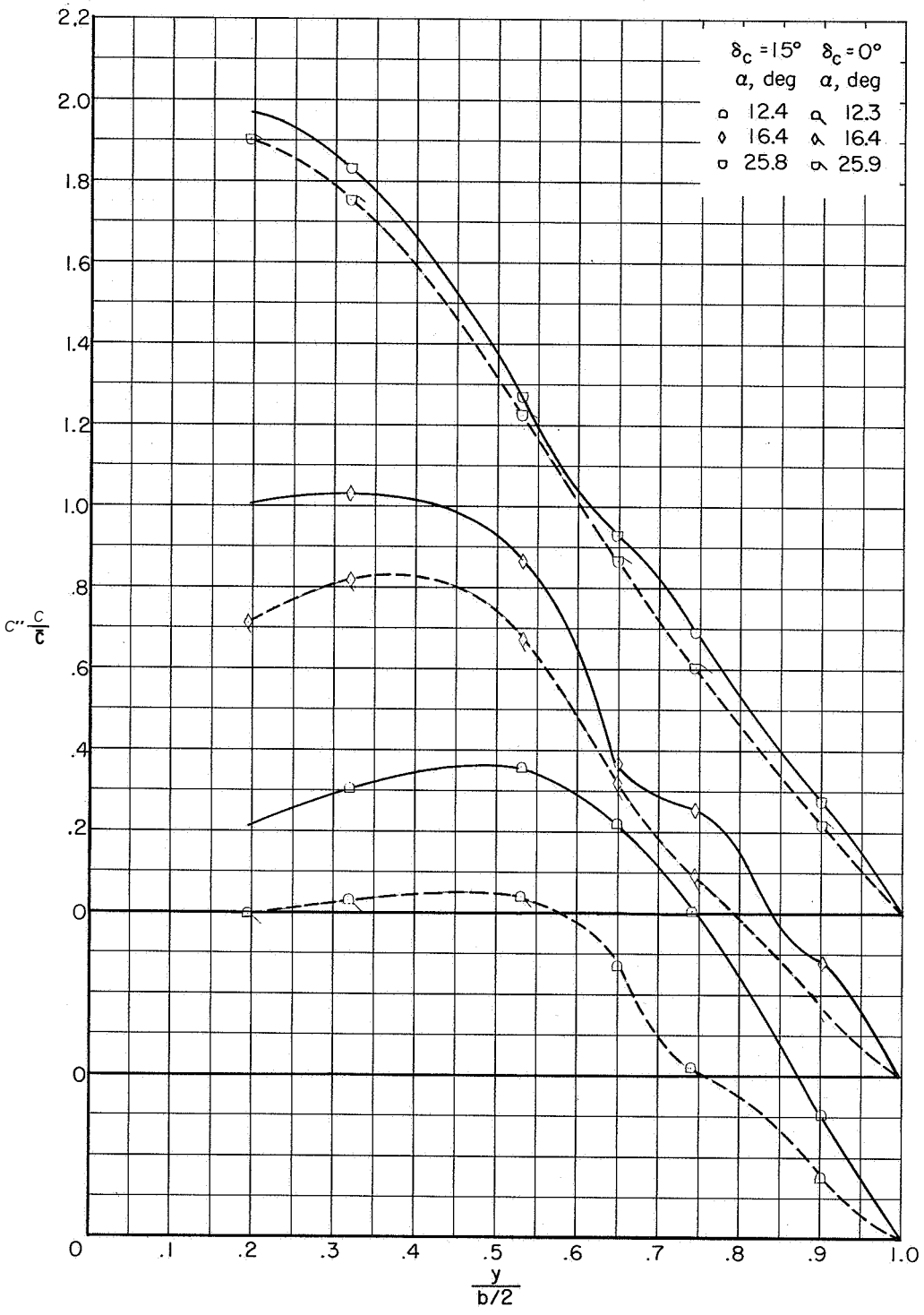

(a) Concluded.

Figure 21.- Continued.

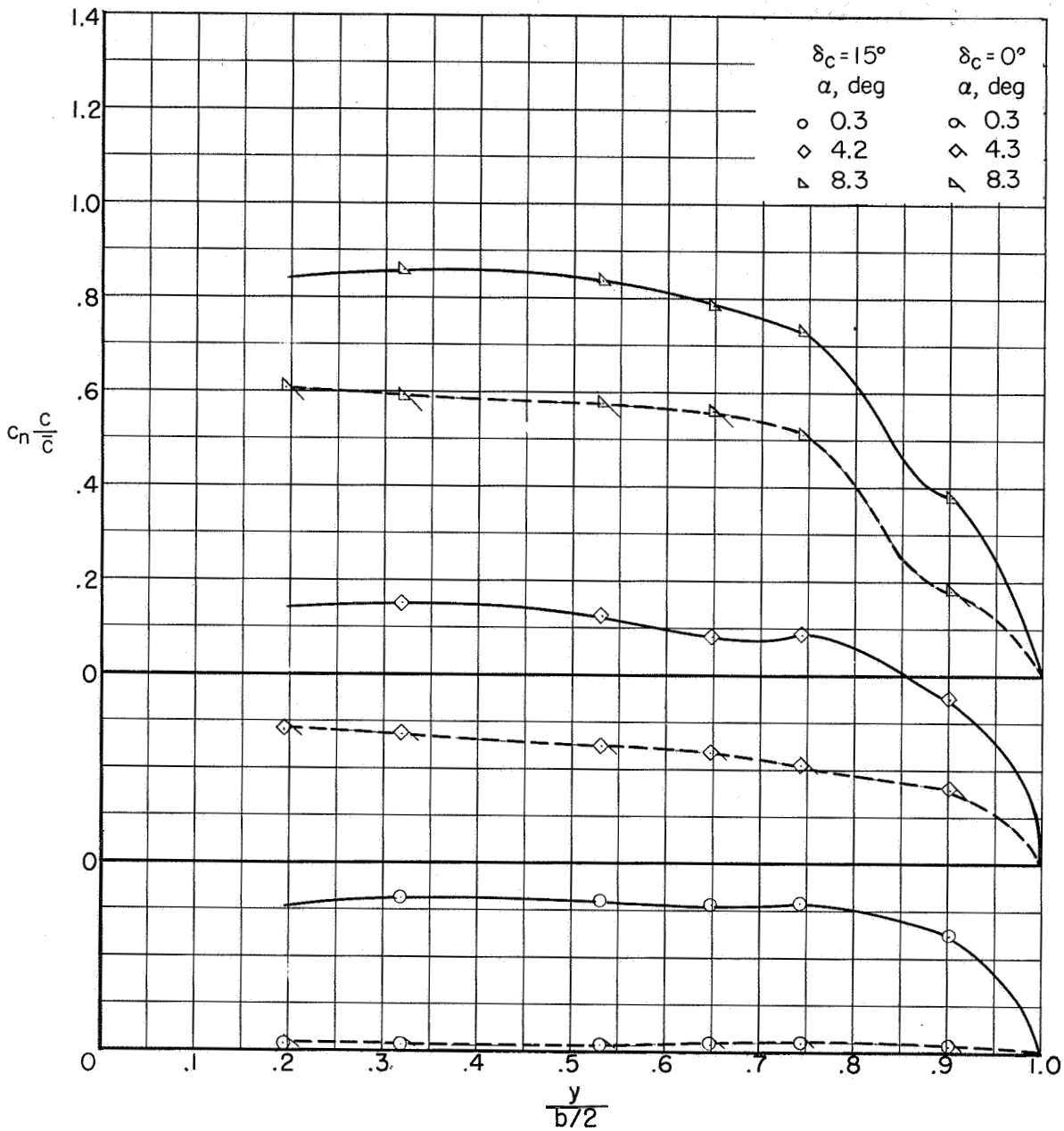

(b) M = 0.94; δ_c = 0° and δ_c = 15°.

Figure 21.- Continued.

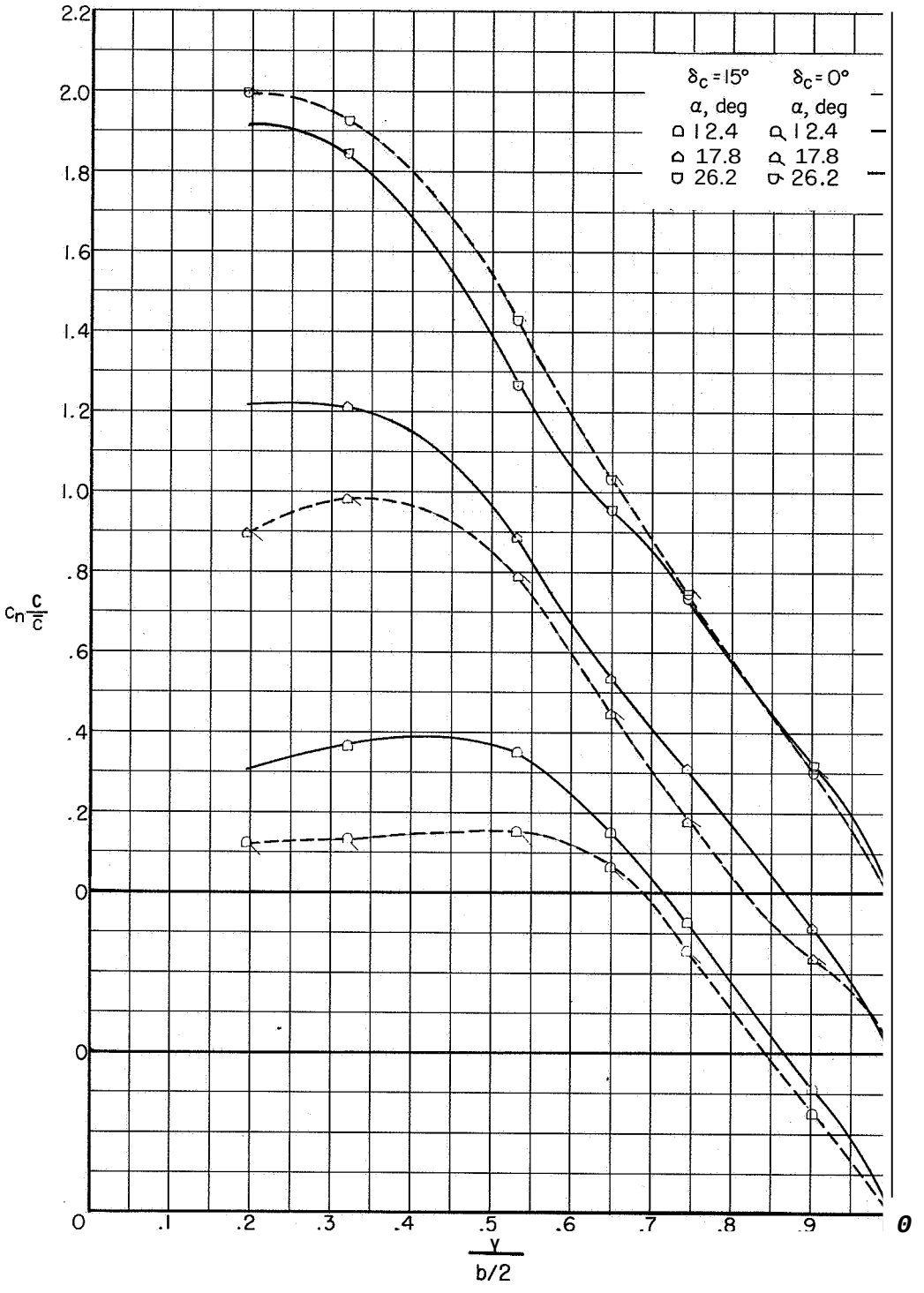

(b) Concluded.

Figure 21. - Continued.

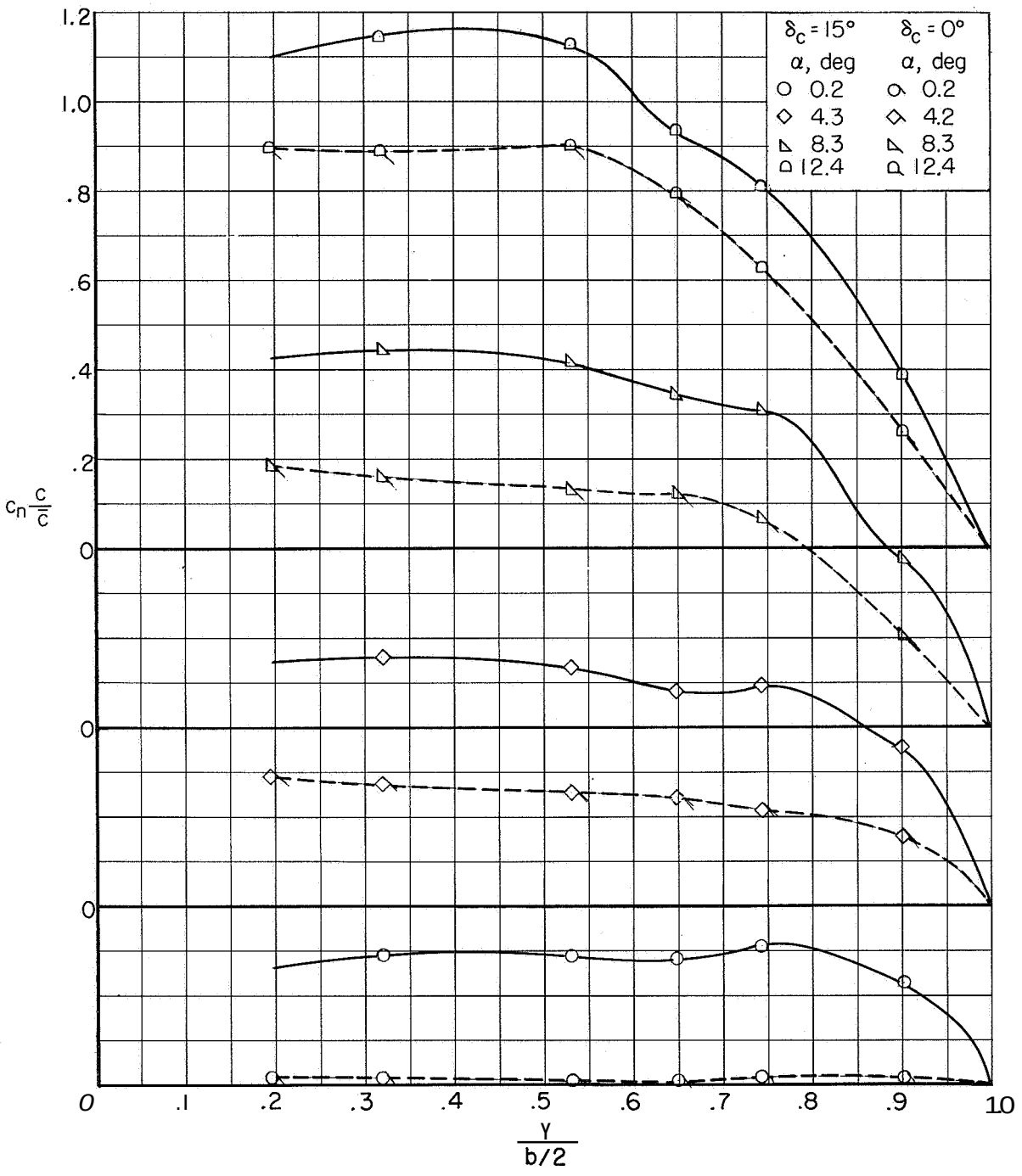

(c) M = 1.05; δ_c = 0° and 6, = 15°.

Figure 21.- Concluded.

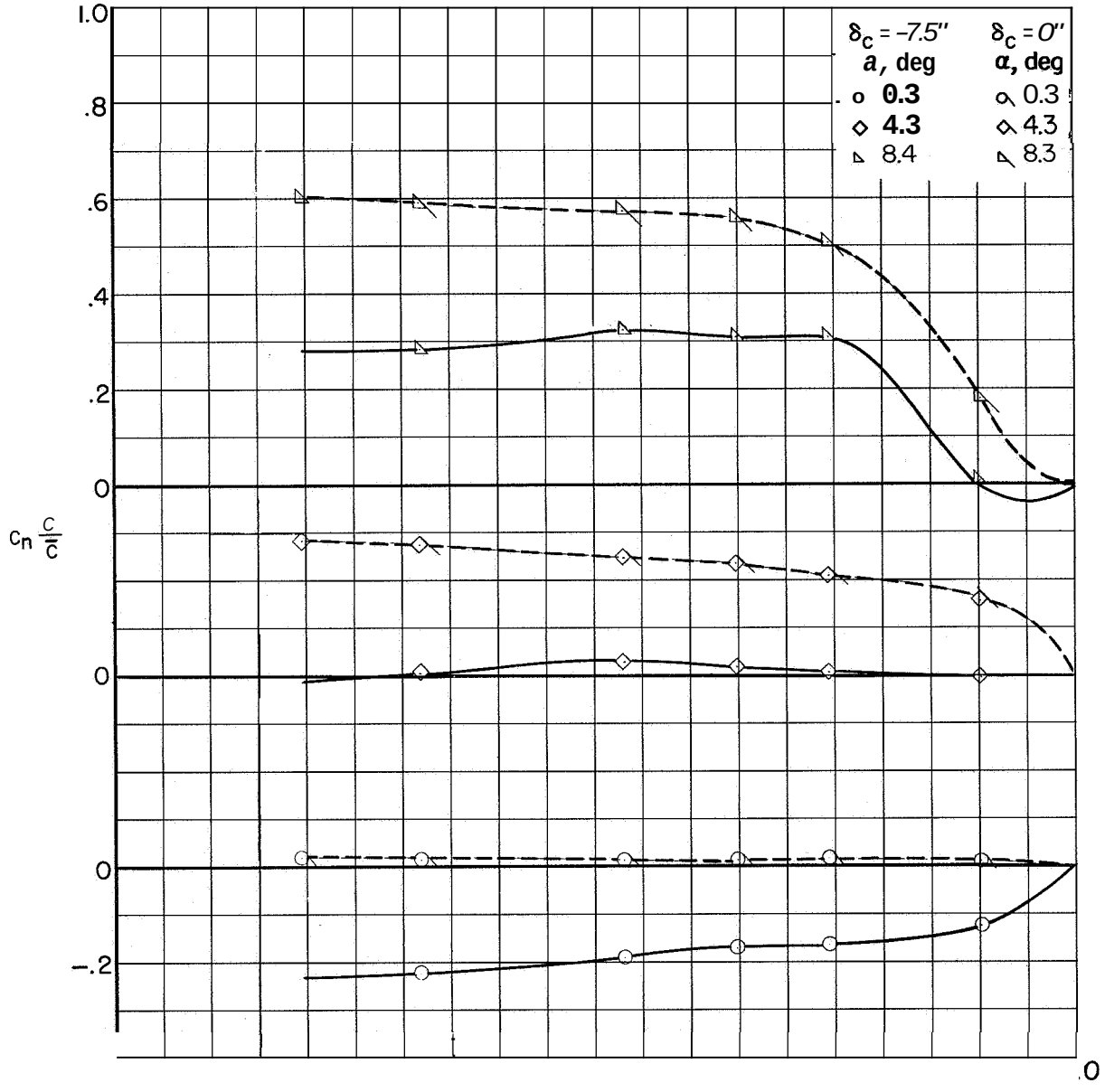

Figure 22.- Variation of section normal-load parameter with wing semispan.

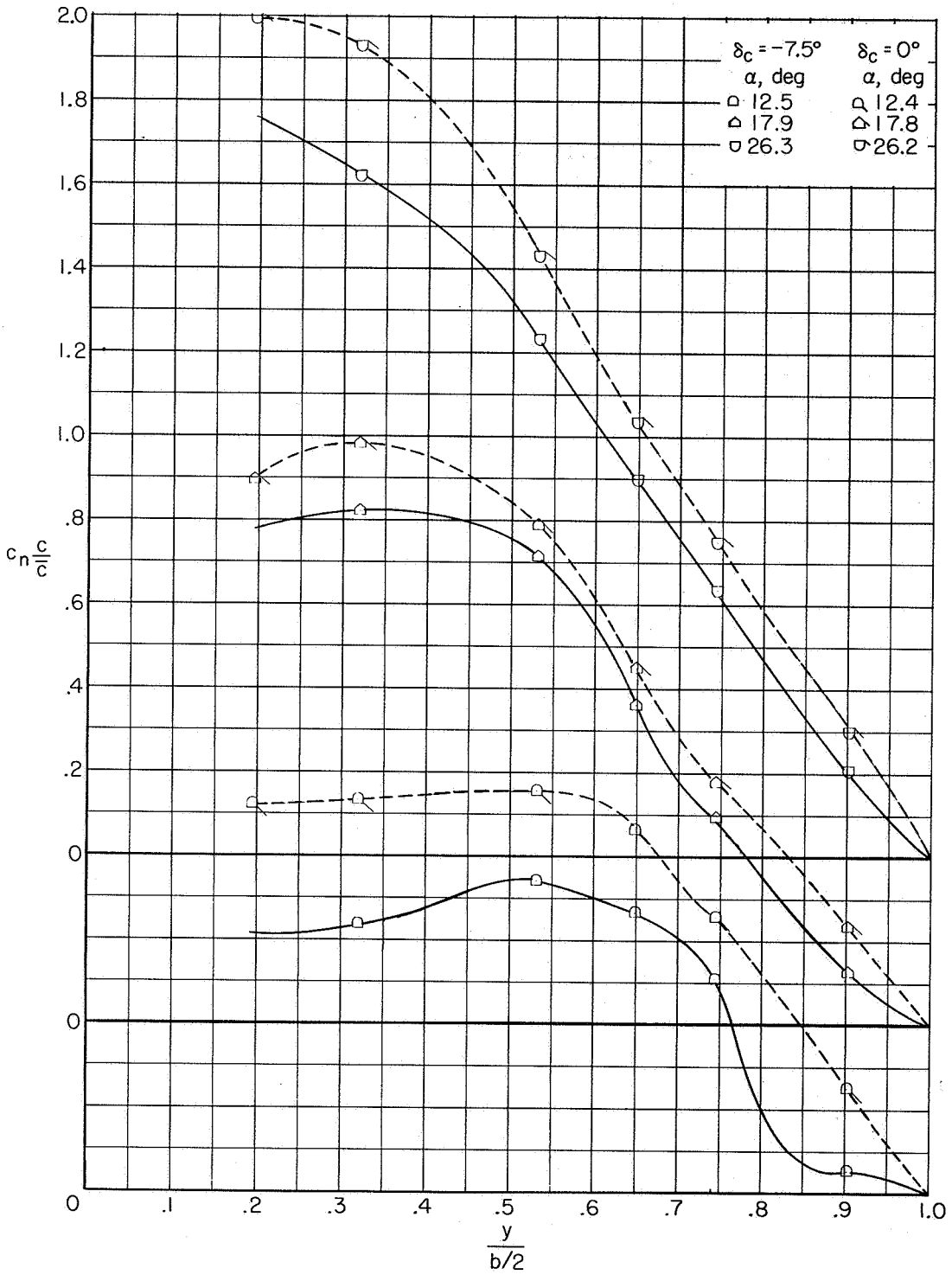

(a) Concluded.

Figure 22.- Concluded.

L-506

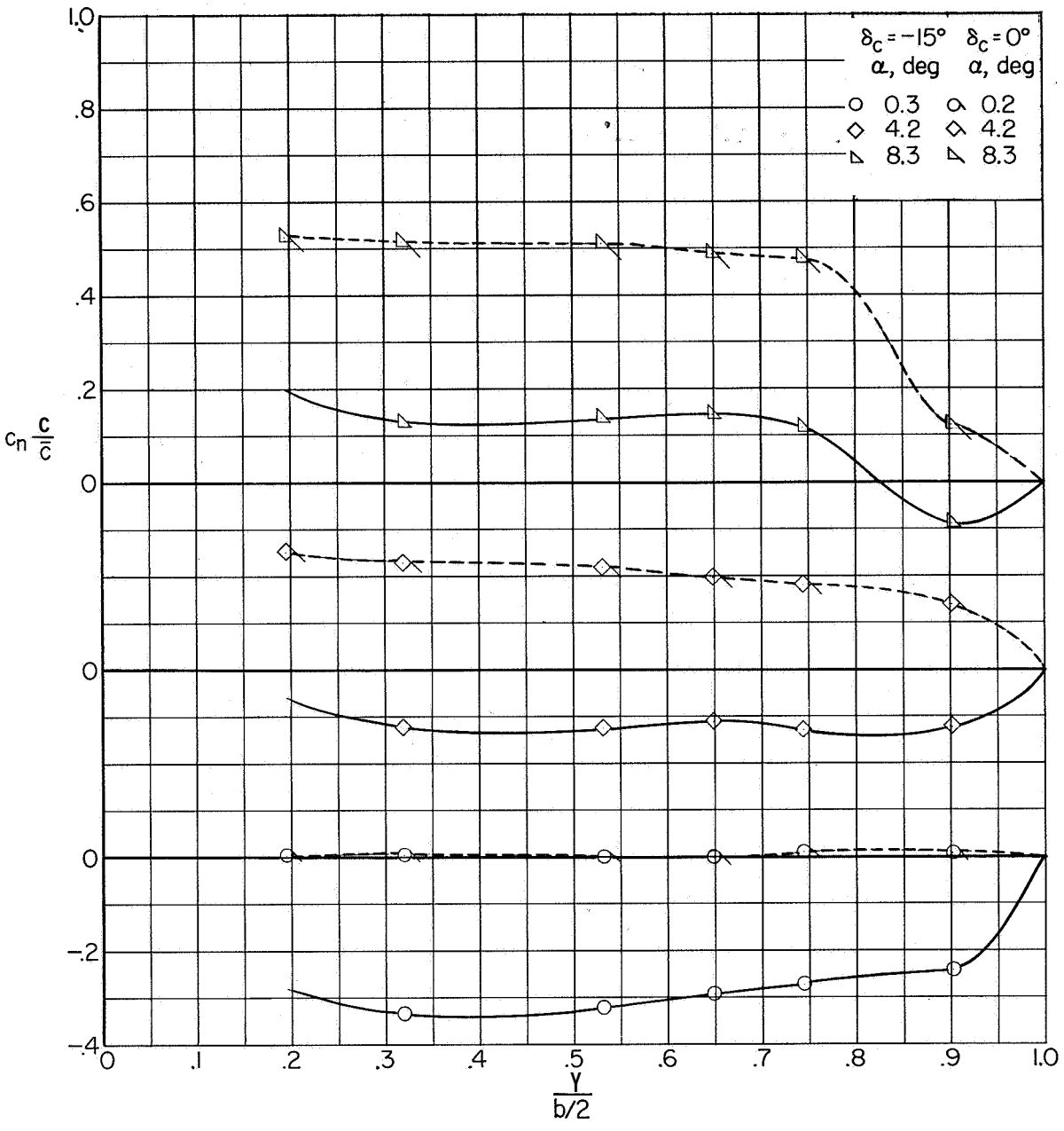

(a) M = 0.80; δ_c = 0° and δ_c = -15°.

Figure 23.- Variation of section normal-load parameter with wing semispan.

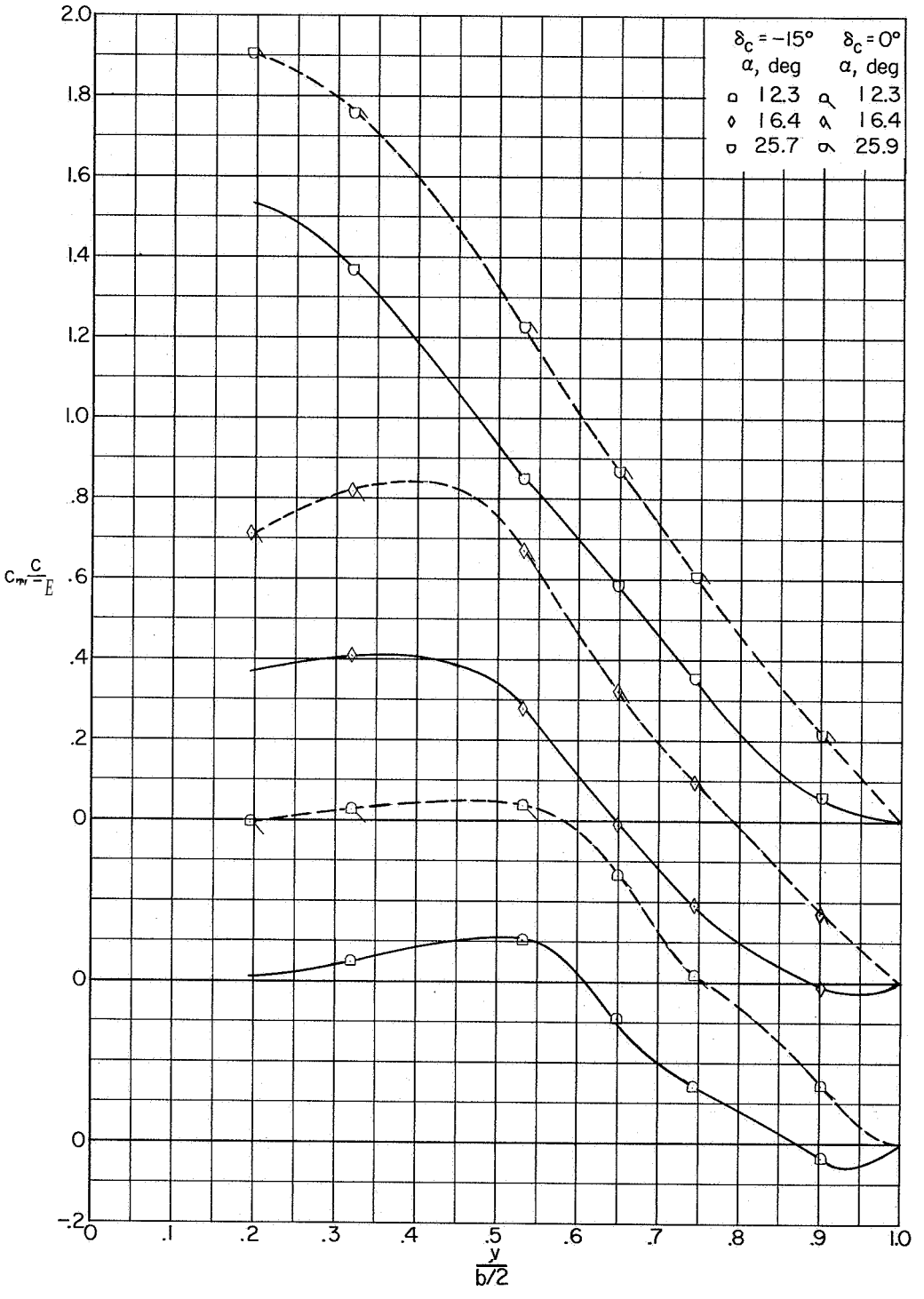

(a) Concluded.

Figure 23.- Continued.

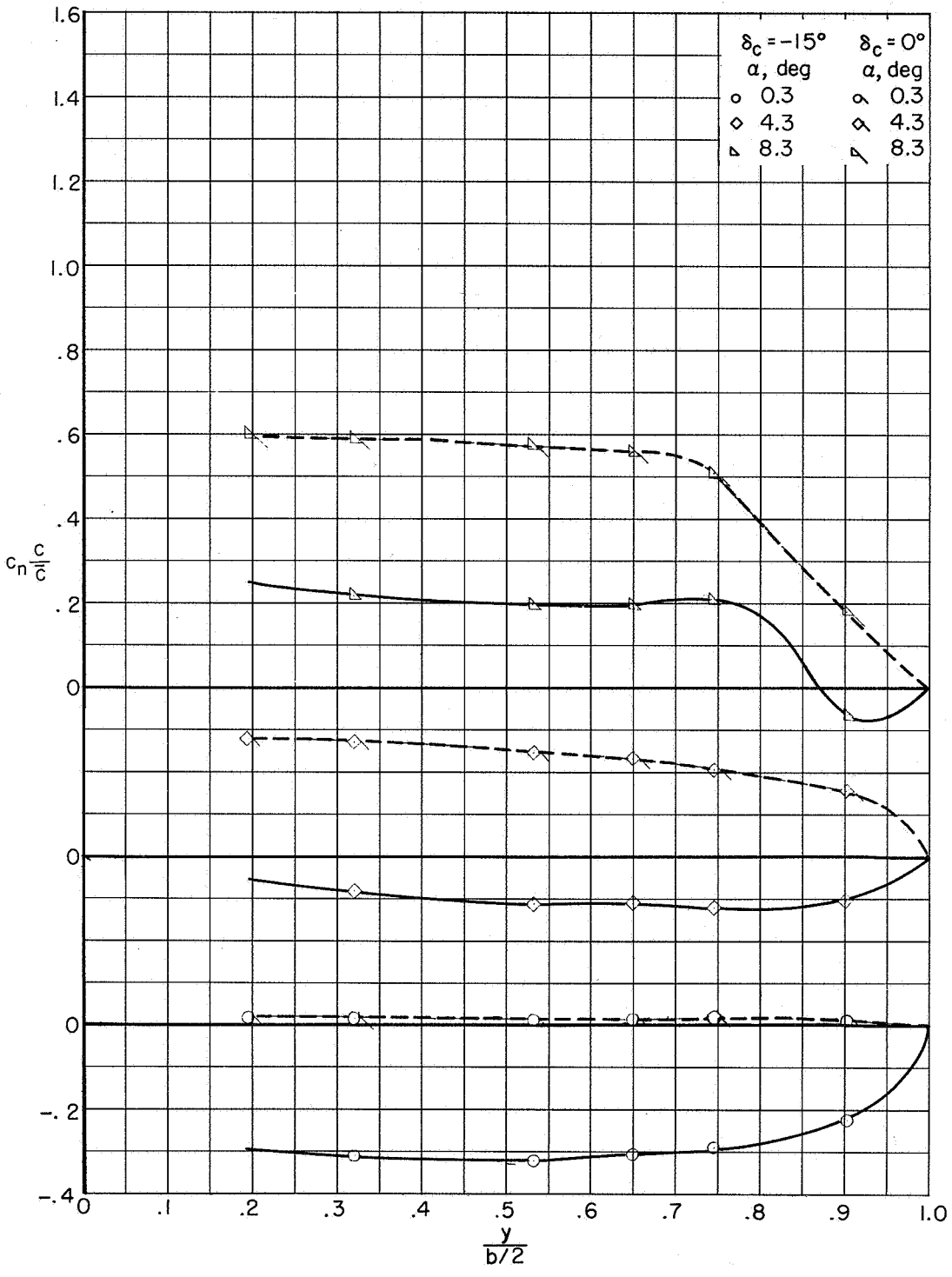

(b) M = 0.94; $\delta_c = 0^\circ$ and $\delta_c = -15^\circ$.

Figure 23.- Continued.

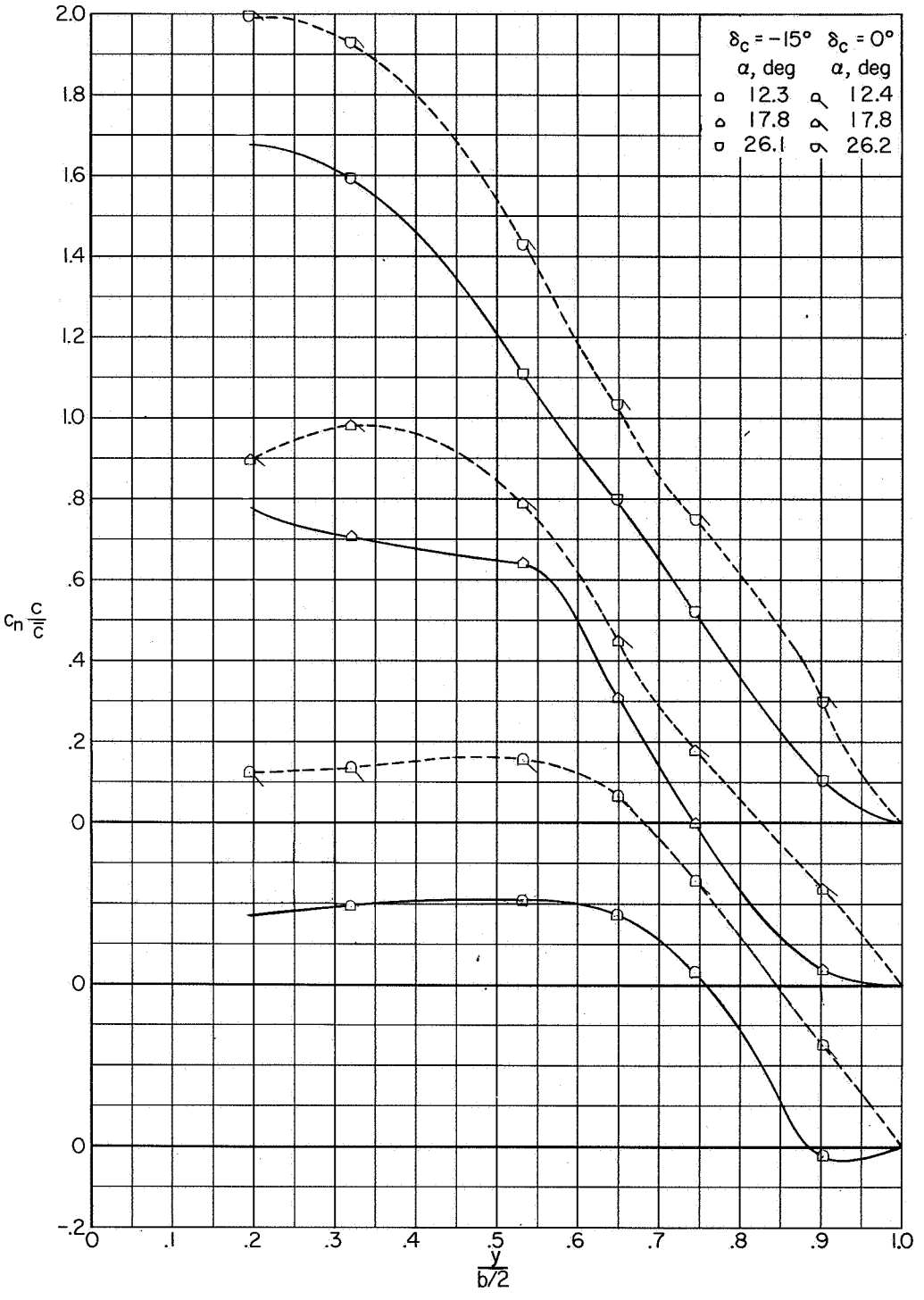

(b) Concluded.

Figure 23.- Continued.

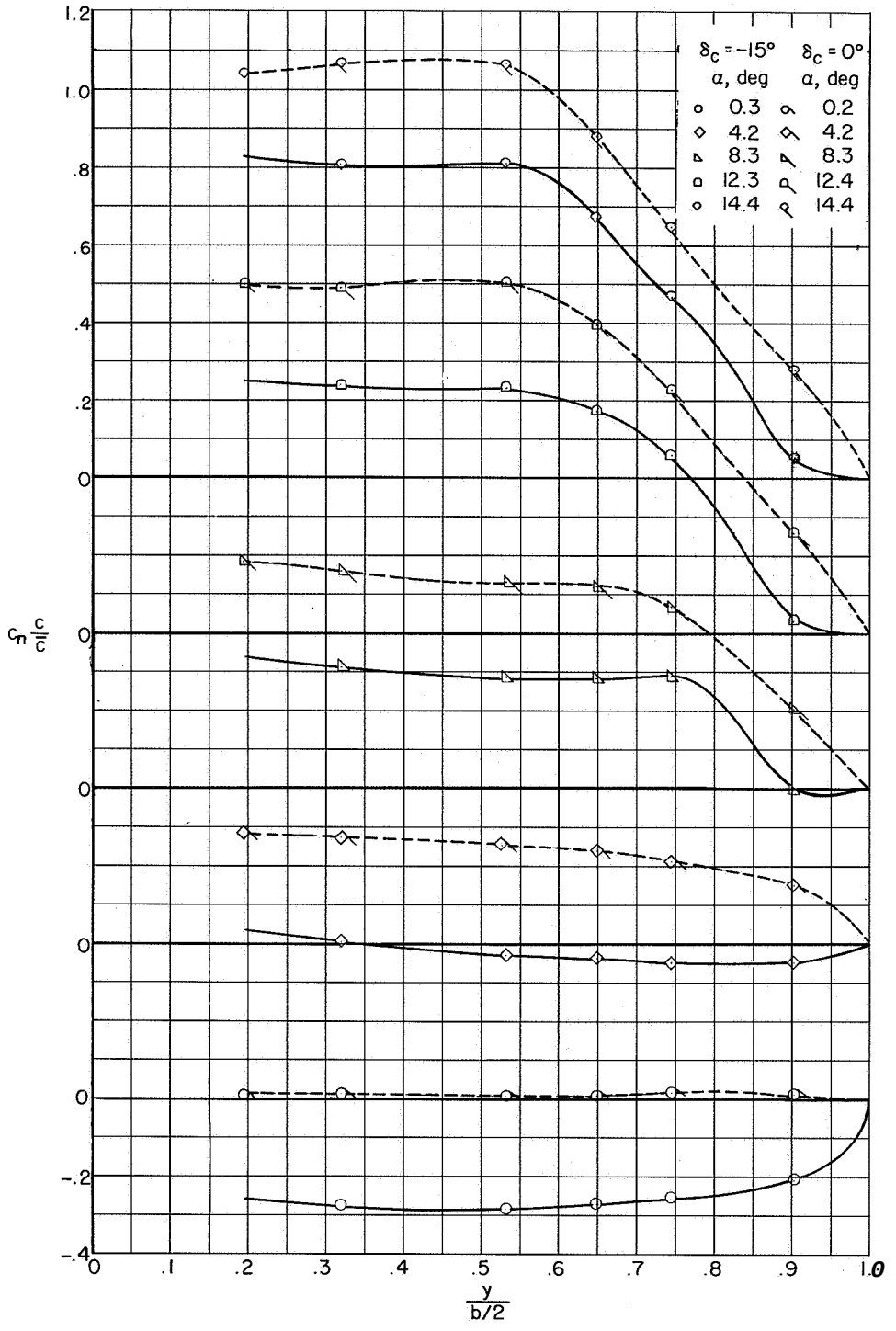

(c) M = 1.05; $\delta_c = 0^\circ$ **and** $\delta_c = -15^\circ$.

Figure 23.- Concluded.

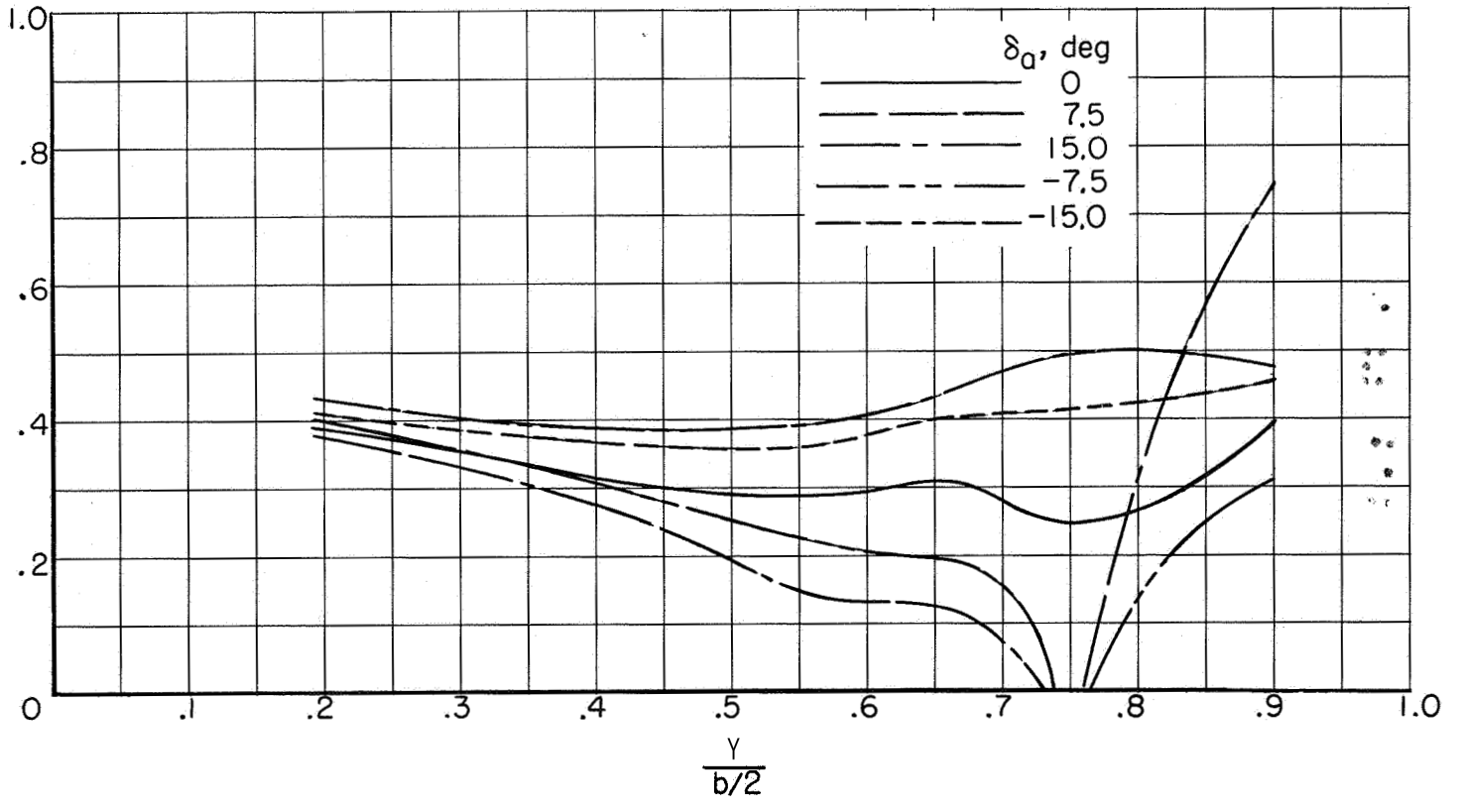

(a) α - 4°.

Figure 24.- Variation of section chordwise center-of-pressure locations along wing semispan for various aileron deflections. M = 0.94.

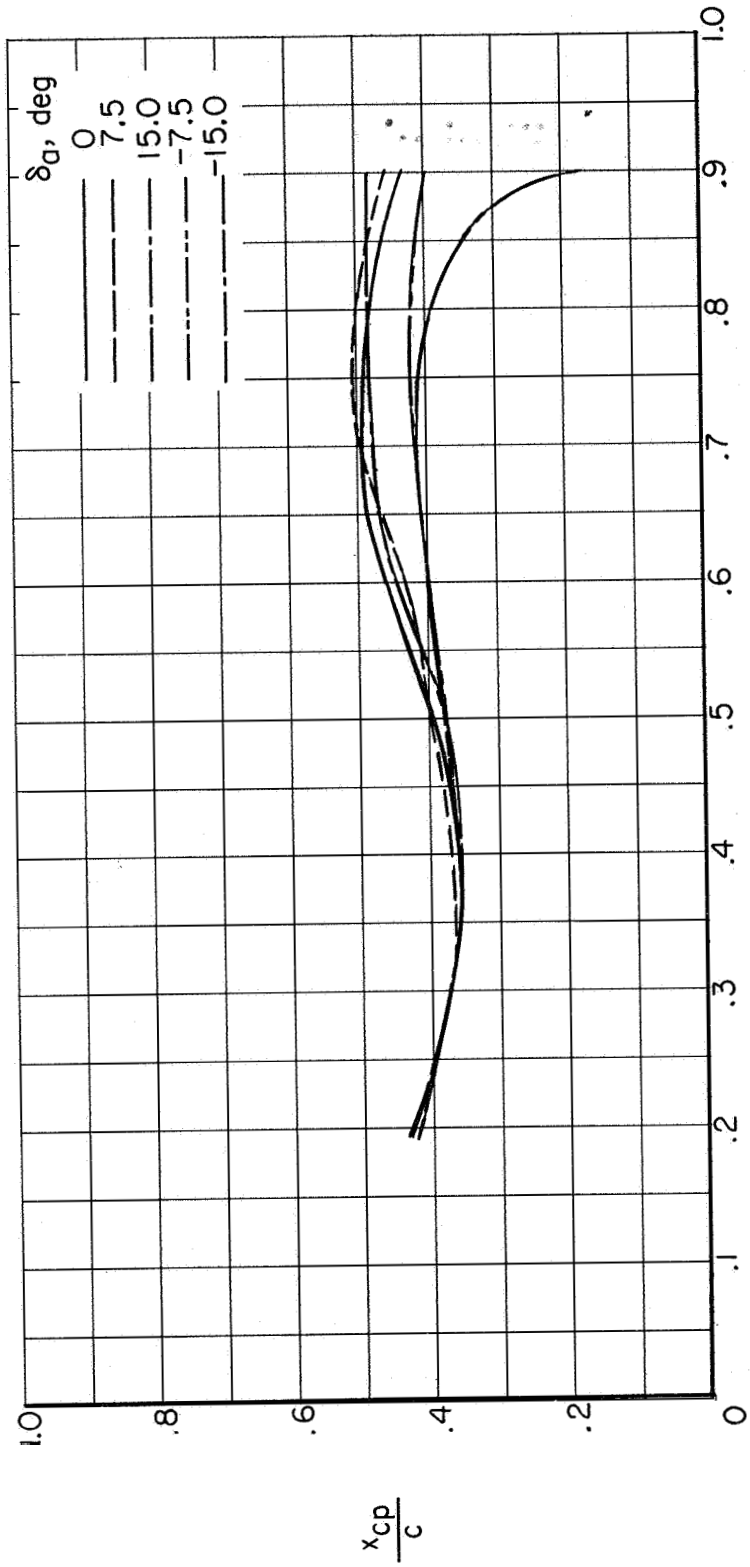

(b) $\alpha \approx 12^\circ$

Figure 24.- Continued.

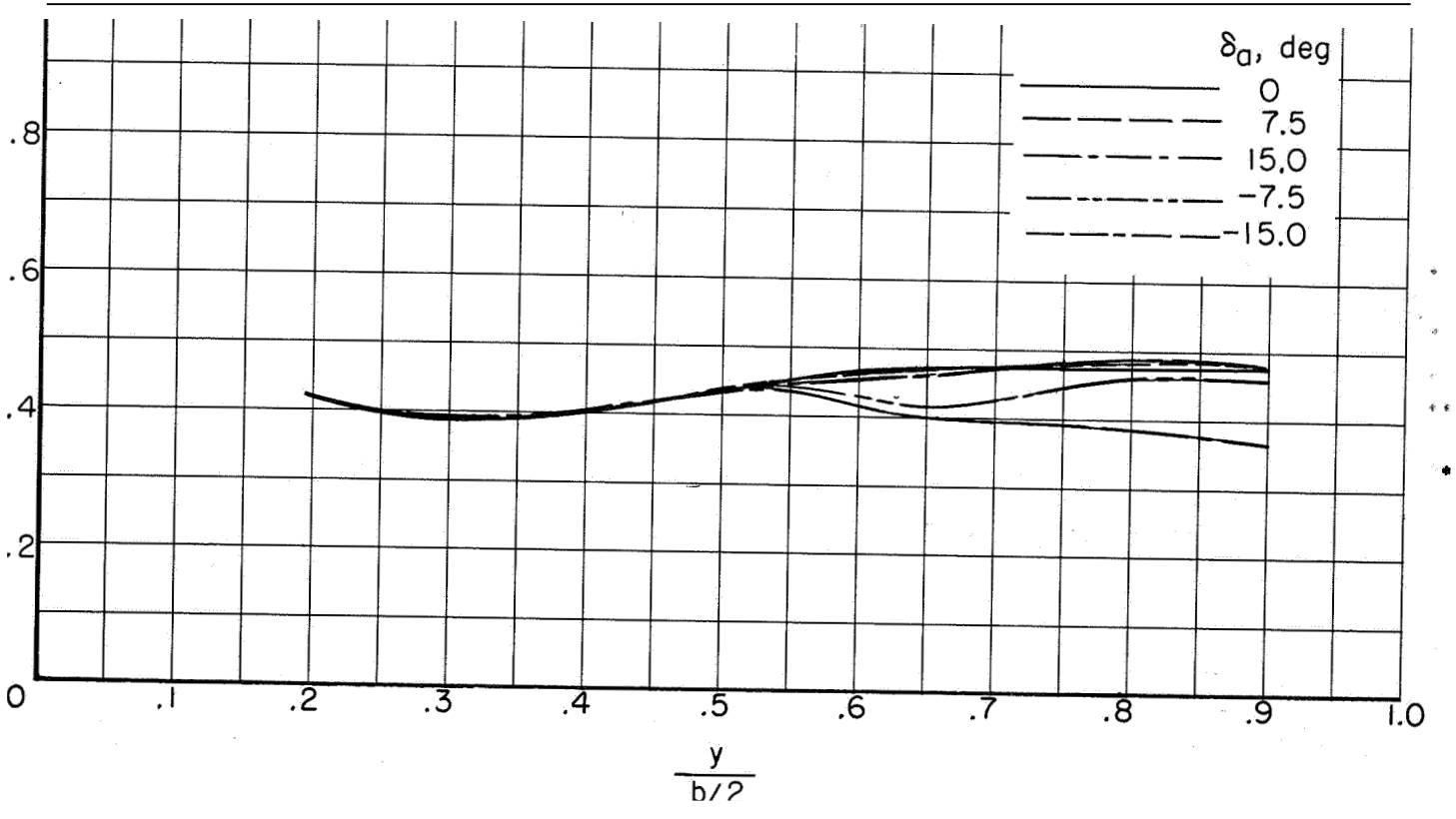

(c) $\alpha \approx 20^\circ$

Figure 24.- Concluded.

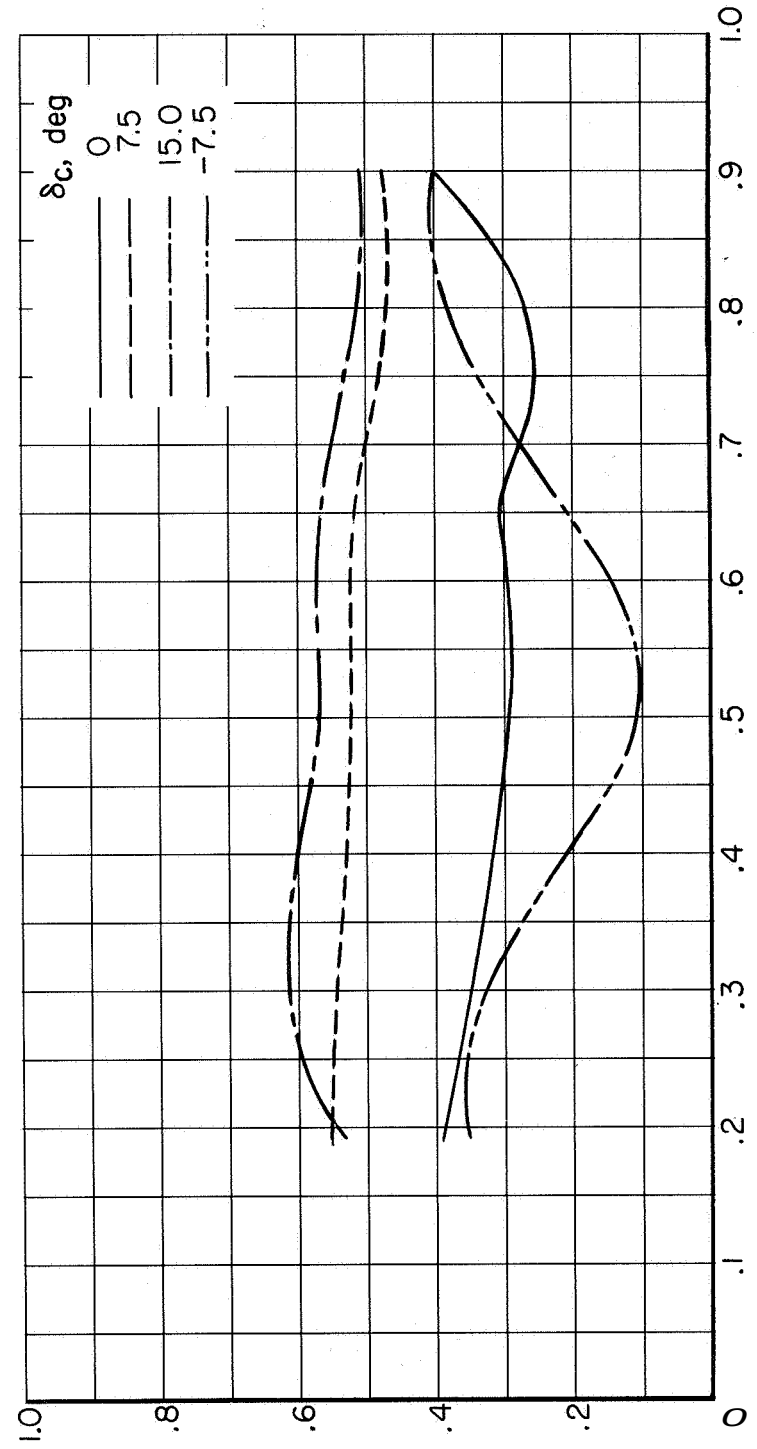

(a) $\alpha \approx 4^\circ$

Figure 25.- Variation of section chordwise center-of-pressure locations along wing semispan for various combined control deflections. M = 0.94.

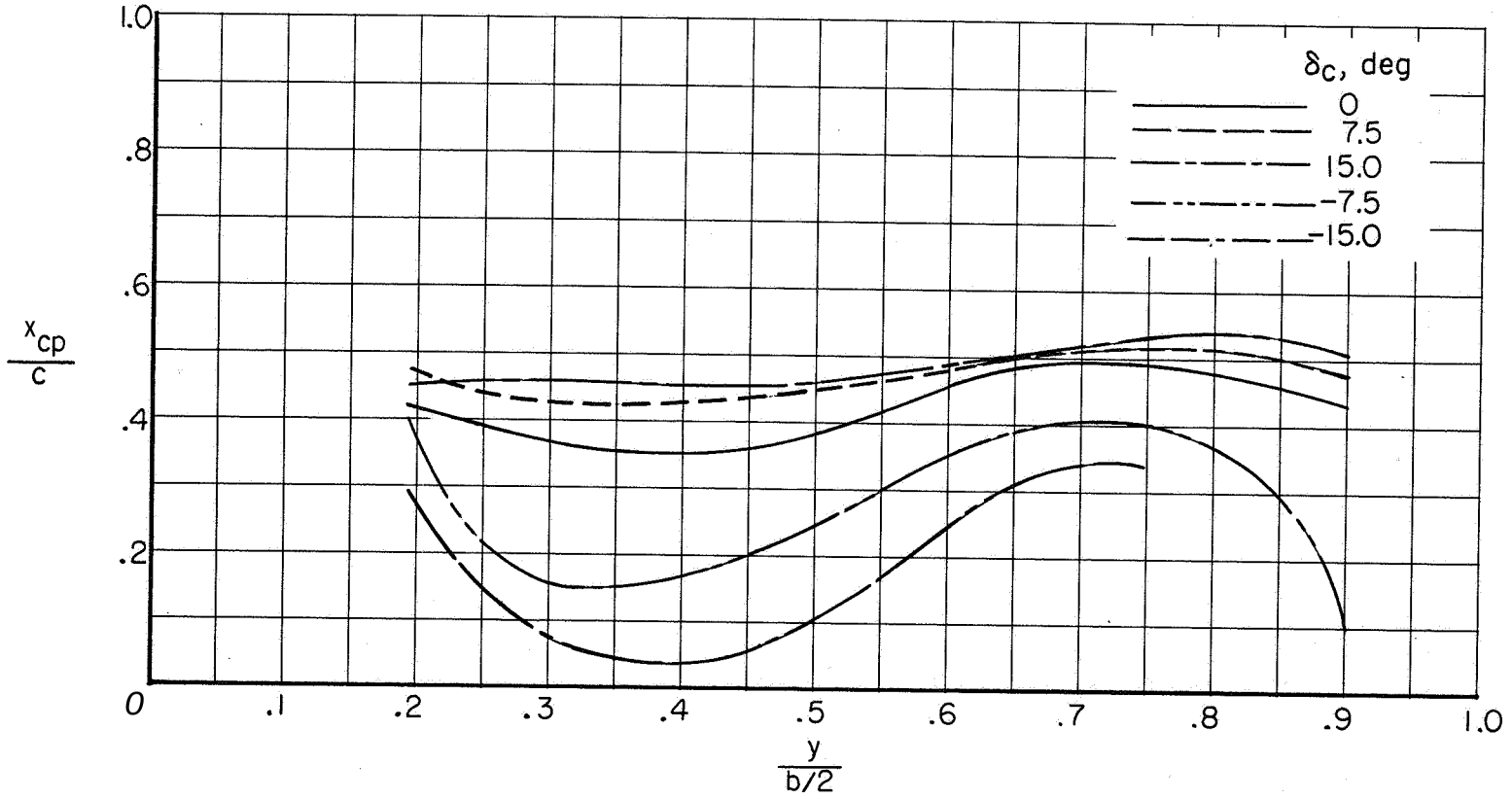

(b) $\alpha \approx 12^\circ$.

Figure 25.- Continued.

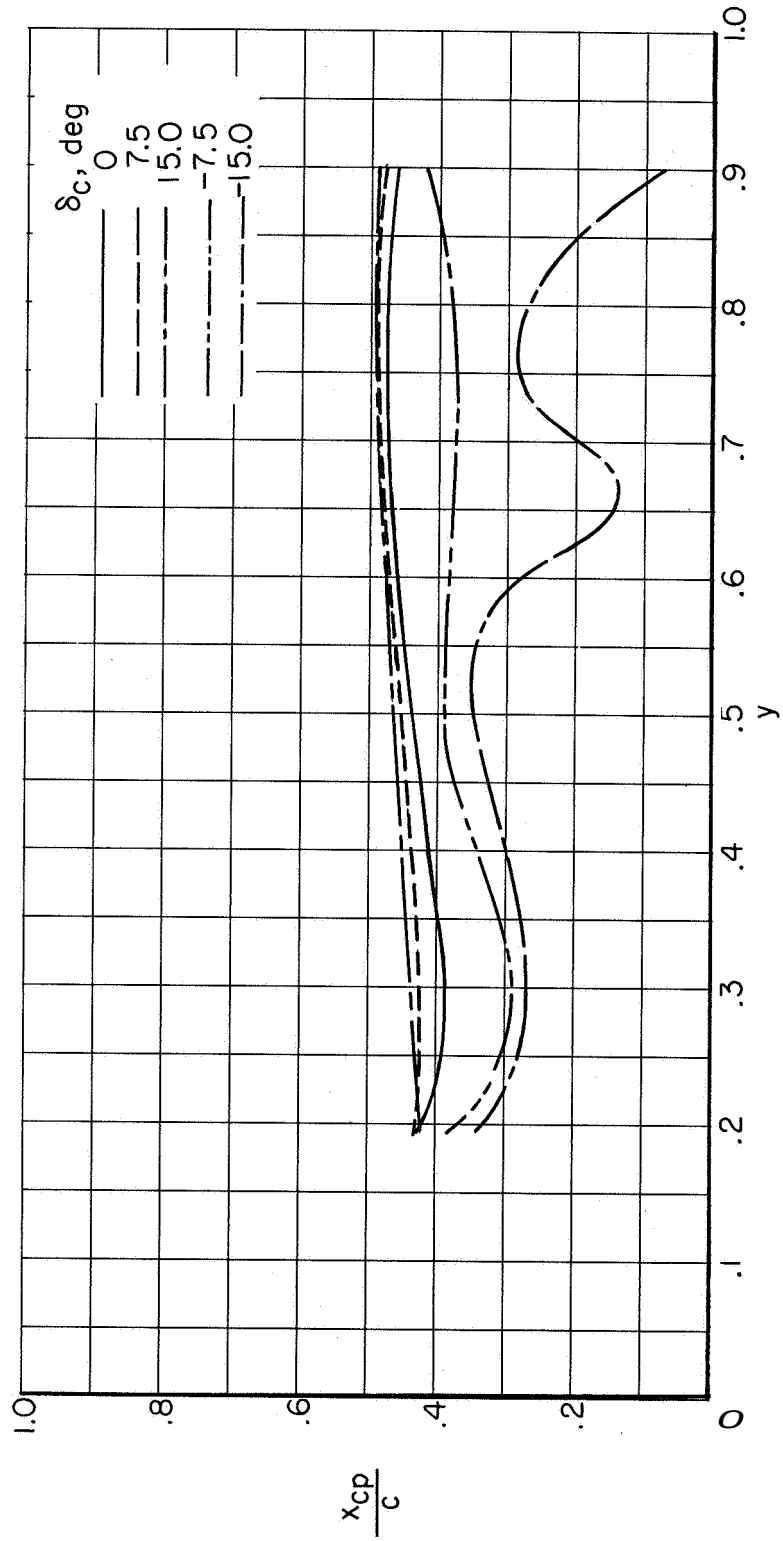

(c) $\alpha \approx 20^\circ$.

Figure 25.- Concluded.

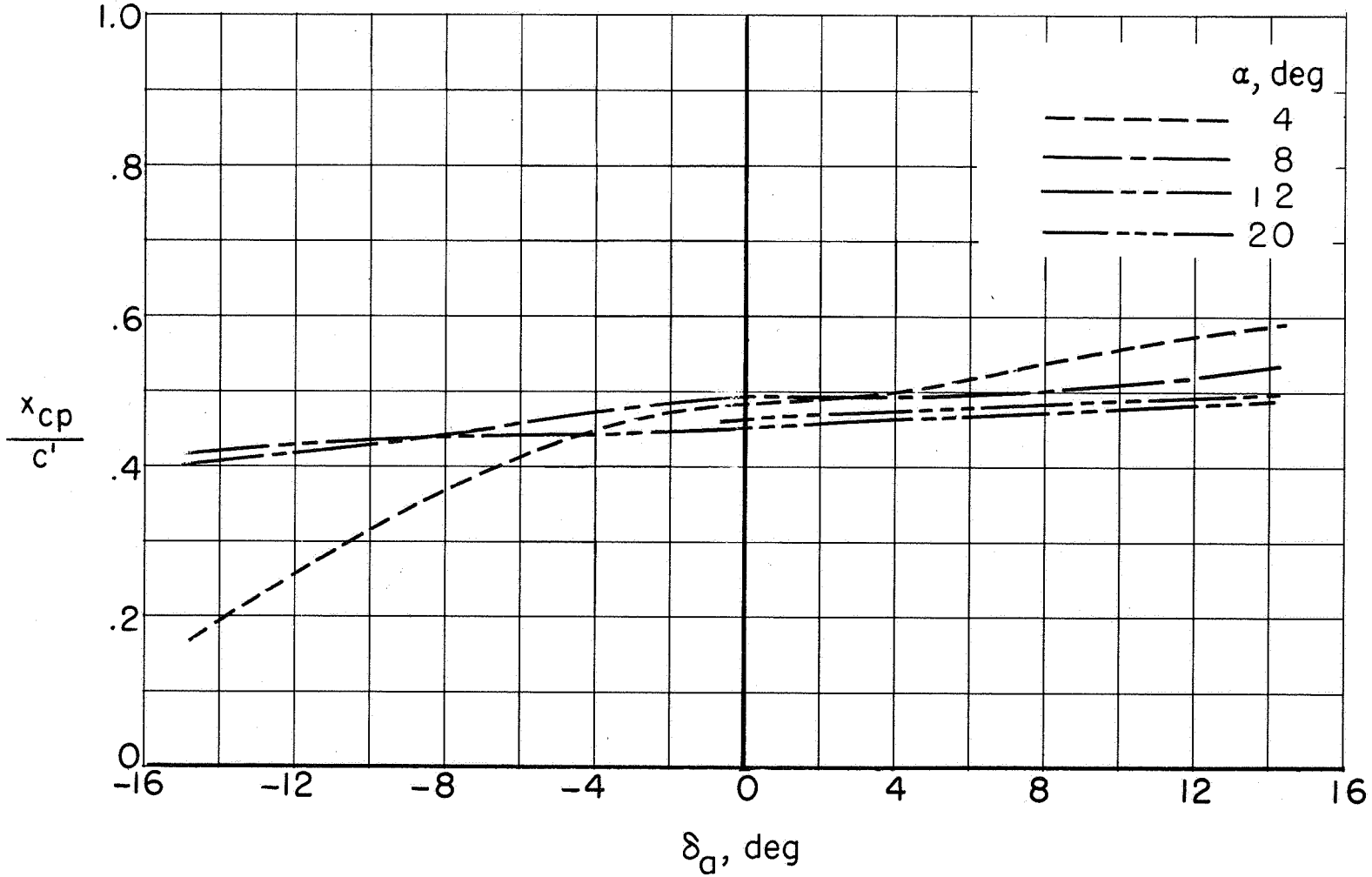

(a) M = 0.80.

Figure 26.- Effect of aileron deflection on wing chordwise center-of-pressure position for various Mach numbers.

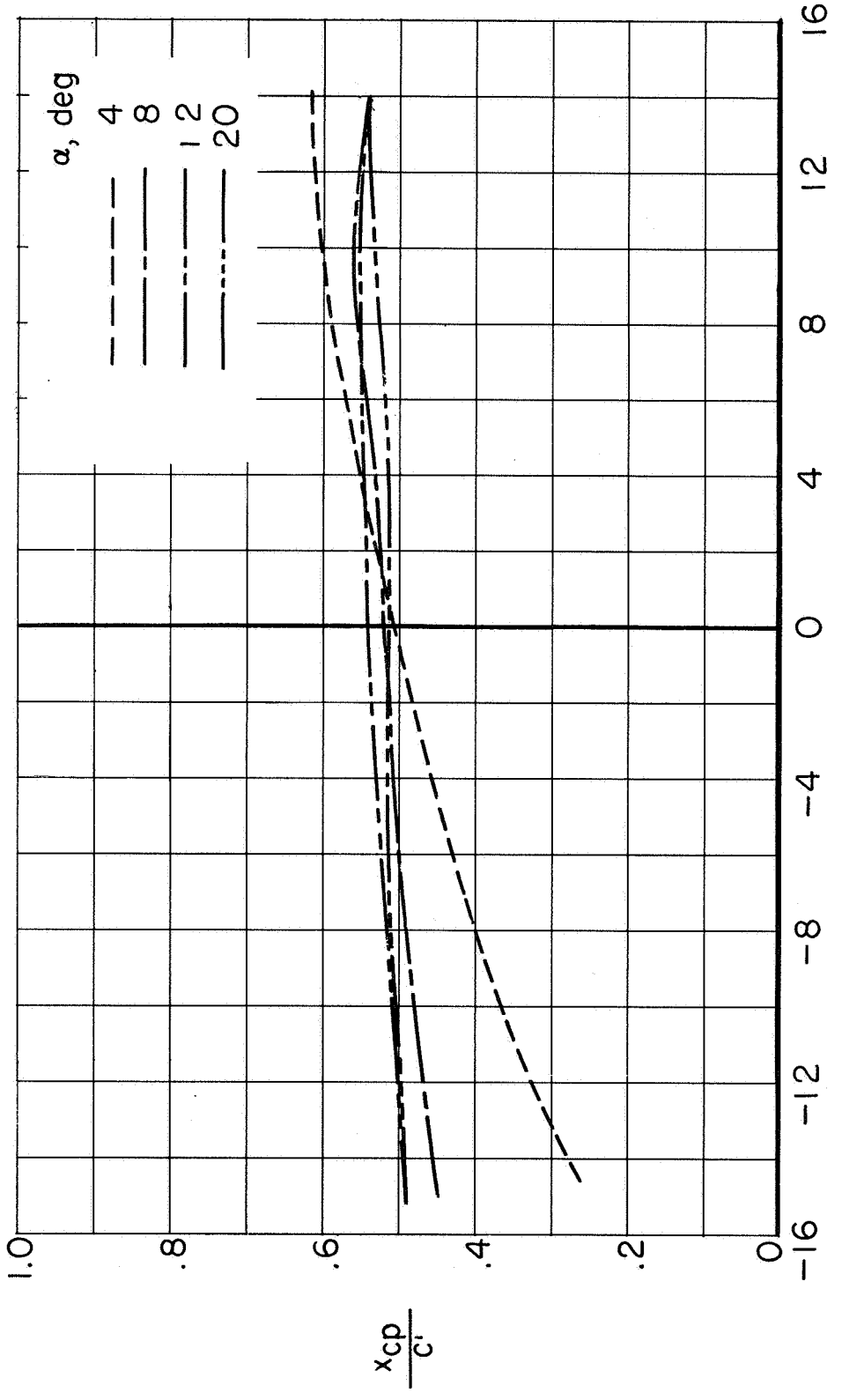

(b) M = 0.94

Figure 26.- Continued.

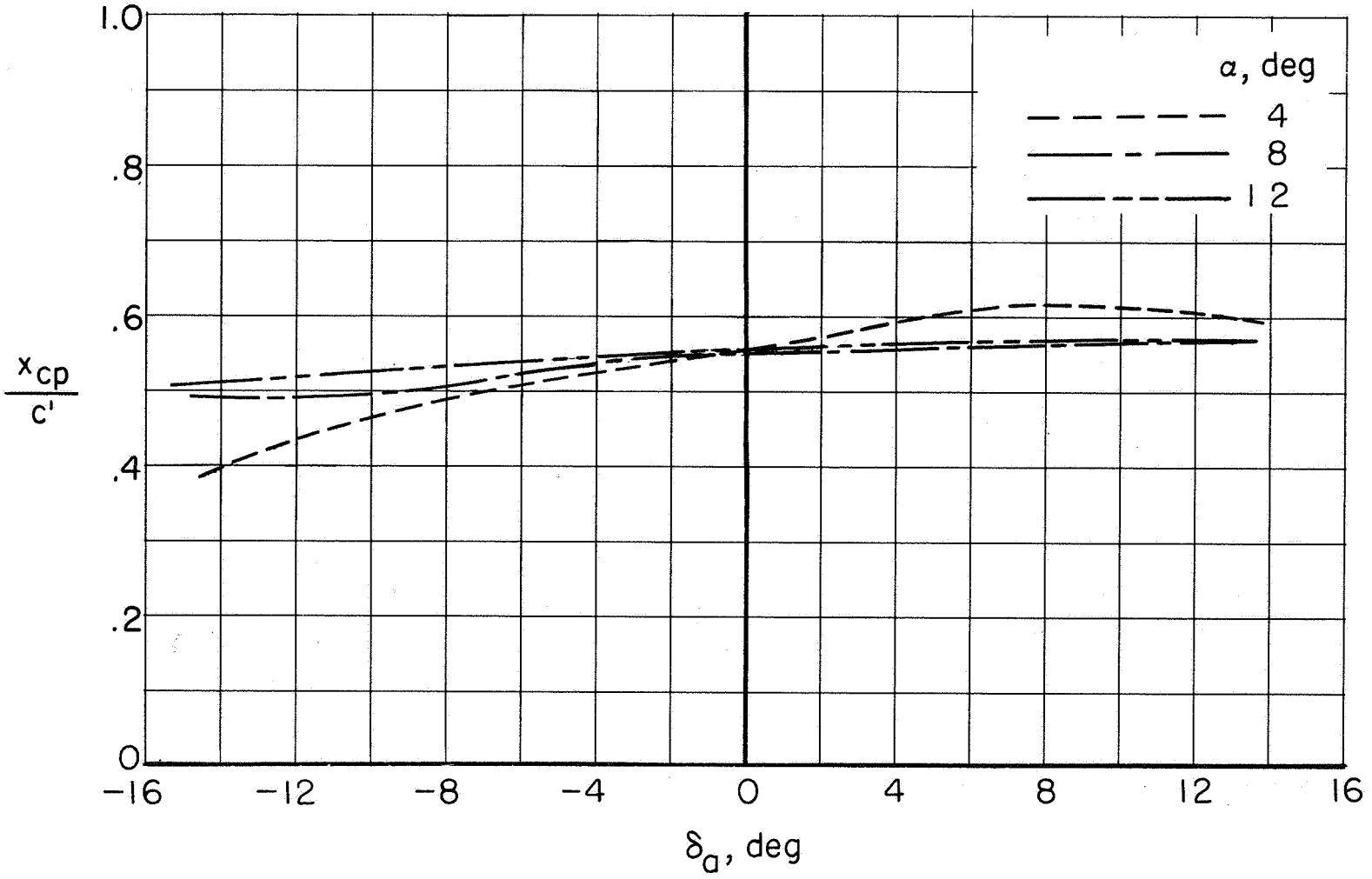

(c) M = 1.05

Figure 26.- Concluded.

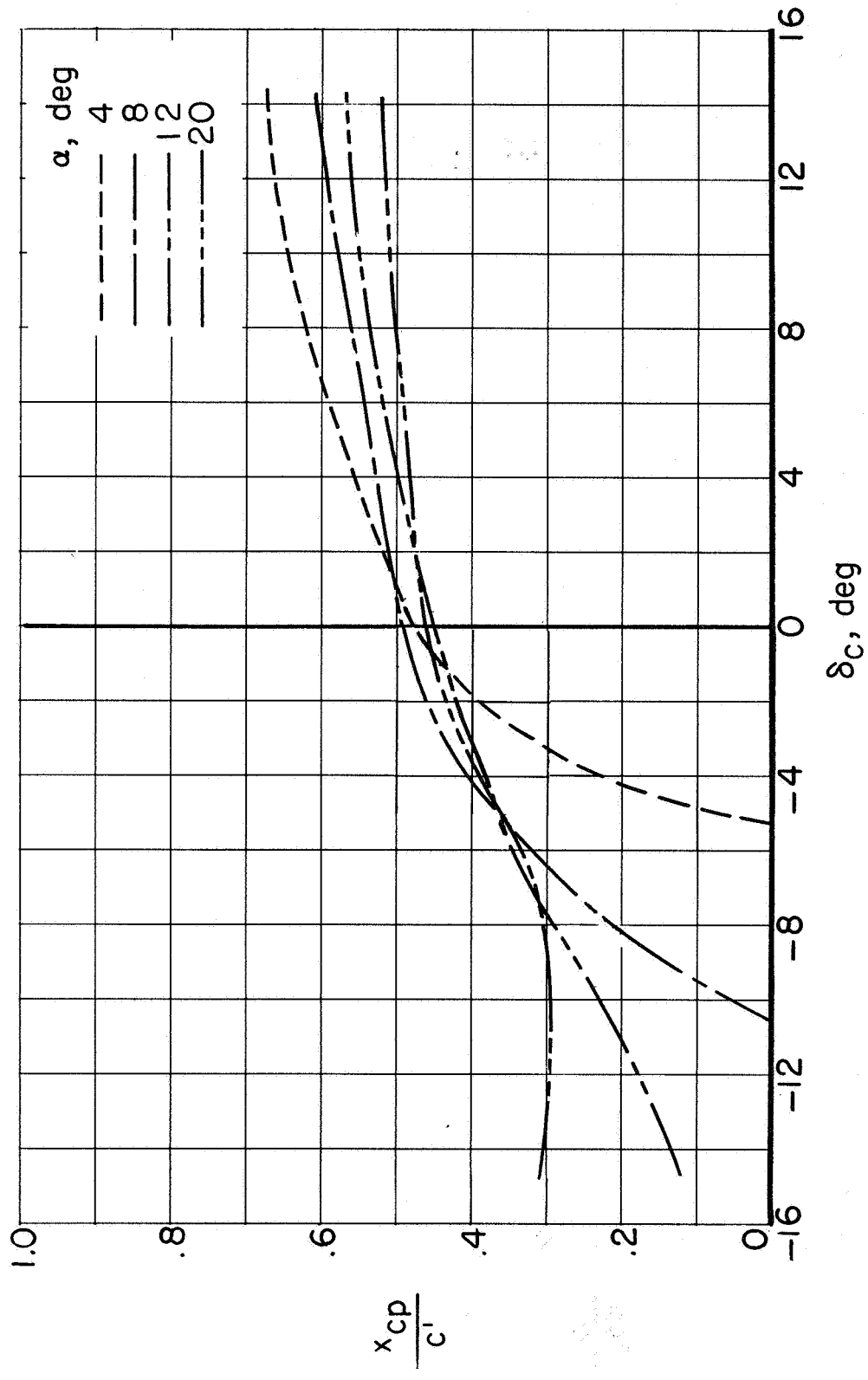

(a) M = 0.80

Figure 27.- Effect of combined control deflection on wing chordwise center-of-pressure location for various Mach numbers.

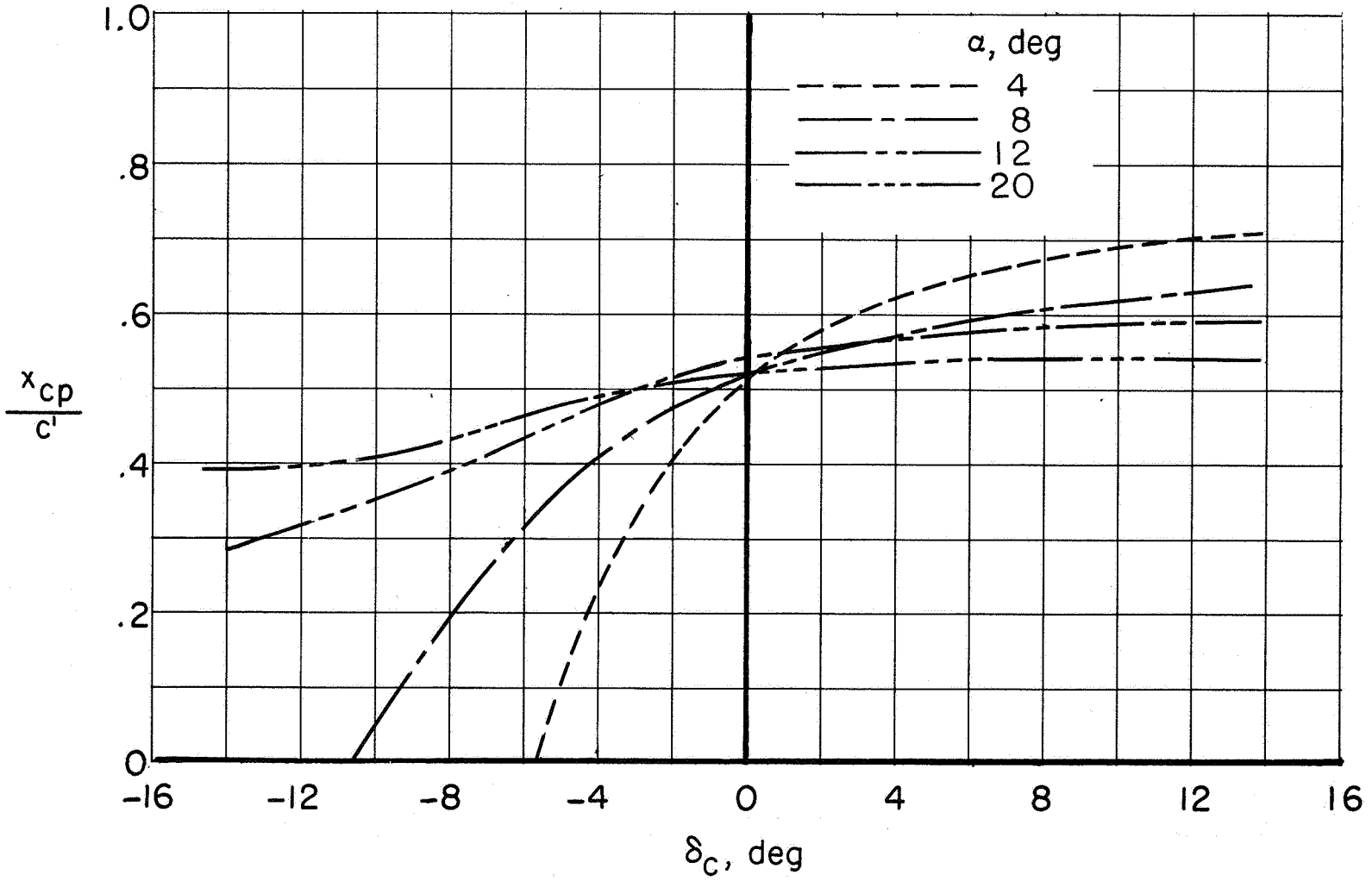

(b) M = 0.94.

Figure 27.- Continued.

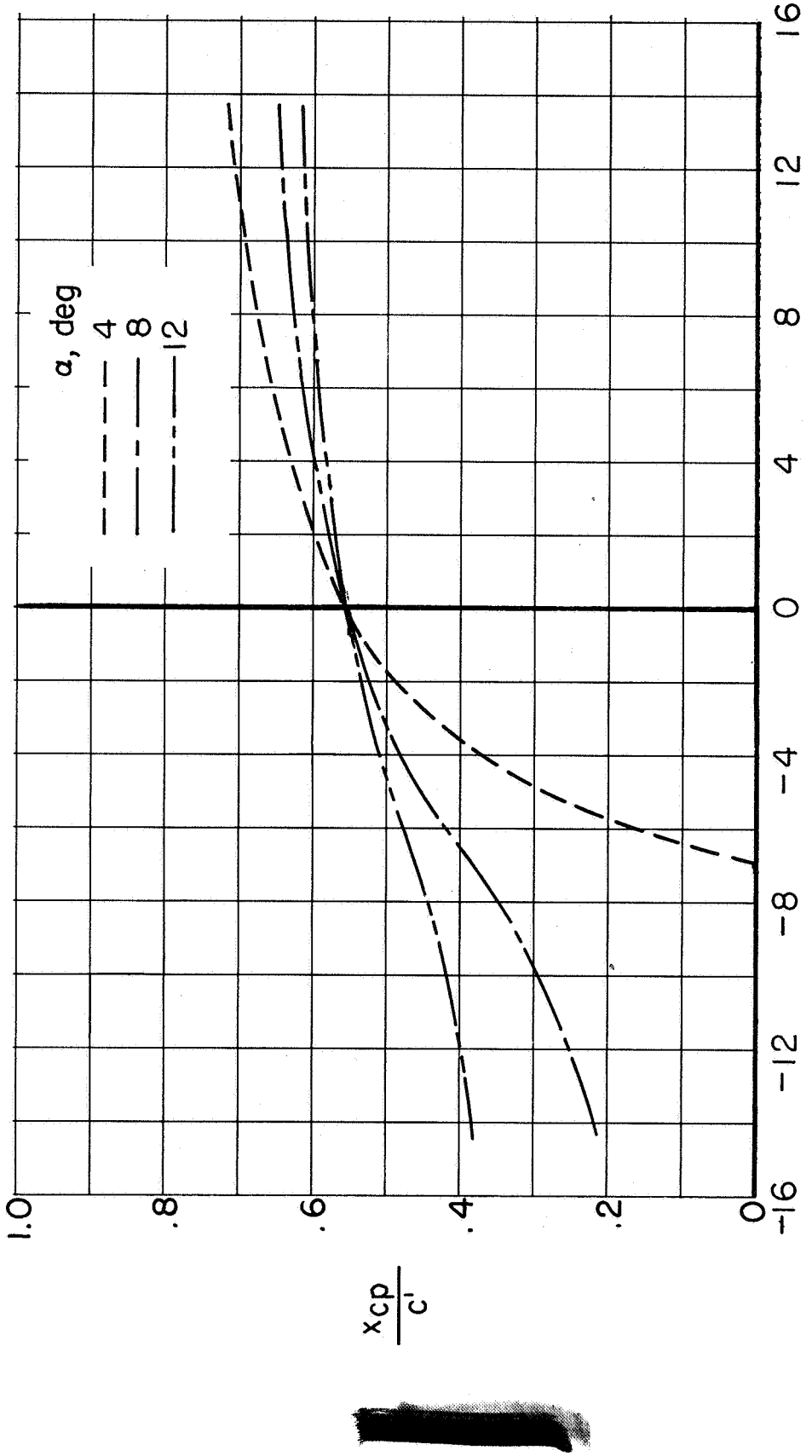

(c) M = 1.05.

Figure 27.- Concluded.

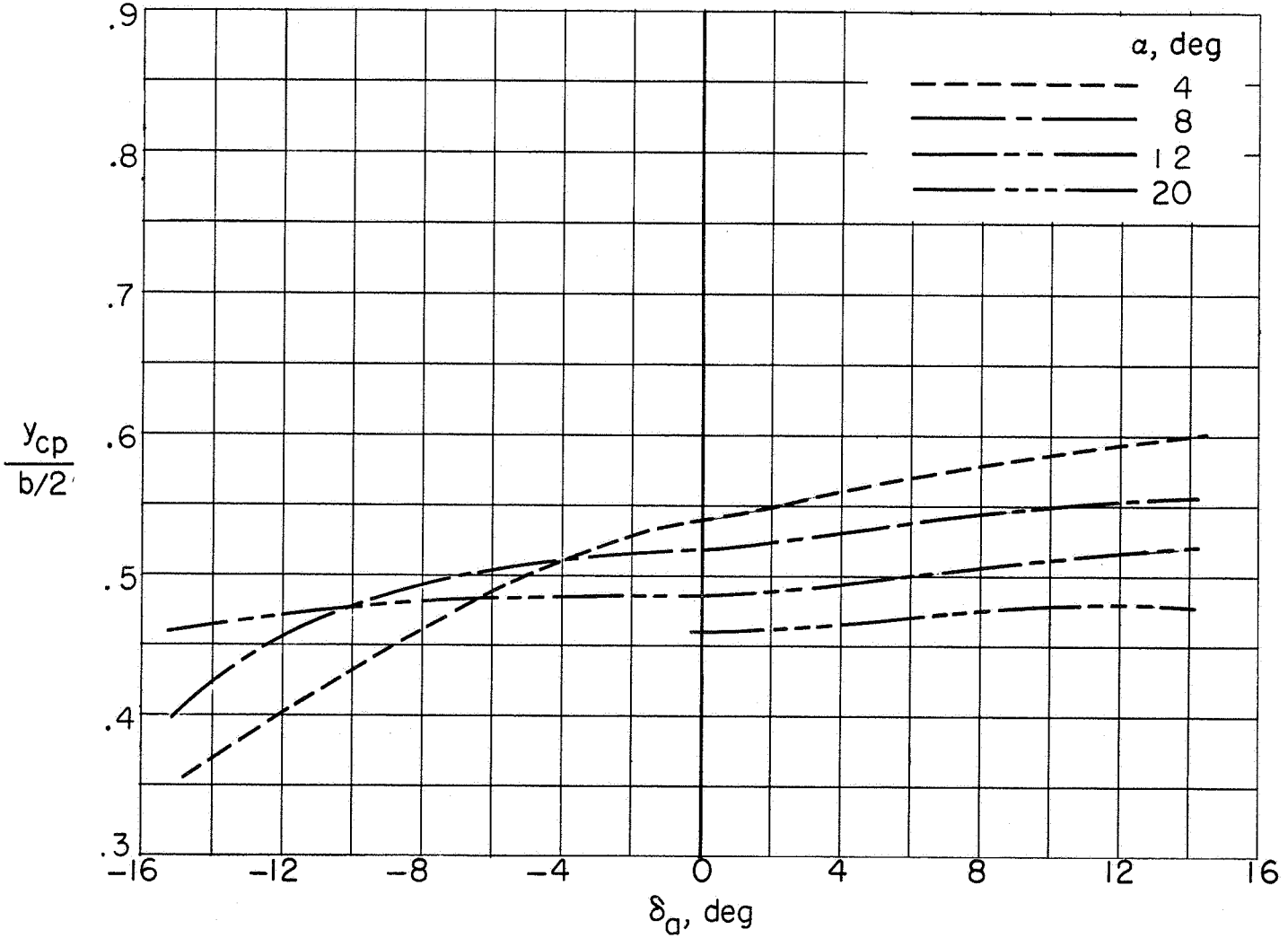

(a) $M_\infty = 0.80$

Figure 28.- Effect of aileron deflection on wing spanwise center-of-pressure location for various Mach numbers.

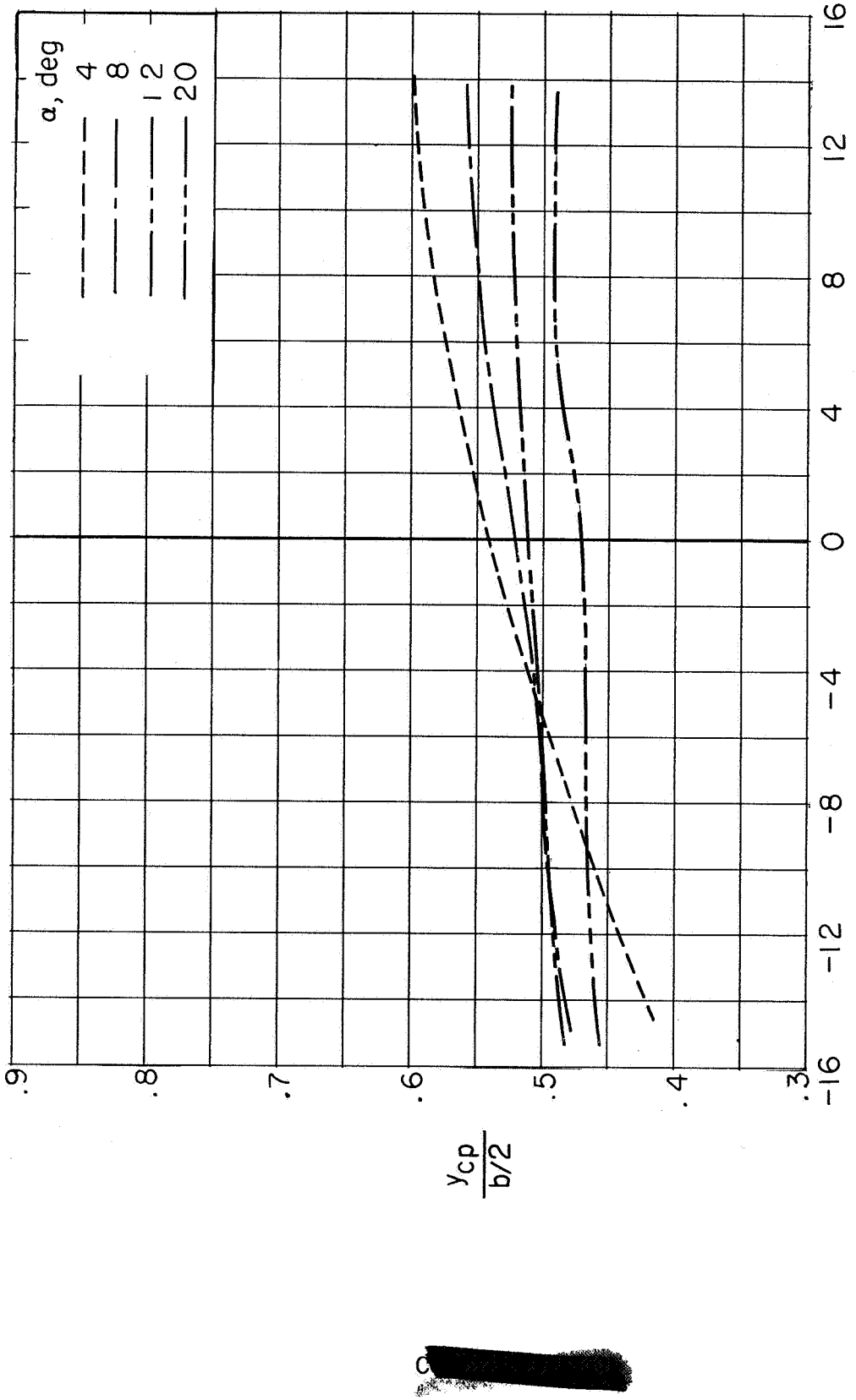

(b) M = 0.94.

Figure 28.- Continued.

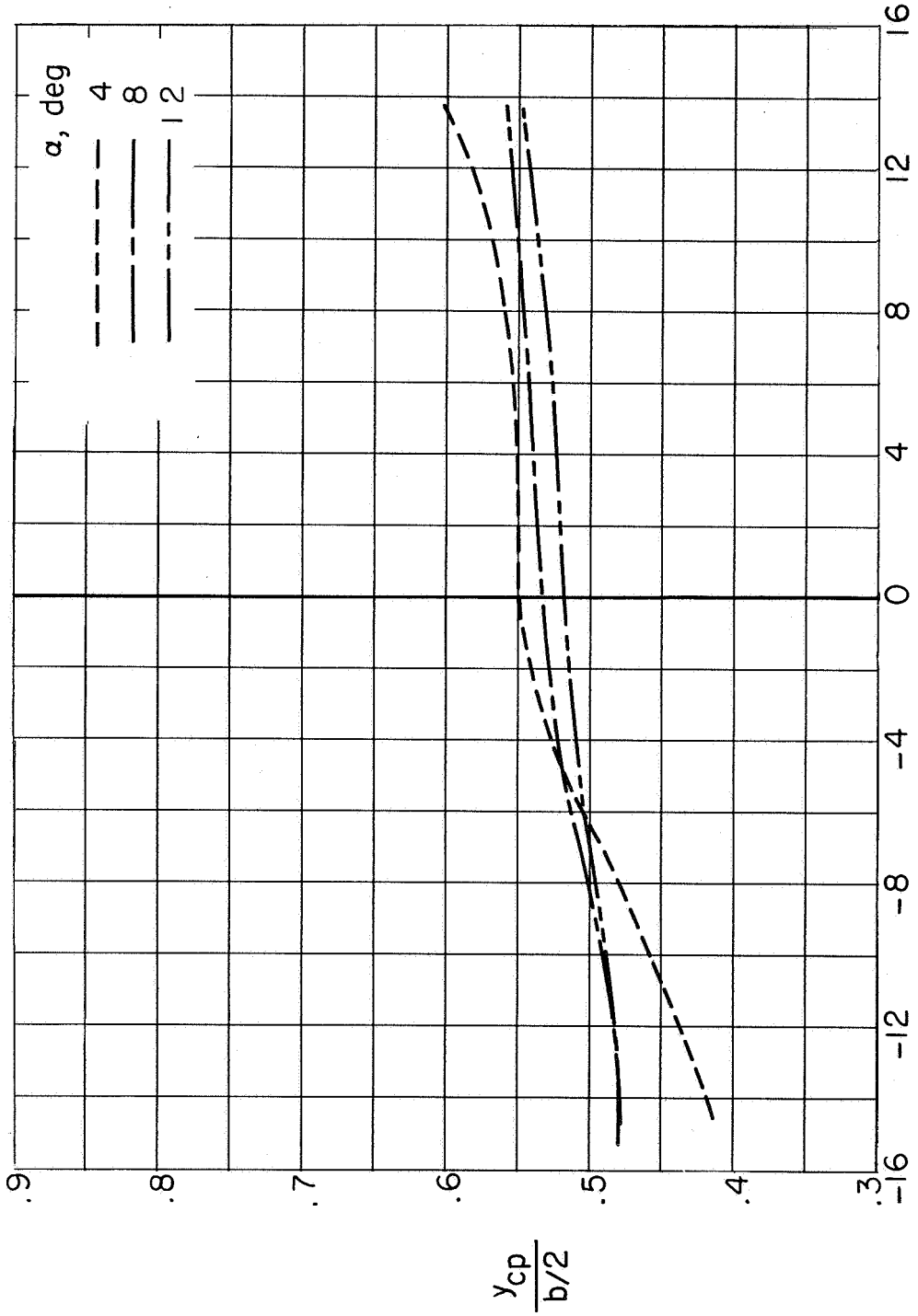

(c) M = 1.05.

Figure 28.- Concluded.

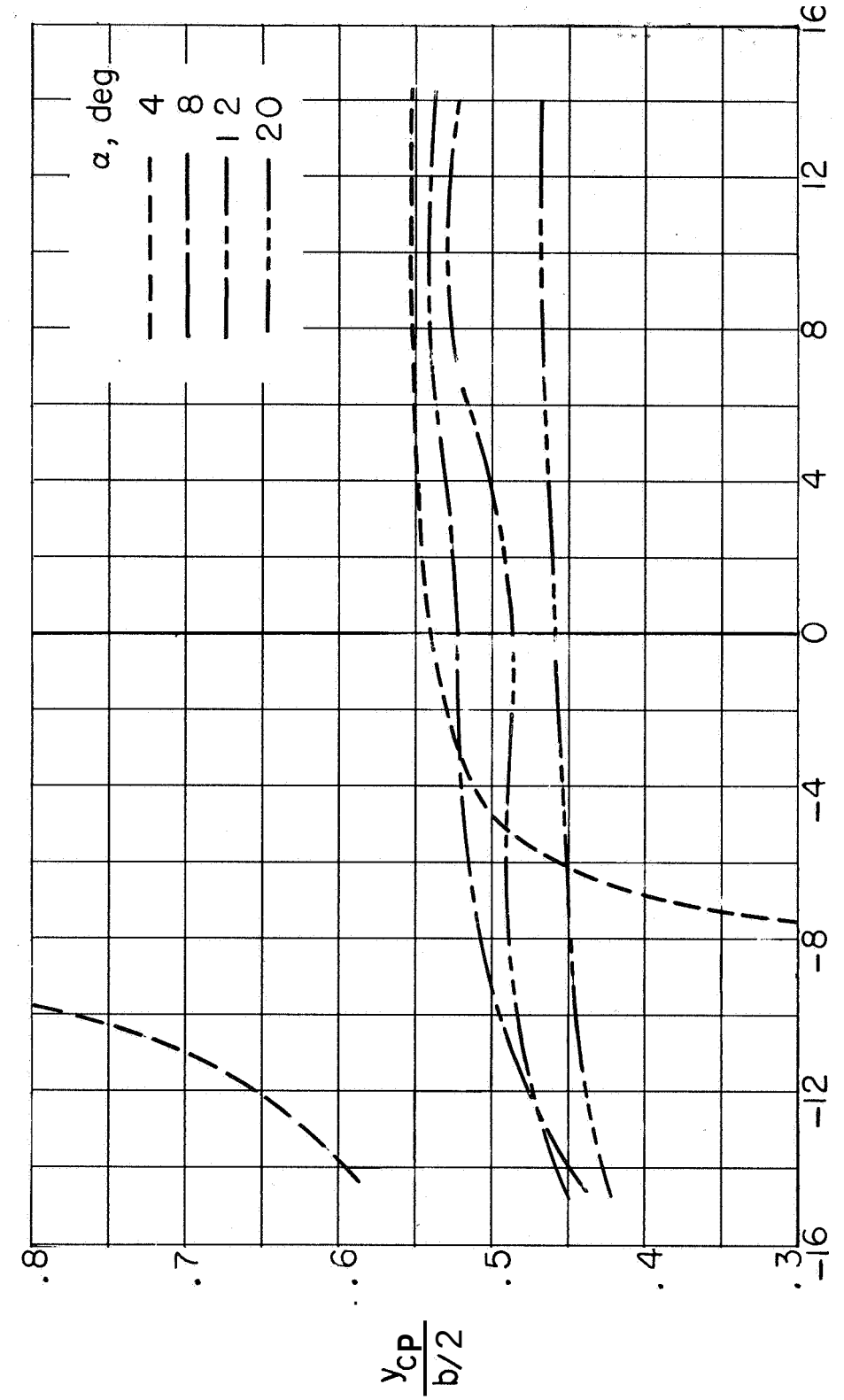

(a) M = 0.80.

Figure 29.- Effect of combined control deflection on wing spanwise center-of-pressure location for various Mach numbers.

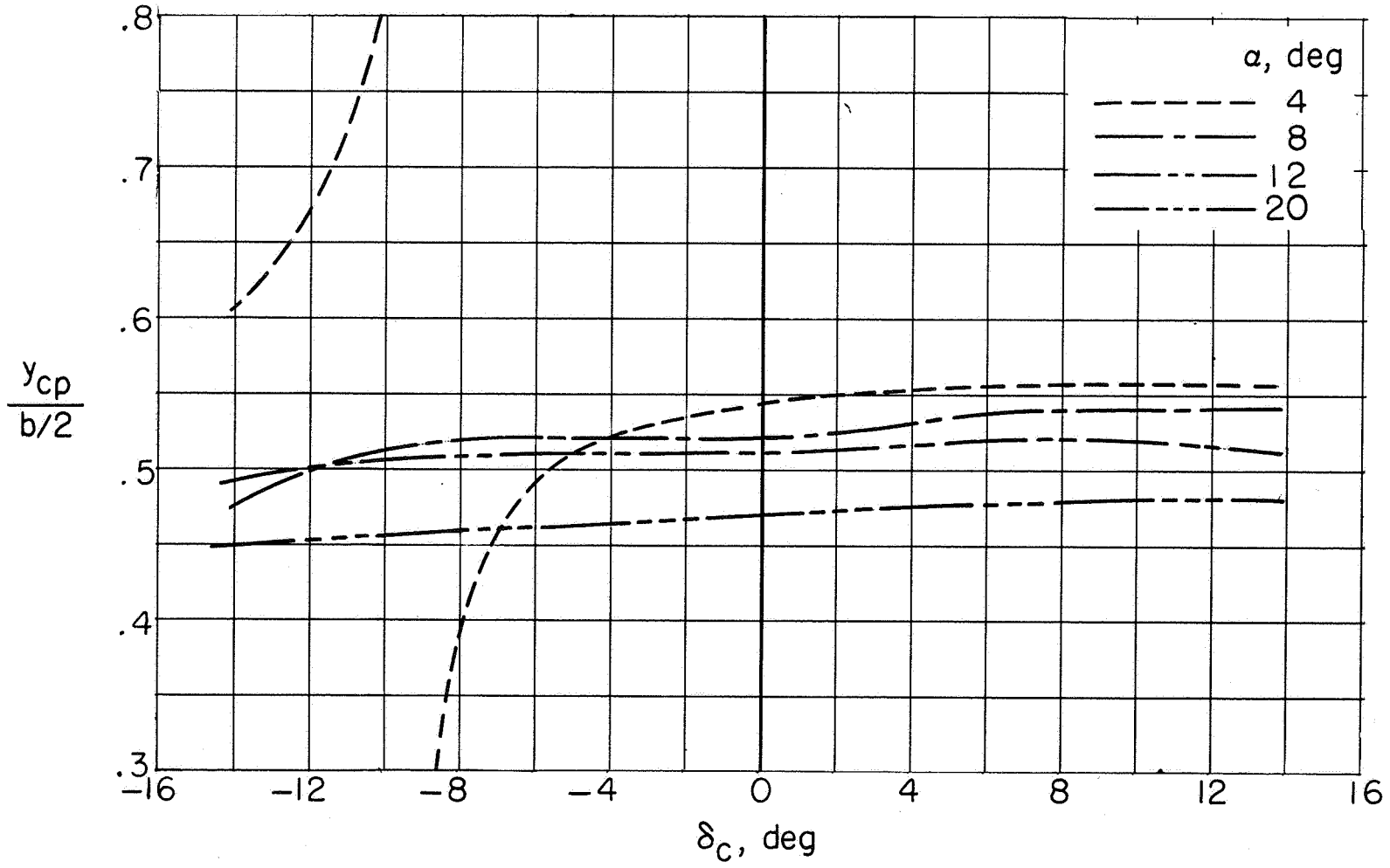

(b) M = 0.94.

Figure 29.- Continued.

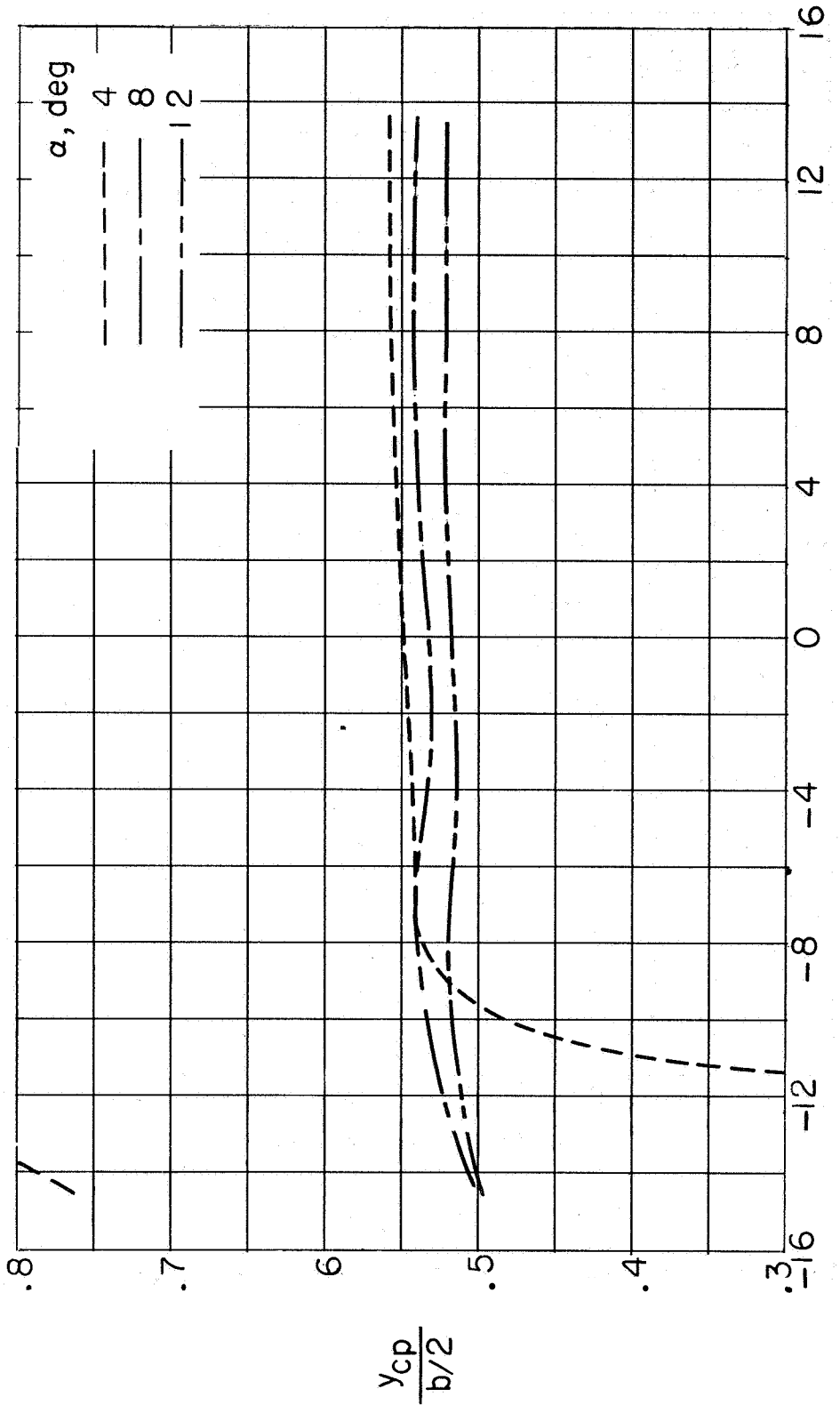

(c) M = 1.05.

Figure 29.- Concluded.

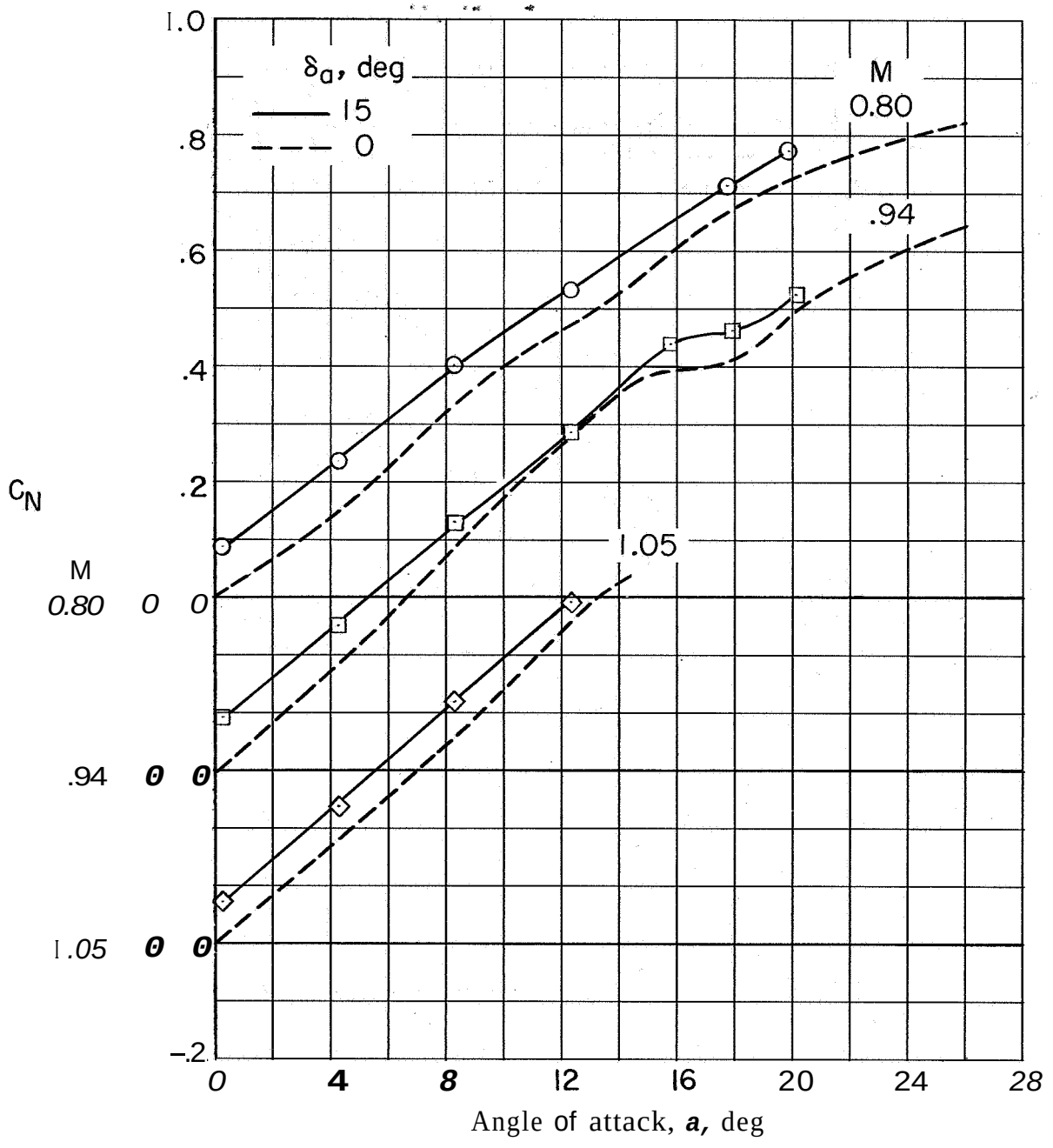

(a) $\delta_a = 15^\circ$ and $\delta_a = 0^\circ$.

Figure 30.- Variation of wing normal-force coefficient with angle of attack with aileron deflected.

L-506

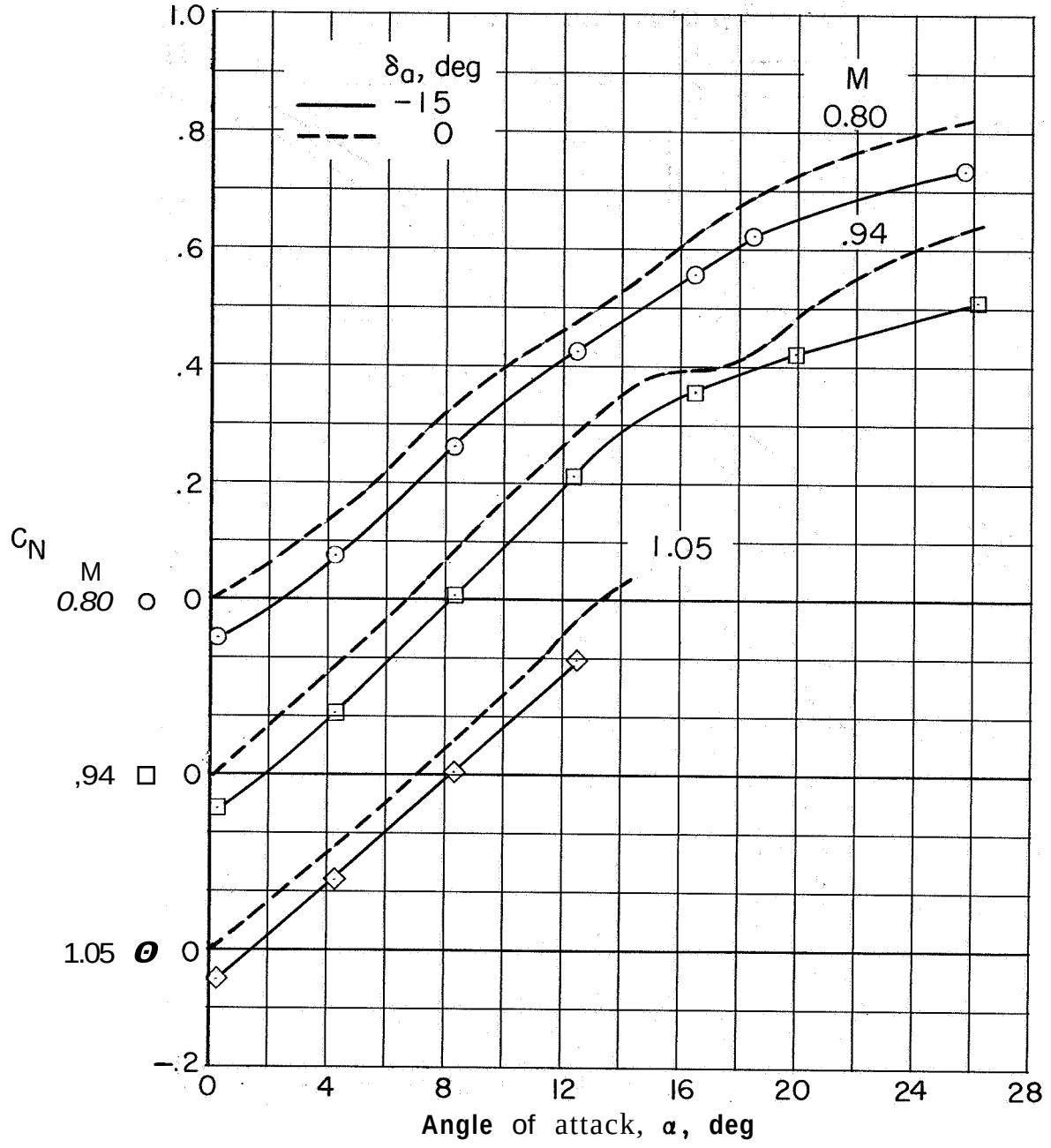

(b) $\delta_a = -15^\circ$ and $\delta_a = 0^\circ$.

Figure 30.- Concluded.

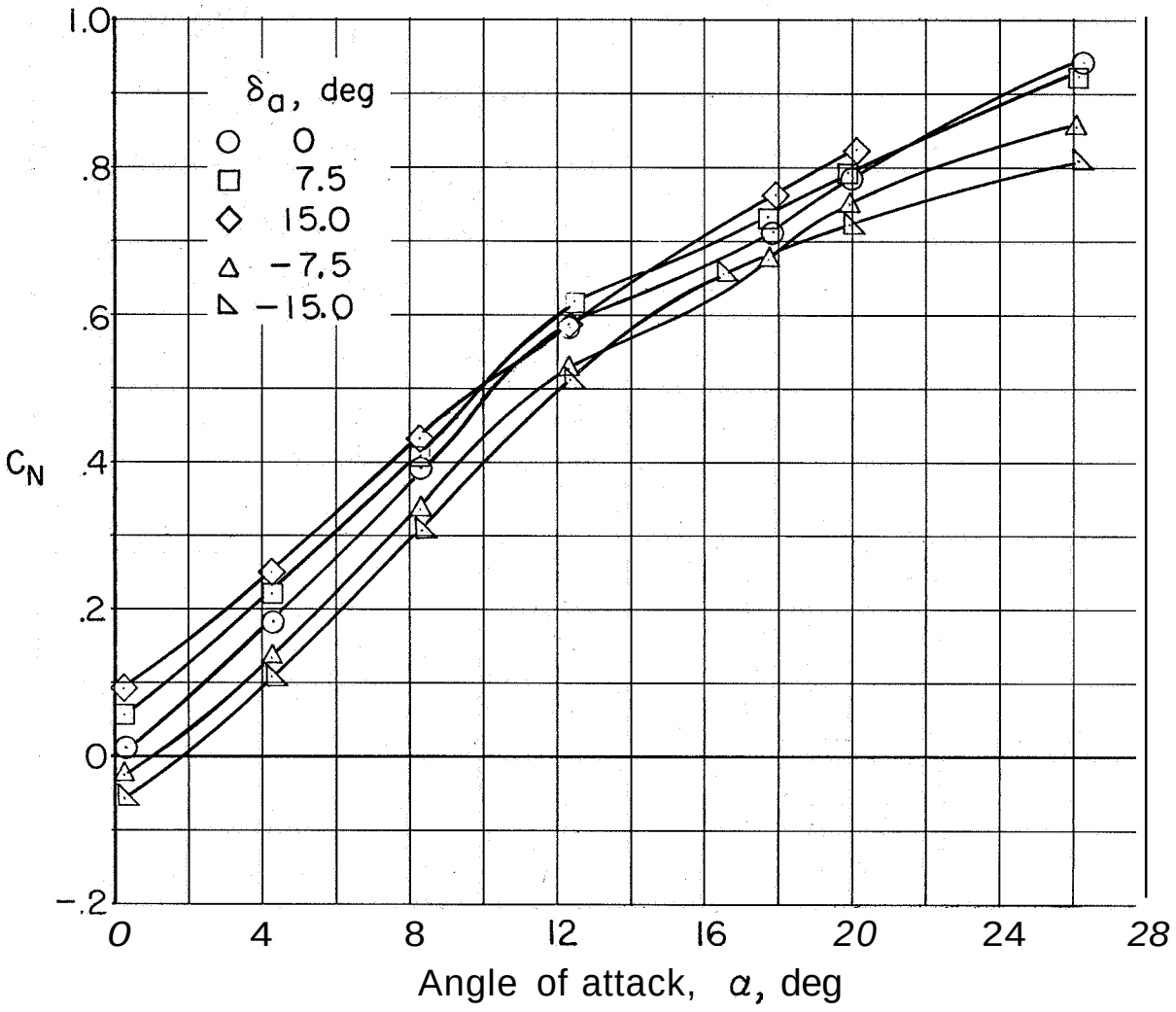

L-506

Figure 31.- Effect of aileron deflection on wing normal-force-coefficient variation with angle of attack. M = 0.94.

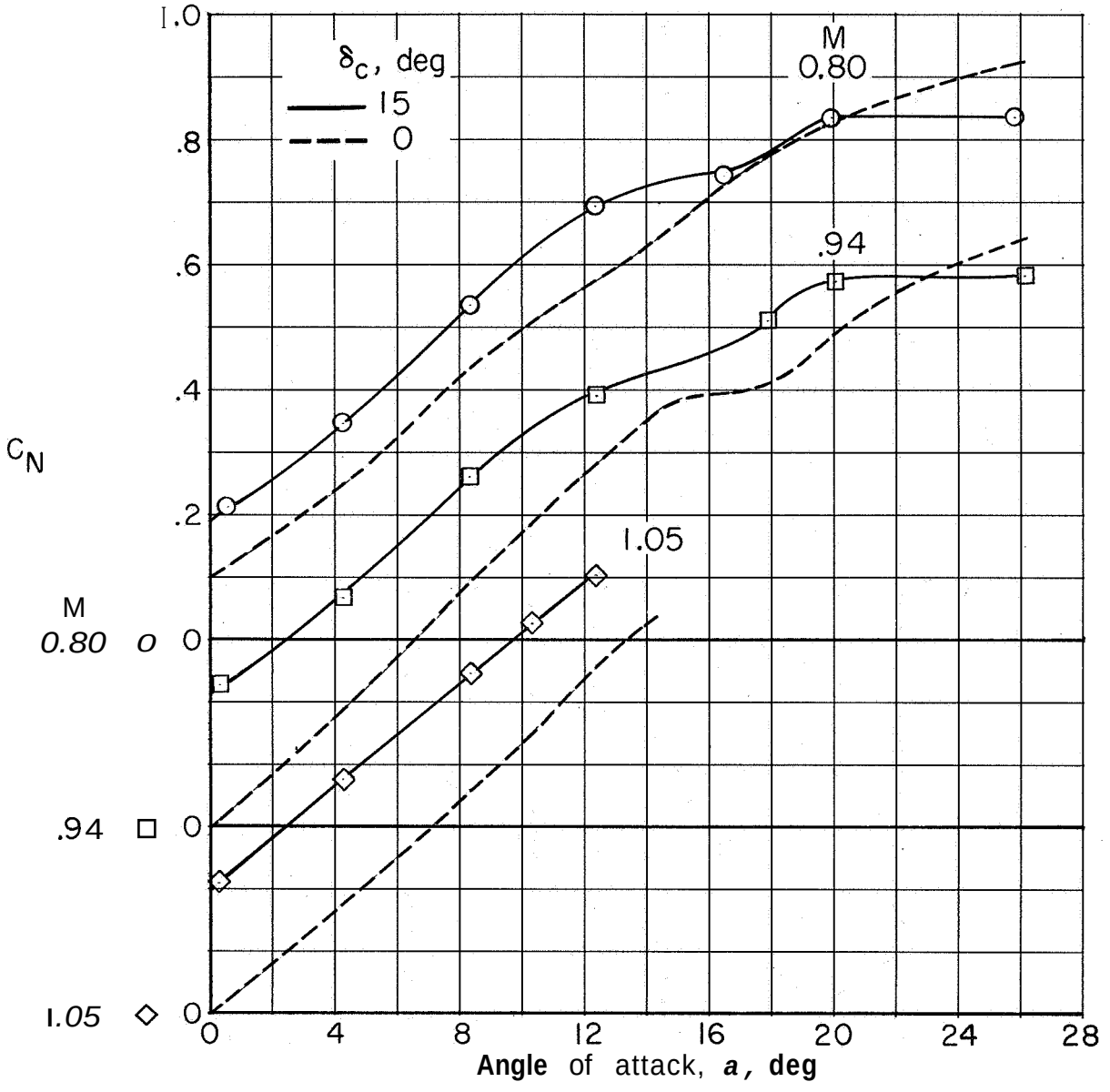

(a) $\delta_c = 15^\circ$ and $\delta_c = 0^\circ$.

Figure 32.- Variation of wing normal-force coefficient with angle of attack for various Mach numbers.

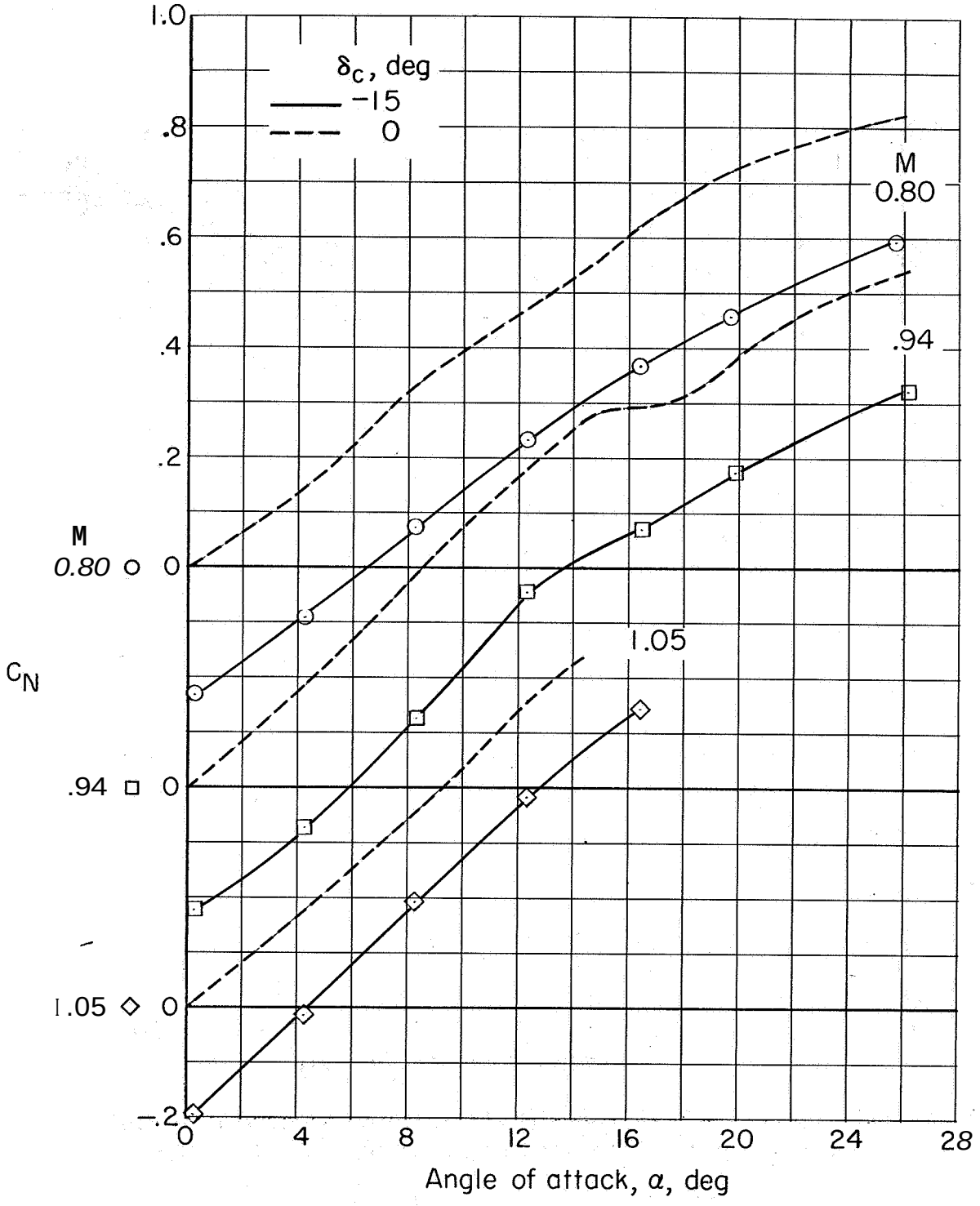

(b) $\delta_c = -15^\circ$ and $\delta_c = 0^\circ$.

Figure 32.- **Concluded.**

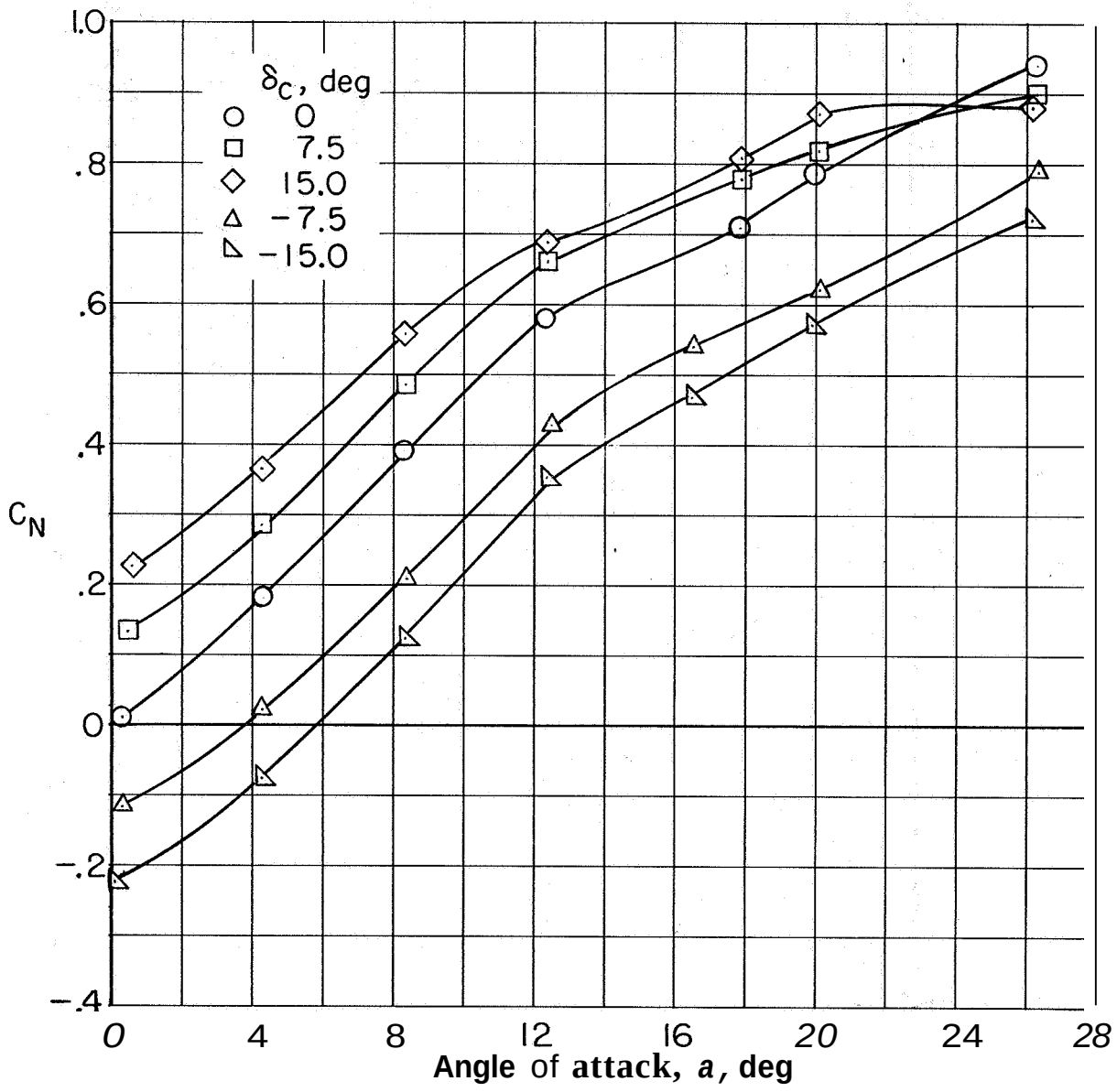

Figure 33.- Effect of combined control deflection on wing normal-force-coefficient variation with angle of attack. M = 0.94.

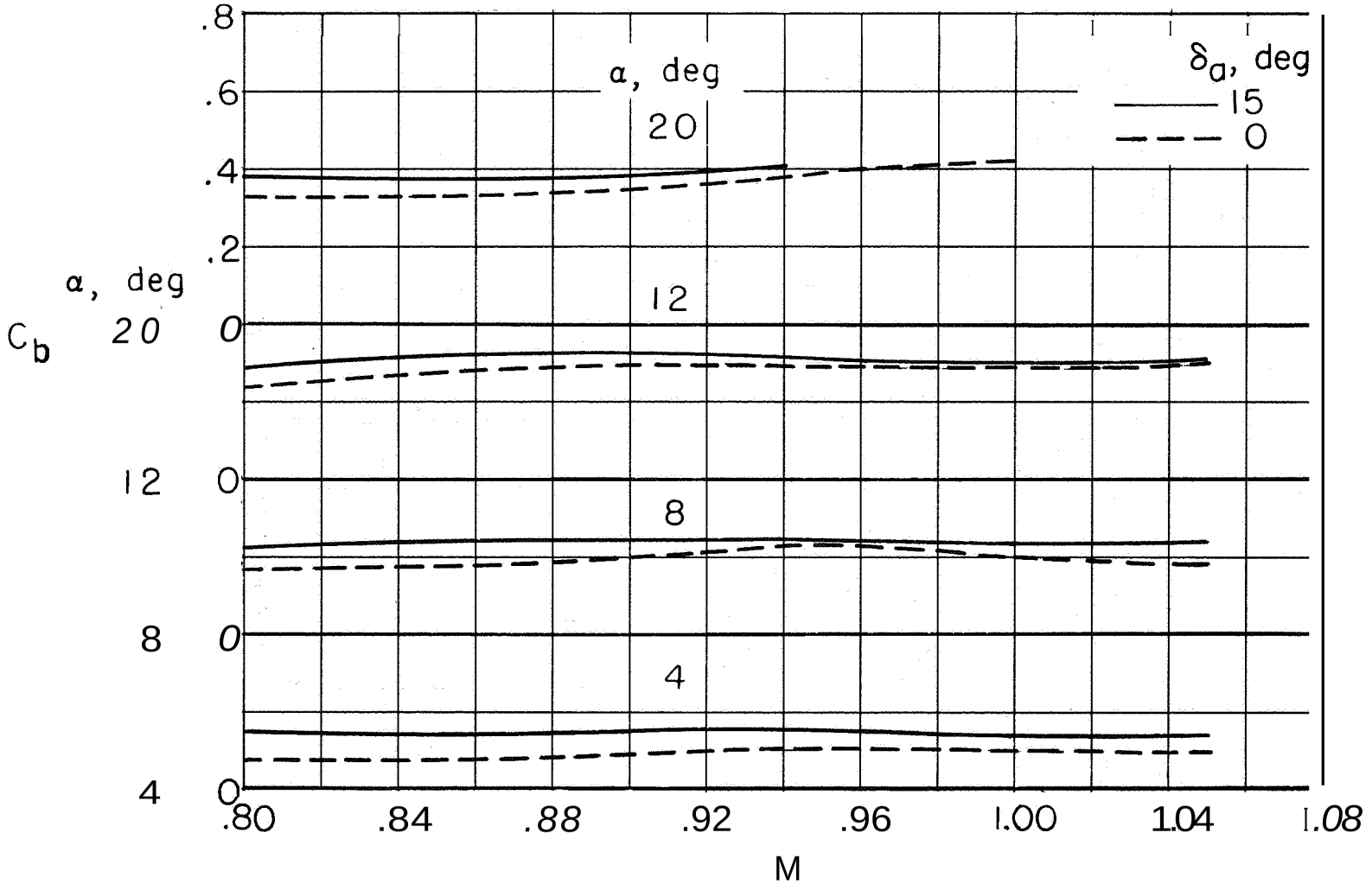

(a) $\delta_a = 15^\circ$ and $\delta = 0^\circ$.

Figure 34.- Effect of Mach number on wing bending-moment coefficient with ailerons deflected for various angles of attack.

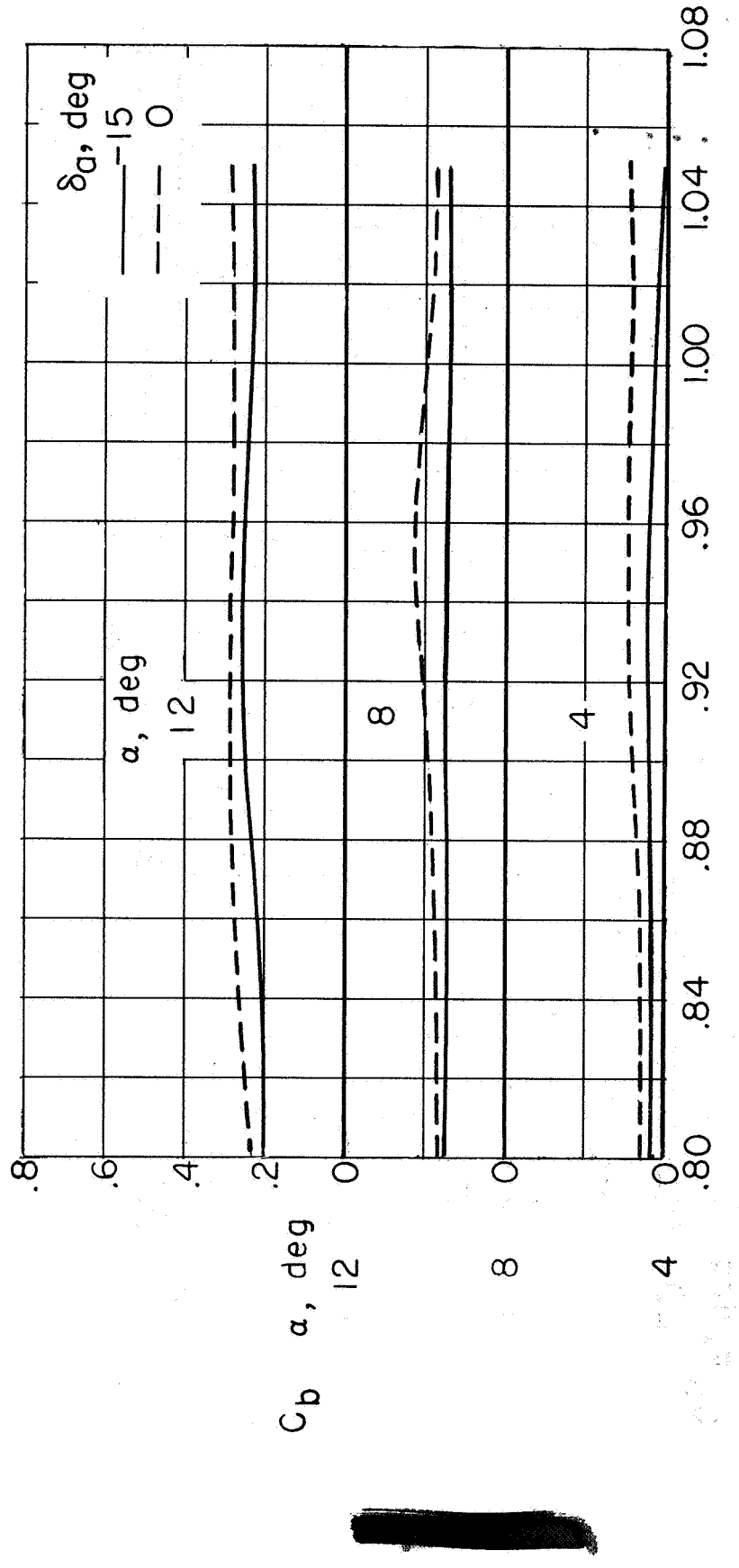

(b) $\delta_a = -15^\circ$ and $\delta_a = 0^\circ$.

Figure 34.- Concluded.

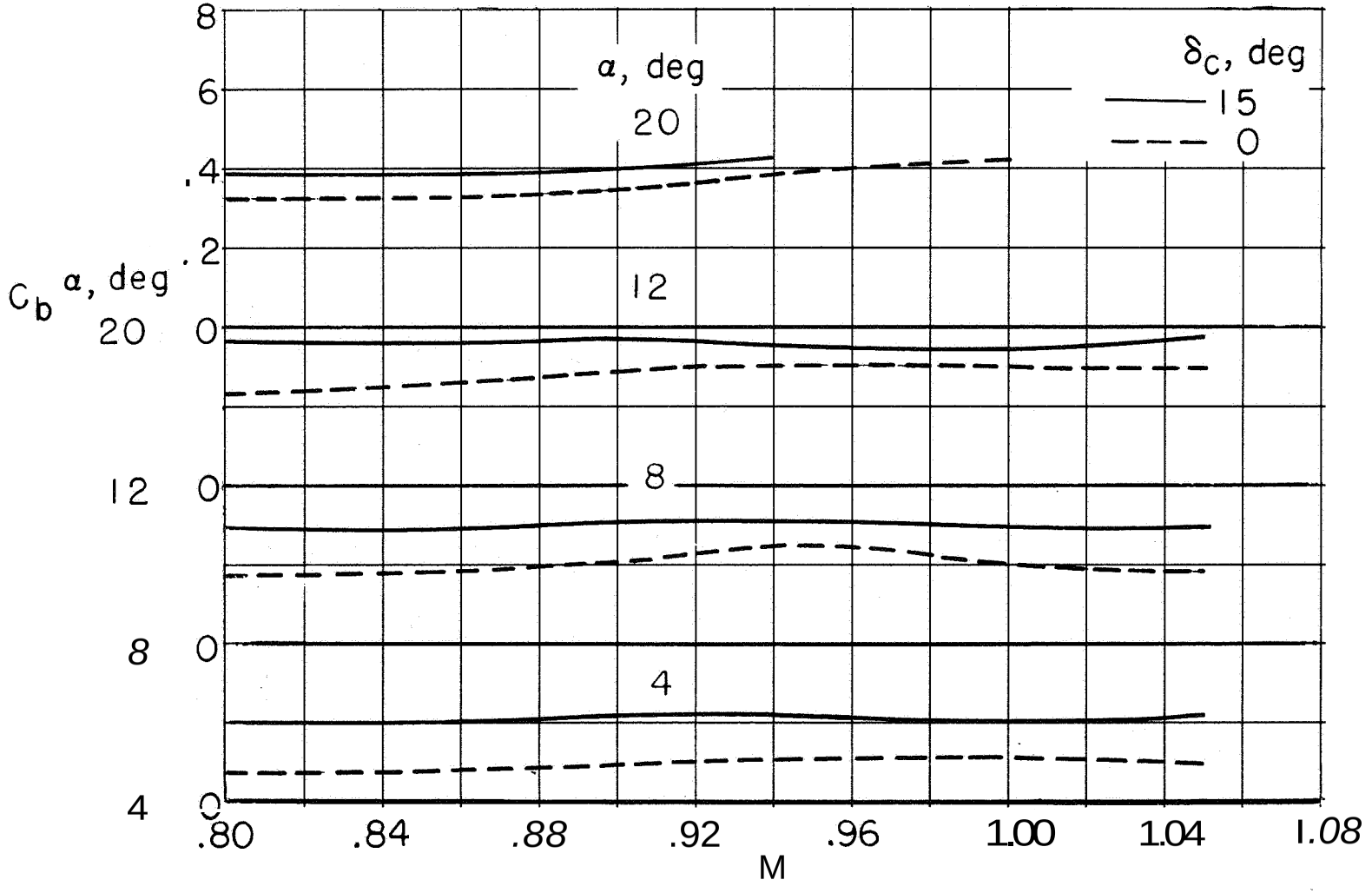

(a) $\delta_c = 15°$ and $\delta_c = 0°$.

Figure 35.- Effect of Mach number on wing bending-moment coefficient with combined controls deflected for various angles of attack.

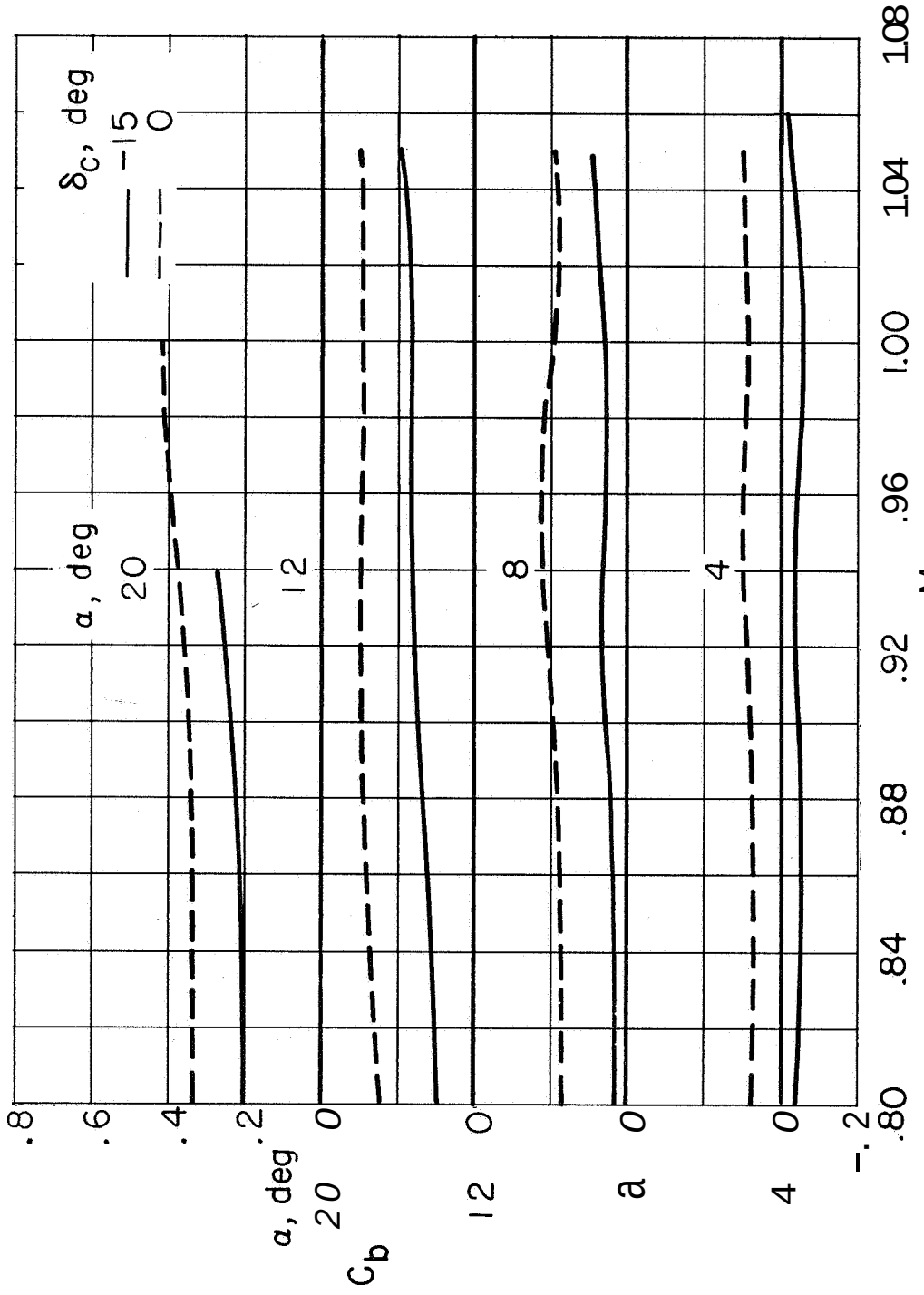

(b) $\delta_s = -15^\circ$ and $\delta_s = 0^\circ$.

Figure 35.- Concluded.